Study of the photophysical properties of oxyluciferin derivatives and their applications to the characterization of interactions between biomolecules

Avisek Ghose

UNIVERSITÉ DE STRASBOURG

ÉCOLE DOCTORALE DES SCIENCES DE LA VIE ET DE LA SANTE (ED-414)

UMR CNRS 7213, Faculté de Pharmacie, Illkirch

THÈSE présentée par :

Avisek GHOSE

Soutenue le : **17 Février 2015**

pour obtenir le grade de : **Docteur de l'université de Strasbourg**

Discipline/ Spécialité : Biophysique

TITRE de la thèse

Etude des propriétés photophysiques de dérivés de l'oxyluciférine et leurs applications à l'étude d'interactions entre biomolécules

THÈSE dirigée par :

M. ARNTZ Youri	Maître de Conférences, Université de Strasbourg

RAPPORTEURS :

Mme. NAVIZET Isabelle	Professeur des Universités, Université Paris-Est
M. GUSTAVSSON Thomas	Directeur de Recherche, CNRS

AUTRES MEMBRES DU JURY :

M. LEONARD Jérémie	Chargé de Recherche, Université de Strasbourg
M. DIDIER Pascal	Maître de Conférences, Université de Strasbourg

UNIVERSITÉ DE STRASBOURG

UNIVERSITÉ DE STRASBOURG

École Doctorale des Sciences de la Vie et de la Santé STRASBOURG

ÉCOLE DOCTORALE DES SCIENCES DE LA VIE ET DE LA SANTE (ED-414)

UMR CNRS 7213, Faculty of Pharmacy, Illkirch

THESIS presented by:

Avisek GHOSE

on **17 Février 2015**

to obtain degree of **Doctorate of University of Strasbourg**

Discipline/ Specialisation : Biophysics

Title of the thesis :

Study of the photophysical properties of Oxyluciferin derivatives and their applications to the characterization of interactions between biomolecules

Thesis Director :

Dr. Youri ARNTZ	Maître de Conférences, Université de Strasbourg

Reporters :

Prof. Isabelle NAVIZET	Professeur des Universités, Université Paris-Est
Dr. Thomas GUSTAVSSON	Directeur de Recherche, CNRS

Other members of the jury :

Dr. Jérémie LEONARD	Chargé de Recherche, Université de Strasbourg
Dr. Pascal DIDIER	Maître de Conférences, Université de Strasbourg

Student: Dr. Einstein, aren't these the same questions as last year's [physics] final exam?

Dr. Einstein: Yes; but this year the "*answers are different*."

—Dr. Albert Einstein

A note of Thank

It's my immense pleasure to express thanks to everyone allied with my three and half years' stay in the Laboratory of Biophotonics and Pharmacology. I am greatly thankful to our beloved director Prof. Yves MELY for providing me an opportunity to pursue my Ph.D under the guidance of my supervisor Dr. Pascal DIDIER. I am deeply thankful to Dr. Guy DUPORTAIL for taking care of me and all my problems, as parent, ahead of my arrival in Strasbourg in January'11. A special note of thanks to Dr. Youri ARNTZ for walking in parallel with us on every step of the project.

I would like to express my special gratitude to Dr. Pascal DIDIER for supervising my work for the entire tenure and to bear with all discussions (scientific or not) and to answer all questions (sometimes silly) of mine with smile on the corner of his lips, always. His kind nature, intelligent troubleshooting capability and forever availability with an open heart and smile were the key for the successful completion of the work.

Thanks to the President of Université de Strasbourg, Director of Ecole Doctorale, Dean of Faculté de Phamacie and all others for their concern. Furthermore, I would like to thank my jury members Prof. Isabelle NAVIZET, Dr. Thomas GUSTAVSSON and Dr. Jérémie LEONARD for accepting my request to evaluate our work. There evaluation will be having an added value to our work.

I am thankful to Dr. Julien GODET, Dr. Ludovic RICHERT, Dr. Eleonore REAL, Dr. Nicolas HUMBERT and Dr. Kamal K. SHARMA for their support to our work. Thanks to Dr. Andrey KLYMCHENKO, Dr. Frédéric PRZYBILLA, Dr. Nicolas ANTON (especially for evaluating our work during mid thesis), Dr. Halina ANTON, Dr. Christian BOUDIER, Dr. Hugues de ROCQUIGNY and other members of LBP for their loving care.

I appreciate involvement of our collaborators Prof. Lukas HINTERMANN, Dr. Panče NAUMOV, Dr. Michel SLIWA, Dr. Mateusz REBARTZ, Dr. Oleg V. MALTSEV, Dr. Jun-ichi HOTTA for their contribution to the pleasant journey of the project.

I have my thanks to Marlyse WERNERT, Ingrid BARTHEL and Ludovic FOUR for their help. Also, I thank my colleagues Hussain, Vanille, Nedal, Rémy, Waseem, Salah, Lesia, Mariana, Manu, Redouane, Rajhans and others for their kind support.

I would like to express my thanks to my friends here, in INDIA and anywhere in the world for their love, care and moral support during the hard times. Special note of thanks for Jasleen K. Bindra (especially for her continuous encouragement and concern during the tenure), Noémie, Bhaskar Mohan, Mohit, Abhineet, Pankaj & Sweta (and their little daughter Anwita), Shashi Kumar, Amita & Deepankar (Yes! the list is endless) for their kindness, motivation, moral support and for sharing their own experiences.

I would be failing on my part if I do not acknowledge the love, affection, encouragement and inspiration given by my parents, who have been behind me in all stages of my life and are the sole reason for my achievements. This work is dedicated to the sacrifices they made for me.

Last but not the least; I am thankful to Human Frontier Science Program for financially supporting our work through the project "*Excited-State Structure of the Emitter and Color-Tuning Mechanism of the Firefly Bioluminescence* (RGY-0081/2011)", Université de Strasbourg, Faculté de Pharmacie and CNRS for providing facilities and associated infrastructure to carry on the project.

Cordially, I wish to express my gratitude to all the people involved in the writing of this thesis but really sorry if I forget someone to enlist.

Mercy beaucoup à tous pour votre présence.

Avisek GHOSE

Illkirch, February 17th, 2015

“In his own time, in his own place, in what he really is and in the stage he has reached–good or bad–every human being is a specific element within the whole of the manifest divine Being. So, why be afraid of difficulties, sufferings and problems? When troubles come, try to understand the relevance of your sufferings. Adversity always presents opportunities for introspection.”

Dr. A P J Abdul Kalam, Wings of Fire (p4-5)

Table of content

Index of tables, figures, schemes and charts

Abbreviations

ATP/AMP	:	Adenosin Triphosphate/Adenosin Monophosphate
CPP	:	Cell Penetrating Peptide
cTAR	:	complementary Transactivation Response Region
ESPT	:	Excited State Proton Transfer
FCS	:	Fluorescence Correlation Spectroscopy
FLIM	:	Fluorescence Lifetime Imaging Microscopy
FRET	:	Föster Resonance Energy Transfer
HIV-1	:	Human Immunodeficiency Syndrome (Type-1)
IPTG	:	Isopropyl β-D-1-thiogalactopyranoside (CAS No. 367-93-1)
Luciferase	:	Latin *lucis-ferre* light bearer, *-ase* an enzyme
Luciferin	:	Latin *lucis*-light, *-ferre-* bearer, *-in* an organic compound
Nucleobase	:	A : Adenine C : Cytosine G : Guanine T : Thiamine
Oligonucleotide	:	Short DNA/RNA nucleobase sequences
$OxyLH_2$	:	Oxyluciferin
PDB	:	Protein Data Bank
PMT	:	Photomultiplier Tube
Protein, C-terminal	:	Carboxyl terminus with a free carboxyl group (–COOH)
Protein, N-terminal	:	Amino/Amine terminus with a free amine group ($–NH_2$)
TCSPC	:	Time Correlated Single Photon Counting
TMR	:	Tetramethyl Rhodamine
Tris	:	2-Amino-2-hydroxymethyl-propane-1,3-diol (CAS No. 77-86-1)

Chapter 01

Introduction: A Bibliographic Review

Introduction: A Bibliographic Review

The very familiar flashing lights of warm summer evenings in shaggy areas produced by fireflies are outstanding examples of bioluminescence in living organisms. The phenomenon of bio-chemi-luminescence (commonly known as *bioluminescence*) is an amazing natural process by which living organisms convert chemical energy into light. This *cold-light* emission from chemically produced excited (*chemi-excited*) state is exhibited by several organisms including certain species of bacteria, beetles, squid, worms etc.[1-4] witnessed by most of the oceans' coasts as delightful show of luminescence during summer sunsets. This extraordinary and fascinating natural phenomenon involves oxidation of photoactive substrate *Luciferin* catalyzed by an enzyme *Luciferase* in presence of Mg^{2+} and Adenosine triphosphate (ATP)[5,6] forming the emitting molecule ***Oxyluciferin***, (**$OxyLH_2$**) in its first excited state[2,10,11]. Presence of molecular oxygen in this process is mandatory to produce bioluminescence. The reaction results in production of Oxyluciferin in singlet excited state[5]. While relaxing to its ground state, **$OxyLH_2$** emits visible photons. The high fluorescence quantum yield (41.0±7.4%, Ando et al.) of this process[5] reflects not only a very efficient catalytic machinery but also, highly favorable micro-environment with strongly deactivated non-radiative pathways.

1.1 Historical review

Study on firefly bioluminescence began in 1885 with French physiologist Raphael Dubois (1849-1929), who described the reaction of Luciferin and Luciferase by observing its change of color in cold and hot water solutions[13]. He studied bioluminescence from *Coleoptera*, an Elateridae beetle, in water at different temperatures. He concluded that the bioluminescence reaction occurs in the presence of a light emitting molecule, named it as **Luciferin** (latin ***lucis***-light, ***-ferre***- bearer, ***-in*** an organic compound), and an enzyme, named it as **Luciferase** (latin ***lucis-ferre*** light bearer, ***-ase*** an enzyme). Following the work of Dubois, Newton Harvey explained the specificity among several Luciferin-Luciferase complexes by observing several bioluminescence systems involving Luciferin and different Luciferase[13]. He showed not only the specificity in the Luciferin-Luciferase system, but also he found that molecular oxygen is mandatory for all these systems to work. More advance studies on this bioluminescence system were initiated by an American biochemist William McElroy (1917-99) in 1940s. The key factor of his experiments, that improved the conclusions of Dubois and Harvey, were the involvement of Adenosine triphosphate (ATP) as an important ingredient for the reaction. In addition, he demonstrated the linear relationship between ATP concentration and the number of emitted photons by using North-American firefly *Photinus pyralis*[13]. Although his suggestive hypothesis that hydrolysis of ATP for the light emission was rejected then and there[13]. During the same time, Aurin M. measured pH dependent absorption spectra of Luciferin extracted and purified from *Cypridina* organisms[14]. Aurin showed, for the first time, spectral changes in absorption of Luciferin and oxidized Luciferin (i.e. Oxyluciferin) with time in buffer at two different

pH (5.10 and 6.80) at room temperature[14]. Several conditions that could influence the reaction mechanism of Luciferin-Luciferase (e.g. temperature, solvent pH, ATP concentration etc.) were studied by different researchers at that time but the interpretation of their results were inadequate[15]. At the beginning of 1950s, it was stated that the bioluminescence reaction is strongly dependent on four key factors: the enzyme Luciferase, the photo emitter Luciferin, molecular oxygen and ATP. In 1953, McElroy proposed a reaction mechanism which relies on the existence of two sequential steps; reaction of Luciferin, Luciferase and ATP, forming an intermediate compound (later on identified as Dioxetanone) in the first step which were then oxidized by molecular oxygen resulting in the emission of light (see scheme 1.1)[16].

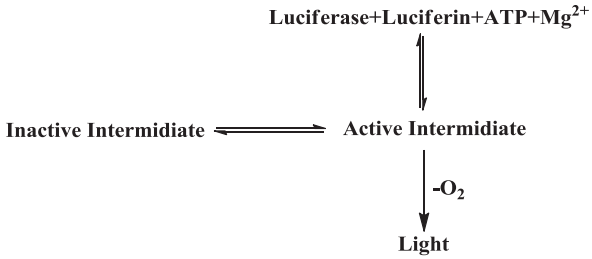

Scheme 1.1: *Reaction mechanism proposed by McElroy et al. (Adapted Form)*[16]

Afterward, 1950s and 1960s could be considered as golden era for characterization of firefly Luciferin-Luciferase bioluminescence system. During this time extensive studies on this system were conducted, mostly pioneered by McElroy. The proposed reaction hypothesis explained in scheme 1.2 came into light for the first time during this period. The production of light in firefly beetle occurs in a very dedicated organ called *Lanterns* which contains specialized photocytes, sandwiched inside a series of cells filled with uric acid crystals. These crystals of uric acid reflect the light produced by photocytes[17]. Luciferase could easily be obtained by grinding these firefly Lanterns and McElroy et al. used this technique in a very sensible way. Purification and crystallization of firefly Luciferase was reported by Green and McElroy in 1956 followed by the purification of 9 mg Luciferase obtained from grinding of 15000 firefly *Lanterns* by Bitler and McElroy in 1957[5,17]. This helped McElroy et al. to achieve partial characterization of the photo-emitter. They suggested the presence of a carboxylic acid group (which was essential for activation of ATP) on one side of the molecule and a phenol group on the other side[13]. In the same year, a very high fluorescence quantum yield (88±25%) of *P. pyralis* in aqueous buffer was measured by Seliger and McElroy[5]. In 1961, Luciferin structure with highly reactive and easily oxydizable thiazole ring came into light[18]. In late 1960's White and McElroy proposed replacement of 6'-OH group of Luciferin with amino group to obtain 6'-aminoluciferin with ~10 fold higher affinity to Luciferase[19] and a red-shifted emission spectrum[11,20-22]. They proposed six structural analogues of firefly Luciferin (see the following chart 1.1) which could be involved in the bioluminescence reaction[13,20].

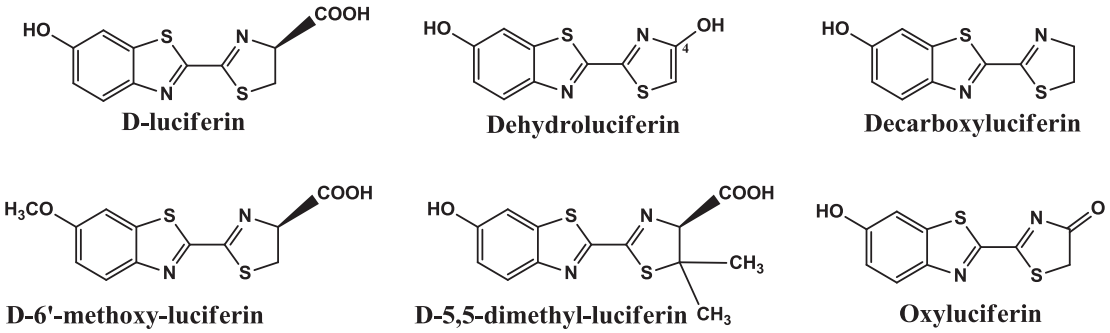

***Chart 1.1**: Analogues of Luciferin proposed by McElroy et al. (Adapted Form)*[13]

Afterwards various structural modifications were proposed by several groups resulting in an improvement in the knowledge of the optical properties of Luciferin-Luciferase complexes[19,23,24]. Theoretically and experimentally different aspects of this system were studied extensively[5,25-36], which includes reaction mechanism,[26,36-41] structural characterization of the complex,[12,37,42,43] change in luminescence spectra of the complex due to alteration in the environment,[5,30,31,37,40,43,44] effect on luminescence due to the structural modification of the photo-emitter,[23,45-47] Excited State Proton Transfer (ESPT) mechanism[6,31,48-51] etc.

With time, behavior of looking in this amazing system developed stepwise. Structure of the Luciferase and its complex with Luciferin has been studied by different researchers globally. The exact structural atlas and the active site of the enzyme had already been predicted. The effect of structural modifications either or both of Luciferin and Luciferase on the bioluminescence spectra has been interpreted extensively to decipher the exact bioluminescence phenomenon[7,52-57]. Computational[33,36] and experimental approaches have been employed in these studies and the effect of these structural modifications on bioluminescence and biological activity of the enzyme complex were explained in detail[20,24,58-63].

In the meantime, another key issue associated with this system; *in-vivo* bio-imaging using Luciferin-Luciferase bioluminescence came into light. Different approaches have been employed to apply this system as an imaging tool either by conjugating Luciferin with distinct functional groups or by monitoring the *in-vivo* enzyme activity. Strategically modified different analogues of this system have been employed to perform *in-vivo* bio-imaging[3,19,64-69].

During the last decade, extensive studies on Oxyluciferin structure either free or bound to Luciferase were performed. Different parameters associated with Luciferin-Luciferase system drew enormous attention in order to reveal the exact photophysical properties of Luciferin-Luciferase complex. Recently, Naumov et al. proposed several structural modifications especially with methyl derivatives of the photo-emitter and they studied the light color modulation as a function of polarity with different solvents ranging from organic to aqueous[4]. In 2009, Naumov et al. proposed a scheme that displays absorption and emission of different analogues of Oxyluciferin in different solvents (DMSO, MeOH, H_2O etc.). This representation was based on the previous experimental

and theoretical studies of Oxyluciferin in different solvents (See figure 1.1). Further, the crystal structure, reaction mechanisms, keto-enol tautomerization between different chemical forms etc. have been studied mainly spectroscopically during this time[12,43,70,71].

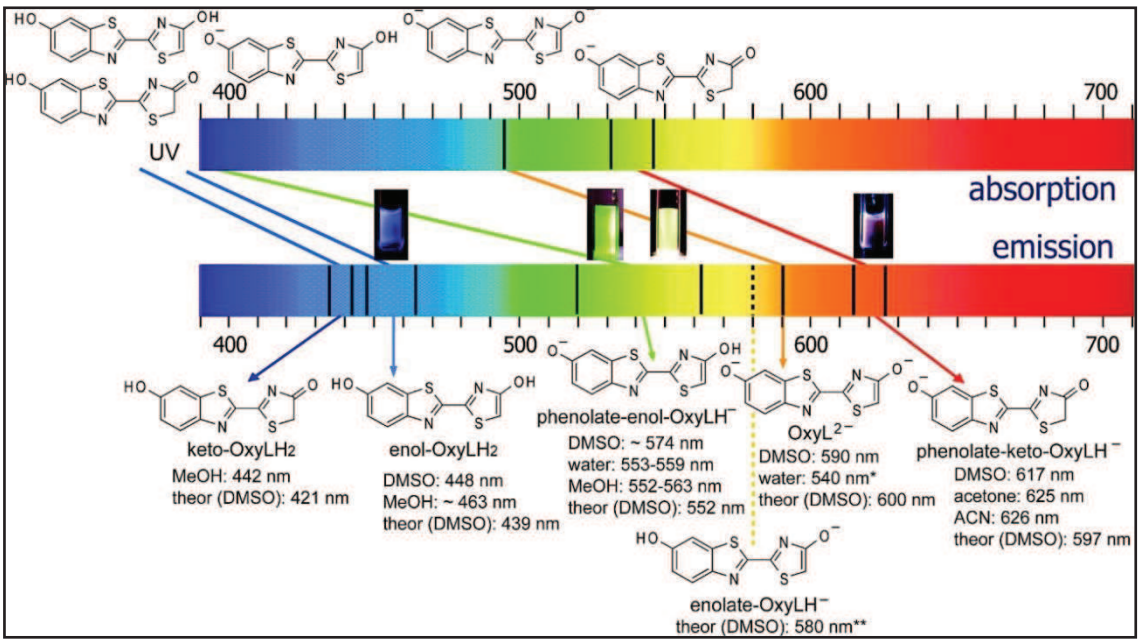

***Figure 1.1**: Absorption and emission color of different Oxyluciferin analogues in different solvents (Naumov et al. Reprinted with permission)[4]*

1.2 The reaction chemistry

The multi-step catalytic reaction, leading to bioluminescence[7,54,55] (scheme 1.2 and 1.3) involves formation of a ternary complex of the substrate Luciferin, enzyme Luciferase and ATP in the first step. In the next step, an acidic anhydride between carboxylic group and Adenosin monophosphate (AMP) are formed by the exclusion of H^+ from 4C-thiazole that creates Pyrophosphate (PPi) as a side product. Later on, through several intermediate steps this anhydride is oxidized by molecular oxygen, producing cyclic peroxide and Dioxetanone. During this intermediate process, radical recombination and annihilation result in the cleavage of covalent bonds leading to the formation of Dioxetanone; a highly unstable compound[72-74]. Decarboxylation of peroxide results in the formation of Oxyluciferin in its electronically first singlet excited state[7,52]. The formation together with the decomposition of Dioxetanone lead to an efficient *chemi-excitation* resulting in the formation of Oxyluciferin in the first excited state[72,73]. This reaction requires high energy (>7kCal/mol), therefore, involvement of molecular oxygen is mandatory in this process. Keto-Oxyluciferin is then rapidly transformed to its enol tautomer by proton removal from 5C-thiazole[52]. De-excitation of excited Oxyluciferin results in the emission of visible light (yellow-green-red) commonly known as firefly bioluminescence. With its high fluorescence quantum yield[5] and exceptionally high signal-to-noise ratio due to the absence of *photo-excitation*, the firefly bioluminescence stands out to be a good candidate of choice for bio-imaging applications[19,39,53,64,75-78].

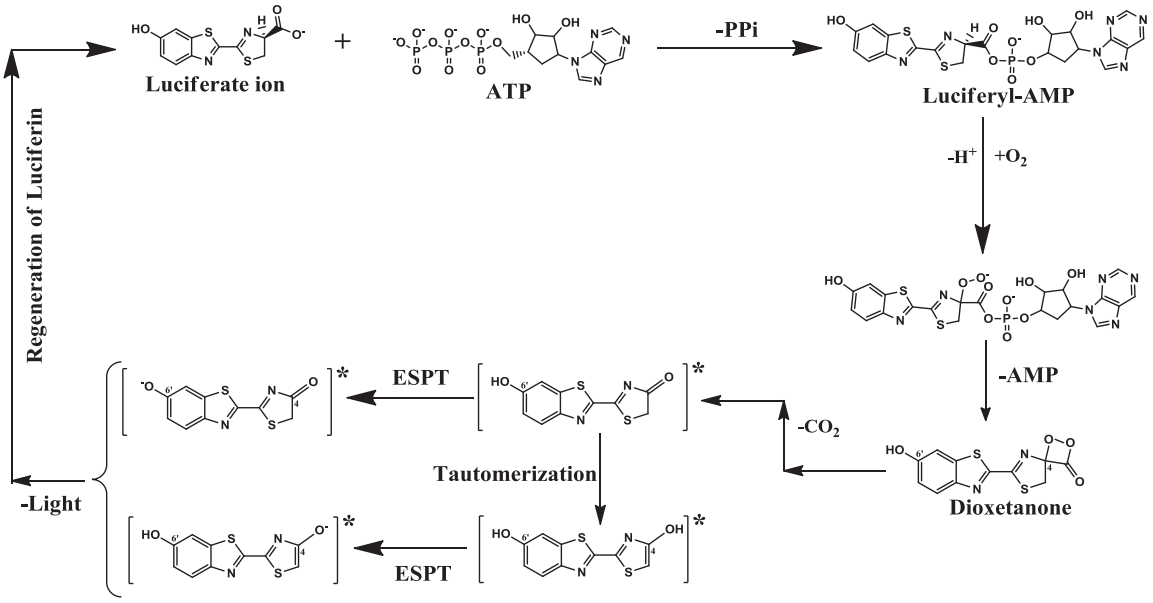

***Scheme 1.2**: Proposed reaction mechanism of firefly bioluminescence and thermal decomposition of Dioxetanone to chemi-excited firefly Oxyluciferin and possible de-excitation pathway of the emitter*[4,48,70]

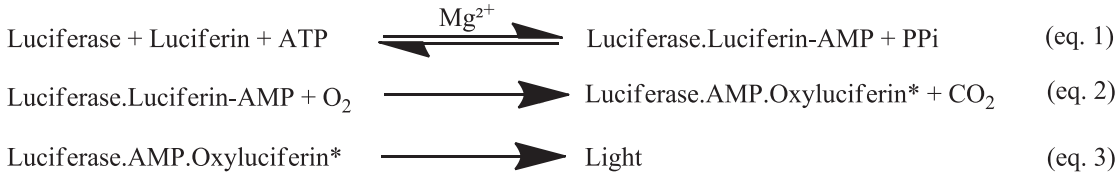

***Scheme 1.3**: Simplified reaction mechanism of firefly bioluminescence*

1.3 The enzymatic regeneration of Oxyluciferin into Luciferin

The enzymatic regeneration of Luciferin from Oxyluciferin may occur through a hypothetical pathway in which Oxyluciferin acts as the substrate of Luciferin for the next cycle[6 79]. This is a two-step process which involves i. transformation of Oxyluciferin into 2-cyano-6-hydroxybenzothiazole and ii. condensation of 2-cyano-6-hydroxybenzothiazole with d-Cysteine to produce Luciferin[79,80]. Gomi et al. indicated that the first process is catalyzed by Luciferin Regenerating Enzyme (LRE)[79]. Active involvement of LRE during the conversion of Oxyluciferin into 2-cyano-6-hydroxybenzothiazole has been proposed by Gomi et al. During a later step, 2-cyano-6-hydroxybenzothiazole is non-enzymatically converted into Luciferin by d-Cysteine. LRE catalyzes the reaction, although the conversion of Oxyluciferin into Luciferin may be completely a non-enzymatic process[79,80]. Strong inhibitory effect of Oxyluciferin on Luciferase over Luciferin is overcome by the involvement of LRE which results rapid turnover of Luciferase for the next light emission cycle[80].

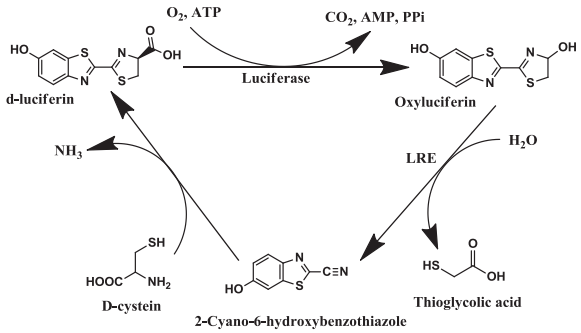

***Scheme 1.4**: Regeneration of Luciferin from Oxyluciferin (Adapted Form)*[66,79]

1.4 The photophysics of firefly bioluminescence

The reaction chemistry and the structure of the photo emitter for all known beetle Luciferase are identical. There are almost 20 Luciferase complexes that can be found in nature, however their luminescence color can vary from yellow to red (536 to 638 nm)[1,26]. One of the key factors on which this variation in the emission wavelength strongly depends is the pH of the solvent[52]. The photo-emitter (the final product) of this bioluminescence system is considered as a good fluorophore as it has distinct spectral properties and strong micro-environment and polarity dependent fluorescence emission[26]. Despite of being indispensable to the development of a new bio-analytical tool, the chemical origin of the color modulation of this molecule remains poorly understood, so far. The photophysical mechanism associated with this bioluminescent system is still a highly debated question. According to several highly argued photophysical processes, the color modulation is likely to occur as an effect of several intramolecular and/or intermolecular factors within the enzyme[81]. The spectral shift observed results from changes in the polarizability and structure of the photo-emitter microenvironment in the enzyme pocket[52]. The photo-emitter, Oxyluciferin, is generated by the decomposition of the highly unstable intermediate compound Dioxetanone with a release of CO_2 (see scheme 1.2). Isolation of this highly unstable species has not been achieved yet. This is the main reason that most of the spectroscopic studies were performed by photo-exciting either **$OxyLH_2$** alone or its complex with the enzyme in solution[82].

A critical limitation of utilization of other chemi-luminescence reactions for analytical applications is their low fluorescence quantum yield, in general ranging from 3 to 5% and very rarely up to 10%[43]. Firefly bioluminescence is the most well-known photo emitter system in biophotonics, particularly known for its extremely high fluorescence quantum yield[5] due to better ability for efficient conversion of chemical energy into light. This process provides exceptionally high signal-to-noise ratio, making it the right candidate for sensitive bio-imaging applications[32]. In recent advancement, it has been demonstrated how strongly acidity can effect spectral properties of the natural Oxyluciferin. Ando et al. showed the effect of pH on the quantum yield of the firefly bioluminescence. They also confirmed the strong effect of pH on the reaction rate kinetics[5,6]. The observed bioluminescence was centered at 560, 620 and 670 nm (shoulder) which originate from different species of the photo-emitter inside the complex

for the pH range 6.4-8.5. According to Ando et al. the intensity of the spectra centered at 560 nm is strongly pH dependent while other two are less sensitive to pH[5,6]. During our studies, we also performed similar experiments and our results are very close to the results of Ando et al. (explained in the section 4.1).

Despite of having significant importance as a bio-analytical tool, a few key aspects of this amazing bioluminescent system have been a subject of disagreement and hypothetical assumption for a long occasion without any direct experimental evidence of excited state structure. One of the main unresolved issues is the molecular origin of the natural or point-mutated emission. The properties of the excited state structure of the firefly emitter is critically important for explaining the key events of firefly luminescence[71]. Considering immense importance of this compound for various bio-analytical applications, which includes probing of the local pH *in-vivo* or *in-vitro*, it is essential to elucidate a set of accurate and reliable pH profile of this compound.

Even though the complex chemistry of **$OxyLH_2$** has spurred extensive experimental[3,5,7,37,44,46,58,82-91] and theoretical[5,25-29,33-35,47,51,90,92-96] studies, the photophysics of this natural photo-emitter remains poorly understood so far. One of the obstacles to complete the understanding of the de-excitation processes is the limited information about the excited-state dynamics of the emitter in aqueous solutions. It can exist in six different chemical forms as a result of ionization of two hydroxyl groups and the keto-enol tautomerism of the 4-thiazolone subunit (see chart 1.2).

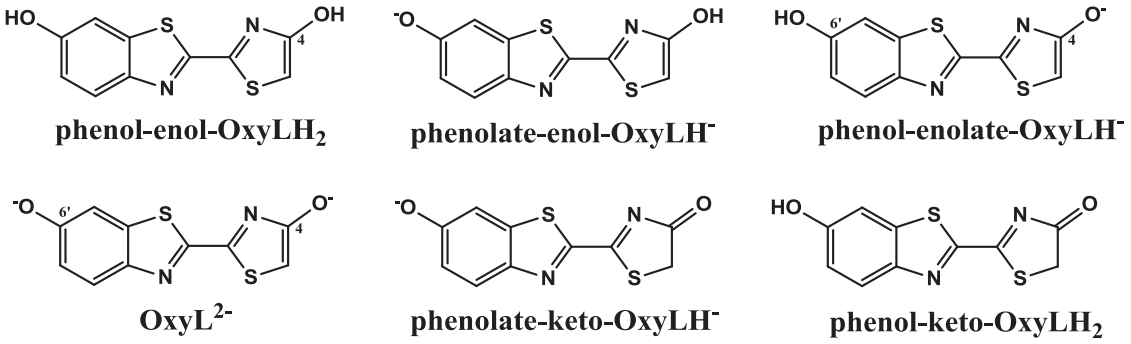

***Chart 1.2**: Possible ground-state chemical forms of firefly Oxyluciferin in aqueous solutions[48]*

The intricate triple dynamic chemical equilibrium in solution is strongly affected by the solvent, pH and specific interactions with bases[9,42,43,70,97]. Experimental[98] and theoretical[99] studies of the firefly Luciferin (the reaction precursor) have shown that the photoluminescence pathways of this closely related molecule are strongly dependent on the solution pH and the excitation wavelength. Moreover, when in complex with Luciferase enzyme, the spectral properties of each chemical forms can additionally be affected by the nature of the active site such as polarity, presence of additional ions and л-л stacking[12,43,48,100]. The variations in bioluminescence spectra results from *keto-enol* tautomerization of Oxyluciferin at different solvent pH is strongly dependent on the location of the alkyl group in proximity to the highly reactive thiazole group of Luciferin[26]. Interaction between enol hydroxyl group and the alkyl group at far proximity of thiazole ring results in formation of an enolate ion, which in turn confirmed by the blue

shift of the emission spectra. But with protonation of solvent, red shift in luminescence occurs which confirms formation of the keto form of Luciferin. In transitional pH (6.5-7.0), both keto and enol forms can be observed, which can likely explain the non-symmetric luminescence for a number of cases[26]. In this natural chemi-luminescent system light is obtained from several electronically excited species rather than from a single one[26]. It can be believed that different emission color at different protonation level (or pH) corresponds to different excited states of the Oxyluciferin molecule in the Luciferin-Luciferase complex[6].

Structural basis for pH sensitivity of Oxyluciferin is the presence of its basic residue, which assists excited Oxyluciferin to undergo tautomerization in the active site (scheme 1.2 and chart 1.2). This hypothesis was originally proposed to explain green (enol & enolate forms) and red (keto form) emission of firefly Luciferin-Luciferase complex[22]. The phenolate-keto species have been considered as the most possible form for the emitting state[33,46,95]. pH sensitivity can be directly related to interacting residues forming a secured active site, enhancing green emission. Also, it can be predicted that pH sensitivity is related to higher active site flexibility, resulting in the production of two different emitters or is related to higher rigidity, allowing the production of single emitter. However, this phenomenon of structural origin of pH sensitivity is still not understood accurately[37]. In addition, contemporary research outcome with di-methyloxyluciferin, whose structure prevents it to undergo tautomerization, indicates that the tautomerization hypothesis is not the only reaction mechanism for green and red bioluminescence[37,46]. Recent studies have shown that the enol tautomer should be considered as emitting species that is generated in the excited state[43,53,71]. In recent time, Excited State Proton Transfer (ESPT) of this system, from either or both hydroxyl groups (scheme 1.2), have been investigated by ultrafast spectroscopic techniques[30,31,71].

1.5 Color tuning mechanism of firefly Luciferin-Luciferase bioluminescence system

Firefly Luciferase, a ~62 kDa protein consists of 542-552 amino acid (AA) residues, catalyzes the bioluminescence reaction by oxidizing the photo-substrate firefly Luciferin in the presence of ATP, Mg^{2+} and molecular oxygen. The reaction proceeds through the activation of Luciferin to form Diaoxetanone, followed by the formation of the final product Oxyluciferin[56]. The enzyme crystallographic studies confirmed that Luciferase has a large N-terminal domain (AA residue 1-436) and a small C-terminal (AA residue 440-550) domain linked through a flexible peptide which creates a wide cleft between these two domains[66,101]. The C-terminal contains Serine-Leucine-Lysine (SLK) motif, which is responsible for peroxisome targeting. The enzyme active site is believed to include the amino acids on the surface of both domains. During the course of reaction significant conformational changes in the enzyme occurs during which both N and C domain come close to each other and cluster the photo-substrate in between them. Majority of the amino acids which play vital roles in the bioluminescence reaction are on the N-terminal domain while only one (Lys529)[101] is on the C-terminal domain[66,101]. A

hydrophobic pocket is created in the enzyme which encapsulates the substrate Luciferin inside it. This hydrophobic pocket enables Luciferase to adopt a « closed form » during the formation of the intermediate compound i.e. Dioxetanone and an « open form » in complex with the photo product Oxyluciferin[66].

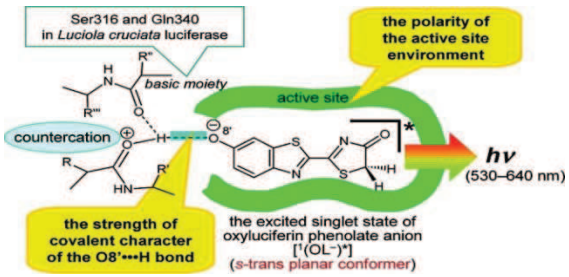

***Figure 1.2**: Schematic representation of firefly bioluminescence mechanism proposed by Hirano et al. (Reprinted with permission)[12]*

The chemistry of the reaction and structure of the substrate and the enzyme is identical for all known beetle Luciferase enzymes isolated from different insects, only the color of bioluminescence is different which is likely associated with the acidification of the reaction mixture i.e. *in-vivo* pH, properties of the enzyme and microenvironment of the emitter in the active site of the enzyme[52]. Several mechanisms have been proposed so far to explain this complex firefly bioluminescence system. Color of the bioluminescence differs in different Luciferase-Luciferin complex; e.g. firefly (Family Lampyridae) emits yellow-green light (540-580 nm), click-beetles (Family Elateridae) emits green to orange (546-560-578-593 nm)[54] and railroad worms (Family Phenogodidae) emits green-red (536-638 nm)[52,54].

Luciferase is a pH sensitive enzyme. In basic media, pH > 7.5, the typical bioluminescence is yellow-green (550-570 nm) centered at 562 nm. However in acidic media, pH ~5-6, this bioluminescence shifts to red with a centre around 620 nm[5,66] (see section 4.1). Ando et al. saw a shoulder around 670 nm as well in their pH dependent study of firefly bioluminescence[5]. White et al. proposed that this spectral shift (or the color modulation) results due change in the polarity at the binding site in Luciferase[102] together with the conformational changes which influence the active site microenvironment. Presence of heavy metal cation and temperature of the microenvironment can also be factors which affect the color of the bioluminescence[66]. Ando et al. concluded that most of the color determination models for firefly bioluminescence systems have two alternative chemical states of excited Oxyluciferin inside the Luciferase active site. The yellow-green emission at higher pH and red emission at low pH correspond to these two states of Oxyluciferin. The equilibrium between keto and enol forms, states of Oxyluciferin in the active pocket of the fluorophore-protein complex, the rotation of the thiazolone fragment around the C2-C2' single bond of Oxyluciferin and most importantly the structural basis of Luciferase are the controlling platform for these two states[5]. An amino acid residue at close proximity to the emitter could react as a base with C5 proton of Oxyluciferin which results in the yellow-green emission of the enol form. But at lower pH (5-6), protonation of this amino

acid residue and the C5 proton of Oxyluciferin become impossible which leads to red colored emission from the keto form. In the intermediate pH region superposition of these two forms can be observed[54].

Excited Oxyluciferin enclosed in the Luciferase active site can exist in two stereo conformations with different energy levels. These stereo conformations result from the rotation of benzothiazole and thiazole rings around the C2-C2' bond. This 90° rotation likely plays an important role in the color tuning of firefly bioluminescence. As per the hypothesis provided by MacCapra et al. this rotation is associated with an intramolecular charge transfer[54]. The energy and color of the emission is dependent on the degree of the rotation. At 90°, the energy is minimum, resulting red colored emission, but the alteration in the microenvironment and more restricted conformation can lead to a rotation with an angle lower than 90°; higher energy thus leads to blue shift in the emission spectra. Temperature and pH also play a role in this isomerization mechanism. Although this hypothesis is quite convincing, it has some drawbacks as it cannot explain green emission from enol-Oxyluciferin[54,103].

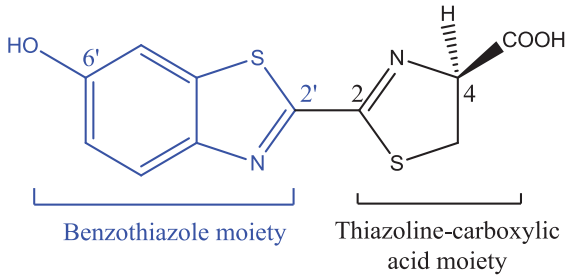

***Scheme 1.5**: Two principle moieties of firefly Luciferin[66]*

Mutation in the amino acid sequence of Luciferase can also affect the color tuning mechanism of firefly bioluminescence[103]. Analysis of bioluminescence from several recombinant Luciferase mutants has shown that modification of the amino acid sequence also results into the red shift of the spectra. Two groups of such amino acids are: (Arg232Glu, Leu238Val) and (Ser247Gly, Asp352Val, Ser358Thr)[54,104]. A review work by Ugarova et al. explains nicely the effect of amino acid mutation on the firefly bioluminescence spectra[54].

Hirano et al. predicted the mechanism of the in vivo bioluminescence color tuning of Luciferase from of *P. pyralis*, *L. cruciata*, and *P. hirtus.* In particular, it depends on the polarities of their active-site environments and the bonding characteristics of the interactions between excited singlet state of phenolate anion and protonated basic moieties. The potential basic moiety consists of multiple amide carbonyls in the luciferase active site. A stronger acidity of the protonated basic moiety, leads to expansion of the color range of bioluminescence. They also found that *L. cruciata* Luciferase active site has a nonpolar character and that the amide carbonyls of Ser316 and Gln340 play an important role as basic moieties. Hirano et al. assumed that the structure of excited phenolate anion for the firefly bioluminescence may have an s-trans planar conformer (see figure 1.2).

1.6 Oxyluciferin as a bio-analytical probe

Being a non-invasive technique, fluorescence emission has been considered to be an ideal tool for monitoring biomolecular interactions *in-vivo* or *in-vitro*. Fluorescence technique has been applied to visualize, measure and characterize biological process of interest at the molecular and/or cellular level[65]. Fluorescent labeling, staining and quenching, while combined with appropriate instrumentations, is a very sensitive and quantitative method that is widely used in molecular biology to understand biomolecular interactions. Its ability to non-invasively monitor the biological activity of the subject promotes it to be a powerful and widely used tool for basic and transitional biological, medical and clinical diagnostic and research purposes.

Transition of the photo-product Oxyluciferin to the ground state is accompanied by the emission of visible light[48,65,74,105]. Because of its better ability to convert chemical energy into light and exceptionally high signal-to-noise ratio, (therefore, having very high fluorescence quantum yield, 41.0±7.4%, Ando et al.),[44,48] Oxyluciferin is well appreciated for sensitive *in-vivo* bio-imaging applications[32], overcoming a major limitation of conventional chemi-luminescence reaction for analytical applications; low fluorescence quantum yield (in general ranging between 3-5% and very rarely up to 10%)[43].

A classical characteristic of fluorescence emission, ESPT, has attracted much attention in last decades due to its application as an environment sensitive probe. The most remarkable photophysical property that is associated with the ESPT is large Stokes Shift compared to the conventional fluorophores e.g. BODIPY, Fluorescein, Rhodamine etc. This large Stokes Shift is desirable to avoid inner-filter effect and self-absorption of the fluorophore[51].

Application of the Luciferin-Luciferase bioluminescence mechanism to visualize and characterize biological/biomolecular activities is not a new technique. Several evidences[19,67-69,106-110] could be found where this specific mechanism has been employed as a fluorescence tool to understand different biomolecular interactions.

In-vivo or *in-vitro* biomolecular imaging was found to be the most ideal technique to obtain molecular and/or cellular information of a target of interest within the host environment. This can provide a better understanding about the molecular basis of the biology. In last decades a continuous progress in the development of new molecular imaging probe could be observed. Large signal amplification from enzyme activities, optical, magnetic resonance and nuclear imaging modalities have been the prime attractions for *in-vivo* or *in-vitro* biological imaging[110]. Characterization of different *in-vivo/in-cellulo* events by observing the photophysical properties of the fluorophore distributed within the subject of interest has great and significant advantages.

Monitoring site specific biomolecular interactions involves either fluorescence quenching technique or FRET measurements. Although FRET is an outstanding mechanism which allows measuring of inter-molecular distances between a pair of fluorophores, the subject of interest needs to be doubly labeled by two adequate

fluorophores. Therefore, single label fluorescence monitoring technique is commonly preferred. In particular, environment sensitive or solvatochromic fluorophore is employed and change in its fluorescence properties can be used to monitor interaction between different biomolecules (e.g. DNA, RNA, protein, peptide etc.). Solvatochromic fluorophores become more promising day by day. Indeed, this property is strongly dependent on the micro-environment of the labeled site and the variation in the emission profile can be correlated with the conformational changes which occur in the complex. For instance, it is possible to monitor interaction between DNA and protein/peptide in different environmental conditions using solvatochromic dyes. One of the classic examples is to monitor interaction between HIV-1 NCp7 or Tat and different DNA/RNA sequences by labeling either one with a solvatochromic fluorophore. Previously reported works and their reviews suggested that different structural properties of HIV-1 NCp7 and/or Tat and their involvement during viral life cycle can be monitored by observing their *in-vitro* interaction with DNA/RNA[105,111-120].

Oxyluciferin is a micro-environment sensitive fluorophore. Thus the fluorescence emission properties of Oxyluciferin and its structural analogues can be used to understand biological events. However, for further applications, its optical properties need to be deciphered in physiologically relevant conditions.

An Overview

An Overview of the Work

During the last decade, understanding of this bioluminescence process is experiencing a growing interest due to the increasing number of applications especially in the field of biological analysis including *in-vivo/in-vitro* imaging, characterization of biomolecular interaction etc. One of the obstacles to complete the understanding of the de-excitation processes of this molecule is limited information about its excited-state dynamics in aqueous solutions. Despite of extensive experimental and theoretical knowledge of this complex chemical reaction, the photophysics of **$OxyLH_2$** still remains poorly understood, so far. Depending upon conditions, **$OxyLH_2$** can exist in six different chemical forms as a result of ionization of both hydroxyl groups and the keto-enol tautomerism of the thiazole subunit. This complex triple dynamic chemical equilibrium in aqueous solution is strongly affected by the nature of the solvent, pH and specific interactions with bases. Moreover, when in complex with the enzyme luciferase, spectral properties of each chemical form of **$OxyLH_2$** can additionally be affected by the nature of the active site such as polarity, presence of additional ions and л-л stacking. According to the recent developments, it has been shown that not only the **phenolate-keto** species generated in the excited state, but also its enol tautomer is a possible form contributing to the fluorescence emission. It includes possible excited-state proton transfer (ESPT) from either or both of the hydroxyl groups. In addition, previous studies of firefly Luciferin (the reaction precursor) have shown that the photoluminescence pathway of the molecule strongly depend on various conditions including solution pH and the excitation wavelength.

This thesis work is a part of the project entitled "*Excited-State Structure of the Emitter and Color-Tuning Mechanism of the Firefly Bioluminescence*" (RGY-0081/2011) financially supported by **Human Frontier Science Program** (HFSP). Four collaborators are involved in this project: i) Prof. Lukas HINTERMANN, Dept. of Chemistry, University of Munich, GERMANY; ii) Dr. Panče NAUMOV, New York University, ABU DHABI; iii) Dr. Pascal DIDIER, University of Strasbourg, FRANCE and iv) Dr. Michel SLIWA, University of Lille, FRANCE. All collaborators play different roles. Briefly saying, different structural analogues of Oxyluciferin were synthesized by the group of Prof. HINTERMANN and their crystallographic structural studies were performed by the team of Dr. NAUMOV. Photophysical profile and their biological applications have been studied by us in Laboratory of Biophotonics and Pharmacology under supervision of Dr. DIDIER. In Lille, Dr. SLIWA and his team studied IR spectroscopic profile of those derivatives.

The first objective of the thesis was to identify the different forms of the **$OxyLH_2$** responsible for the color tuning of the fluorescence emission in aqueous solutions ranging from blue to red (445-637 nm). Also, it was important to understand the ESPT mechanism involved in this process to provide a model mechanism which can explain the de-excitation processes of **$OxyLH_2$** in aqueous solutions.

To understand the exact emission mechanism of **$OxyLH_2$**, Prof. Lukas HINTERMANN chemically synthesized different analogues of **$OxyLH_2$** where different

–H atoms are replaced by $–CH_3$, so that they can be prevented from undergoing any protonation/deprotonation (chemical) reactions in aqueous solutions (see the chart below). Different experimental procedures involving steady state and time resolved fluorescence spectroscopy techniques have been employed to decipher the optical properties of these structurally modified derivatives. Absorption, emission spectra and excited state fluorescence lifetime of different analogues of **$OxyLH_2$** have been recorded at different experimental conditions in aqueous solution at different pH.

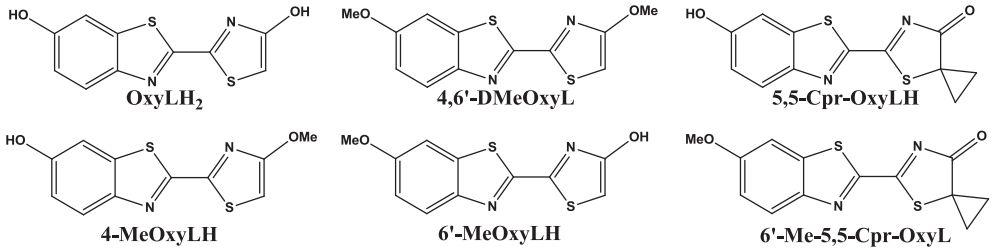

*Chemical structures of **$OxyLH_2$** and its structural analogues used in this study*

The steady-state and time-resolved emission experiments, performed in aqueous buffered solutions within a physiologically relevant pH range, provided for the first time the individual absorption and emission spectra of all neutral, tautomeric and anionic variants of **$OxyLH_2$** as well as the ground state and excited state equilibrium constants. In addition, the rate constants of the fundamental photoreaction processes were also determined. With these pH dependent fluorescence emission and time resolved results, we proposed a model of photoluminescence pathway of **$OxyLH_2$** in aqueous solutions. These results have already been communicated to ACS Journal of Physical Chemistry B and the article has been accepted for publication.

In the second step, we have produced and purified the enzyme Luciferase (expressed in *E. coli* bacteria and purified by FPLC technique) in order to study the photophysical properties of $OxyLH_2$-Luciferase complex in aqueous buffer at different pH. Different analogues of Oxyluciferin in complex with Luciferase have been studied (by mimicking the natural Oxyluciferin-Luciferase complex) to unravel the photodynamics of the natural complex. We first determined the best suitable concentration ratio of Oxyluciferin to Luciferase by using fluorescence anisotropy. Next, we employed steady state fluorescence spectroscopy and time resolved fluorescence spectroscopy by selectively exciting each chemical forms of Oxyluciferin to study different parameters of the Oxyluciferin-Luciferase complex for different experimental conditions. From the spectral and time resolved results we could interpret the effect of the local environment on the optical properties of the Oxyluciferin within the protein pocket.

From the observations of photophysical parameters of Oxyluciferin-Luciferase complex in aqueous buffers and by comparing them with unbound Oxyluciferin in aqueous buffer, we could decipher the spectral behaviour and photodynamics of each chemical from of the photo-emitter when in complex with the enzyme. ESPT mechanism involved in this process could also be described from these results. The exact excited state structure of the photo emitter in natural conditions and factors that affect the color

modulation mechanism of this bioluminescence mechanism can now be explained with a great extent with these results.

In the last part of our work, **$OxyLH_2$** and its two structural analogues; **4-MeOxyLH** and **4,6'-DMeOxyL** (see above chart) were selected to demonstrate the potential ability of using Oxyluciferin derivatives for suitable bio-analytical experiments. These derivatives were further chemically modified and coupled to HIV-1 peptides Tat(44-61) and/or NCp7(11-55) by solid phase synthesis method. Different analytical approaches were employed to use the optical properties of **$OxyLH_2$** derivatives to monitor biomolecular interaction *in cell* or *in vitro*. These experimental approaches involves Fluorescence Lifetime Imaging Microscopy (FLIM) with HeLa cells incubated with HIV-1 Tat peptide labeled with Oxyluciferin, steady state and fluorescence time-resolved study of fluorescence quenching of HIV-1 NCp7 labeled with **4-MeOxyLH** in complex with different oligonucleotide sequences at different concentrations.

Fluorescence Lifetime Imaging Microscopy (FLIM) is an imaging technique in which fluorescence decay of a fluorophore is measured for constructing an image which represents a map of fluorescence lifetime in the form of an image. From the FLIM experiments we have observed different distribution pattern of excited state fluorescence lifetime for different Oxyluciferin derivatives responding to the heterogeneous pH environment inside the cytoplasm of HeLa cells. **$OxyLH_2$**, that displays pH dependent fluorescence lifetime, shows a broader lifetime distribution histogram inside the HeLa cell, while narrower distribution could be observed with the cells incubated with Tat peptide labeled with **4,6'-DMeOxyL**. Results obtained in these FLIM experiments proved that Oxyluciferin can be used as an analytical tool for bio-imaging purposes to recognize and to monitor small variation of the intracellular pH.

In parallel, we labeled HIV-1 NCp-7(11-55) with **4-MeOxyLH** and observed its fluorescence quenching in presence of different single-strand and stem-loop oligonucleotide sequences. We measured fluorescence anisotropy by titrating labeled peptide with increasing concentration of oligonucleotide in physiological pH. Fluorescence anisotropy and Neutral/Anionic (N*/A*) emission ratio calculated from dual emission of **4-MeOxyLH** coupled to NCp7 for these different complexes were used to obtain the dissociation constant for these complexes. Our results have been further validated by the time resolved fluorescence spectroscopy data. These results show that the particular optical properties of **4-MeOxyLH** can be used to monitor biomolecular interactions. The results obtained from these experiments are in complete agreement with the fact that the firefly emitter is an appropriate bio-analytical tool for studying and to monitor biomolecular interactions *in-vivo* or *in-vitro*.

To stabilize a specific chemical form of the of **$OxyLH_2$** (keto form), **5,5-Cpr-OxyLH** (see above figure) was synthesized in order to perform fluorescence labeling of protein. This compound displays the ability to specifically react with Cysteine (Cys) residue in basic condition. Without any Cys residue in the solution, **5,5-Cpr-OxyLH** has an emission spectra centered at 637 nm. But in presence of Cysteine, the emission maximum is significantly blue shifted (about 70 nm). We postulated that in presence of

thiol of Cys, the spiro-cycle ring at C5 thiazole opens and =O reacts with the thiol group of Cys and as a result, tautomerization likely occurs. As a result, emission originates from the enol form of Oxyluciferin and blue shift of the spectra is observed. Amine and thiol groups are widely distributed in biomolecules. Compared to other non-specific amine-labeling techniques for large biomolecules, thiol (or Cys) labeling strategies are more prominent. About 88% of all proteins have at least one Cys residue. Different favorable strategies also encourage fluorescent label using Cys as a promising bio-analytical tool. **5,5-Cpr-OxyLH** derivative was used to label human *Alpha-1 Antitrypsin* (α1-AT), the protease inhibitor (412 amino acid long protein) where a solvent accessible Cys232 residue is available. A significant change has been recorded in emission spectra (~75 nm) before and after the labeling has been done. After the completion of the labeling procedure and purification, fluorescence quenching of the labeled α1-AT with increasing concentration of Procine Pancreatic Elastase (PPE) has been studied. In presence of PPE fluorescence quenching of labeled α1-AT has been observed confirming the biological integrity of the protein in physiological buffer.

The results obtained in these experiments are currently integrated in other manuscripts which will be submitted shortly.

In summary;

i. we deciphered different chemical forms of Oxyluciferin involved in the color tuning mechanism of firefly bioluminescence by studying photodynamics of its different analogues in aqueous buffers.

ii. we proposed a photoluminescence pathway of Oxyluciferin in aqueous buffer.

iii. we did an interpretation that the exact excited state structure of the photo emitter in natural conditions in complex with the enzyme Luciferase and ESPT involved in this color tuning mechanism of firefly bioluminescence.

iv. we showed that Oxyluciferin can be used as a promising bio-analytical tool specially to monitor biomolecular interactions *in-vivo* or *in-vitro*.

Chapter 02

Materials and Methods

Materials and Methods

2.1 Synthesis and ^{1}HNMR study of Oxyluciferin derivatives

Structurally modified analogues of Oxyluciferin derivatives have been synthesized by the group of our project collaborator Prof. Lukas HINTERMANN at Department of Chemistry, Technical University of Munich, GERMANY. Synthesis method and ^{1}HNMR study of most of these derivatives discussed herein have already been published[9,48,97] and remaining of them will be reported separately in shortly coming communications.

2.2 Sample preparation

Stock solutions of all Oxyluciferin derivatives were prepared by dissolving them in spectroscopic grade DMSO (CAS No. 67-68-5 purchased from Sigma-Aldrich). To maintain minimum freeze-thaw cycle, stock solutions of Oxyluciferin were stored in several aliquots of 20 µl at -20°C temperature. For spectral measurements, they were further diluted about 500 folds to final concentrations of about a few micromolar in aqueous buffers with different pH in 10 mm path length quartz cuvette purchased from Hellma Analytics. Aqueous buffer solutions used in this study were prepared as follows: 75mM NaCl/20mM KH_2PO_4/0.2mM $MgCl_2$ for pH $\leq$ 7.0 and 75mM NaCl/25mM Tris/0.2mM $MgCl_2$ for pH > 7.0 (unless mentioned specifically). The aqueous buffered solutions were prepared by diluting their 1M stock solutions in de-ionized water (18.2 MΩ) purified by Millipore system. The buffer solutions were separated into several fractions and their pH (error ±0.02) was adjusted by 250mM HCl or by 250mM NaOH at 20°C (ΔpH ≈0.25). For all spectral measurements separate buffers at different pH were used.

2.3 Steady-state spectroscopic measurements

Absorption spectra were measured by using a dual beam Cary-4000 (Agilent Technologies) spectrometer, equipped with thermostated sample holder, at the rate of 100 nm/min with a PMT detector. Signal was recorded after correcting their baseline factor (against the same buffer) and optical density was plotted as a function of wavelength. For fluorescence spectra, same Oxyluciferin concentration as for absorption spectra was used and collected at the rate of 150 nm/min by the detector, photomultiplier tube of Fluorolog or Fluoromax, Jobin Yvon, equipped with a Peltier thermostated sample holder, with 2 to 3 nm of excitation and emission slits. Fluorescence signal obtained has been corrected from the instrument's response characteristics to avoid potentially misleading trace and finally have been plotted as a function of wavelength. Emission spectra were collected at different excitation wavelengths by eliminating contribution from Raman and Rayleigh scatterings. Similarly, excitation spectra have been recorded by observing fluorescence from different emission maxima (data not shown). While observing time dependent fluorescence emission, excitation and emission

wavelength have been fixed at the point of interest with 2-3 nm excitation and emission slits.

Absolute fluorescence quantum yield of **4,6′-DMeOxyL**, **4-MeOxyLH** and **5,5-Cpr-OxyLH** have been measured independently in Phosphate Buffered Solution (PBS, pH 7.4 at 20°C purchased from Bio Whittaker, diluted 1/10 times in de-ionized water) with Jobin Yvon Fluorolog equipped with a integrating sphere[121,122]. These three compounds were found to be good candidate as reference for the calculation of quantum yield for other compounds, since they have three different and distinct emission band centered at 445, 560 and 637 nm respectively in PBS. Their absorption spectra are also comparable to that of other compounds. Measured absolute fluorescence quantum yield for these three reference compounds have been found to be 0.49±0.05 for **4,6′-DMeOxyL**, 0.65±0.07 for **4-MeOxyLH** and 0.19±0.02 for **5,5-Cpr-OxyLH**.

Relative fluorescence quantum yield (Φ_S) for other compounds (and also for these three reference compounds) in buffer with different pH were determined by comparative method where the ratio-metric equation $\mathbf{\Phi_S = \Phi_R*(I_S/I_R)*(OD_R/OD_S)*(\eta_S^2/\eta_R^2)}$[123] was used. Absolute area (I) under the curve for sample (S) emission and reference (R) emission spectra was calculated by integrating them between desired ranges. Refractive Index (η) was 1.333 for buffer. Optical Density (OD) was the absorbance of sample and reference at the excitation wavelength.

2.4 Time resolved fluorescence spectroscopic measurements

To study excited state photodynamics of different derivatives of Oxyluciferin in aqueous buffer, two different approaches of Time Correlated Single Photon Counting (TCSPC) have been employed to monitor time-resolved fluorescence decay of each compound at different excitation and emission wavelength.

In the first approach, the excitation pulse at 376 nm was provided by frequency doubling infrared pulses delivered by a 80 MHz Ti:Sapphire femtosecond laser (Tsunami, Spectra Physics) pumped by a Millenia X laser (Spectra Physics). The pulsed UV excitation was obtained with a BBO (β-Barium Borate) crystal with its crystal axis properly oriented with respect to the propagation direction fixed by the incoming beam. The excitation beam was collimated over 10 mm path length quartz cuvette. The fluorescence emission was collected at 90° with respect to the excitation beam through a monochromator. The incident beam intensity was adjusted to ensure an intensity-linear dependence of the fluorescence over the whole spectral range. The emission was collected through a polarizer set at the magic angle (54.7°) and a 16 nm band-pass monochromator (Jobin-Yvon H10). The single-photon events were collected by a microchannel plate photomultiplier tube (Hamamatsu) coupled to a pulse pre-amplifier HFAC (Becker-Hickl) and recorded on a SPC-630 board (Becker-Hickl). The instrumental response function was recorded using a polished aluminum reflector. Its full width at half-maximum was ~40 ps. Integrated counts of 10^6 were collected for all of the lifetime measurements[124]. Lifetime decay has been acquired by the Becker-Hickl Single

Photon Counter (SPC) software (*ver. 9.55*) and analyzed by Becker-Hickl SPC Image Data Analysis software (*ver. 4.9.7*)[124,125] which minimizes the χ^2 value (preferably to below 1.2) between the data and the model function of incomplete multiexponential fluorescence decay during the analysis.

During initial experiments it has been observed that all compounds could be excited at a common wavelength (376 nm) at 80 MHz (12.5 ns repetition rate of the excitation pulse) and their decay could be analyzed by considering an incomplete multiexponential fit. But with this approach, it was difficult to determine very short lifetime values. Indeed, it was necessary to observe fluorescence decay with a selective multiple excitation wavelengths ranging about 370 to 520 nm with lower repetition rate of the laser. To overcome these difficulties, later on, we employed another TCSPC approach, where selective excitation was possible with 4 MHz crystal (250 ns repetition rate of the excitation pulse) and also the analysis software was able to fit the decay with more than 3 lifetime components.

On the second approach, the excitation pulse was provided by a femtosecond Ti:Sapphire laser (Coherent Chameleon Ultra II, 80 MHz, 200 fs, 3.8 W) coupled to either a pulse picker (4 MHz) and a harmonic generator (SHG/THG, APE) for excitation from 300 to 500 nm, or an intracavity frequency doubled OPO (APE) and a pulse picker (4 MHz) for 500 to 700 nm excitation. The measurement of fluorescence decay were performed using the FT200 from Picoquant spectrophotometer and the emission was collected through a polarizer set at the magic angle (54.7°) and Czerny-Turner type computer controlled monochromator for the selection of wavelength of detection. The single-photon events were collected by a cooled microchannel plate photomultiplier tube R3809U (Hamamatsu) and were recorded by PicoHarp 300 TCSPC system (PicoQuant). The instrumental response function was recorded using colloidal silica (Ludox) and its full width at half-maximum was ~50 ps. All decays were collected until the number of events reached 10^4 at the maximum. The recorded decays were analyzed by FluoFit software package *ver.* 4.6.6 (PicoQuant). The reduced χ^2 was below 1.1, weighted residuals and autocorrelation function were used to check the quality of the fits. In case of non-exponential decays the stretched exponential model was used to estimate the time constants[48].

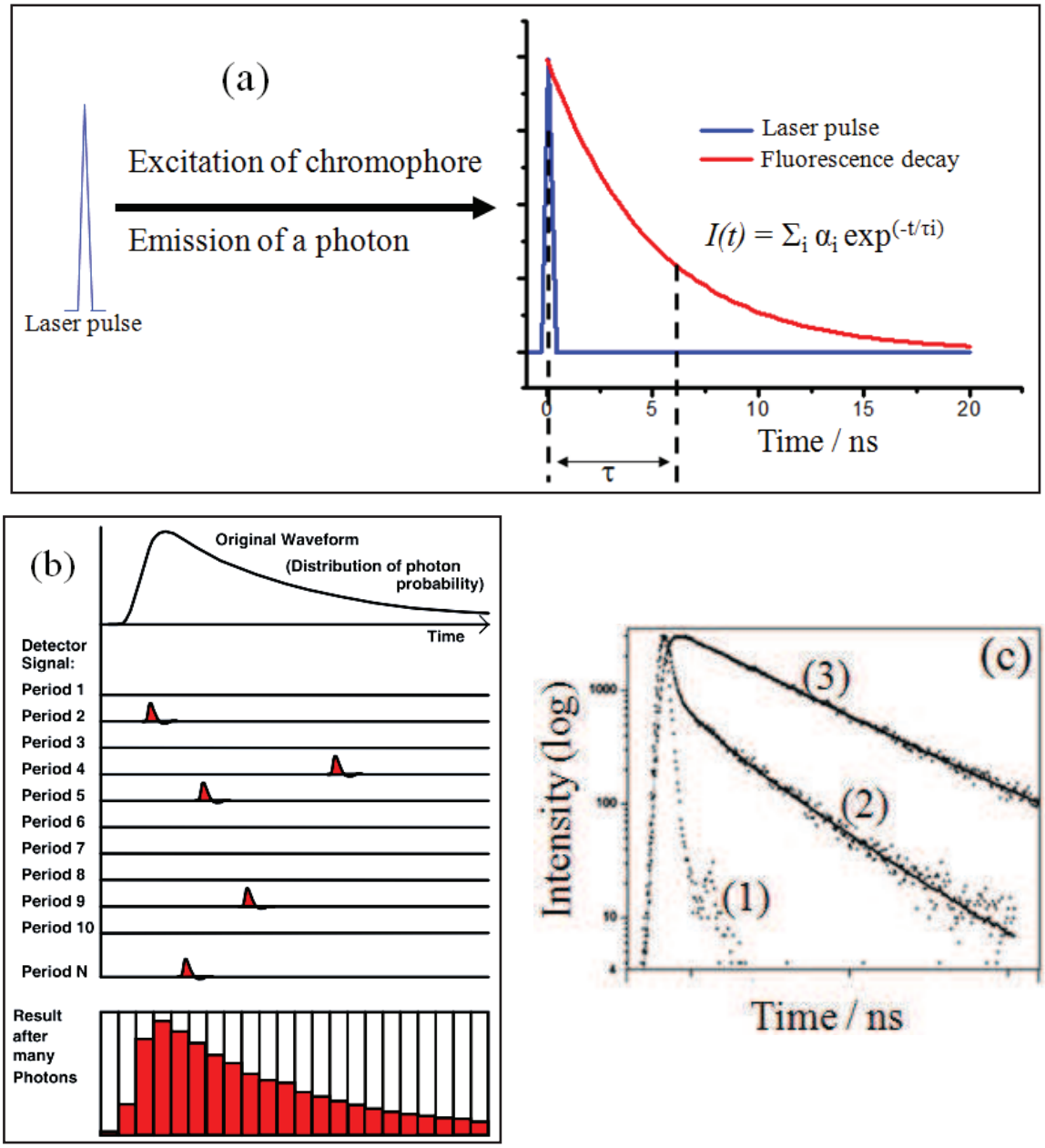

Figure 2.1: *(a) Excitation of a fluorophore by laser pulse and its time resolved emission decay (Becker W. et al. Adapted Form)*[124], *(b) Principle of TCSPC (Becker W. et al. Adapted Form)*[124] *and (c) Instrument Response Function (1) and Multiexponential fluorescence decay curve with fit (2-3)(Reprinted with permission)*[126]. *Lifetime (τ) values are calculated from the multiexponential decay fit using the equation* $\mathbf{I(t) = \Sigma_i\ \alpha_i.exp^{-t/\tau i}}$

2.5 Expression and purification of firefly Luciferase[60,127,128]

The enzyme Luciferase was expressed in BL-21 (DE3*) *E. coli* bacteria cells using the plasmid extracted from Japanese firefly (*Luciola cruciata*) kindly provided by Prof. Jun-ichi HOTTA, Graduate School of Science and Engineering, Yamagata University, Yonezawa, JAPAN.

The Luciferase plasmid were incubated with BL-21 (DE3*) cells overnight at 37°C on Lysogency Broth (LB) Agar media (supplemented with Ampicillin) to grow bacterial colony. Then a colony was further incubated in LB media supplemented with 100 µg/ml of Ampicillin for 4-6 hours at 37°C. As the colony grows, absorbance of the LB solution at 595 nm has been recorded periodically. When OD_{595} was about 0.8, 200 µM IPTG has been added to stop further bacterial growth and kept at 18°C overnight. Then the palette was removed by centrifugation at 9000 rpm at 4°C for 10 min and washed with PBS. Protease inhibitor has been added to it followed by addition of Lysozyme at 1 mg/ml at room temperature. Lysozyme has been mixed properly with gentle rotation. Short burst sonication was used to rupture the cell wall and finally after a centrifugation at 10000 rpm at 4°C for 2 hours the solution was ready for purification.

To purify Luciferase, Fast Protein Liquid Chromatography (FPLC) technique has been employed using Nickel affinity chromatography column in PBS with 200 mM Imidazole solution with a linear gradient of 0 to 100% in 60 min and monitored at 280 nm. Purified protein has been observed in 10% SDS Electrophoresis Gel and a band appeared around 62 kDa which was in good agreement with theoretical molecular mass of the protein. Further, to remove Imidazole and any other impurities (e.g. DTT etc.) the protein solution was passed through two filters with cut off at 10 kDa and 30 kDa. Final solution was mixed with 10% (v/v) Glycerol and its N_2 shock-freezed aliquots were kept at -80°C. Concentration of the Luciferase solution has been calculated from ε_{280}: 37290 $M^{-1}.cm^{-1}$ (Ref. SIB database).

2.6 HIV-1 peptide synthesis & labeling

With the development of new reagents and techniques, the classical approach of synthesis of biologically active peptides, by solid phase method, has been developed intensively in recent decades[129].

In order to couple different Oxyluciferin analogues (**$OxyLH_2$**, **4-MeOxyLH** & **4,6'-DMeOxyL**) with HIV-1 Tat(44-61) and NCp7(11-55) peptides, they were further modified at thiazole moiety with carbon chain and a carboxyl group. Their modified structures have been shown in Appendix-C.2 and described in the following scheme and table. Instead of synthesizing the full-length HIV-1 proteins, we have selected specific amino acid (AA) sequences of these HIV-1 proteins; for Tat the synthesis was done for the AA sequence Gly44 to Gly61 and for NCp7 the synthesized sequence was Lys11 to Asn55. The reason of synthesizing these particular amino acid sequences will be explained in the chapter five. **$OxyLH_2$** and **4,6'-DMeOxyL** were coupled to Tat(44-61) (separately) and **4-MeOxyLH** was coupled to NCp7(11-55). A β-alanine (3-

aminopropanoic acid) derivative was used as a spacer in between the peptide and Oxyluciferin[130].

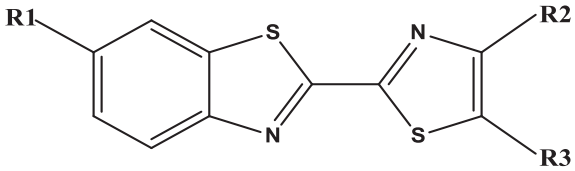

***Scheme 2.1**: Schematic of Oxyluciferin coupled to HIV-1 peptides*

***Table 2.1**: Different Oxyluciferin derivatives coupled to HIV-1 peptides*

Compound	R1	R2	R3	Peptide	Molecular mass* (g/mol)
$OxyLH_2$	-OH	-OH	~COOH	Tat(44-61)	2680
4,6'-DMeOxyL	$-OCH_3$	~COOH	-H	Tat(44-61)	2634
4-MeOxyLH	-OH	~COOH	-H	NCp7(11-55)	5561

*Theoretical (refer section C.1 for more detailed chemical structures)

Peptides were synthesized by solid phase peptide synthesis method using a 433A synthesizer (ABI, Foster City, CA). The synthesis were performed at 0.1 mmol scale using standard side-chain protected fluorenylmethyloxycarbonyl (Fmoc)-amino acids and HBTU/HOBt coupling protocol[131]. Fmoc-Gly-Wang resin LL (Novabiochem, 0.38 mmol/g reactive group concentrations) or Fmoc-Asn(trt)-Wang resin (Activotec, 0.52 mmol/g reactive group concentration) were used as a solid support for the synthesis of Oxyluciferin functionalized to N-terminal of Tat(44-61) or to NCp7(11-55) peptides. After the completion of the synthesis, peptidylresins were isolated and washed twice with MeOH and CH_2Cl_2. Figure 2.2 represents amino acid sequences of HIV-1 peptides obtained from different articles published earlier[105,111,132,133].

Three to five equivalents of the label (Oxyluciferin derivatives) were dissolved in 500 µl of DMF and mixed with six equivalents of HBTU/HOBt coupling solution (in DMF) and further added to Fmoc deprotected peptidyl resin swelled in 500 µl of DMF. After a few minutes of gentle shaking, six equivalents of DIEA solution were added and the reaction mixture was stirred overnight at 37°C. Afterwards the peptidylresins were washed with MeOH and CH_2Cl_2.

Cleavage and deprotection of peptidylresins of labeled Tat(44-61) were performed by addition of 10 ml Trifluoroacetic Acid (TFA) solution containing 5% (v/v) water and 5% (v/v) TIS $(iPr)_3SiH$. In addition to the previous protocol, 1% (w/v) phenol, 5% (v/v) thioanisole and 2.5% (v/v) ethanedithiol were added to the mixture for the cleavage of peptidylresin of labeled NCp7(11-55). The peptidylresins were then precipitated by using cold diethyl ether and then pelleted by centrifugation at 3000 rpm for 10 min. Then the pellets were dried at room temperature. The labeled peptides were then solubilized with aqueous TFA (0.05% v/v) and were lyophilized under vacuum.

All labeled peptides were purified by High Performance Liquid Chromatography (HPLC) technique using a C18 column (Nucleosil 100A, 5 µm; 250x10, Macherey-Nagel) in an aqueous-acetonitrile mixture containing 0.05% TFA with linear gradients

(15 to 70% of aqueous-acetonitrile during 90 min for Tat(44-61) or 20 to 50% aqueous-acetonitrile during 90 min for NCp7(11-55) labeled peptides) and monitored at 220 nm or 370 nm.

All purified labeled peptides were analyzed by ESI Mass Spectrometry. Molecular mass obtained from the analysis, were in good agreement with the theoretical molecular mass of the labeled peptides (mentioned in table 2.1). Prior to use, lyophilized peptides were stored at -20°C. All HPLC quality grade chemicals used for the synthesis and purifications were purchased from Sigma-Aldrich or Fluka, unless mentioned otherwise.

During experiments, the concentration of aqueous solution of labeled Tat(44-61) peptides were determined from the absorbance at 375 nm using, molar extinction coefficients $\varepsilon_{375} = 4.80 \times 10^4\ M^{-1}.cm^{-1}$ for **4,6'-DMeOxyL** and $\varepsilon_{375} = 2.23 \times 10^4\ M^{-1}.cm^{-1}$ for **$OxyLH_2$** (refer Appendix-C.4 for ε calculation). The zinc-bound form of Oxyluciferin labeled NCp7(11-55) were prepared by reacting the peptide with a 2.5 fold molar excess of zinc sulphate in aqueous buffer of 25mM Tris-HCl/30mM NaCl/0.2mM $MgCl_2$ at pH 7.4 at 20°C. The pH was increased only after the addition of zinc to the labeled NCp7 in order to avoid oxidation of zinc-free peptide. The peptide concentration were determined by using an $\varepsilon_{280} = 5.70 \times 10^3\ M^{-1}.cm^{-1}$[119]. The solution of peptide was stored at -20°C in small aliquots.

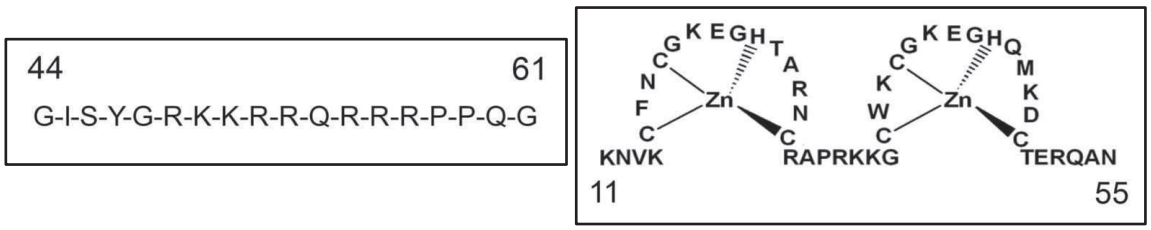

***Figure 2.2**: Amino acid sequence of HIV-1 peptides used in this study: left, Tat(44-61) and right, NCp7(11-55)*[105,111,132,133]

2.7 Two-photon excitation microscopy

Fluorescence Correlation Spectroscopy (FCS) and Fluorescence Lifetime Imaging Microscopy (FLIM) experiments were performed using an in-house constructed multi-photon laser scanning system Olympus IX70 inverted microscope with an Olympus 60X 1.2NA water immersion objective[134]. TCSPC-FLIM uses multidimensional Time-Correlated Single Photon Counting (TCSPC) process in which the sample is scanned by a focused beam of 80 MHz pulsed (mode-locked Ti:Sapphire) laser (Tsunami, Spectra Physics). Two-photon excitation was fixed at 780 nm and the laser power was adjusted to give a count rates with peaks up to as small as 10^6 photons/sec, to avoid pile-up effect. Photons were collected using two-photon short pass filter with a cut-off wavelength of 680 nm (F75-680, AHF, GERMANY). The fluorescence was directed by an optical fiber coupled APD (SPCM-AQR-14-FC, Perkin Elmer), which was connected to a TCSPC module (SPC830, Becker & Hickl, GERMANY), operates in the reversed start-stop mode. Typically, the samples were scanned continuously for about 180 seconds to achieve appropriate photon statistics to analyze the fluorescence decays. Data were

analyzed using commercial software package (SPCImage *ver*. 4.9.7, Becker & Hickl, GERMANY), which uses an iterative deconvolution method to recover the lifetimes from the fluorescence decays[134].

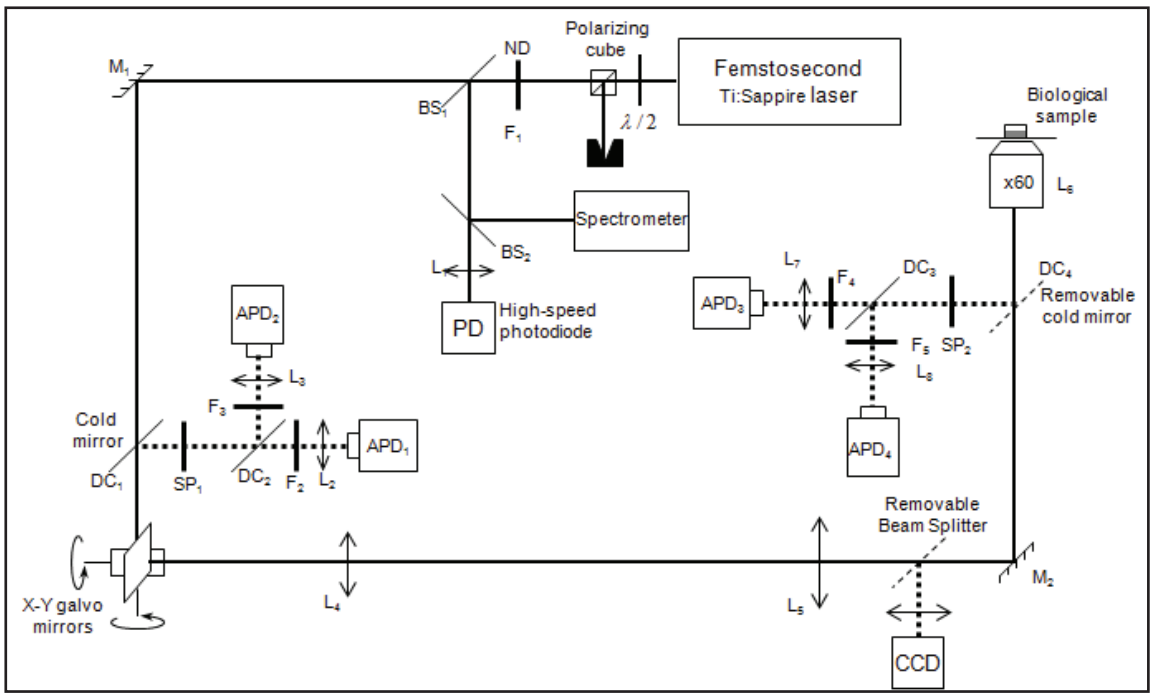

***Figure 2.3**: Schematic of architecture of two-photon excitation instrumentation*

2.8 Fluorescence Lifetime Imaging Microscopy (FLIM)

Optical methods are considered to be finest way to study biophysical properties of molecules. Although direct optical examination of active biomolecules is not a very suitable approach, as their light-protective defense mechanism prevent themselves from photodamage[135,192]. Classical optical microscopic techniques employ chemical fixation and refraction index-matched technique to visualize and to analyze with improved optical transparency of the dehydrated biomolecules[192]. This complicated endeavor does not allow the biologist to study intracellular and intercellular dynamics as well as to study subcellular structure of a fixed specimen[192]. The histology of the living biomolecules can be understood in a better manner by observing them with a non-invasive approach[192].

In-vivo or *in-vitro* bio-imaging technique applies principle of physics, chemistry and biology together to non-invasively visualize and characterize biological process of interest at molecular as well as cellular level in the living subjects[65]. Fluorescent labeling and staining, while combined with an appropriate imaging instrument, is a sensitive and quantitative method that is widely used in molecular and cellular biology.

In particular, fluorescence based microscopy techniques are one of the most widely used tool for imaging active biomolecules in the field of biophysical research[135]. It has undergone a renaissance in last decade by the introduction of GFP and 2-photon microscopy technique[192] and more recently with the advent of nanoscopy[193]. In 1980s, the use of fluorescence microscopy expanded from staining biomolecules within cells to

study the intracellular concentration of ions and for the detection of association of reactions within the cell[135]. Although the most limiting aspect of this technique is the knowledge of local probe concentrations within the cell which is usually variable based on the affinity of the fluorophore for the various biomolecules within the cell[135]. This emphasis on intracellular physiology required different types of fluorophore, ones which changed their optical properties in response to the ion or in response to the binding reaction of interest[135].

When a molecule, specially a fluorophore, absorbs a photon it reaches its electronically excited state and during its return to the ground state (S0) the molecule releases its absorbed energy in the form of photon[135]. The time a molecule spends at the excited vibrational states (S1, S2 …. Sn) is much lower than the time it takes for transition from S1 to S0. This is determined by the sum of all kinetic constants of the return pathways possible (K = transitions per molecule per unit of time)[135] and is known as excited state lifetime (τ) of that fluorophore and expressed as $\mathbf{I(t) = \Sigma_i\ \alpha_i.exp^{-t/\tau i}}$ (see figure 2.1). Lifetime is strongly dependent on the solvent polarity as larger dipole moment in polar solvents enhances the efficiency of energy transfer, lowering the fluorophore's lifetime[135]. Lifetime of the fluorophore is directly proportional to fluorescence quantum yield (Φ) but it is found to be more robust as Φ is directly calculated from fluorescence emission intensity with respect to its excitation intensity.

FLIM is an imaging technique in which fluorescence decay of a fluorophore is measured for constructing an image that represents a map of fluorescence lifetime within the sample. One of the main advantage of FLIM when used with environment sensitive dye relies on the fact that fluorescence lifetime of the fluorophore is dependent on its molecular micro-environment but not in its local concentration. Time domain FLIM is performed by using Time Correlated Single Photon Counting (TCSPC) devices[135] [124]. Data acquisition is based on the detection of arrival time of the single photon with respect to the position of the excitation pulse at the time of photon detection. The result is 3-D data array comprising distribution of photons over spatial coordinates (*x, y*) and time delay of the photon (t) which represents the array of pixels of the 2-D scan with each pixel containing large number of photons of time channels (generally in the scale of nanoseconds)[124] (see figure 2.3).

Iterative convolution method is used to obtain fluorescence decay parameter form such array of pixels. First a suitable decay model is convoluted with instrument response function (IRF), calculated/measured form the excitation pulse, and set as model parameter. Then the fit procedure optimizes the model parameter until the best fit to the photon numbers per time channel is achieved[124]. Profile of this decay model can be single or multiple exponential functions depending upon the environmental condition and structure of the fluorophore. The decay profile, described several decay time and amplitude coefficients, finally construct a FLIM image by assigning the intensity (brightness) to the total number of photons in the pixel and color to the selected decay parameter where color scale determines the fluorophore lifetime and its distribution over the image. FLIM image also build up a 2-D histogram plot of pixel intensity as a function of time where signature of fluorophore's lifetime distribution can be obtained[124].

2.9 Fluorescence anisotropy measurements

Rotational diffusion causes change in the direction of the transition moment which is the reason for depolarization. From anisotropy, average angular displacement of a fluorophore that occurs between absorption and subsequent emission can be monitored. The angular displacement is dependent on the rate and extent of the rotational diffusion during the excited state lifetime. This diffusion rate depends on several factors mainly including the shape and the size of the fluorophore-protein complex. The fluorophore, free of the protein is much smaller in size and has faster rotational diffusion than the emission rate which leads to a almost depolarized emission and thus to a nearly zero anisotropy[135]. But when bound to a protein, the shape of the complex changes and size increases (as well as the molecular weight), results in slower rotation diffusion and therefore anisotropy increases.

Emission intensity (I) of complexes were measured through a polarizer oriented parallel (∥) or perpendicular (⊥) to the polarized excitation. Anisotropy (r) is calculated from $\mathbf{r = (I_{\parallel}-I_{\perp})/(I_{\parallel}+2I_{\perp})}$[135]. Anisotropy is a dimensionless quantity independent of the fluorophore concentration and is defined as the total intensity of the sample as difference in emission intensity ($I_{\parallel}$-I⊥) is normalized to the total intensity ($I_{\parallel}$+2I⊥) of the sample.

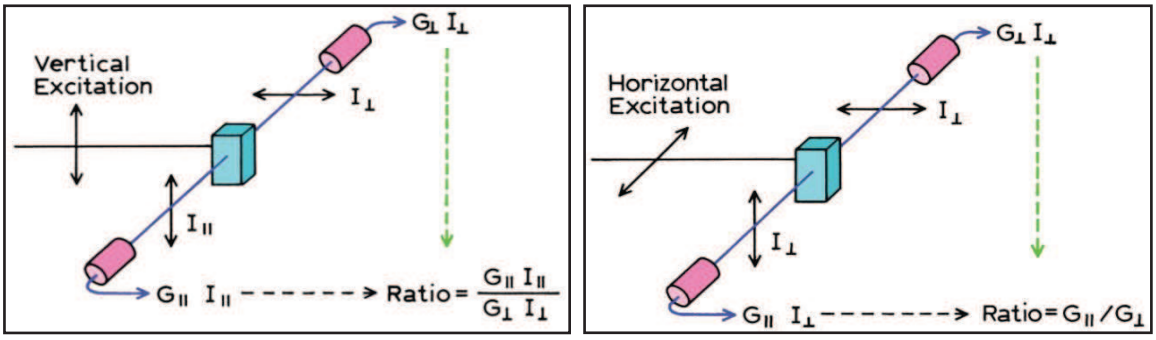

***Figure 2.4**: Schematic of fluorescence anisotropy measurement by T-format spectrofluorometer (Princ. of Flr. Spetr; J. Lakowicz, Reprinted with permission)*[135]

Anisotropy measurements were done by SLM-AMINCO (Model MH-116, SLM Instruments Inc. USA) T-format spectrofluorometer where fluorescence emission was collected by two PMT placed at 90° with respect of excitation light (Exc. slit: 4 nm). Mechanically orienting polarizers have been used to select different combination of vertical (⊥) and horizontal (∥) excitation lights. Emission was collected through suitable long pass filters (Kodak, USA) to minimize scattered lights from the excitation. In T-format method, intensities are measured by two PMTs and emission polarizes are kept perpendicular for one and vertical for the other. For vertical (V) excitation, the ratio of parallel and perpendicular signals (R_V) is given by $G_{\parallel}.I_{\parallel}/G_{\perp}.I_{\perp}$ (factor G is the sensitivity the channel measured from the individual intensity ratio). Similarly, for horizontal (H) excitation polarizer, the ratio (R_H) is given by $G_{\parallel}/G_{\perp}$. The ratio, R_V/R_H is used to

calculate the anisotropy (r). Theoretically this ratio should always be less than 3 (hence $r \leq 0.4$). Greater the value indicates presence of artifact in the measurement system. (Average of 10 calculations have been accepted as final result)[135].

2.10 Cell culture

HeLa cells (ATCC CCL-2) were cultured (¢2.00E+5) on a 35 mm glass bottom µ-petridish (Ibidi, GERMANY) in DMEM (Dulbecco's Modified Eagle Medium) from Gibco, Life Technologies, supplemented with 10% FBS (Fetal Bovine Serum, Gibco) and 0.1% PEN-STREP (Lonza) for 24 hr. at 37°C in 5% CO_2 atmosphere. After the incubation of 18-24 hr., the cells were washed with PBS and Opti-MEM (Gibco). Oxyluciferin labeled Tat, dissolved in water, was added to them with final concentration of 0.3-0.7 µg/ml in Opti-MEM. Then the cells were incubated further for 30-45 min. After incubation, cells were again washed with PBS and Opti-MEM and further incubated in Opti-MEM, next observed under the microscope placed in a thermally incubated chamber at 37°C. Later to quantify fluorescence lifetime differently, 30 µM (~20 µg/ml) Monensin Sodium salt was added directly over the cells, three minutes prior to observe, to neutralize the intracellular acidic media (concentration of H^+)[136] inside the cell.

2.11 Oligonucleotide sequences

Double HPLC grade purified custom-made oligonucleotide sequences were purchased from IBA GmbH, GERMANY and their stock solution was prepared in de-ionized water and concentration was calculated from their molar absorption coefficient provided by IBA GmbH.

2.12 Software used

For different analytical purposes Origin software (*ver. 8.6*) academic license to LBP-UMR7213 has been used. Chemical structures, schemes and charts have been prepared with ChemBioDraw software (*ver. 12.0*) valid with personal academic license. Other software mentioned otherwise wherever required.

Chapter 03

Results & Discussions

pH dependent photophysical profile of Oxyluciferin in aqueous buffer

pH Dependent Spectra of Oxyluciferin in Aqueous Buffer

In this work, we investigated the color tuning mechanism of firefly bioluminescence, by performing the first systematic steady-state and time-resolved fluorescence study of firefly Oxyluciferin and its analogues in aqueous buffered solutions to provide the individual absorption and emission spectra of all possible chemical forms of the photo-emitter and to unravel the exact factors that affect the emission of Oxyluciferin (**$OxyLH_2$**). In particular, the steady-state and time-resolved fluorescence emission experiments performed in aqueous solutions within a physiologically relevant pH range, provided the individual emission spectra of all tautomeric and anionic **$OxyLH_2$** variants as well as their ground and excited states equilibrium constants[48]. In addition, the rate constants of the fundamental photoreaction processes were also determined. New synthetic strategies have been applied to access large variety of non-natural structurally modified Oxyluciferin analogues (see chart 3.2). The excited-state structure of these structurally modified derivatives and their equilibrium constants in strongly polar environment with strong hydrogen bonding potential has been studied in/ex situ with conventional spectroscopic method. Different mathematical and chemometric approaches allow us to decipher the chemical equilibrium and kinetic profile among six hypothetically possible chemical forms (see chart 3.1) that govern this complex phenomenon associated with changes in emission wavelength. Spectral study of different chemical forms of Oxyluciferin (e.g. phenol-enol, phenolate-enol, phenol-keto, phenolate-keto etc.) in aqueous solutions confirms that the proton transfer from the enol group (thiazole subunit) is more favorable than that from benzothiazole group[48]. It has been observed that in aqueous solutions, the phenol-keto form is the strongest photoacid among all other isomers of Oxyluciferin and phenolate-keto has the lowest emission energy. From the pH-dependent absorption and emission spectra and the respective fluorescence lifetimes we concluded that the keto-enol tautomerism reaction is not favored in aqueous solutions unlike in non-polar solvents. Although these results do not directly apply to the Luciferase-Oxyluciferin complex where the active site is considered to be of low polarity, they provide support to the hypothesis that the excited state potential energy surface and the related dynamics are affected by the environment of the active site[48].

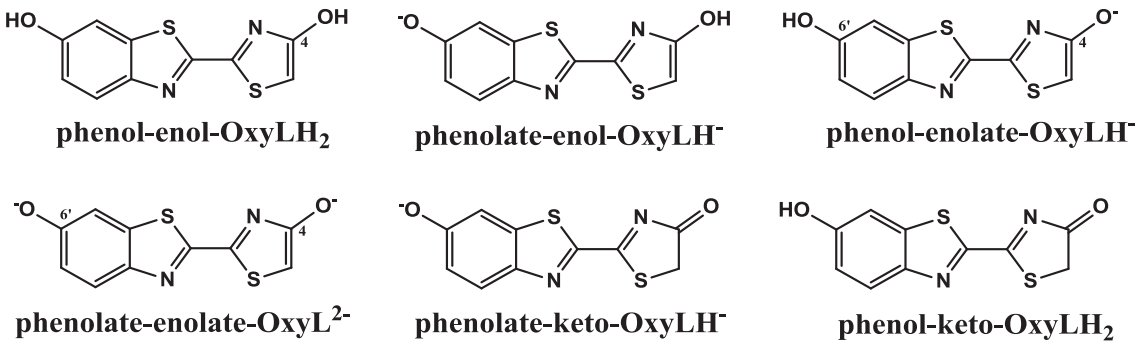

***Chart 3.1**: Possible ground-state chemical forms of Oxyluciferin in aqueous solution*

We investigated the absorption, emission spectra and the excited state equilibrium constants for all chemical forms of **$OxyLH_2$** presented in chart 3.1. These parameters

have not been determined previously, even though they are essential for the understanding of the photophysical properties of the molecule. Our project collaborator Prof. Lukas HINTERMANN from Dept. of Chemistry at University of Munich, chemically synthesized different analogues of **$OxyLH_2$** where different –H atoms are replaced by $–CH_3$. This site specific methylation prevents the analogue to undergo any protonation/deprotonation (chemical) reactions. Spectroscopic studies for five prime structural analogues of firefly Oxyluciferin (see chart 3.2) have been studied in aqueous buffers[48].

Chart 3.2 represents correlation between different chemical forms of firefly Oxyluciferin (shown in blue) in aqueous buffer and different structural analogues or model compounds (shown in black) studied in this work. Model compounds **4,6′-DMeOxyL** and **6′-Me-5,5-Cpr-OxyL** can represent **phenol-enol-$OxyLH_2$** and **phenol-keto-$OxyLH_2$** respectively in deprotonated (basic) aqueous buffer. On the other hand, **4-MeOxyLH** can mimic **phenol-enolate-$OxyLH^-$** form of Oxyluciferin in completely deprotonated aqueous buffer. In similar condition, **6′-MeOxyLH** can mimic **phenolate-enol-$OxyLH^-$** form and **phenolate-keto-$OxyLH^-$** form can be represented by keto variant **5,5-Cpr-OxyLH**. Depending upon solution pH, **$OxyLH_2$** can represent all these six chemical forms of firefly oxyluciferin including **phenolate-enolate-$OxyL^{2-}$**.

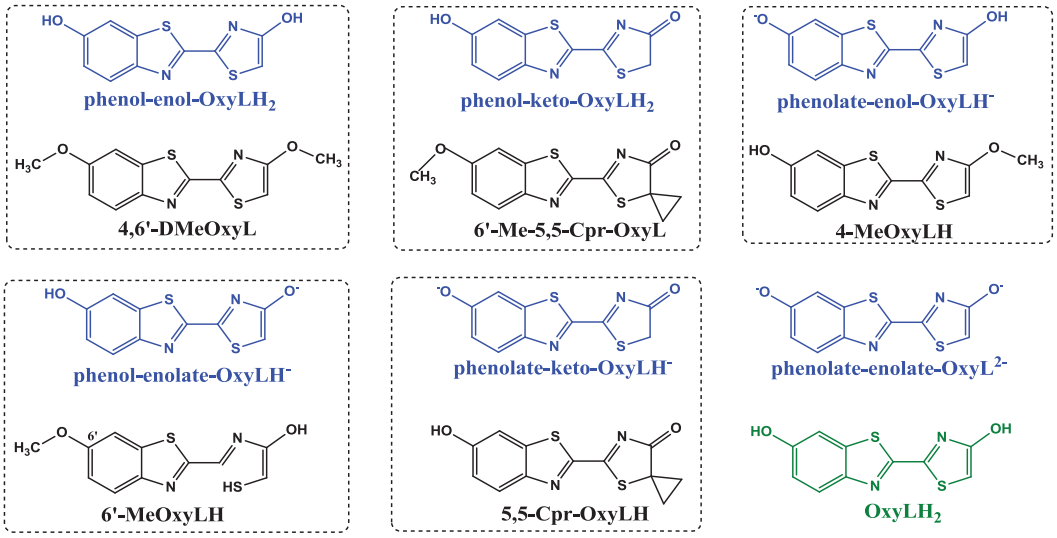

***Chart 3.2**: Chemical structure and corresponding molecular weight of firefly emitter $OxyLH_2$ and its five analogues used in this study*

Spectral properties of several structural analogues of Oxyluciferin have been studied in aqueous buffers at pH ranging 5 to 11. Their pH dependent steady state absorption, emission spectra and time resolved fluorescence decay has been studied to decipher the exact color tuning mechanism of firefly bioluminescence. Six different chemical forms of firefly Luciferin that are actively involved in this process have been used. Their spectral properties, excited state dynamics (ESPT), ground state and excited state equilibrium etc. have been characterized and reported in *"Emission Properties of Oxyluciferin and its Derivatives in Water: Revealing the Nature of the Emissive Species in Firefly Bioluminescence"* Ghose et al. J. Phys. Chem. B, **119**, 2015

(doi: 10.1021/jp508905m). In this chapter we explain those results in a more detailed way (all data reprinted with permission).

3.1 Selection of model compounds

To simulate a micro-environment close enough to the physiological conditions used in the bioluminescence reaction involving Luciferin-Luciferase complex and to decipher the effect of pH on Oxyluciferin emission and its equilibrium, aqueous buffers at different pH have been used in this study. To facilitate comparative assignments, the absorption, emission spectra and fluorescence decays of all structurally modified derivatives were recorded under identical conditions for pH ranging 5 to 11 that spans over all pKa values so far reported for Oxyluciferin[137]. Indeed, bioluminescence reaction of Luciferin-Luciferase is strongly dependent in pH region 6-10[6,44,137,138]. Monopotassium di-hydrogen phosphate (KH_2PO_4) buffer has been used for pH between 5 to 7 as this is well known to be an ideal buffer in the 5.8-8.0 range. While to prepare buffer pH > 7.0, Tris has been used as it has a pKa that lies at 7.4 and is well known for buffers ranging from 6.8 to 8.2. It has been expected that at pH 5.0, Oxyluciferin will be in completely protonated form while at pH 11.0 it will be in completely deprotonated form. Concentrations of theses derivatives used for absorption and emission spectra are mentioned in the following table:

Compound	Mol. Wt. (g/mol)	Conc. (μM)	Compound	Mol. Wt. (g/mol)	Conc. (μM)
4,6'-DMeOxyL	278.35	0.9	6'-Me-5,5-Cpr-OxyL	290.36	1.0
4-MeOxyLH	264.32	6.0	5,5-Cpr-OxyLH	276.33	1.1
6'-MeOxyLH	264.32	4.0	$OxyLH_2$	250.30	3.0

Ionization of both hydroxyl groups and keto-enol tautomerization of the thiazole moiety (triple equilibrium of Oxyluciferin) make photochemistry of Oxyluciferin more complex. A strategy of selective blocking of both or either one hydroxyl group has been used in this study. We mainly target five structural analogues (see chart 3.2) which can model different tautomeric and anionic variants of Oxyluciferin. **4,6′-DMeOxyL** is a model for **phenol-enol-OxyLH$_2$** form (neutral form) while **4-MeOxyLH** and **6′-MeOxyLH** are analogous of **phenolate-enol-OxyLH$^-$** and **phenol-enolate-OxyLH$^-$** forms that can normally be generated in basic conditions. In **4,6′-DMeOxyL** both hydroxyl groups (benzothiazole and thiazole) are blocked by $-CH_3$ and in **4-MeOxyLH** and **6′-MeOxyLH** 4C-thiazole and 6C-benzothiazole are blocked respectively (see chart 3.2). Apart from this, we also included keto-variant of Oxyluciferin **5,5-Cpr-OxyLH** where due to very specific 5,5 thiazole distribution pattern it is restricted to keto tautomeric form (see chart 3.2) and benzothiazole group can undergo deprotonatation in basic media. This can mimic **phenolate-keto-OxyLH$^-$** form of Oxyluciferin. Also, we considered another keto variant **6′-Me-5,5-Cpr-OxyL** which is model for neutral **phenol-**

keto-OxyLH$_2$ form similar to neutral enol form i.e. **4,6′-DMeOxyL** (benzothiazole is restricted by –CH_3).

3.2 Optical properties of Oxyluciferin in organic solvent

Prior to understand the photophysics of Oxyluciferin and its analogues in aqueous buffers, their spectral properties have been observed in pure and 50% (v/v) DMSO. Investigation of Oxyluciferin and d-Luciferin in organic solvents is not a new idea. Understanding the proton transfer mechanism of different analogues of Oxyluciferin in pure organic solvent or in a mixture is a well-established approach reported in earlier times. In recent years photophysical study of Oxyluciferin in non-aqueous solvents, especially in binary mixtures, has been investigated widely[4,12,31,139,140]. To understand the ESPT mechanism of newly synthesized structural analogues of Oxyluciferin, primarily, we also used the same approach and characterized the steady state properties in DMSO-H_2O mixture. Absorption and fluorescence emission spectra of Oxyluciferin (**OxyLH$_2$**) and its four structural analogues (**4-MeOxyLH**, **6'-MeOxyLH**, **4,6'-DMeOxyL** and **5,5-Cpr-OxyLH**) were measured in DMSO-H_2O system. In particular, we recorded their spectra in pure (100%) DMSO and 50% (v/v) DMSO-H_2O binary mixture. DMSO-H_2O solution is more polar than pure DMSO. Water is polar-protic solvent while DMSO is polar-aprotic solvent. However, the change in pH of the system was unknown. This polarity variation plays a significant role in the ESPT mechanism involved in the process. Their steady state optical properties are summarized and represented in the figure. 3.1.

The absorption spectra of Oxyluciferin and its analogues are dominated by single band centered about 371-376 nm (except for keto form i.e. 391 nm) and almost not sensitive to the change in solvent polarity. **OxyLH$_2$** and its 6'C methylated analogue (**6'-MeOxyLH**) absorbs at 376 nm while its neutral and 4C methylated analogue (**4-MeOxyLH**) absorbs at 371 nm. Naumov et al. reported the absorption maxima of **OxyLH$_2$** in pure DMSO as 377 nm[4] similar to the value we obtained. Effect of methylation can be clearly visible; a small blue shift of the absorption maxima with 4C-thiazole methylation could be recorded. Keto-Oxyluciferin (**5,5-Cpr-OxyLH)** has a red-shifted absorption maxima centered at 391 nm likely due to a different electronic structure.

Effect of solvent polarity on Oxyluciferin and its analogues are much visible in their emission spectra due to more pronounced fluorophore-solvent interactions in the excited state than the ground state[4]. Except the keto analogue, all other analogues display a single emission band centered in between 434-443 nm in pure DMSO (polar-aprotic solvent). **OxyLH$_2$** has an emission band centered at 443 nm in pure DMSO resulting from the excited neutral form (**OxyLH$_2^*$**). Its 6'methylated analogue shares the same emission maxima with **OxyLH$_2^*$**, while its 4-thiazole and neutral analogues have blue shifted emission band. The single band in the emission spectra obtained in pure DMSO confirms presence of single specie in the excited state due to the absence of ESPT in pure DMSO (see figure. 3.1).

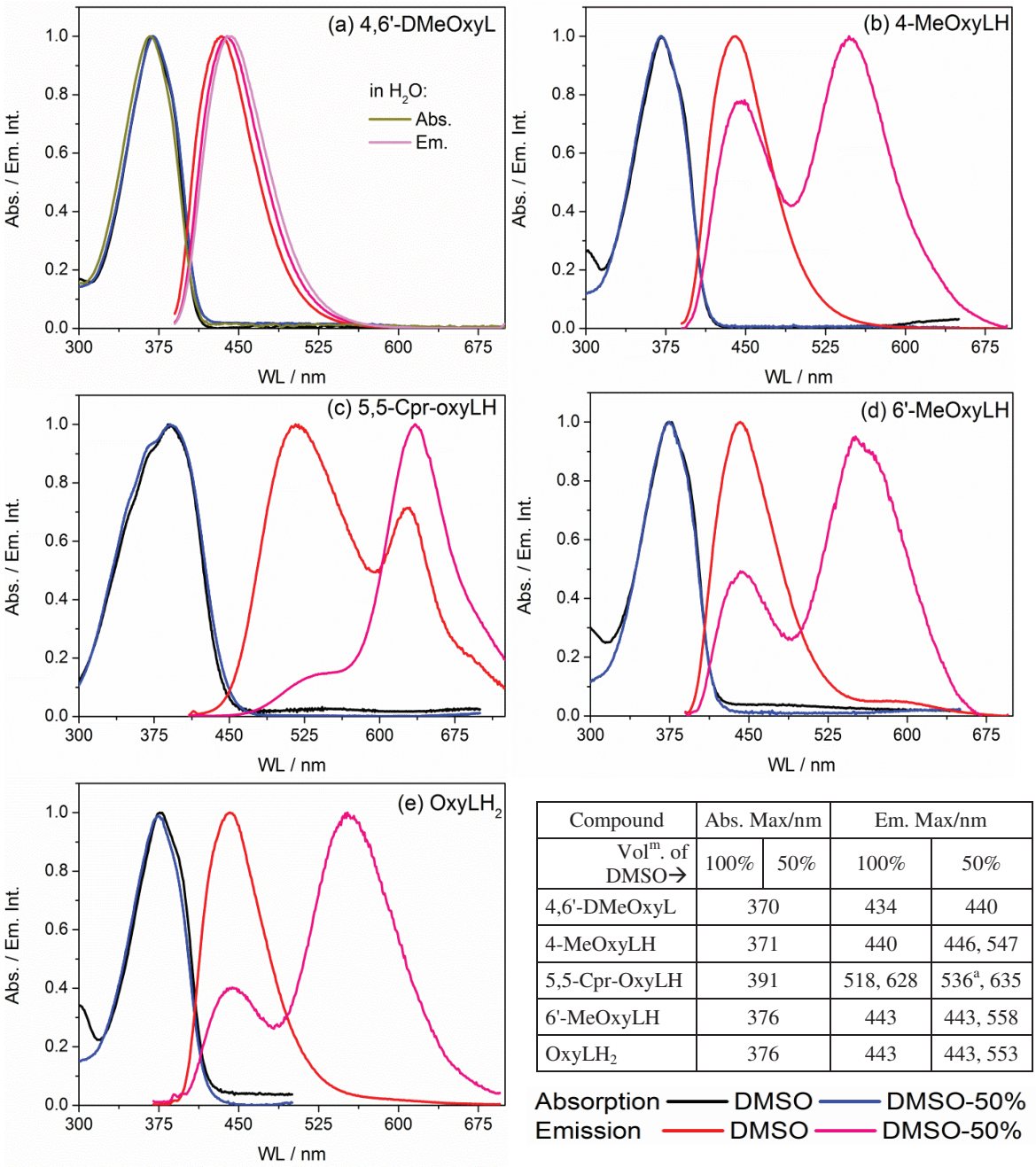

Compound	Abs. Max/nm		Em. Max/nm	
Vol[m]. of DMSO→	100%	50%	100%	50%
4,6'-DMeOxyL	370		434	440
4-MeOxyLH	371		440	446, 547
5,5-Cpr-OxyLH	391		518, 628	536[a], 635
6'-MeOxyLH	376		443	443, 558
$OxyLH_2$	376		443	443, 553

***Figure 3.1**: Absorption, emission spectra of (a) **4,6'-DMeOxyL**, (b) **4-MeOxyLH**, (c) **5,5-Cpr-OxyLH** (d) **6'-MeOxyLH** and (e) **$OxyLH_2$** in DMSO-H_2O. In the table we have reported the absorption and emission maxima (while excited at absorption maxima) of those analogues (a: shoulder/tail).*

Increased solvent polarity due to addition of water has a strong effect on the emission spectra. Due to specific interactions and enhanced hydrogen bonding capability in the comparatively deprotonated solvent, a strongly red shifted and more intense secondary emission band (centered around 547-558 nm) could be observed in 50% (v/v) DMSO-H_2O binary mixture (more polar in nature than pure DMSO). This dual emission band evidences existence of more than one species in the excited state and can likely b e associated to an efficient ESPT involved in the emission mechanism. The hypothesis relying on the presence of both neutral and anionic species in the excited state is supported by the single emission spectra of neutral compound **4,6'-DMeOxyL** in both

solvents (100% and 50% DMSO). Due to dual methylation at both benzothiazole and thiazole groups, this compound cannot undergo ESPT. So the emission even in 50% DMSO is originating from the neutral state. To confirm that there is no effect of solvent polarity which can lead to generation of another ionic specie in the excited state in the emission of this compound, figure 3.1a is supplemented with additional Abs/Em spectra of **4,6'-DMeOxyL** in 100% water. No secondary emission band could be observed even in highly polar (protic) solvent like water. Although, a very small red shift in the emission maxima has been noticed.

The keto-Oxyluciferin, **5,5-Cpr-OxyLH**, is unique in terms of its photophysics. This compound is a strong photoacid (we will discuss about the photoacidity of **5,5-Cpr-OxyLH** later in section 3.5) and the presence of neutral and anionic species can be observed in pure DMSO. Absence of –OH in the thiazole subunit is the reason that the compound is already in the deprotonated state even in pure organic solvent. Its red-shifted absorption spectra support this hypothesis. Fluorescence emission occurs from both **phenol-keto-OxyLH$_2$** (~518 nm) and **phenolate-keto-OxyLH$^-$** (~635 nm) form. In addition, with increasing solvent polarity, the contribution of **phenolate-keto OxyLH$^-$** in the emission dominates the **phenol-keto-OxyLH$_2$** emission which finally appears as a shoulder. Therefore it can be postulated that solvent polarity plays a significant role in the emission and ESPT mechanism of Oxyluciferin and its derivatives. Time resolved fluorescence decay of **4,6'-DMeoxyL**, **4-MeOxyLH** and **OxyLH$_2$** in DMSO-H_2O has been reported in Appendix-A.2.

3.3 pH dependent absorption spectra

To understand the ground state equilibrium of Oxyluciferin in aqueous buffer, we first measured the absorption spectra of each analogue at different pH in the range 5 to 11. The interpretation of the color tuning luminescence mechanism of firefly Luciferin required intense characterization of composition, concentration and absorbance of **OxyLH$_2$** and its analogues. The pH-dependent steady-state absorption spectra of Oxyluciferin analogues are presented in figure 3.2. **4-MeOxyLH** and **5,5-Cpr-OxyLH** display clear isosbestic points that can be unambiguously associated with the presence of two chemical forms. The absorption spectra of these two analogues evidenced that the phenol-phenolate equilibrium occurs in the pH range 5 to 11. Phenol/phenolate species has their absorption maxima at 367/406 nm and 388/482 nm for **4-MeOxyLH** and **5,5-Cpr-OxyLH** respectively. Absorption spectrum of **5,5-Cpr-OxyLH** indicates that the spectral maximum of the phenolate ion of the keto form is strongly red shifted (482 nm) relative to its neutral form (388 nm). In this case, the absorption is mainly due to a л-л* transition of the keto group and n-л* transition from –OH at benzothiazole group. The hypothesis is supported by the spectra of **4-MeOxyLH** (only n-л* transition of C4-methoxy is relevant in this case) where absorption from phenolate ion (anionic/deprotonated form) also has a red-shift to 406 nm compared to its neutral form (367 nm). The relative ground state pKa of 7.8 and 8.7 has been calculated for **5,5-Cpr-OxyLH** and **4-MeOxyLH** respectively (see table 3.2 and figure 3.2).

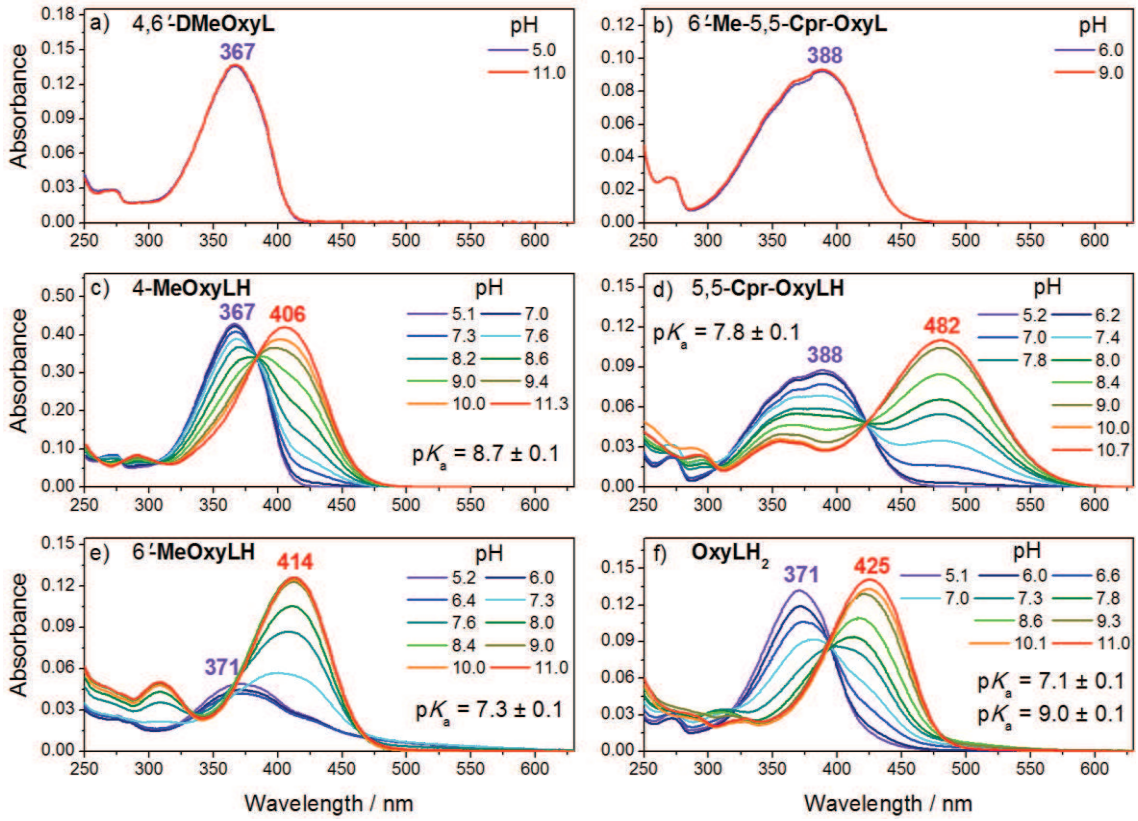

***Figure 3.2**: Dependence of the absorption spectra of firefly Oxyluciferin (**OxyLH$_2$**) and its derivatives on solvent pH and their corresponding pKa values. The chemical structures are shown in chart 3.2. The spectra were recorded in aqueous buffers at different pH at 20^{o}C. The concentration was 0.9, 6.0, 4.0, 1.0, 1.1 and 3.0 µM for **4,6′-DMeOxyL**, **4-MeOxyLH**, **6′-MeOxyLH**, **6′-Me-5,5-Cpr-OxyL**, **5,5-Cpr-OxyLH** and **OxyLH$_2$**, respectively.*

Deciphering pure spectral signature of the species that evolve from **6′-MeOxyLH** and **OxyLH$_2$** was complicated and required a multi-set data analysis approach of the pH-dependent absorption spectra. In the case of **6′-MeOxyLH**, the complexity is introduced by the presence of three coexisting species due to keto-enol and enol-enolate equilibrium in the studied pH range. For **6′-MeOxyLH** a strong absorption band centered at 371 nm and a shoulder at ~440 nm has been observed at pH 6. By comparing this spectrum with the one obtained with **4,6'-DMeOxyL** in the same conditions (where the phenol-enol species absorbs at 367 nm without any shoulder) we conclude that this band is likely assigned to the enol form. At pH 11, the maximum absorption shifts to 414 nm without any shoulder and can be assigned to the enolate form (neutral keto form cannot exists in such a strong basic media).

The absorption spectra of **OxyLH$_2$** display two pH dependent absorption bands in the range of 371-425 nm and 309-313 nm. At pH 9 the stronger band is red shifted to 417 nm but the weaker band remains at the same position above pH 7.7. The more intense band shows an additional red shit to 425 nm in between pH 9-11 and remain at same position at pH >10 (see figure 3.2). In figure 3.3, absorption maxima of **OxyLH$_2$** and its two model compounds **6′-MeOxyLH** and **4-MeOxyLH** have been plotted as a function of pH

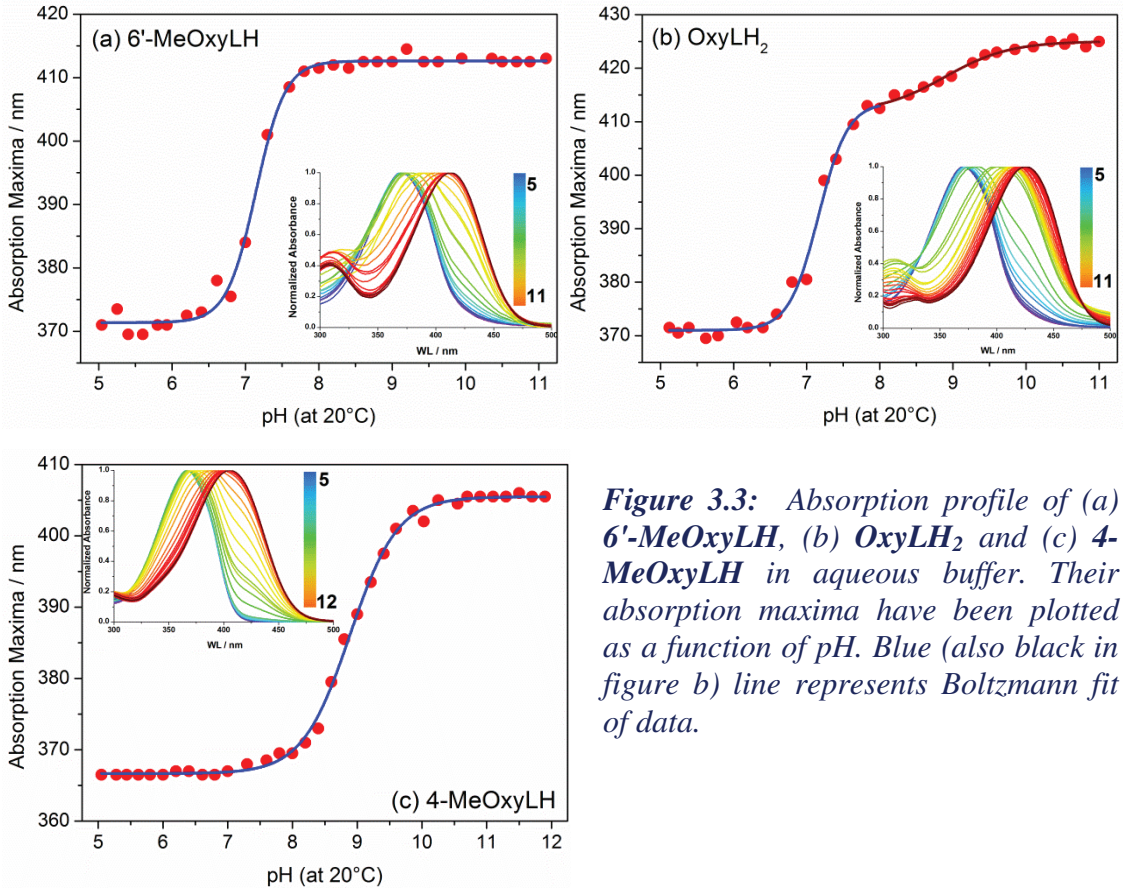

Figure 3.3: *Absorption profile of (a)* ***6'-MeOxyLH****, (b)* ***OxyLH$_2$*** *and (c)* ***4-MeOxyLH*** *in aqueous buffer. Their absorption maxima have been plotted as a function of pH. Blue (also black in figure b) line represents Boltzmann fit of data.*

To determine the accurate ground-state equilibrium constants of **OxyLH$_2$**, recently our project-collaborators *Rebarz M. et al.* applied a chemometric approach (**M**ultivariate **C**urve **R**esolution–**A**lternating **L**east **S**quares / MCR-ALS) to decipher the pH-dependent spectra of model compounds where some ESPT processes or the enol-keto equilibrium are blocked[9]. The analysis provided the absorption spectra of individual chemical forms of the emitter devoid from the other species and their pH-dependent concentration profiles.

MCR method is a powerful approach to study complex tautomerization equilibrium from spectral data with an assumption that the data follow a bilinear model. The spectroscopic data can be completely resolved and the concentration profile **C** and spectra **S** of the components can be calculated from a spectroscopic mixture represented by a matrix **D** according to the equation $\mathbf{D} = \mathbf{CS}^{\mathbf{T}} + \mathbf{E}$[9].

In this equation, matrix **D** contains *m* number of pH-dependent spectra (rows) recorded at *n* wavelength (columns). The matrices C(*m* x *N*) and S^T(*N* x *n*) contain pH dependent concentration profiles and the characteristic spectra of **N** absorbing species in the mixture, respectively[9]. The matrix ***E***(*m* x *n*) contains the residual signal, caused mostly by the experimental noise. The most outstanding advantage of this MCR approach is the possibility to perform a multiple dataset analysis. The studied datasets correspond to the experimental data that observe the same chemical system, while the focus is on the

processes that is being developed under different experimental conditions and, consequently, exhibits complementary behaviors[9].

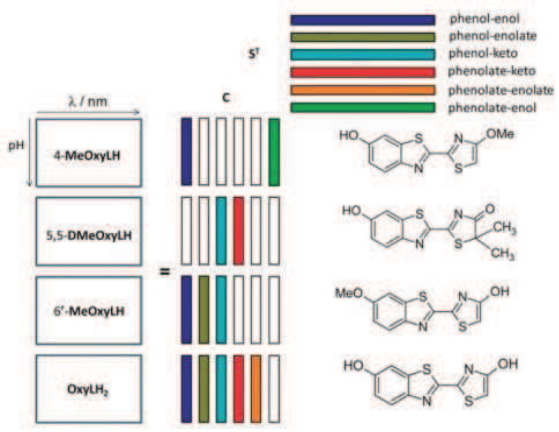

***Figure 3.4**: Multi-set data arrangement for MCR-ALS analysis of Oxyluciferin (Rebarz et al. Reprinted with permission)*[9]

In their work *Rebarz M. et al.* employed MCR-ALS to perform a simultaneous analysis of the pH-dependent spectroscopic data of **$OxyLH_2$** and its derivatives. Briefly, individual series of pH-dependent absorption spectra are arranged in data matrices $\boldsymbol{D_i}$ (I = Oxyluciferin derivatives) where each row corresponds to the absorption spectrum measured at a given pH. Multi-set data arrangement can also be built corresponding to augmented matrices where the single data matrices are appended column-wise. The augmented data matrices built for multi-set spectral data analysis correspond to experiments performed for several Oxyluciferin derivatives having some common chemical forms in aqueous buffers[9].

To interpret the data, they assumed a bilinear model in the single-set analysis and/or in multi-set analysis. In multi-set analysis, the matrix $\boldsymbol{S^T}$ contains the pure spectra of the species present in the different mixtures of chemical forms and the concentration matrix **C** is the augmented data matrix describing the pH-dependent profile of each species in each individual data set (see figure 3.4). However, it is to be noted that multi-set data configuration neither involve all species that are present in all experiments nor all experiments share the same pH evolutions. Multi-set analysis also contributes to reduce significantly the amount of improbability in the results[9].

To understand the absorption behavior of Oxyluciferin in aqueous buffer and to identify exact chemical forms that are contributing to absorption spectra, it was necessary to analyze them in a different and unique way. Multivariate deconvolution technique was required to overcome possible inaccuracies associated with conventional univariate analytical approach. Application of such analytical technique allowed us to decipher the pH-dependent concentration profiles and the absorption spectra of each individual chemical forms of Oxyluciferin (see figure. 3.5) at different pH extracted from their pH dependent absorption spectra. Encouraged by the results of *Rebarz M. et al.*, we thus applied Multivariate Curve Resolution-Alternate Least Squares (MCR-ALS) technique to identify the absorption spectra of each species in the ground state.

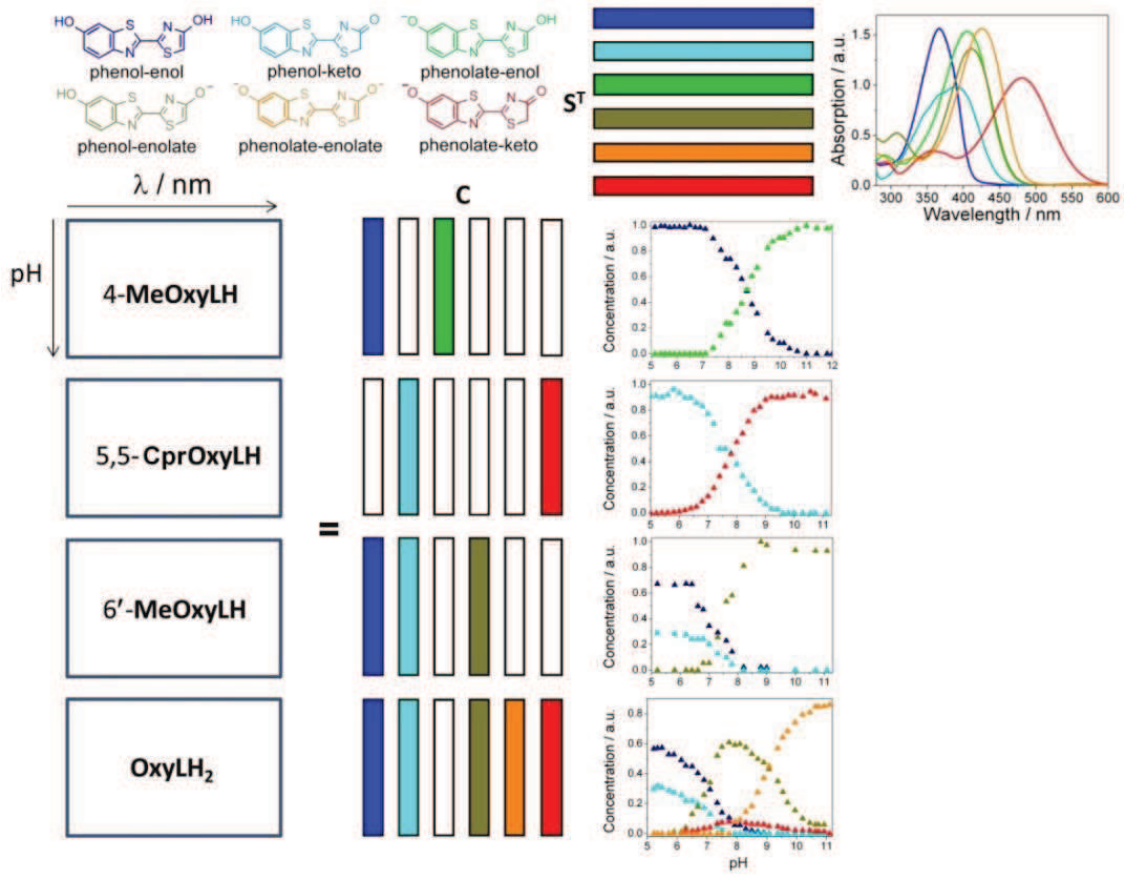

***Figure 3.5**: Absorption spectra and corresponding concentration profiles for **OxyLH$_2$** and three model compounds (**4-MeOxyLH, 5,5-Cpr-OxyLH** and **6'-MeOxyLH**) obtained by multi-set MCR-ALS analysis.*

In line with the earlier results obtained by our project collaborators,[137] the ground state spectral maxima of all the chemical forms can be arranged in the following order: *phenol-enol-OxyLH$_2$ (367 nm) < phenol-keto-OxyLH$_2$ (388 nm) < phenolate-enol-OxyLH$^-$ (406 nm) < phenol-enolate-OxyLH$^-$ (412 nm) < phenolate-enolate-OxyL^{2-} (425 nm) < phenolate-keto-OxyLH$^-$ (482 nm).* The distribution diagram (see figure 3.6) shows that the contribution of the **phenolate-enol-OxyLH$^-$** form is negligible due to the significantly higher pKa value of the phenol group relative to the enol group. In practice the presence of this species in the case of OxyLH$_2$ can be ignored.

pKa values for each derivatives has been calculated from the concentration profile presented in the figure 3.6. pKa was calculated by fitting the concentration profile (solid line/figure 3.6) with Henderson-Hasselbach equation (pKa = pH + log([HA]/[A$^-$]).[137] By fitting these data with MCR-ALS, pKa value for each chemical form of Oxyluciferin could be calculated. The pKa values for few derivatives determined in Tris buffer are slightly lower than those in phosphate buffers as shown earlier by Rebarz M. et al.[137] In particular, the phenol-phenolate equilibrium for **4-MeOxyLH** was found at 8.7 which is lower by 0.2 p*K* units. Whereas the pKa value for **OxyLH$_2$** are lowered by 0.3 units for the phenol-enol/phenol-enolate (pKa 7.1) and 0.1 units for the phenol-enolate/phenolate-enolate (pKa 9.0) equilibrium respectively. Lowering of the pKa constants is another

proof of Oxyluciferin sensitivity towards ionic strength of the buffer. The combination of concentration profile and absorption spectra of each chemical forms determined by using MCR-ALS can be used to evaluate the contribution of each species at a given pH value (see figure 3.5 and 3.6). It also facilitates us to determine precisely the excitation wavelength that can be employed to preferentially excite a particular chemical form of Oxyluciferin at a given pH value. For example, at pH 8–9 it is possible to excite the **phenolate-keto-OxyLH$^-$** selectively or **phenol-enolate-OxyLH$^-$** forms and to characterize its optical properties without any significant contribution from the other chemical forms.

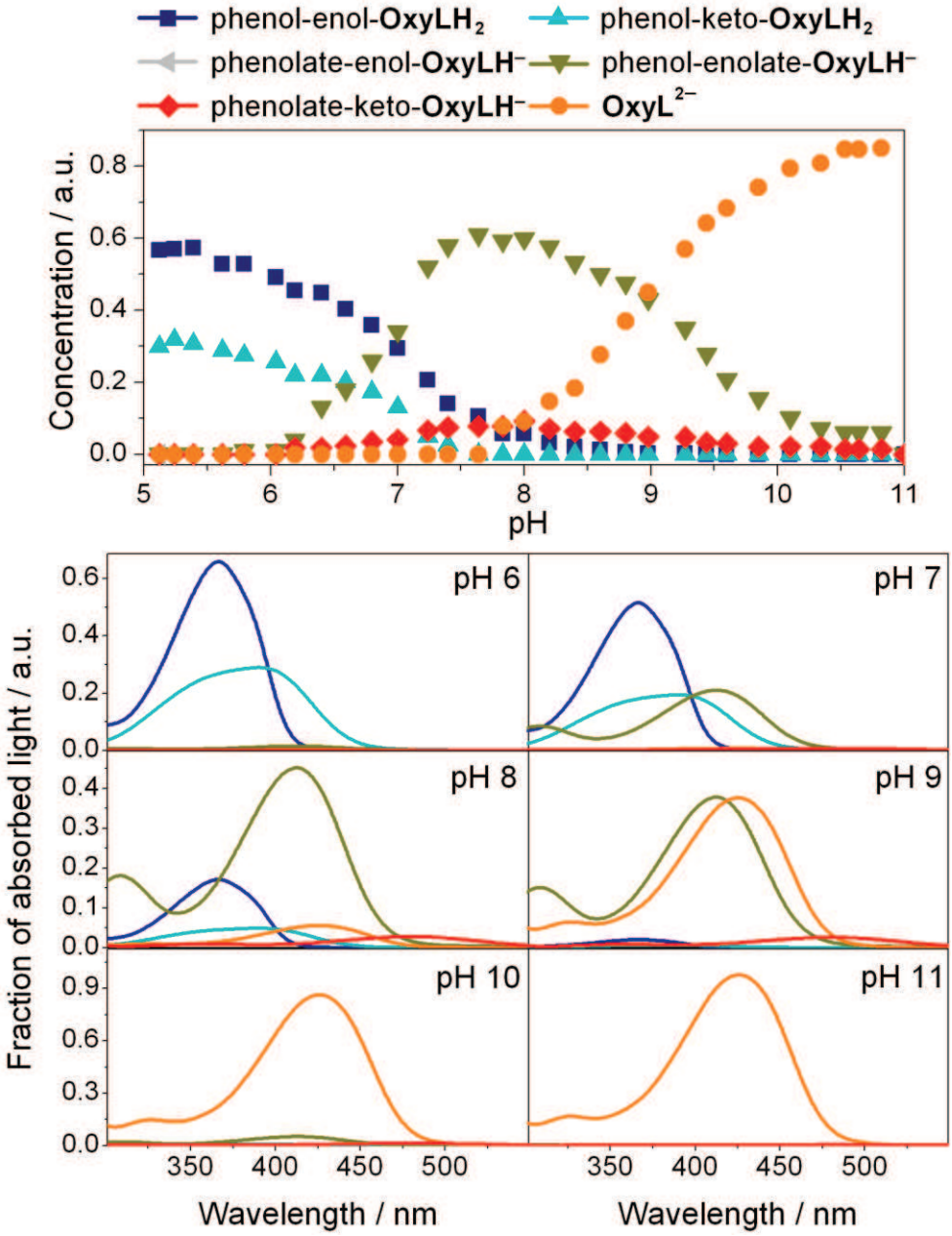

***Figure 3.6**: Absorption spectra and concentration profiles of five forms of firefly Oxyluciferin obtained from MCR-ALS analysis. (The concentration of the **phenolate-enol-OxyLH$^-$** form under these conditions is negligible)*

3.4 pH dependent emission spectra and their time-resolved fluorescence decay

Understanding of ground state equilibrium and absorption spectra of the conjugated acids and bases set the foundation for the interpretation of fluorescence emission mechanism and estimation of the corresponding equilibrium constants in the excited state (pKa*) by evaluating excited state proton transfer (ESPT) mechanism by means of the Förster Cycle[123,140].

3.4.1 Emission spectra of the non-ionizable model compounds

The fluorescence emission spectra of non-ionizable model compounds **4,6′-DMeOxyL** and **6′-Me-5,5-Cpr-OxyL** recorded in aqueous solutions in pH region 5-11 are presented in figure 3.8. Their concentration was kept exactly similar to their absorption spectra and their corresponding time-resolved fluorescence decays are shown in figure 3.7. The position and the shape of their emission spectra as well as their relative fluorescence quantum yield and excited state lifetimes do not evolve with pH in the studied range (see figure 3.8 and table 3.1). This is because of the absence of acidic groups on the compound (both benzothiazole and thazole are blocked). **4,6′-DMeOxyL** exhibits a single broad emission band centered at 445 nm while excited at 370 nm which is in very good agreement with the fluorescence emission associated to the neutral **phenol-enol-OxyLH$_2$** form (450–455 nm)[141,142]. Relative fluorescence quantum yield (Φ_R) of **4,6′-DMeOxyL** was found to be 0.49 throughout the pH region and its fluorescence emission decayed monoexponentially with an excited state lifetime of 3.1 ns in this pH region. On the other hand, the emission maximum of other model compound **6′-Me-5,5-Cpr-OxyL**, the **phenol-keto-OxyLH$_2$** analogue, was significantly red shifted by 80 nm from that of the **phenol-enol-OxyLH$_2$** counterpart i.e. **4,6′-DMeOxyL**, with maximum at 525 nm. The shape and position of the emission spectra while excited at 370 nm does not evolve with pH. Fluorescence decays monoexponentially with an excited state time constant of 0.9 ns. Shortening of this lifetime can be attributed to the increased contribution of non-radiative pathways associated with the relatively smaller energy band gap which is also supported by the five-fold decrease in relative fluorescence quantum yield calculated for this compound.

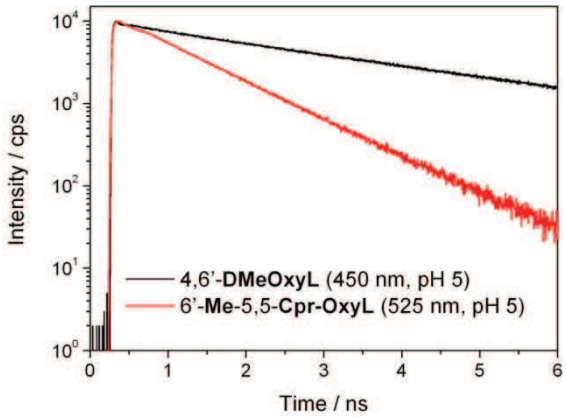

***Figure 3.7**: Fluorescence decays of two model compounds (**4,6'-DMeOxyL** and **6'-Me 5,5-Cpr-OxyL**) recorded in aqueous solutions.*

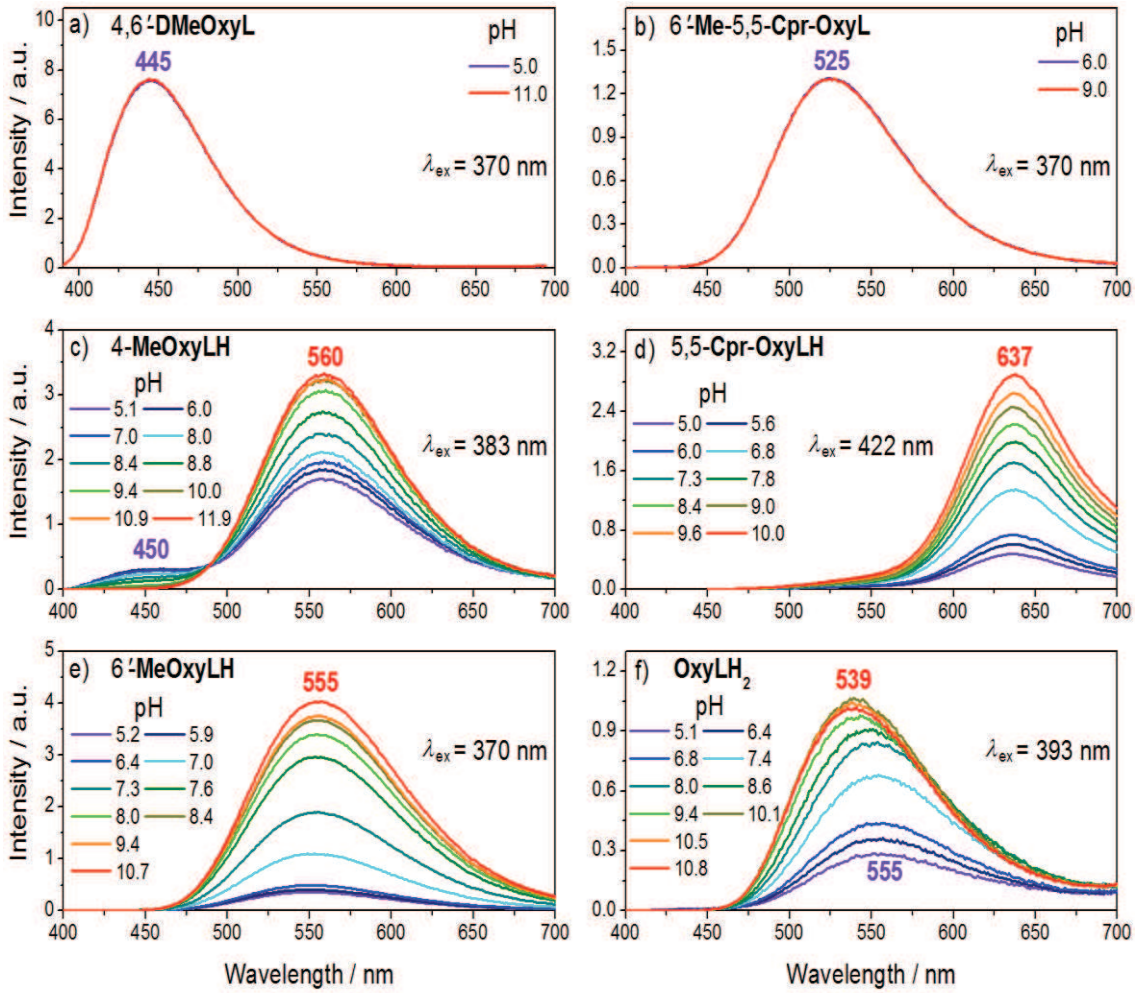

***Figure 3.8**: Emission spectra of firefly Oxyluciferin (**OxyLH$_2$**) and its derivatives recorded in aqueous solutions at different pH. The chemical structures are shown in chart 3.2. Measurements were performed at room temperature (20°C) in aqueous buffers at different pH and the concentration was 0.9, 6.0, 4.0, 1.0, 1.1 and 3.0 μM for **4,6′-DMeOxyL**, **4-MeOxyLH**, **6′-MeOxyLH**, **6′-Me-5,5-Cpr-OxyL**, **5,5-Cpr-OxyLH** and **OxyLH$_2$**, respectively.*

3.4.2 Emission spectra of the ionizable model compounds

The fluorescence emission spectra of other model compounds **4-MeOxyLH**, **5,5-Cpr-OxyLH** and **6′-MeOxyLH** were recorded in aqueous solutions within the pH range 5–11 in the similar way as before and are presented in figure 3.8. The emission spectra of **4-MeOxyLH** and **5,5-Cpr-OxyLH** were recorded at excitation wavelengths that correspond to their isosbestic points at 383 nm and 422 nm respectively (see figure 3.2). **5,5-Cpr-OxyLH** was always irradiated in the visible region; excitation to higher excited states leads to formation of a new photo-product which has a characteristic specific emission at 530 nm, which was particularly pronounced in basic conditions (see Appendix-A.3). **6′-MeOxyLH** was excited at 370 nm where the absorption was least sensitive to solvent pH (see figure 3.2).

The emission spectra of **4-MeOxyLH** in acidic solutions are composed of two distinct bands. At pH 5.0 the strong band is centered at 560 nm from the ionic form and is accompanied by a weaker band centered at ~450 nm originating from the neutral form which is in accordance with the spectrum of **4,6′-DMeOxyL** (see figure 3.8). This assignment is fully supported by the time-resolved fluorescence decay of this compound recorded at both emission maxima in acidic solution (pH 5.0). By exciting the neutral form at 370 nm the emission band at 450 nm is strongly quenched and decays non-exponentially with a very short lifetime component of 0.24 ns. Simultaneously the time resolved fluorescence decay observed at 560 nm at pH 5.0 rises with an average time constant corresponding to ESPT rate and disappears biexponentially with excited state lifetimes of 1.6 and 4.9 ns (see figure 3.9 and table 3.1). The first component corresponds to the geminate proton quenching. In agreement with a pKa* value of about 3.4 the emission band at 450 nm disappears completely in highly basic solution (pH > 9) where only the deprotonated excited state contributes to the fluorescence emission (see figure 3.8). At high pH (>10) the deprotonation occurs already in the ground state and expectedly, geminate recombination[143-149] of proton was not observed with the growing part of the time resolved fluorescence decay. Hence, the fluorescence emission of **4-MeOxyLH** at 560 nm at pH 10 was characterized by a monoexponential decay with time constant of 4.88 ns, identical to that of the longer component measured at pH 5 (see table 3.1). Therefore, the spectrum recorded at high pH establishes a model for the photophysical properties of the **phenolate-enol-OxyLH**$^-$ form. To obtain the spectral signature of the **phenolate-keto-OxyLH**$^-$ form, the emission spectra of **5,5-Cpr-OxyLH** were recorded by exciting at 422 nm. The shape and the position of the emission spectra did not evolve with pH and only one emission band centered at 637 nm was observed in contrast to **4-MeOxyLH**. This can be explained by the higher photo acidity of **5,5-Cpr-OxyLH**, which experiences highly efficient ESPT throughout the whole pH range. The time-resolved fluorescence decay recorded at 520 nm with an excitation at 390 nm in acidic solution, corresponds to the neutral form of **keto-OxyLH$_2$** and reveals a bimodal process (see figure 3.9 and table 3.1) with a very short lifetime component corresponds to the instrumental response function (IRF) of the setup (<50 ps). Therefore it can be postulated that, ESPT from the phenol group is a very fast, thus only emission from the deprotonated form of **5,5-Cpr-OxyLH** can be observed with steady-state spectroscopy. The emission maximum at 637 nm is in very good agreement with the data reported previously for the phenolate-keto emission from **5,5-DMeOxyLH** derivative[12,150]. It is noteworthy that de-excitation of the phenolate-keto anionic emission exhibits time constant of 0.6 ns, while recorded at 640 nm and is several times faster than the one corresponding to the phenolate-enol form (4.9 ns) (see figure 3.9 and table 3.1). The weak emission and the long tail observed at 530 nm at basic pH are likely caused by photo-degradation of the molecule and should not be taken into account while considering emission spectra of the phenolate-keto form.

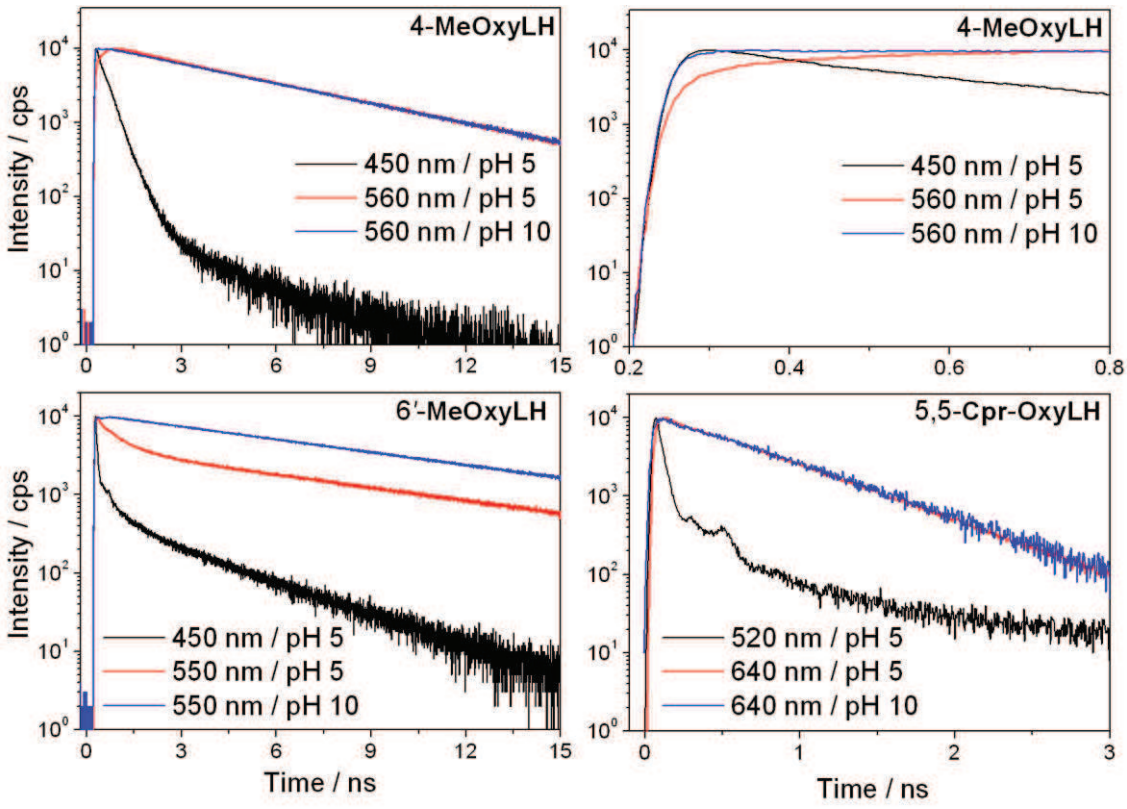

***Figure 3.9**: Fluorescence decays of derivatives of firefly Oxyluciferin measured in acidic and basic buffered aqueous solutions. The chemical structures are shown in chart 3.2.*

To understand the emission mechanism of **phenol-enolate-OxyLH$^-$,** we focused on the other ionizable model compound **6′-MeOxyLH**, where the dissociation of the phenol group is purposefully blocked. This derivative exhibits a broad intense emission spectra centered at ~550 nm while excited at 370 nm. Because of the strong photoacidity the fluorescence emission of **6′-MeOxyLH** originates mainly from the enolate ion. The time-resolved fluorescence decay of **6′-MeOxyLH** recorded at 450 nm in acidic pH has a non-exponential character with a very short component (< 50ps) which is quite similar to IRF. This is the result of very fast and efficient ESPT from the enol group at lower pH. It is already known from the absorption spectra[137] that this compound can exist with ~30% keto form at pH 5. The contribution of this tautomer (exclusively in the neutral form due to blocked phenol deprotonation) in the fluorescence emission of **6′-MeOxyLH** cannot be excluded especially at acidic pH. A detailed analysis of pH dependent emission spectra of **6′-MeOxyLH** (see figure 3.8) reveals a very small blue shift from 555 nm at pH 11 to 550 nm at pH 5. This blue shift may be explained by the superposition of two strongly overlapped components in the emission spectra in acidic media: a major component originates from enolate anion with a maxima at 555 nm associated with a minor one that corresponds to the emission from neutral keto tautomer that centered around 525 nm (compared with **6′-Me-5,5-Cpr-OxyL**). At basic pH, the minor component was depleted and only emission from pure enolate species could be observed (λ_{max} 555 nm). To support this interpretation, the emission spectra of **6′-MeOxyLH** in pH

5 has been recorded by exciting at 430 nm (see figure 3.10). For this condition, excitation of the keto tautomer is highly increased because of its superior absorption coefficient relative to the other species[137]. Apparently, the contribution of the keto tautomer into the resultant emission spectrum of **6′-MeOxyLH** was stronger and a maximum blue shift to 535 nm could be observed. The presence of the keto tautomer in acidic media was also noticeable in the time-resolved fluorescence decay. The decay recorded in acidic solution at 550 nm (λ_{Exc} 370 nm) was multiexponential with time constants of 0.17, 0.8 and 7.9 ns (see figure 3.9 and table 3.1). The shortest lifetime (0.17 ns) is attributed to the geminate quenching while the second component corresponds to the excited state lifetime of **6′-Me-5,5-Cpr-OxyL** (0.9 ns). On the contrary, in basic solution (pH 10) the decay recorded at 550 nm was monoexponential with a time constant of 8 ns. This result strongly support that the keto tautomer is not present in basic solution and the spectra recorded under such conditions correspond to emission from the **phenol-enolate-OxyLH$^-$** form.

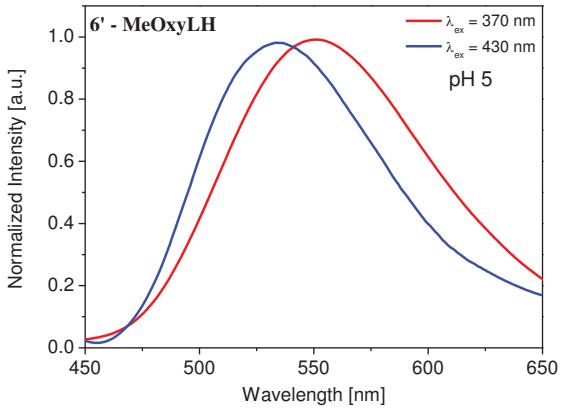

***Figure 3.10**: Emission spectra of **6'-MeOxyLH** recorded in aqueous solutions at pH 5 and excitation at 370 nm (red line) and 430 nm (blue line).*

3.4.3 Emission spectra of Oxyluciferin (**OxyLH$_2$**)

The presence of five chemical forms provides an accurate spectral characterization of the most intricate part of the analysis; the pH-dependent fluorescence emission of the real emitter **OxyLH$_2$**. The **phenolate-enol-OxyLH$^-$** form can be excluded from the analysis of emission spectra because of its higher pKa of the phenol group with respect to enol group. To decipher the individual contributions of each chemical form, the fluorescence emission spectra of **OxyLH$_2$** were recorded at two different excitation wavelengths: 370 and 510 nm (see figure 3.11). The interpretation of the emission spectra was greatly facilitated by this selective photo-excitation of **OxyLH$_2$**. The relative absorbance of all six chemical forms of **OxyLH$_2$** at a specific pH are listed in figure 3.2 and 3.6.

***Table 3.1**: Time resolved and fluorescence quantum yield (Φ_R) data for firefly Oxyluciferin and its derivatives (see chart 3.2) in aqueous solutions (the constants for **$OxyLH_2$** obtained by using the global analysis method for all the decays are highlighted in boldface font)*

Compound	Neutral emission				Anionic emission					Φ_R
	pH	λ_{ex} / nm	λ_{em} / nm	τ / ns	pH	λ_{ex} / nm	λ_{em} / nm	τ / ns (%)		
4,6′-DMeOxyL	5–11	370	450	3.10	-					0.49
4-MeOxyLH	5	370	450	0.24[a]	5	370	560	0.21[b] 1.60 (11) 4.86 (89)		0.32
					10	430	560	4.88		0.47
6′-Me-5,5-Cpr-OxyL	5–9	390	525	0.93	-					0.11
5,5-Cpr-OxyLH	5	390	520	< 0.05[a]	5	390	640	0.16 (25) 0.61 (75)		0.18
					10	520	640	0.63		0.26
6′-MeOxyLH	5	370	450	< 0.05[a]	5	370	550	0.17 (42) 0.78 (32) 7.88 (26)		0.18
					10	430	550	7.97		0.35
$OxyLH_2$	5	370	450	< 0.05[a]	5	370	550	0.16 (52) 1.04 (8) 7.63 (40)	**0.17 (50)** **0.48 (7)** **7.82 (43)**	0.15
						370	640	0.16 (12) 0.56 (80) 7.28 (8)	**0.17 (41)** **0.48 (49)** **7.82 (10)**	
					7.6	430	550	0.17 (32) 0.53 (19) 3.95 (6) 7.68 (43)	**0.17 (17)** **0.48 (7)** **5.80 (19)** **7.82 (55)**	0.35
						510	640	0.41	**0.17 (2)** **0.48 (98)**	
					10	430	540	5.91	**5.80**	0.50

[a]Short component of non-exponential decay, [b]Average time constant of the growing part.

Excitation at 370 nm.

In acidic conditions (pH < 8), the dominant species that can be excited at 370 nm are **phenol-enol-$OxyLH_2$** and **phenol-keto-$OxyLH_2$** (see figure 3.6). Assuming a strong photo-acidity in the excited state for both phenol and enol groups, it can be predicted that the first species should be deprotonated to **phenol-enolate-$OxyLH^-$** followed by the second one to **phenolate-keto-$OxyLH^-$**. The time-resolved fluorescence decay is a strong evidence of efficient ESPT from the enol group recorded at emission wavelength that corresponds to the emission from **phenol-enol-$OxyLH_2$** form (λ_{max} 450 nm) (see figure 3.8). The decay recorded indicates that the emission from the neutral **phenol-enol-$OxyLH_2$** form is strongly quenched and the proton transfer time constant is <50 ps (see

figure 3.11 and table 3.1). In comparison, the value estimated by Erez et al. is 45 ps[73]. Considering the possible deprotonation of the phenol group, the fluorescence spectrum contains contributions from both species. Because of higher abundance and higher fluorescence quantum yield relative to **phenolate-keto-OxyLH$^-$** (637 nm) form, the dominant contribution comes from the **phenol-enolate-OxyLH$^-$** form (555 nm). The recorded emission spectra have maxima at 555 nm and possess long tail that extends beyond 600 nm.

Time resolved fluorescence decay recorded at 640 nm in pH 5.0 clearly shows two populations with exited state lifetime of ~0.56 ns and ~7.3 ns (see table 3.1) together with the geminate recombination[143-149] associated with a time constant of 0.16 ns. The value of first component (0.56 ns) is fully in line with the lifetime of **phenolate-keto-OxyLH$^-$** form determined by considering **5,5-Cpr-OxyLH** exited state lifetime whereas the lifetime of second component (7.3 ns) is in a very good agreement with the fluorescence lifetime of **phenol-enolate-OxyLH$^-$** (7.9 ns; table 3.1) determined for **6′-MeOxyLH.**

With increasing pH, in basic condition, the contribution from keto-tautomer becomes negligible, and the most abundant species are **phenol-enolate-OxyLH$^-$** and **phenolate-enolate-OxyL^{2-}** (see figure 3.6). This results in a slight blue shift of the emission spectra that are attributed to a mixture of monoanionic and dianionic form. Due to negligible concentration of other species in the ground state (see figure 3.6), the fluorescence emission from the dianionic form becomes more dominant at pH > 9 and the emission spectra recorded at pH 11 displays a maximum at 539 nm which can be attributed to the **phenolate-enolate-OxyL^{2-}** form. The blue-shifted emission from mono-deprotonated **phenol-enolate-OxyLH$^-$** form had a shorter exited state lifetime of ~5.9 ns (see table 3.1).

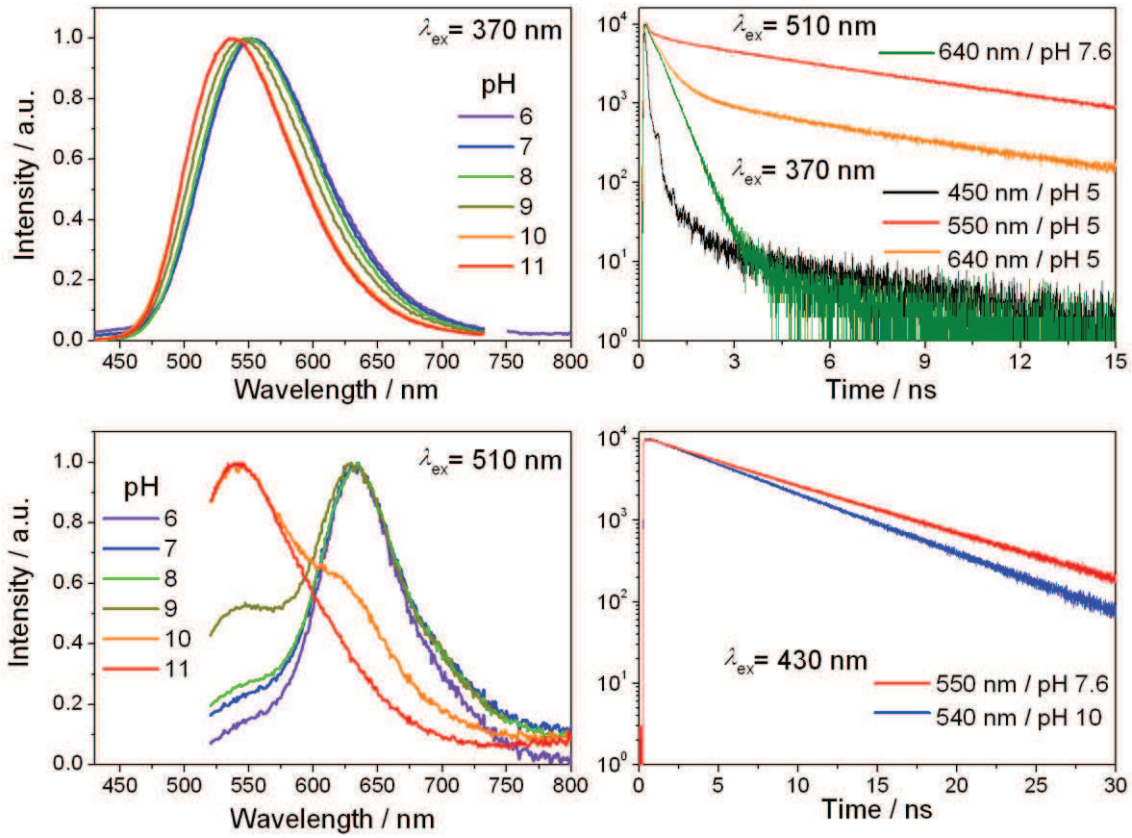

***Figure 3.11**: Normalized emission spectra of firefly Oxyluciferin in aqueous solution at different pH and excitation wavelengths*

Excitation with visible light at 510 nm.

Photo-excitation at lower energy leads to different de-excitation pathways of **OxyLH$_2$**. In acidic solutions (pH 6-7) the major absorbing species is the **phenolate-keto-OxyLH$^-$** form. Also, minor contributions from **phenol-keto-OxyLH$_2$** and **phenol-enolate-OxyLH$^-$** could be observed. Therefore, **phenolate-keto-OxyLH$^-$** form dominates the fluorescence emission at this pH and features a band centered at 634 nm, slightly blue shifted (3 nm) compared to the emission from **5,5-Cpr-OxyLH**. Nearly monoexponential fluorescence decay could be observed at 640 nm (see figure 3.11) with a time constant of 0.4 ns (see table 3.1) which indicates that the **phenolate-keto-OxyLH$^-$** is the dominant species in this condition.

At higher pH 8-9, a shoulder around 540 nm appears due to **phenolate-enolate-OxyL^{2-}** contribution. This is because of the increased abundance of **phenolate-enolate-OxyL^{2-}** resulting from deprotonation of **phenol-enolate-OxyLH$^-$** in the ground state. At highly basic solution (pH >10), the intensity of the red band decreases considerably at ~634 nm in favor of the green emission intensity from **phenolate-enolate-OxyL^{2-}** at ~540 nm which becomes more dominant at pH 11 with an exited state lifetime of 5.91 ns (see table 3.1). Time resolved fluorescence emission decay at pH 7.6 has a strong importance to characterize the spectral properties of **OxyLH$_2$**. With an excitation at 430 nm and by monitoring the emission decay at 550 nm, a mixture of phenolate-keto

(0.53 ns), **phenolate-enolate-OxyL^{2-}** (3.95 ns) and **phenol-enolate-OxyLH^{-}** (7.68 ns) could be observed (see table 3.1).

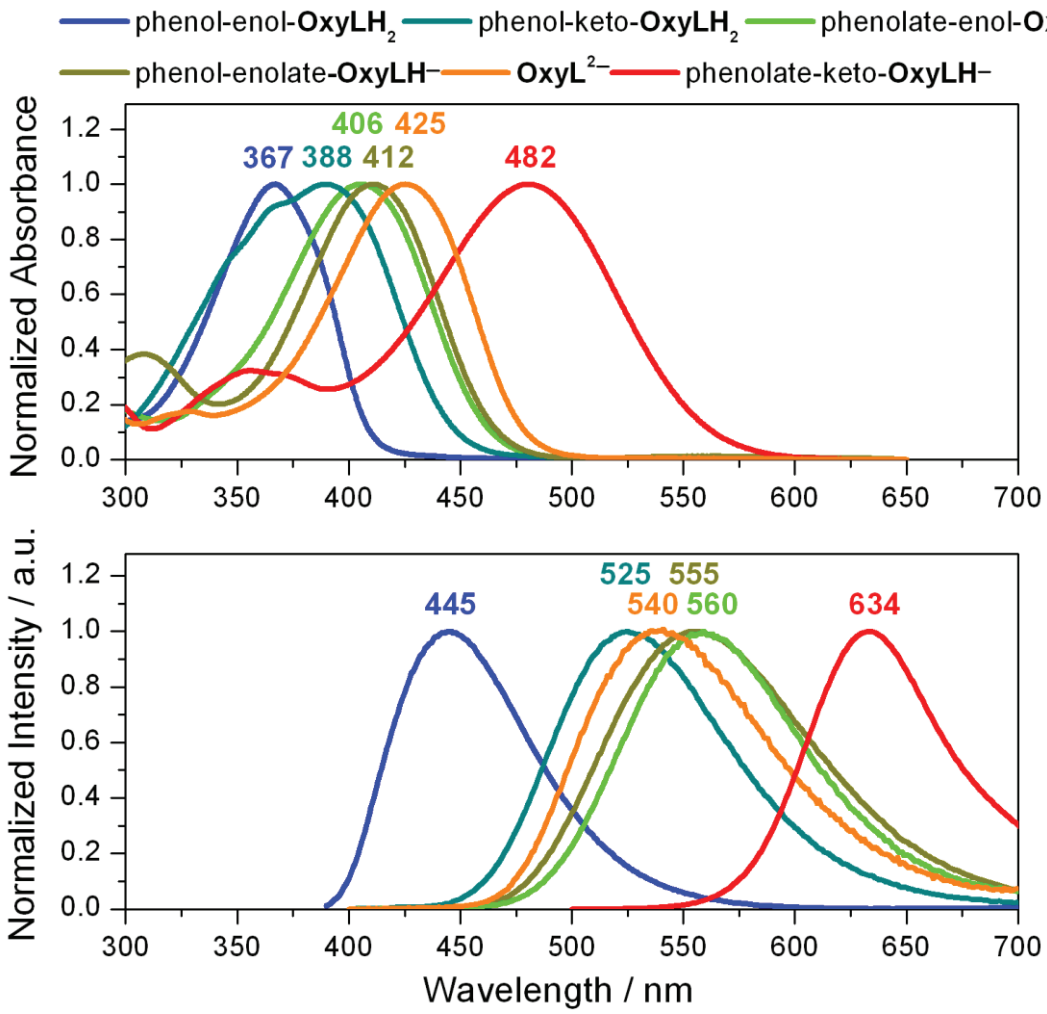

***Figure 3.12**: Absorption (top panel) and emission (bottom panel) spectra of individual chemical forms of firefly Oxyluciferin based on the Multivariate Curve Resolution–Alternating Least Squares (MCR-ALS) procedure.*

The spectral data recorded for different analogues at different pH with selective excitation (thus exciting the particular chemical form of Oxyluciferin) and their analysis provides the fluorescence emission spectra of each individual chemical forms associated with the color tuning mechanism of firefly Luciferin (see figure 3.12). The order of emission energies does not match exactly the same order of the absorption energies. The order of emission energies is *phenol-enol-OxyLH$_2$ (445 nm) > phenol-keto-OxyLH$_2$ (525 nm) > phenolate-enolate-OxyL^{2-} (540 nm) > phenol-enolate-OxyLH^{-} (555 nm) > phenolate-enol-OxyLH^{-} (560 nm) > phenolate-keto-OxyLH^{-} (634 nm)*. In the excited state, we could observe in the emission decay only the contribution from three species: phenol-enolate, phenolate-keto and phenolate-enolate that are associated with one geminate recombination with decay of 0.17 ns without any ESPT growing signal. Such

observation can be explained by the fact that the enol group in the phenol-enol form and the phenol group in the phenol-keto form are strong photoacids. In addition to this single wavelength lifetime analysis, a global decay analysis with four time constants was performed, one for each species and one for geminate recombination (see table 3.2) to obtain more reliable values for phenol-enolate (7.82 ns), phenolate-keto (0.48 ns) and phenolate-enolate (5.80 ns) forms.

3.5 Equilibrium and photodynamics in the excited state

Five chemical equilibriums could be considered in the case of **OxyLH$_2$***: phenol-enol/phenol-enolate, phenol-enolate/phenolate-enolate, phenol-enol/phenolate-enol, phenolate-enol/phenolate-enolate and phenol-keto/phenolate-keto. In the ground state, where the enol group is more acidic than the phenol group, the pathway including phenol-enol/phenolate-enol deprotonation and subsequent phenolate-enol/phenolate-enolate deprotonation can be excluded from the consideration. The equilibrium between phenol-enolate/phenolate-enolate is accompanied with a minor difference between their respective absorption spectra. This excludes calculation based on the Förster cycle theory and implies absence of ESPT. The deprotonation of the enol group was estimated at pKa* = 1.5 for the phenol-enol/phenol-enolate equilibrium. This value is higher than the previously reported values (–0.5 to 0.5)[73,142]. For the phenol-keto/phenolate-keto equilibrium, the constant calculated is identical with that obtained for **5,5-Cpr-OxyLH** (pKa* = –2.6), indicating that only anionic species can be observed after photoexcitation.

5,5-Cpr-OxyLH was estimated to be the most photo-acidic compound (pKa* = –2.6) and this analogue of Oxyluciferin can be placed in the group of « super-photoacids » (pK* < 0) which can undergo deprotonation even in alcohols and some other organic solvents[151]. On the contrary, **4-MeOxyLH** has a much higher estimated pKa* = 3.4. This comparison shows that the keto-enol tautomerism on the opposite terminus of the emitter strongly affect the photoacidity of the phenol group. A similar effect could be observed for the acidity in the ground state also. For the enol-enolate equilibrium in **6′-MeOxyLH**, pKa* of 1.7 was estimated.

So far, **phenol-keto-OxyLH$_2$** has been regularly reported as blue emitter[4,142,150]. The hypothesis was mainly based on results obtained for another model compound **5,5-DMeOxyLH** in organic solvents. Due to extremely high photoacidity of this compound (pK* = -3.91)[150] the fluorescence emission of its neutral form could not be recorded in water, not even in very acidic aqueous buffered solution. The spectrum of the phenolate anion could be observed. Hirano et al. showed that the emission of **5,5-DMeOxyLH** depends on solvent polarity[12]. The results obtained in organic solvents (deprotonation is inhibited in many organic solvents, such as benzene, chloroform, acetonitrile etc.) cannot be extrapolated to very polar solution (water). Although Hirano et al. provided an insight into the emission mechanism of the **keto-OxyLH$_2$** in water by inhibiting the ionization of the 6′-OH group by methylation of **5,5-DMeOxyLH**. The product **6′-Me-5,5-DMeOxyL** was photo-unstable in aqueous solvent and the emission could only be estimated as green light (λ_{max}~535 nm). On the contrary, the derivative **6′-Me-5,5-Cpr-OxyL** is quite stable

in aqueous buffer within the pH range 5–9, and its green emission could be recorded without any difficulties. The results indicate that the **phenol-keto-OxyLH$_2$** form, which is normally identified as blue emitter in non-aqueous solutions could emit green light in a very polar and strong hydrogen acceptor/donor solvent such as water. However, similar to the case of **6′-Me-5,5-DMeOxyL**, the electronic effects should not be excluded as a possible reason for the observed spectral shift. Thus position of the emission maximum of **phenol-keto-OxyLH$_2$** in aqueous buffer becomes noteworthy.

To determine the exact excited state equilibrium (pKa*) of all chemical forms of Oxyluciferin, further interpretation of their emission spectra were required. From the interpretation of emission energies of all model compounds (in their neutral and anionic forms, wherever possible) the values for the estimated excited-state equilibrium constants could be corrected and refined. The pKa* values of all analogues were recalculated by using the Förster cycle theory and the intersection points of the mutually normalized absorption and emission spectra of the conjugated acid-base pairs presented in table 3.2. Information about the excited-state equilibrium constants can also be derived by fitting nonexponential fluorescence time-resolved decays of a conjugated acid to the numerical solution of the Debye-Smoluchowski equation[152,153]. This method, known as spherically symmetric diffusion problem (SSDP) approach, was recently successfully applied to decipher excited state equilibrium constants for various photoacids.[154] The time resolved fluorescence decay recorded at wavelength corresponds to neutral emission displays a typical bimodal character. The neutral emission quenched by ESPT (with rate constant k_{PT}) is observed as a short decay component while the long emission tail is attributed to reversible geminate recombination process (k_r). In the case of emission from **4-MeOxyLH** recorded at 450 nm (see figure 3.9), such nonexponential decay is clearly visible. The SSDP fitting procedure employed software of Krissnel and Agmon[154] calculates the rate constants of the excited state proton transfer, k_{PT} = 4.1 x10^9 s^{-1}, and geminate recombination in the excited state, k_r = 17 x10^9 Å s^{-1}. The ratio k_{PT}/k_r[151] gives pKa* = 2.0. This is in reasonable agreement with the value obtained by Förster cycle analysis. Unfortunately, the emission decays of the non-dissociated forms of the other compounds are nearly as short as our instrumental response function (~50 ps) and the SSDP approach could not be applied.

The irreversible process that takes the molecule to the ground state can be characterized by the presence of a very short component in the fluorescence decay of anionic species in acidic conditions. But this component is absent in basic solutions because the molecule is already deprotonated before the excitation (see figure 3.2 & 3.5 and table 3.1). The functional group of the photoacid decides the relative contribution of this short component throughout the decay. The time constant for **4-MeOxyLH** and **6′-MeOxyLH** are ~1.6 and 0.17 ns with relative amplitude of 11% and 42% respectively. This result shows that for the enol group, the irreversible geminate proton quenching is significantly more effective. In **OxyLH$_2$** the quenching takes place at both deprotonation sites, thus has the highest contribution from the short decay component (46%).

In scheme 3.1 ESPT mechanism involved in between enol tautomers of Oxyluciferin has been explained. Equillibrum between different chemical forms and associated quenching pathways among them have been have been explained with the help of this model rrepresentation.

***Table 3.2**: Spectroscopic parameters and equilibrium constants for firefly Oxyluciferin and its analogues in aqueous solutions*

Compound	λ_{Abs} / nm		pKa	λ_{Em} / nm		pKa*
	neutral	anion		neutral	anion	
4,6′-DMeOxyL	367	-	-	445	-	-
4-MeOxyLH	367	406	8.7	~450	560	0.9 ± 0.3
6′-MeOxyLH	371	414	7.3	~450	555	–0.3± 0.3
6′-Me-5,5-Cpr-OxyL	388	-	-	525	-	-
5,5-Cpr-OxyLH	388	482	7.8	n.d.	637	–1.0 ± 0.5
$OxyLH_2$	371	414[a] 425[b]	7.1[d] 9.0[e]	~450	539[b] 555[g] 634[c]	–0.9 ± 0.5[f] –0.5 ± 0.3[d]

[b]$OxyL^{2-}$, [c]Phenolate-keto-$OxyLH^-$, [d]Phenol-enol/phenol-enolate, [e]Phenol-enolate/phenolate-enolate, [f]Phenol-keto/phenolate-keto, [g]Phenol-enolate-$OxyLH^-$ (n.d. – not detectable).

The following table briefly represents Oxyluciferin analogue that corresponds to particular chemical form of the photo emitter with designated excitation wavelength in basic aqueous buffer.

Chemical form of Oxyluciferin	**Compound**	λ_{Exc}	λ_{Em}
Phenol-enol-$OxyLH_2$	4,6'-DMeOxyL	370	445
Phenol-keto-$OxyLH_2$	6'-Me-5,5-Cpr-OxyL	390	525
Phenolate-enolate-$OxyL^{2-}$	$OxyLH_2$	370	540
Phenol-enolate-$OxyLH^-$	6'-MeOxyLH	370	555
Phenolate-enol-$OxyLH^-$	4-MeOxyLH	383	560
Phenolate-keto-$OxyLH^-$	5,5-Cpr-OxyLH	422	637

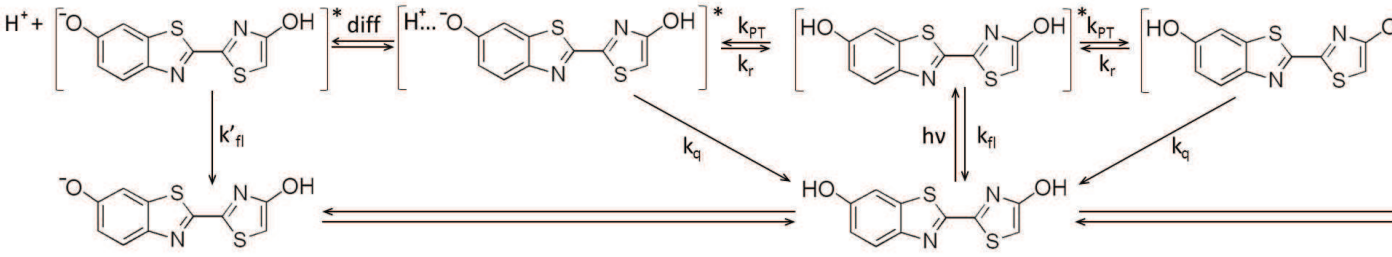

***Scheme 3.1**: ESPT mechanism for enol tautomer of Oxyluciferin*

3.6 Photoluminescence pathways of Oxyluciferin in aqueous solution

The absorption, emission spectra and fluorescence lifetimes of all model compounds of firefly Oxyluciferin in buffered aqueous solutions were studied thoroughly and their tautomeric forms and protonation states were revealed. Their excited state equilibrium constants were calculated by using Förster cycle approach.

i. we found that contrary to the previous conclusions for the blue emission from the neutral phenol-keto isomer in non-aqueous solutions, a keto-Oxyluciferin analogue (a cyclopropyl derivative) of this species is a green emitter (525 nm) in aqueous solutions;

ii. we confirmed the earlier conclusions[155] that ESPT from the enol group of the phenol-enol form is more favorable event in the excited state relative to ESPT from the phenol group;

iii. the phenol-keto form is the strongest photoacid among the isomers;

iv. the phenolate-keto ion has the lowest emission energy (634 nm);

v. the order of emission energies of the chemical forms of Oxyluciferin and global analysis of the fluorescence decay indicates that some processes in the first excited state are not likely to take place in very polar and strong hydrogen-accepting solvent, such as water. In particular, a second deprotonation at the phenol group after the enol deprotonation (i.e. deprotonation of the phenol-enolate) is not likely to occur in the excited state. Moreover, the keto-enol tautomerism reaction, observed previously in toluene in presence of a strong base,[155] is not favorable in aqueous solutions.

Finally by combining these data with previous results[6,31,43,44,49,70,137] as well as with the equilibrium constants determined in this work[48], we could propose the reactions in scheme 3.2 for the complete photoluminescence cycle of **$OxyLH_2$** in a wide pH range in buffered aqueous solution. These results could be useful to gain better insight into the firefly bioluminescence.

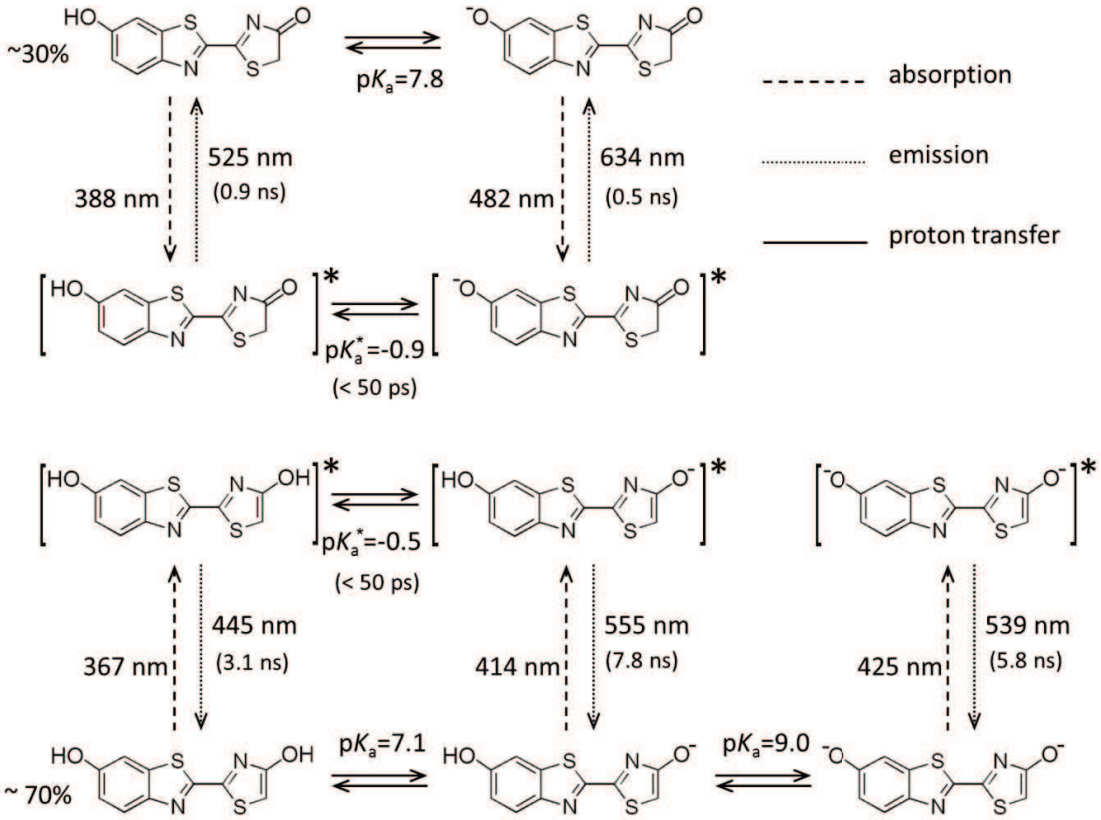

***Scheme 3.2**: Photoluminescence pathway of Oxyluciferin in aqueous solution*

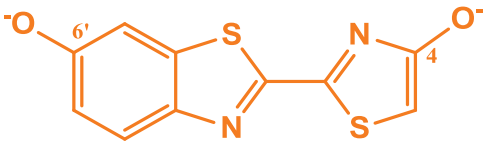

phenolate-enolate-OxyL^{2-}

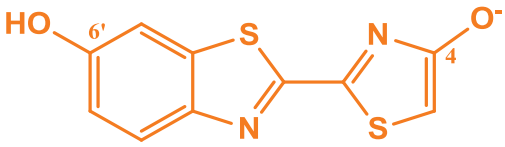

phenol-enolate-OxyLH^{-}

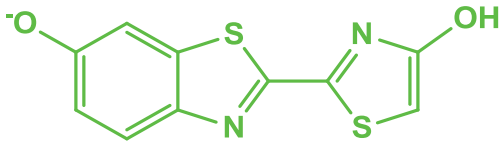

phenolate-enol-OxyLH^{-}

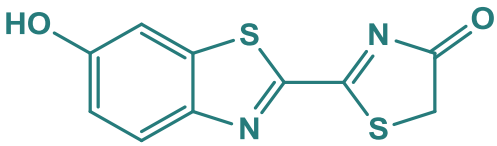

phenol-keto-OxyLH$_2$

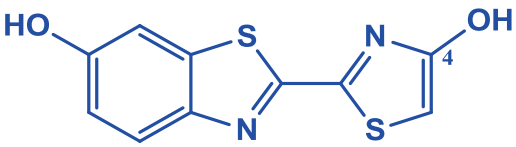

phenol-enol-OxyLH$_2$

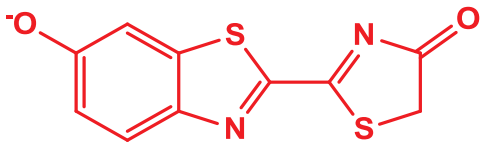

phenolate-keto-OxyLH^{-}

Appendix-A

A.1 Geminate Recombination (GR) Process[143-149]

One of the most important factor on which the excited state lifetime of photogenerated ions depends is the forward and backward proton transfer parameter. Geminate Recombination of photogenerated electron-hole pairs is an unique aspect of chemical reactivity governing the efficiency of the photophysical process. The ability of the solvent molecules to confine the photofragments, created by the photo-excitation, results in a back proton transfer reaction of the photoproducts trapped inside the solvent "cage". The time window for this process is known as Geminate Recombination. Photoinduced proton transfer from a neutral donor to a neutral acceptor in a randomly distributed system gives birth to radical pairs that are in close proximity.

The organic compounds which become more acidic upon excitation are known as « Photo-acids ». The sudden increase in acidity causes the photo-acids to dissociate in the aqueous solutions within its excited-state lifetime. A recombination anion results from this dissociation reaction. Although a less reactive weaker base in the excited state can still react with this protons. Many photoacids exhibit acid-base equilibrium in their excited state, where both proton dissociation and recombination reactions occur reversibly in the excited-state. Therefore, similar to the ground state, the acidic strength of the photoacids can be characterized by assigning an excited-state equilibrium constant (Ka*) to the proton dissociation reaction. To achieve the equilibrium in such conditions, both the proton dissociation and recombination reactions must be fast enough compared to the excited-state lifetime of the molecule.

A.2 Time resolved fluorescence decay of Oxyluciferin and its two derivatives in DMSO-H_2O system

Furthermore, to confirm ESPT involved in the emission mechanism of Oxyluciferin in DMSO/H_2O system (see section 3.2 and figure 3.1), time resolved fluorescence emission decays of **4,6'-DMeOxyL, 4-MeOxyLH** and **$OxyLH_2$** were recorded with an excitation at 376 nm in pure DMSO and 50%(v/v) DMSO at their emission maxima. Effect of solvent polarity, and presence of efficient ESPT (except for **4,6'-DMeOxyL** where ESPT is not feasible) due to polarity change is clearly visible in the decays presented in the following figure.

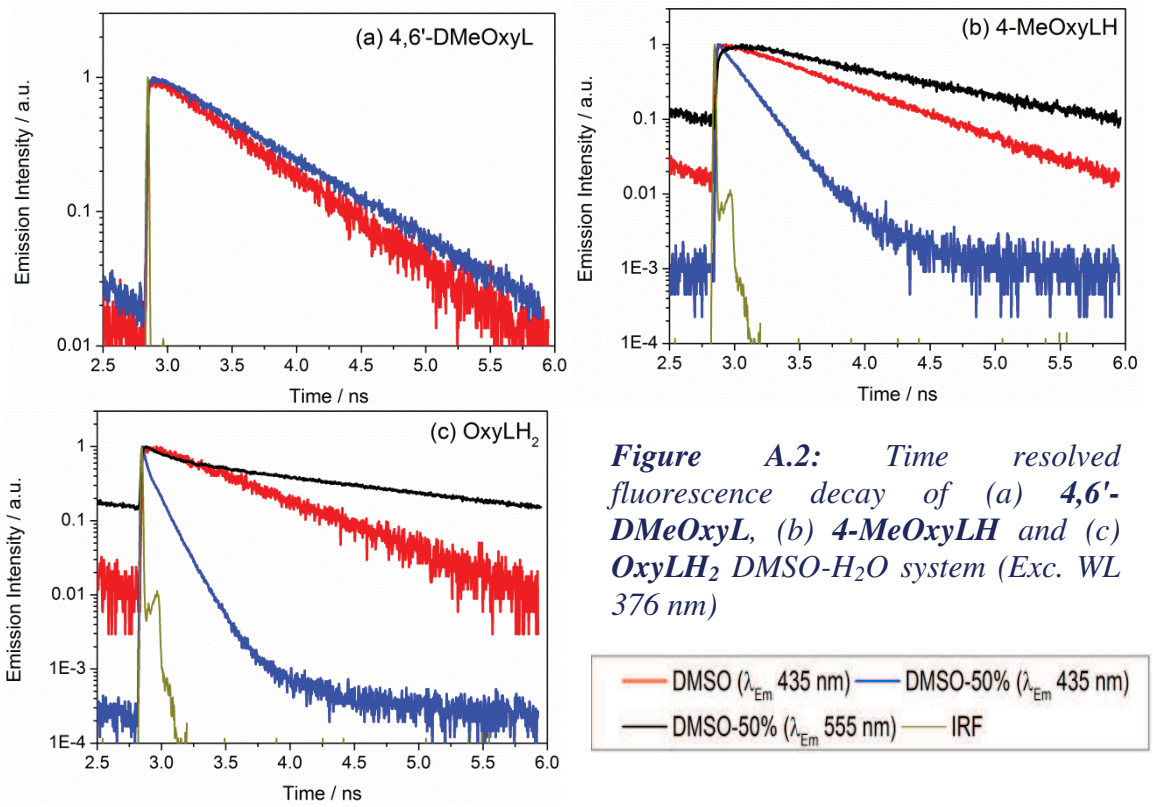

Figure A.2: *Time resolved fluorescence decay of (a)* ***4,6'-DMeOxyL****, (b)* ***4-MeOxyLH*** *and (c)* ***OxyLH$_2$*** *DMSO-H_2O system (Exc. WL 376 nm)*

A.3 Relative stability and photo-stability of keto-Oxyluciferin[48]

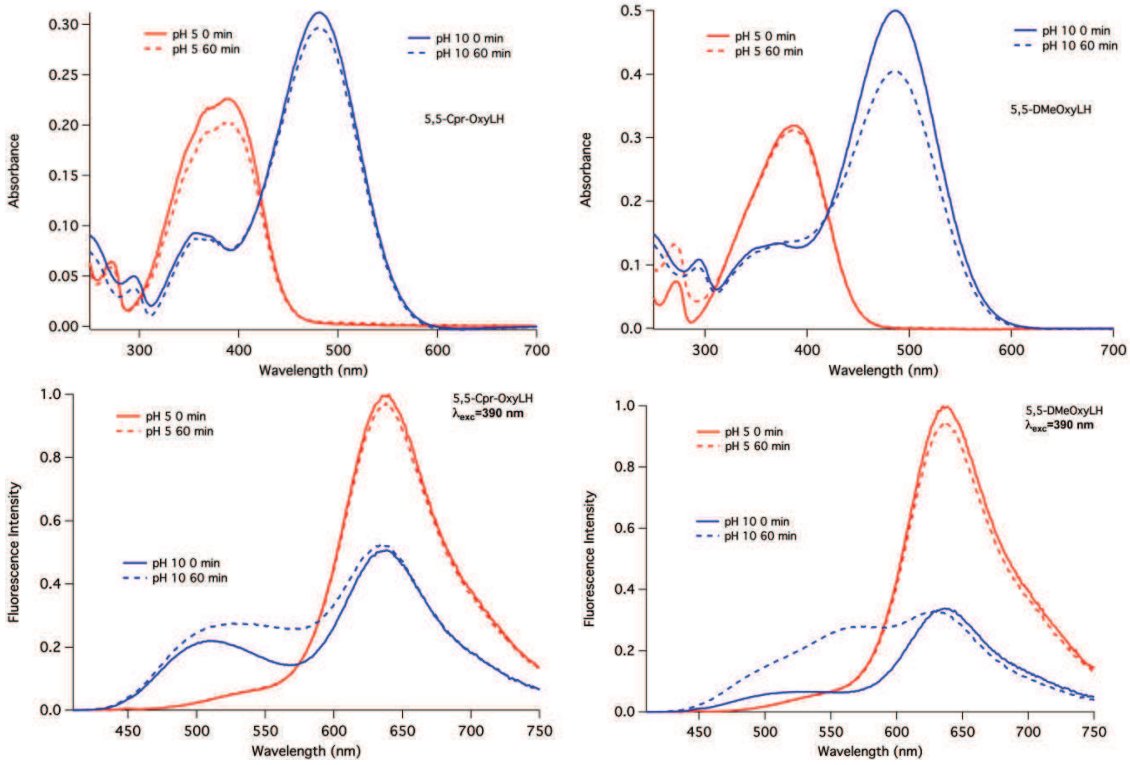

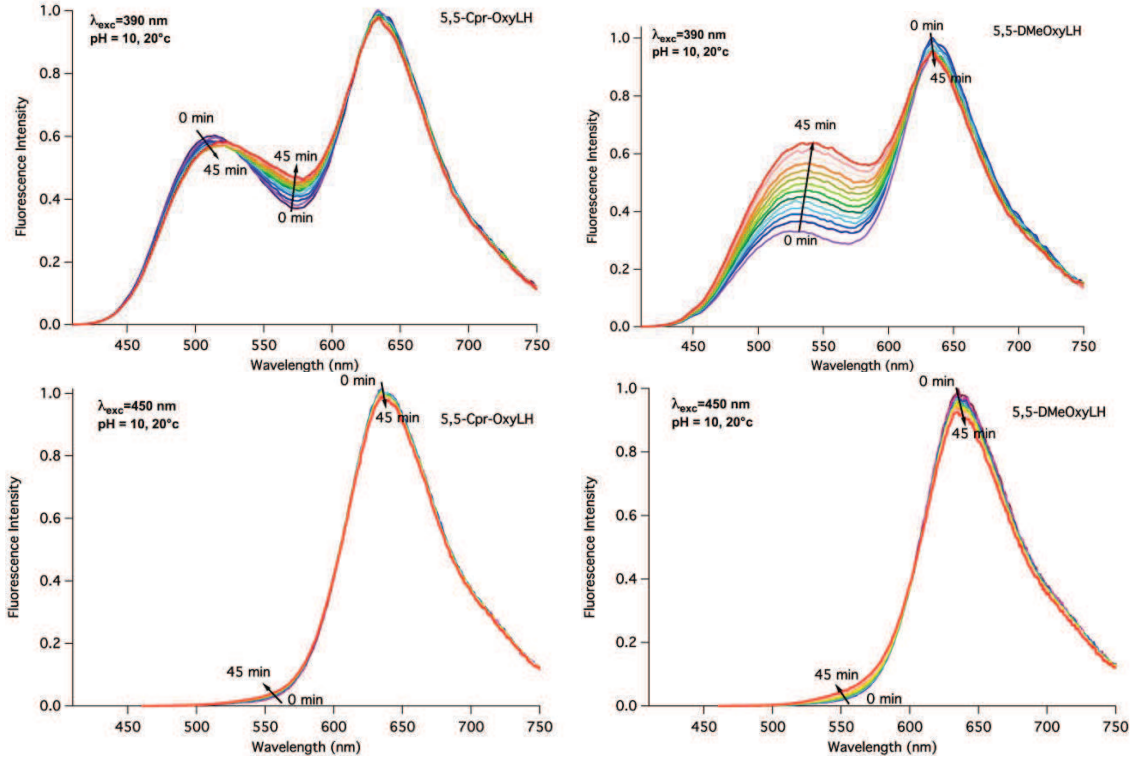

Figure A.3: *Relative stability and photo-stability of* ***5,5-Cpr-OxyLH*** *and* ***5,5-DMeOxyLH****. Row 1 and 2: absorption and emission changes measured at t=0 min and t=60 min at pH 5 and 10. Row 3 and 4: time dependent emission under continuous illumination at 390 and 450 nm measured at pH 10. All experiments were performed at T=20°C*[48]*.*

In our study we have included two derivatives which represent keto form of Oxyluciferin; **5,5-Cpr-OxyLH** and **6′-Me-5,5-Cpr-OxyL**. 5,5-disubstitution group in these two derivatives restricts the thiazole section to the keto tautomeric form. **5,5-Cpr-OxyLH**, whose phenol group is deprotonated in basic media, mimics the **phenolate-keto-OxyLH**$^-$ form and **6′-Me-5,5-Cpr-OxyL** is a model for the neutral **phenol-keto-OxyLH$_2$** form as we have already discussed before.

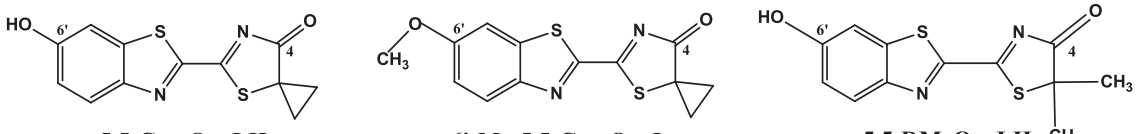

In earlier studies doubly methylated analogue **5,5-DMeOxyLH** has been considered as the model keto form[21,97,156]. However, it has been observed in our experiments that **5,5-DMeOxyLH** is poorly photostable in aqueous solutions, especially in basic conditions and under UV excitation (see figure A.3/right panel). From the pH dependent absorption and emission spectra of **5,5-Cpr-OxyLH** it could be concluded that they show better stability and photostability in aqueous buffer (see figure A.3/left panel). Therefore, these two cyclopropyl derivatives (**5,5-Cpr-OxyLH** and **6′-Me-5,5-Cpr-OxyL**) have been included in our study.

For **5,5-DMeOxyLH** and **5,5-Cpr-OxyLH** in basic conditions and under UV excitation, a new photoproduct with emission band centered at 530 nm is formed, which is likely to be assigned to dianionic species that evolves after isomerization and hydrolysis. The cyclopropyl group minimized such photoreaction and increased the global stability in the ground state and in the excited state. A minor influence of cyclopropyl group can be observed on the absorption spectrum (see figure 3.2): the existence of a shoulder about 370 nm that does not exist for **5,5-DMeOxyLH**. This shoulder can be assigned to a certain geometry constrained by the cyclopropyl group on the thiazole ring. Indeed theoretical calculations predict that the lowest excitation for **5,5-DMeOxyLH** as well as **phenol-keto-OxyLH$_2$** is a charge transfer transition (HOMO–LUMO) from phenol part to thiazole ring and that the geometry of the thiazole ring is nearly planar[29,97] without a cyclopropyl group.

Article 01

Emission Properties of Oxyluciferin and Its Derivatives in Water: Revealing the Nature of the Emissive Species in Firefly Bioluminescence

THE JOURNAL OF PHYSICAL CHEMISTRY B

Article

pubs.acs.org/JPCB

Emission Properties of Oxyluciferin and Its Derivatives in Water: Revealing the Nature of the Emissive Species in Firefly Bioluminescence

Avisek Ghose,[†,#] Mateusz Rebarz,[‡,#] Oleg V. Maltsev,[§] Lukas Hintermann,[§] Cyril Ruckebusch,[‡] Eduard Fron,[∥] Johan Hofkens,[∥] Yves Mély,[†] Panče Naumov,*[,⊥] Michel Sliwa,*[,‡] and Pascal Didier*[,†]

[†]Laboratoire de Biophotonique et Pharmacologie, UMR 7213 du CNRS, Faculté de Pharmacie, Université de Strasbourg, 74, Route du Rhin, 67401 Illkirch Cedex, France

[‡]Laboratoire de Spectrochimie Infrarouge et Raman (LASIR), CNRS UMR 8516/Université Lille Nord de France, Université Lille1 – Sciences et Technologies/Chemistry Department, bât C5/59655 Villeneuve d'Ascq Cedex, France

[§]Department Chemie, Technische Universität München, Lichtenbergstrasse 4, 85748 Garching bei München, Germany

[∥]Laboratory of Photochemistry and Spectroscopy, Department of Chemistry, KU Leuven, Celestijnenlaan 200F, 3001 Heverlee, Belgium

[⊥]New York University Abu Dhabi, P.O. Box 129188, Abu Dhabi, United Arab Emirates

Supporting Information

ABSTRACT: The first systematic steady-state and time-resolved emission study of firefly oxyluciferin (emitter in firefly bioluminescence) and its analogues in aqueous buffers provided the individual emission spectra of all chemical forms of the emitter and the excited-state equilibrium constants in strongly polar environment with strong hydrogen bonding potential. The results confirmed the earlier hypothesis that excited-state proton transfer from the enol group is favored over proton transfer from the phenol group. In water, the phenol-keto form is the strongest photoacid among the isomers and its conjugate base (phenolate-keto) has the lowest emission energy (634 nm). Furthermore, for the first time we observed green emission (525 nm) from a neutral phenol-keto isomer constrained to the keto form by cyclopropyl substitution. The order of emission energies indicates that in aqueous solution a second deprotonation at the phenol group after the enol group had dissociated (that is, deprotonation of the phenol-enolate) does not occur in the first excited state. The pH-dependent emission spectra and the time-resolved fluorescence parameters revealed that the keto-enol tautomerism reaction, which can occur in a nonpolar environment (toluene) in the presence of a base, is not favored in water.

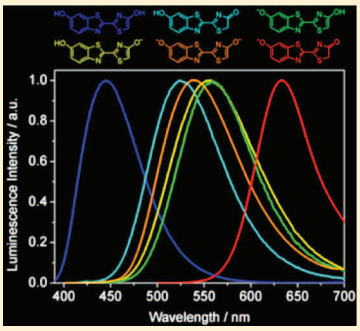

1. INTRODUCTION

1.1. Background. The phenomenon of biochemiluminescence (commonly known as bioluminescence) is a fascinating natural process by which living organisms convert chemical energy into light. Such cold-light emission from a chemically produced excited (chemiexcited) state is known for several organisms, including certain species of bacteria, beetles, squid, and worms.[1−3] In the case of fireflies, the light-generating reaction involves an enzyme (luciferase) that catalyzes oxidation of the substrate (luciferin) by molecular oxygen, in the presence of adenosine-5′-triphosphate (ATP) and Mg^{2+}, leading to formation of the emitting molecule (oxyluciferin, **OxyLH$_2$**) in its first excited state.[2,4,5] While relaxing to its ground state, **OxyLH$_2$** emits a photon in the visible part of the electromagnetic spectrum. The high luminescence quantum yield of this process[6] reflects not only a very efficient catalytic machinery, but also a highly favorable microenvironment with strongly deactivated nonradiative pathways. With its high quantum yield[6] and the exceptionally high signal-to-noise ratio due to the absence of photoexcitation, the firefly bioluminescence stands out as the best candidate of choice for bioimaging applications.[7−12]

The reaction chemistry and structure of the emitter are identical for all known beetle luciferases;[1,13] however, the emission wavelength depends on the conditions and can vary between 536 and 638 nm.[14] Despite being essential to the development of new bioanalytical tools, the chemical origin of the color modulation remains poorly understood. According to several debated photophysical mechanisms, the color modulation likely occurs as a result of intramolecular and/or intermolecular factors within the enzyme.[15] The emitter is generated by decomposition of the dioxetanone and release of CO_2 (Scheme 1). Because isolation of this highly unstable species has not been achieved yet, most spectroscopic studies

Special Issue: Photoinduced Proton Transfer in Chemistry and Biology Symposium

Received: September 4, 2014
Revised: October 29, 2014
Published: November 3, 2014

Scheme 1. Thermal Decomposition of Dioxetanone (Unstable Intermediate) to Chemiexcited Firefly Oxyluciferin and Possible Deexcitation Pathways of the Emitter

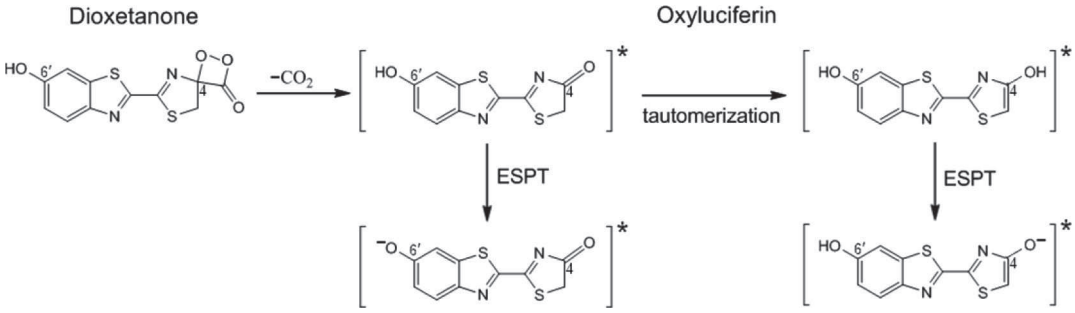

were performed by photoexcitation of either **OxyLH$_2$** alone or its complex with the enzyme in solution.[16]

Even though the complex chemistry of **OxyLH$_2$** has spurred extensive experimental[3,6,16−27] and theoretical[28−40] studies, the photophysics of this "phantom molecule" remains poorly characterized. It can exist in six different forms as a result of ionization of two hydroxyl groups and the keto-enol tautomerism of the 4-thiazolone subunit (Chart 1). The

Chart 1. Possible Ground-State Chemical Forms of Firefly Oxyluciferin in Solution

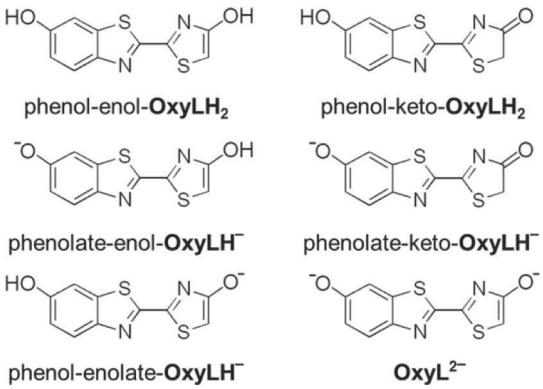

intricate triple dynamic chemical equilibrium in solution is strongly affected by the solvent, pH, and specific interactions with bases.[41−44] Moreover, the spectral properties of each chemical form could be additionally affected in the enzyme by the nature of the active site such as polarity, presence of additional ions, and $\pi-\pi$ stacking.[42,45,46] Historically, the phenolate-keto species has been considered the most viable form for the emitting state.[17,35,40] However, recent studies have shown that the enol tautomer should not be excluded as emitting species that is generated in the excited state.[42,47,48] Moreover, ultrafast spectroscopic results have indicated possible excited-state proton transfer (ESPT) from either of the two hydroxyl groups (Scheme 1).[47,49] Experimental[50] and theoretical[51] studies of the firefly luciferin (the reaction precursor) have shown that the photoluminescence pathways of this closely related molecule also depend strongly on pH and excitation wavelength.

One of the obstacles to complete understanding of the deexcitation processes is the limited information on the excited-state dynamics of the emitter in aqueous solutions. To determine the accurate ground-state equilibrium constants of **OxyLH$_2$**, we have recently applied the multivariate curve resolution−alternating least-squares (MCR-ALS) procedure and deciphered the pH-dependent spectra of model compounds where some ESPT processes or the enol-keto equilibrium are blocked.[43] The analysis provided for the first time the absorption spectra and the pH-dependent concentration profiles of the individual chemical forms of the emitter devoid from the other species. Encouraged by this result, here we apply a similar approach to investigate the *emission* spectra and equilibrium constants in the excited state for all chemical forms of **OxyLH$_2$**. These parameters have not been determined, even though they are essential for clarification of the related photophysics. We prepared five analogues of firefly oxyluciferin, including two new structural variants, 5,5-**Cpr-OxyLH** (Cpr = (spiro)cyclopropyl) and 6′-**Me**-5,5-**Cpr-OxyL** (Chart 2).[52] The

Chart 2. Derivatives of Firefly Oxyluciferin Studied in This Work

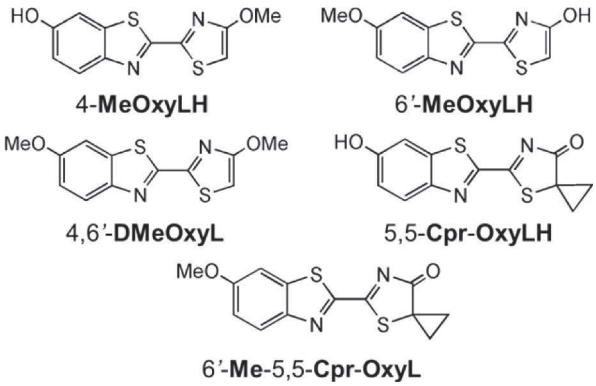

latter two compounds were used instead of the 5,5-dimethyl analogue (5,5-**DMeOxyLH**), which in our hands proved to be unstable under photoexcitation. The steady-state and time-resolved emission experiments, performed in aqueous buffered solutions within a physiologically relevant pH range, provided for the first time the individual emission spectra of all tautomeric and anionic variants of **OxyLH$_2$** as well as the equilibrium constants in the excited state. In addition, the rate constants of the fundamental photoreaction processes were also determined.

2. EXPERIMENTAL SECTION

2.1. Sample Preparation. The synthesis of **OxyLH$_2$** was performed by our improved procedure.[44] The model analogues 4-**MeOxyLH**, 6′-**MeOxyLH**, and 4,6′-**DMeOxyL** were synthesized as previously reported.[43] The synthesis and characterization of the new spirocyclic analogues 5,5-**Cpr-OxyLH** and 6′-**Me**-5,5-**Cpr-OxyL** will be reported elsewhere. Stock

dx.doi.org/10.1021/jp508905m | J. Phys. Chem. B 2015, 119, 2638−2649

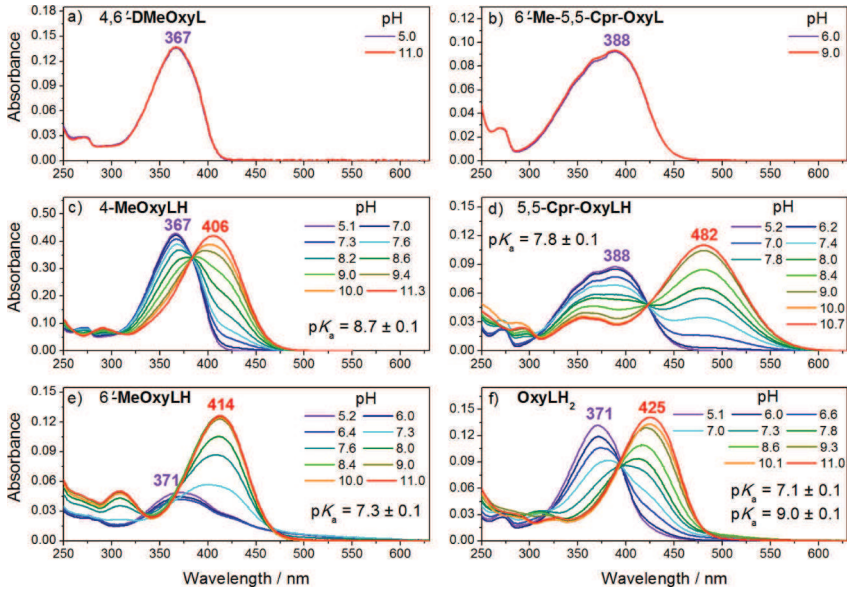

Figure 1. Dependence of the absorption spectra of firefly oxyluciferin (**OxyLH$_2$**) and its derivatives in aqueous solutions at different pH and determination of the corresponding pK_a values. The structural formulas are given in Chart 2. The spectra were recorded in aqueous buffers at different pH (see section 2.1) at 20 °C. The concentration was 0.9, 6.0, 4.0, 1.0, 1.1, and 3.0 μM for 4,6′-**DMeOxyL**, 4-**MeOxyLH**, 6′-**MeOxyLH**, 6′-**Me**-5,5-**Cpr**-**OxyL**, 5,5-**Cpr**-**OxyLH**, and **OxyLH$_2$**, respectively.

solutions of all compounds were prepared in spectroscopic grade DMSO (Sigma-Aldrich) and stored in several aliquots at −20 °C to minimize the freeze−thaw cycle. They were further diluted 1000-fold to a final concentration of about a few μM in aqueous buffer with different pH. The buffers were prepared by diluting a 1 M stock solution in deionized, Millipore-purified water (18.2 MΩ). Buffered stock solutions were prepared as follows: 75 mM NaCl/20 mM KH_2PO_4/0.2 mM $MgCl_2$ for pH ≤ 7.0 and 75 mM NaCl/25 mM Tris(hydroxymethyl)-aminomethane (TRIS)/0.2 mM $MgCl_2$ for pH > 7.0. The buffer was separated into several fractions, and their pH (error ±0.02) was adjusted by 250 mM HCl or by 250 mM NaOH separately at 20 °C (ΔpH ≈ 0.25). Separate buffers at different pH were used in all spectral measurements.

2.2. Spectroscopy. Absorption spectra were recorded with a Cary-4000 spectrometer (Agilent Technologies). Steady-state fluorescence spectra were recorded with Fluorolog 3 spectrofluorometer (Horiba Jobin Yvon) with 3 nm excitation/emission slit and corrected for the instrumental response characteristics. The absolute quantum yield determined for three selected compounds in phosphate buffered solution (Bio Whittaker) at pH 7.4 and 20 °C was 0.49 ± 0.05 for 4,6′-**DMeOxyL**, 0.65 ± 0.07 for 4-**MeOxyLH**, and 0.19 ± 0.02 for 5,5-**Cpr**-**OxyLH**. These compounds were selected as references because they exhibit distinct emission band centered at 445, 560, and 637 nm, respectively. The fluorescence quantum yields of the other compounds were determined by the comparative method, using the equation $\Phi_S = \Phi_R \cdot (I_S/I_R) \cdot (OD_R/OD_S) \cdot (n_S^2/n_R^2)$.[53]

The fluorescence decays of all compounds were measured by the time-correlated single photon counting (TCSPC) technique. Excitation pulse was provided by a femtosecond Ti:sapphire laser (Coherent Chameleon Ultra II, 80 MHz, 200 fs, 3.8 W) coupled to either a pulse picker (4 MHz) and a harmonic generator (SHG/THG, APE) for excitation from 300 to 500 nm, or an intracavity frequency doubled OPO (APE) and a pulse picker (4 MHz) for 500 to 700 nm excitation. The measurements of fluorescence lifetimes were performed using the FT200 Picoquant spectrometer. The emission was collected through a polarizer set at the magic angle and a Czerny-Turner type monochromator, computer-controlled for the selection of wavelength detection. The single-photon events were collected by a cooled microchannel plate photomultiplier tube R3809U (Hamamatsu) and recorded by a PicoHarp 300 TCSPC system (PicoQuant). The instrumental response function was recorded using colloidal silica (Ludox), and its full width at half-maximum was ∼50 ps. All decays were collected until the number of events reached 10^4 at the maximum. The recorded decays were analyzed by the FluoFit software package version 4.6.6 (PicoQuant). The reduced χ^2 was below 1.1. Weighted residuals and autocorrelation function were used to check the quality of the fits. In the case of nonexponential decays, the stretched exponential model was used to estimate the time constants.

3. RESULTS AND DISCUSSION

3.1. Selection of Model Compounds and Their pH-Dependent Absorption Spectra. The photochemistry of **OxyLH$_2$** in aqueous solution is quite complex because of its triple equilibrium (ionization of both hydroxyl groups and keto-enol tautomerization of the thiazole moiety). Similar to the strategy of selective blocking of either hydroxyl group employed earlier,[42,43,54] we chose to study five compounds that model different tautomeric and anionic variants of **OxyLH$_2$** (Chart 2). Specifically, 4,6′-**DMeOxyL** is a model for the phenol-enol-**OxyLH$_2$** form, whereas 4-**MeOxyLH** and 6′-**MeOxyLH** are analogous to the phenolate-enol-**OxyLH$^-$** and phenol-enolate-**OxyLH$^-$** forms that are normally generated in basic conditions. We also included in the analysis two derivatives in which the 5,5-disubstitution pattern restricts the thiazole portion to the keto tautomeric form; 5,5-**Cpr**-**OxyLH**, whose phenol group is deprotonated in basic media, mimics the phenolate-keto-**OxyLH$^-$** form, while 6′-**Me**-5,5-**Cpr**-**OxyLH** is a model for the neutral phenol-keto-**OxyLH$_2$** form. Notably,

dx.doi.org/10.1021/jp508905m | J. Phys. Chem. B 2015, 119, 2638−2649

previous studies have relied on the doubly methylated analogue, 5,5-**DMeOxyLH**, to model the keto form.[45,54,55] However, our experiments indicated that this compound is not stable and in fact, it is very photounstable (an important parameter for our studies) in aqueous solutions, especially in basic conditions and under UV excitation. Instead, we used cyclopropyl derivatives, 5,5-**Cpr-OxyLH** and 6′-**Me**-5,5-**Cpr-OxyL** (Chart 2), which exhibit significantly better stability and photostability, as it was concluded from the comparison of pH-dependent absorption and emission spectra between 5,5-**Cpr-OxyLH** and 5,5-**DMeOxyLH** (see Figure S1 in the Supporting Information, SI). For 5,5-**DMeOxyLH** and 5,5-**Cpr-OxyLH** in basic conditions and under UV excitation, a new photoproduct with emission band at 530 nm is formed, which is assigned to dianionic species (see section 3.4) that evolves after isomerization and hydrolysis. The cyclopropyl group minimized such photoreaction and increased the global stability in the ground state and in the excited state. A minor influence of cyclopropyl group can be observed on the absorption spectrum (Figure 1b,d, and SI Figure S1): the existence of a shoulder about 370 nm that does not exist for 5,5-**DMeOxyLH**. This shoulder is assigned to a certain geometry constrained by the cyclopropyl group on the thiazole ring. Indeed theoretical calculations predict that the lowest excitation for 5,5-**DMeOxyLH** as well as phenol-keto-**OxyLH$_2$** is a charge transfer transition (HOMO−LUMO) from phenol part to thiazole ring and that the geometry of the thiazole ring is nearly planar[37,45] without a cyclopropyl group.

The interpretation of the emission spectra required characterization of the composition, concentration, and absorbance spectra of **OxyLH$_2$** and its derivatives in the pH range 5−11. The pH-dependent steady-state absorption spectra are presented in Figure 1. The molecules that are constrained to only two chemical forms (5,5-**Cpr-OxyLH** and 4-**MeOxyLH**) present clear isosbestic points. The spectrum of 5,5-**Cpr-OxyLH** (Figure, 1d) indicates that the spectral maximum of the phenolate ion of the keto form is strongly red-shifted (482 nm) relative to the neutral form (388 nm). The pK_a = 7.8 is identical to and confirms the value previously determined for 5,5-**DMeOxyLH**.[43]

However, extraction of the pure spectra of the species that evolve from 6′-**MeOxyLH** and **OxyLH$_2$** was not straightforward and required a multiset-data analysis of the pH-dependent absorption spectra of **OxyLH$_2$** and its derivatives. Following the previously described approach,[43] we used here different buffers (see the Experimental Section) together with the new cyclopropyl derivatives to evaluate eventual effects of the buffer on the spectra. Application of such analysis (SI Figure S2) afforded the pH-dependent concentration profiles and the absorption spectra of the individual chemical forms at various pH (Figure 2). In line with earlier results,[43] the spectral maxima of the chemical forms are aligned in the following order (Figure 6 and Figure S2, SI): phenol-enol-**OxyLH$_2$** (367 nm) < phenol-keto-**OxyLH$_2$** (388 nm) < phenolate-enol-**OxyLH$^-$** (406 nm) < phenol-enolate-**OxyLH$^-$** (414 nm) < **OxyL^{2-}** (425 nm) < phenolate-keto-**OxyLH$^-$** (482 nm). The distribution diagram (Figure 2) shows that the contribution of the phenolate-enol-**OxyLH$^-$** form is negligible due to the significantly higher pK_a value of the phenol (pK_a = 9.0) relative to the enol (pK_a = 7.1) group. In practice, the presence of this species in solutions of **OxyLH$_2$** can be ignored.

The pK_a values determined in TRIS buffer are slightly lower than those in phosphate buffer.[43] In particular, the phenol-

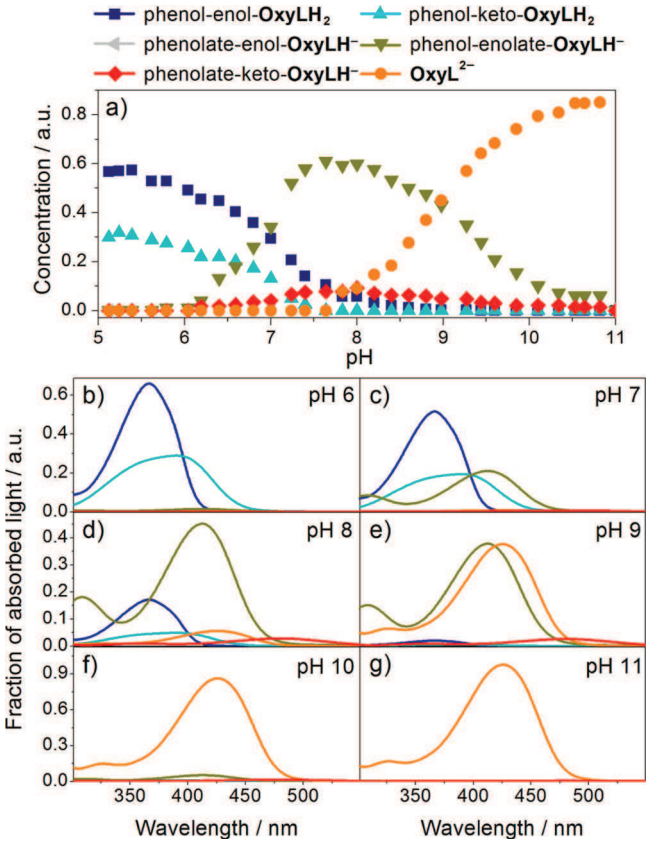

Figure 2. Absorption spectra and pH-concentration profiles of five forms of firefly oxyluciferin obtained by MCR-ALS analysis. The concentration of the phenolate-enol-**OxyLH$^-$** form under these conditions is negligible.

phenolate equilibrium for 4-**MeOxyLH** is lower by 0.2 pK units, whereas the pK_a constants for **OxyLH$_2$** are lowered by 0.3 units for the phenol-enol/phenol-enolate and 0.1 units for the phenol-enolate/phenolate-enolate equilibrium, respectively. Apparently, the chemical equilibria of **OxyLH$_2$** and its derivatives are slightly sensitive to the ionic strength of the buffer. Finally, the combination of the concentration profiles and absorption spectra allows us to determine the absorption contribution of each individual component at a given pH value (Figure 2a). In turn, it is possible to precisely select the excitation wavelength to preferentially excite a particular chemical form of the emitter. For instance, at pH 8−9 (Figure, 2d and 2e) it is possible to selectively excite the phenolate-keto-**OxyLH$^-$** form (SI Figure S7) and to study its photodynamics without significant contribution from the other forms.

The ground-state equilibria and the absorption spectra of the conjugated acids and bases set the basis for the estimation of the corresponding equilibrium constants in the excited state (pK_a*) by means of the Förster cycle.[53,56] Although this method can only provide a qualitative estimate, it can be used for assignment of the emissive species in the excited state (vide infra). With an estimated pK_a* = −2.6, the most photoacidic of the studied compounds is 5,5-**Cpr-OxyLH**. This value places this derivative in the group of "super-photoacids" (pK* < 0) which undergo deprotonation even in alcohols and some other organic solvents.[57] On the other hand, 4-**MeOxyLH** has a much higher pK_a* value, estimated to 3.4. The comparison of these values shows that the photoacidity of the phenol group is strongly affected by the keto-enol tautomerism on the opposite

dx.doi.org/10.1021/jp508905m | J. Phys. Chem. B 2015, 119, 2638−2649

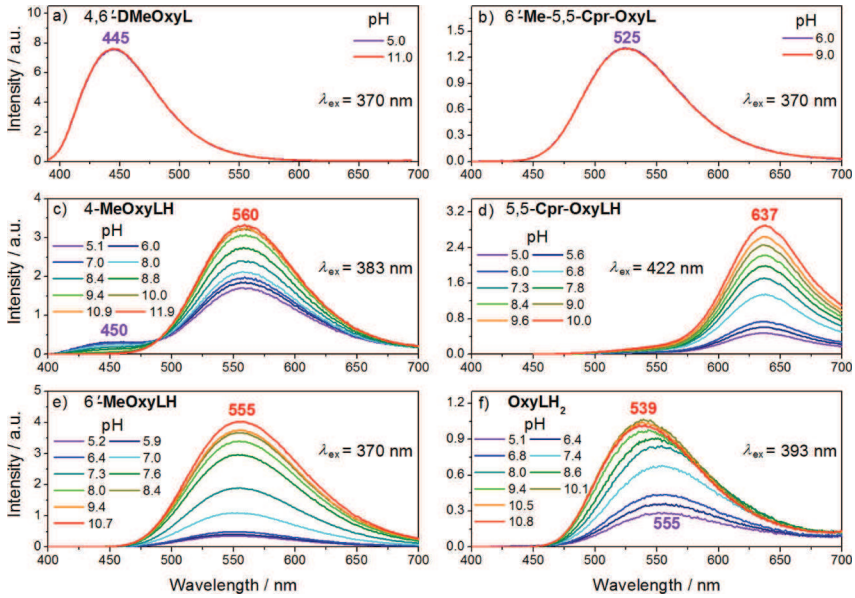

Figure 3. Emission spectra of firefly oxyluciferin (**OxyLH$_2$**) and its derivatives recorded in aqueous solutions at different pH. The chemical formulas are given in Chart 2. Measurements were performed at room temperature (20 °C) in aqueous buffers at different pH (see section 2.1) and the concentration was 0.9, 6, 4, 1, 1.1, and 3 μM for 4,6′-**DMeOxyL**, 4-**MeOxyLH**, 6′-**MeOxyLH**, 6′-**Me**-5,5-**Cpr-OxyL**, 5,5-**Cpr-OxyLH**, and **OxyLH$_2$**, respectively.

Table 1. Time-Resolved and Fluorescence Quantum Yield Fluorescence Data for Firefly Oxyluciferin and Its Derivatives (Chart 2) in Aqueous Solutions[a]

	neutral emission				anionic emission					
compound	pH	λ_{ex}/nm	λ_{em}/nm	τ/ns	pH	λ_{ex}/nm	λ_{em}/nm	τ/ns (%)		Φ_{Fl}
4,6′-**DMeOxyL**	5−11	370	450	3.10			-			0.49
4-**MeOxyLH**	5	370	450	0.24[b]	5	370	560	0.21[c]		0.32
								1.47 (11)		
								4.86 (89)		
					10	430	560	4.88		0.47
6′-**Me**-5,5-**Cpr-OxyL**	5−9	390	525	0.93			-			0.11
5,5-**Cpr-OxyLH**	5	390	525	<0.05[b]	5	390	640	0.16 (25)		0.18
								0.61 (75)		
					10	520	640	0.63		0.26
6′-**MeOxyLH**	5	370	450	<0.05[b]	5	370	550	0.17 (42)		0.18
								0.78 (32)		
								7.88 (26)		
					10	430	550	7.97		0.35
OxyLH$_2$	5	370	450	<0.05[b]	5	370	550	0.16 (52)	**0.17 (50)**	0.15
								1.04 (8)	**0.48 (7)**	
								7.63 (40)	**7.82 (43)**	
						370	640	0.16 (12)	**0.17 (41)**	
								0.56 (80)	**0.48 (49)**	
								7.28 (8)	**7.82 (10)**	
					7.6	430	550	0.17 (32)	**0.17 (17)**	0.35
								0.53 (19)	**0.48 (7)**	
								3.95 (6)	**5.80 (19)**	
								7.68 (43)	**7.82 (55)**	
						510	640	0.41	**0.17 (2)**	
									0.48 (98)	
					10	430	540	5.91	**5.80**	0.50

[a]The constants for **OxyLH$_2$** obtained by using the global analysis method for all the decay are highlighted in boldface font. [b]Short component of nonexponential decay. [c]Time constant of the growing part.

terminus of the emitter. A similar effect was observed for the acidity in the ground state. For the enol-enolate equilibrium in 6′-**MeOxyLH**, we estimate a pK_a* value of 1.7.

In the case of **OxyLH$_2$***, five equilibria should be considered: phenol-enol/phenol-enolate, phenol-enolate/phenolate-enolate, phenol-enol/phenolate-enol, phenolate-enol/phenolate-

dx.doi.org/10.1021/jp508905m | J. Phys. Chem. B 2015, 119, 2638−2649

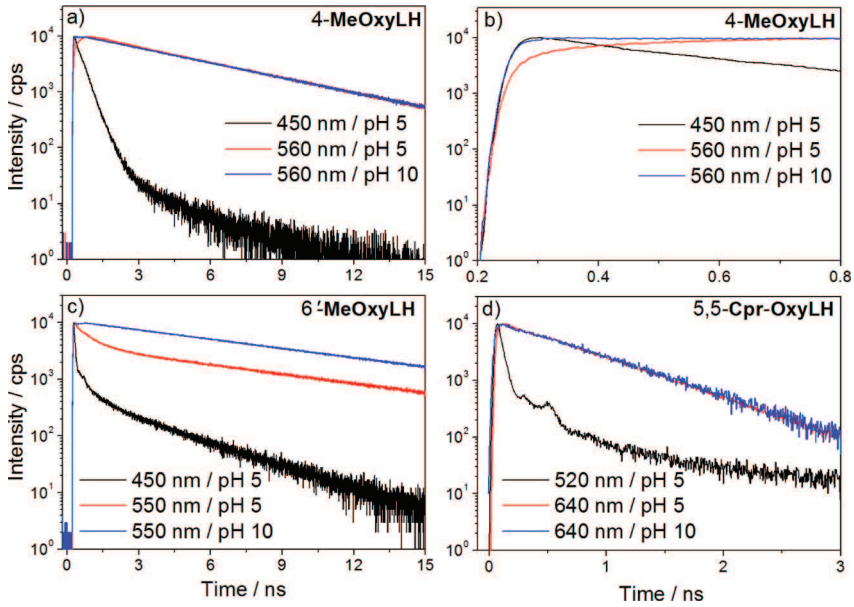

Figure 4. Fluorescence decays of derivatives of firefly oxyluciferin measured in acidic and basic buffered aqueous solutions. The chemical formulas are given in Chart 2.

enolate and phenol-keto/phenolate-keto. In the ground state, where the enol group is more acidic than the phenol group (pK_a = 7.1 versus pK_a = 9.0), the pathway including phenol-enol/phenolate-enol deprotonation (this is confirmed in section 3.4, where the phenol group has a lower photoacidity than the enol one in phenol-enol form, Table 2) and subsequent phenolate-enol/phenolate-enolate deprotonation can be excluded from consideration. Moreover, the equilibrium phenol-enolate/phenolate-enolate is accompanied by a minor difference between the respective absorption spectra, which gives a pK_a* of 7.5 and implies absence of ESPT in acidic and neutral conditions. The deprotonation of the enol group gives an estimated pK_a* of 1.5 for the phenol-enol/phenol-enolate equilibrium (note that this value is higher than the previously reported values, between −0.5 and 0.5,[49,58] and should be corrected with the emission spectra; see section 3.4). For the phenol-keto/phenolate-keto equilibrium, the calculated constant is identical to that obtained for 5,5-**Cpr-OxyLH** (pK_a* = −2.6), indicating that only anionic species will be observed after photoexcitation.

3.2. Emission Spectra of the Nonionizable Model Compounds. The fluorescence spectra of 4,6′-**DMeOxyL** and 6′-**Me**-5,5-**Cpr-OxyL** recorded in buffered aqueous solutions are presented in Figure 3a and 3b, and the corresponding fluorescence decays are deposited as SI Figure S3. As expected from the absence of acidic groups, the position and shape of their spectra as well as the total fluorescence quantum yield and fluorescence lifetimes do not evolve with pH in the studied range (Figure 3, Table 1). 4,6′-**DMeOxyL** exhibits a single broad band with a maximum at 445 nm, in good agreement with the emission assigned to the neutral phenol-enol-**OxyLH$_2$** form (450−455 nm).[54,58] The fluorescence quantum yield of this compound was 49%, and the emission decayed monoexponentially with a lifetime of 3.1 ns. On the other hand, the emission maximum of 6′-**Me**-5,5-**Cpr-OxyL**, an analogue of the phenol-keto-**OxyLH$_2$** form, was significantly red-shifted from that of the phenol-enol-**OxyLH$_2$** model (4,6′-**DMeOxyL**) counterpart, with a maximum at 525 nm and monoexponential decay with a time constant of 0.9 ns. This lifetime shortening could be attributed to increased contribution from nonradiative pathways due to the smaller energy gap.

The position of the emission maximum of 6′-**Me**-5,5-**Cpr-OxyL** is noteworthy because phenol-keto-**OxyLH$_2$** has so far been regularly reported as a blue emitter.[42,55,58] That assignment was based mainly on results obtained for the model compound 5,5-**DMeOxyLH** in organic solvents. Due to the very high photoacidity of this compound (pK* = −3.91),[55] the emission of its neutral form cannot be recorded in water, even in quite acidic solution, and only the spectrum of the phenolate anion is observed. The deprotonation is inhibited in many organic solvents, such as benzene, chloroform, and acetonitrile. However, Hirano et al. showed that the emission of 5,5-**DMeOxyLH** depends on polarity.[45] Hence, the results obtained in organic solvents cannot be merely extrapolated to very polar solution (water). The same authors provided insight into the emission of the keto-**OxyLH$_2$** form in water by blocking the ionization of the 6′-OH group by methylation of 5,5-**DMeOxyLH.** However, the product (6′-**Me-5,5-DMeOxyL**) was unstable, and the emission could only be estimated as green light (∼535 nm). By contrast, the derivative studied here 6′-**Me**-5,5-**Cpr-OxyL** is stable in water within the pH range 5−9, and its green emission could be recorded without difficulties. This result indicates that the phenol-keto-**OxyLH$_2$** form, normally identified in nonaqueous solutions as a blue emitter, could emit green light in very polar and strong hydrogen acceptor solvent such as water. However, similar to the case of 6′-**Me**-5,5-**DMeOxyL**,[45] the electronic effects could not be excluded[42] as a possible reason for the observed shift.

3.3. Emission Spectra of the Ionizable Model Compounds. The fluorescence spectra of 4-**MeOxyLH**, 5,5-**Cpr-OxyLH**, and 6′-**MeOxyLH** recorded in aqueous solutions within the pH range 5−11 are presented in Figure 3. The spectra of 4-**MeOxyLH** and 5,5-**Cpr-OxyLH** were recorded at an excitation wavelength that corresponds to the isosbestic points of 383 and 422 nm (Figure 1a and 1b). 5,5-**Cpr-OxyLH** was always irradiated in the visible region. Excitation to higher excited states leads to the formation of a new photoproduct that has a characteristic specific emission at 530 nm, which was

dx.doi.org/10.1021/jp508905m | J. Phys. Chem. B 2015, 119, 2638−2649

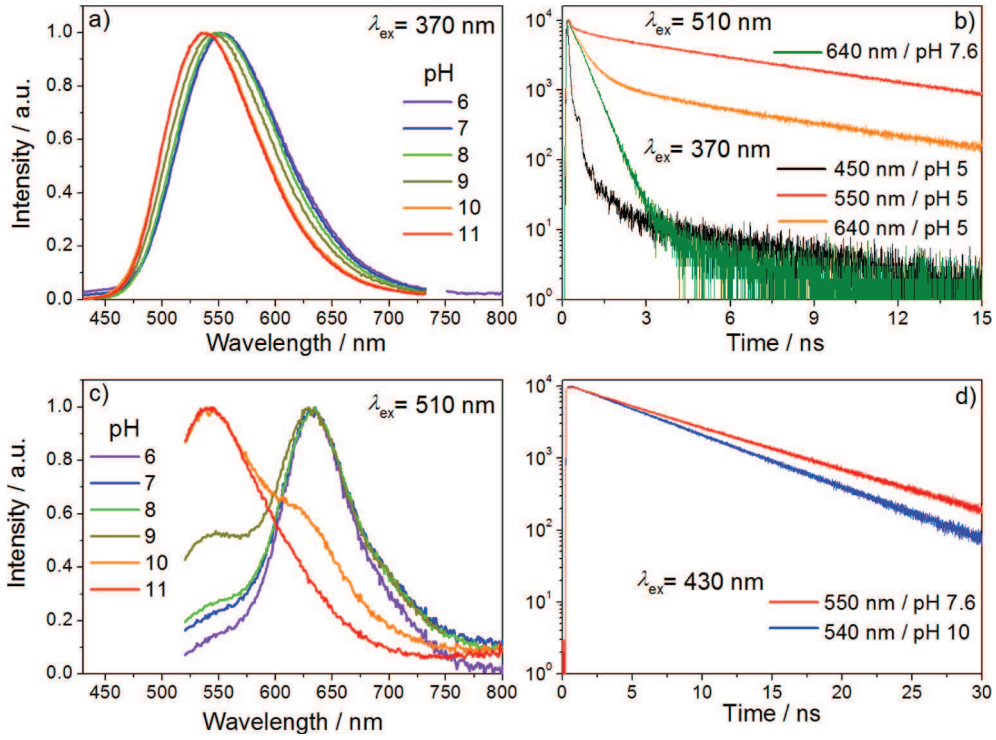

Figure 5. Normalized emission spectra of firefly oxyluciferin in aqueous solution at different pH and excitation wavelengths.

particularly pronounced in basic conditions for UV excitation (SI Figure S1). 6′-**MeOxyLH** was excited at 370 nm where the absorption was least sensitive to pH.

The spectra of 4-**MeOxyLH** in acidic solutions are composed of two bands (Figure 3c). At the lowest studied pH (5) the strong band centered at 560 nm from the ion is accompanied by a weaker band at ∼450 nm from the neutral form, in accordance with the spectrum of 4,6′-**DMeOxyL**. This assignment is supported by the time-resolved fluorescence decays recorded in acidic solution (pH 5). As shown in Figure 4a, by excitation of the neutral form (absorption at 370 nm), the emission band at 450 nm is strongly quenched and decays nonexponentially. Simultaneously, the fluorescence band at 560 nm rises (Figure 4a) with a time constant corresponding to proton transfer rate and disappears biexponentially with lifetimes 1.5 and 4.9 ns (Figure 4, Table 1), where the first component corresponds to geminate proton quenching (SI Figure S6). In agreement with a pK_a* value of about 3.4 (see section 3.1), the 450 nm band completely vanishes in basic solution where only the deprotonated excited state contributes to the emission (Figure 3c). At pH 10, the deprotonation occurs already in the ground state so that growing of the luminescence and, expectedly, geminate recombination was not observed. The emission at 560 nm was thus characterized by a monoexponential decay with a time constant identical to that of the longer component (4.9 ns) measured at pH 5 (Table 1). Thus, the spectrum recorded at high pH establishes a viable model for the fluorescence signature of the phenolate-enol-**OxyLH**$^-$ form.

To obtain the spectral signature of the phenolate-keto-**OxyLH**$^-$ form, we examined the spectra of 5,5-**Cpr-OxyLH**. In contrast to 4-**MeOxyLH**, the shape and position of the spectra did not evolve with pH, and only one band with a maximum at 637 nm was observed (Figure 3d). This result can be explained by the much higher photoacidity of this compound, which undergoes very efficient ESPT throughout the whole pH range studied here. The fluorescence decay recorded at 520 nm, corresponding to the neutral form keto-**OxyLH$_2$**, reveals a bimodal process (Figure 4d) with the short component corresponding to the instrumental response function (IRF) of the setup (<50 ps). Thus, ESPT from the phenol group is a very fast process, and only emission from the deprotonated form of the molecule could be observed with steady-state spectroscopy. The maximum at 637 nm is in very good agreement with the data reported previously for the phenolate-keto emission based on the 5,5-**DMeOxyLH** derivative.[45,55] It is worthy of note that deexcitation of the phenolate-keto anion exhibits a time constant τ = 0.6 ns and is several times faster than the corresponding phenolate-enol form (τ = 4.9 ns; compare with the data in Figure 4a and Table 1). As mentioned above, the weak emission and the long tail at 530 nm at basic pH are due to photodegradation and should not be taken into account when the spectra of the phenolate-keto form are considered.

To obtain insight into the emission properties of phenol-enolate-**OxyLH**$^-$, we turned to 6′-**MeOxyLH**, where the dissociation of the phenol group is blocked. This derivative exhibits a broad intense emission at ∼550 nm (Figure 3e). The strong photoacidity that was qualitatively evaluated above indicates that in the studied pH range, the emission of 6′-**MeOxyLH** originates mainly from the enolate ion. Indeed, the fluorescence decay recorded at 450 nm has a nonexponential character with IRF signature at short time scale (Figure 4c), confirming the very fast and efficient ESPT from the enol group. However, it is already known from the absorption spectra[43] that this compound can exist as a mixture with ∼30% keto form at pH = 5. As a consequence, the contribution of this tautomer (exclusively in the neutral form due to blocked phenol deprotonation) to the emission spectra of 6′-**MeOxyLH** cannot be excluded, especially at acidic pHs. Indeed, thorough

dx.doi.org/10.1021/jp508905m | J. Phys. Chem. B 2015, 119, 2638−2649

analysis of the pH-dependent spectra (Figure 3e) reveals a small blue shift of the spectrum from 555 nm at pH 11 to 550 nm at pH 5. This energy change could be explained by superposition of two broad and strongly overlapping components in the spectrum recorded in acidic medium: a minor component that corresponds to the neutral keto tautomer that emits at ∼525 nm (compare with 6′-**Me**-5,5-**Cpr**-**OxyL**) and a major component that originates from the enolate anion, with a maximum at 555 nm. At higher pH, the first species is depleted, and at basic pH only emission from the pure enolate form could be observed.

To support this interpretation, we recorded the emission spectrum of 6′-**MeOxyLH** at pH 5 after excitation at 430 nm (SI Figure S4). Under these conditions, the excitation of the keto tautomer is strongly favored because of the superior absorption coefficient relative to the other species.[43] Its contribution to the emission in the resultant spectrum was more pronounced, and the blue shift of the maximum toward 535 nm became more apparent. Moreover, the presence of the keto tautomer was also manifested in the time-resolved fluorescence. The decay recorded in acidic solution at 550 nm was multiexponential with time constants of 0.17, 0.8, and 7.9 ns (Figure 4 and Table 1). The first value is attributed to geminate quenching. The second component corresponds well to the lifetime of 6′-**Me**-5,5-**Cpr**-**OxyL** (0.9 ns, compare with the data in Table 1). At pH 10 the decay recorded at 550 nm was monoexponential with time constant ∼8 ns. This result shows that the keto tautomer is not present in basic solution, and the spectra recorded under such conditions correspond to emission from the phenol-enolate-**OxyLH**$^-$.

3.4. Emission Spectra of Oxyluciferin (OxyLH$_2$). The presence of five chemical forms strongly complicates the accurate spectral characterization of the pH-dependent emission of the real emitter (**OxyLH$_2$**), which also is the most intricate part of the analysis. To decipher the individual contributions, the fluorescence spectra of **OxyLH$_2$** were recorded at three different excitation wavelengths, UV excitation at 370 nm, and visible excitation at 430 and 510 nm (Figure 5). The selective photoexcitation greatly facilitated the interpretation of the spectra. The relative absorption intensities of the six chemical forms of **OxyLH$_2$** at selected pH are listed in Figure 2.

Excitation at 370 nm. In acidic conditions (pH < 8), the dominant species excited at 370 nm are phenol-enol-**OxyLH$_2$** and phenol-keto-**OxyLH$_2$** (Figure 2b,c). Assuming strong photoacidity in the excited state for enol group for phenol-enol form (pK_a* is higher for enol than for phenol comparing results obtained for 6′-**MeOxyLH** and 4-**MeOxyLH**, Table 2) and for phenol group for phenol-keto form, we can conclude that the first species should be deprotonated to phenol-enolate-**OxyLH**$^-$, whereas the second should be deprotonated to phenolate-keto-**OxyLH**$^-$. The efficient ESPT from the enol group is clearly visible in the time-resolved curve recorded at wavelength corresponding to the phenol-enol-**OxyLH$_2$** form (450 nm). The recorded decay indicates that the emission from the neutral form is strongly quenched and the proton transfer time constant is <50 ps (instrument response function) (Figure 5b, Table 1). Erez et al. evaluated this value to 45 ps.[49] Taking into account the possible deprotonation of the phenol group, the fluorescence spectrum measured under such conditions should contain contributions from both species. In line with our expectations, a dominant contribution comes from the phenol-enolate-**OxyLH**$^-$ form (555 nm) because of its higher abundance and higher fluorescence quantum yield relative to phenolate-keto-**OxyLH**$^-$ (637 nm). Moreover, the contribution of this last species is clearly seen from the long wavelength tail of the recorded spectrum that extends beyond 600 nm (compare with the emission of 6′-**MeOxyLH** in Figure 3e).

In addition to geminate recombination, at pH 5 the fluorescence decay recorded at 640 nm clearly shows two species with fluorescence time constants ∼0.5 ns and ∼7.3 ns. The former value is fully in line with the lifetime of the phenolate-keto-**OxyLH**$^-$ form determined by consideration of 5,5-**Cpr**-**OxyLH** (see section 3.3), whereas the latter is in good agreement with the fluorescence lifetime of phenol-enolate-**OxyLH**$^-$ (7.9 ns; Table 1) determined for 6′-**MeOxyLH**. By increase of pH, the contribution from the keto tautomer becomes marginal and the most abundant species are phenol-enolate-**OxyLH**$^-$ and **OxyL**$^{2-}$ (Figure 2d and 2e). As a result, the observed emission spectra are slightly blue-shifted and are attributed to a mixture of monoanionic and dianionic form. The emission of the dianion becomes dominant for pH > 9 due to negligible concentration of other species in the ground state (Figure 2f,g). Therefore, the spectrum recorded at pH = 11 with maximum at 539 nm can be assigned to **OxyL**$^{2-}$. This emission is blue-shifted compared to that of the monodeprotonated form (phenol-enolate-**OxyLH**$^-$) and also has a shorter lifetime, ∼5.9 ns (Table 1).

Excitation with Visible Light. Photoexcitation at lower energy leads to different photoluminescence pathways. In acidic solutions (pH 6 and 7) after 510 nm excitation, the major absorbing species is the phenolate-keto-**OxyLH**$^-$ form (SI Figure S7). Thus, the emission spectrum after 510 nm excitation is dominated by the phenolate-keto-**OxyLH**$^-$ form and features a band at 634 nm, which is slightly blue-shifted when compared to the 637 nm band of 5,5-**Cpr**-**OxyLH** in basic solution. The fluorescence decay at 640 nm is nearly monoexponential with a lifetime of 0.4 ns (Figure 5b, Table 1), indicating that the phenolate-keto-**OxyLH**$^-$ is the dominant species. At pH 8 and 9, a shoulder around 540 nm appears from **OxyL**$^{2-}$, in line with a pH-dependent increasing abundance of this species due to deprotonation of phenol-enolate-**OxyLH**$^-$ in the ground state. The emission decay at pH 7.6 after excitation at 430 nm detected at 550 nm shows a mixture of all species (Figure 5d, Table 1) and by comparison with excitation at 510 nm, phenolate-keto (0.53 ns), **OxyL**$^{2-}$ (3.95 ns) and phenol-enolate-**OxyLH**$^-$ (7.68 ns). At pH 10, the intensity of the red band decreases considerably in favor of the green emission from **OxyL**$^{2-}$ (∼540 nm), which becomes dominant at pH 11 with a lifetime of 5.91 ns.

The above analysis provides arguments for assigning the emission spectra of the individual chemical forms of firefly **OxyLH$_2$**, plotted in Figure 6. Interestingly, the order of emission energies does not exactly reflect the order of the absorption energies (Table 2). The order of emission energies is phenol-enol-**OxyLH$_2$** (445 nm) > phenol-keto-**OxyLH$_2$** (525 nm) > phenolate-enolate-**OxyL**$^{2-}$ (539 nm) > phenol-enolate-**OxyLH**$^-$ (555 nm) > phenolate-enol-**OxyLH**$^-$ (560 nm) > phenolate-keto-**OxyLH**$^-$ (634 nm). Furthermore, for **OxyLH$_2$** the decay luminescence analysis shows that in excited state only three species (phenol-enolate, phenolate-keto, and phenolate-enolate) are observed with one decay for geminate recombination (0.17 ns) without any ESPT growing signal. This is in line with the results that the enol group in the phenol-enol form (phenol group has higher pK_a*, Table 2) and the phenol group in the phenol-keto form are strong photoacids.

dx.doi.org/10.1021/jp508905m | J. Phys. Chem. B 2015, 119, 2638−2649

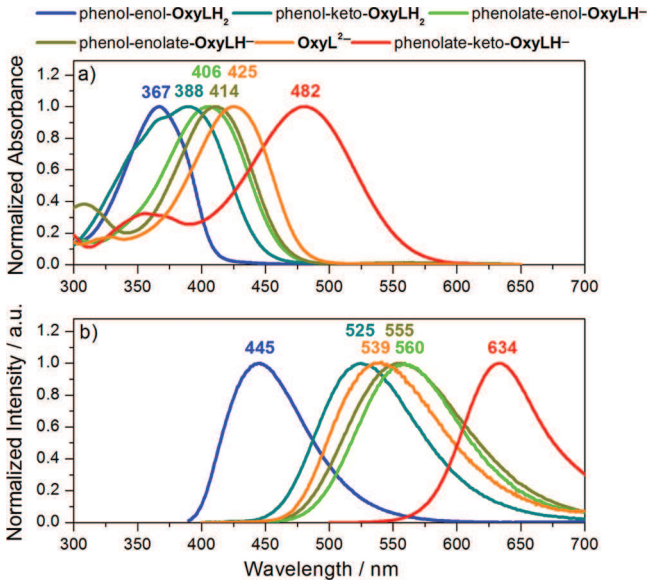

Figure 6. Absorption (top panel) and emission (bottom panel) spectra of individual chemical forms of firefly oxyluciferin based on the MCR-ALS procedure.

Accordingly, in addition to single wavelength lifetime analysis, a global decay analysis with four time constants was performed, one for each species and one for geminate recombination (Table 1) to arrive at more precise values for the phenol-enolate (7.82 ns), phenolate-keto (0.48 ns) and phenolate-enolate (5.80 ns) forms. At different excitation wavelengths and pH range, no growing signals were found in water contrary to time-resolved spectra in toluene,[47] which were indicative of isomerization or ionization from the phenolate-keto form or the phenol-enolate form to the phenolate-enolate form. This is in agreement with the order of emission energies of the phenolate-keto and phenol-enolate forms (adding to that, monoionic species were reported to be more stable in the ground state than dianionic species[37]), which seem to prevent conversion in the first excited state to phenolate-enolate form because they are at lower energy.

3.5. Equilibria and Photodynamics in the Excited State. Having determined the emission energies of all model compounds in their neutral and (wherever possible) anionic forms, the values for the estimated excited-state equilibrium constants (see section 3.1) can be corrected and refined. The pK_a* values recalculated by using the Förster cycle theory and the intersection points of the mutually normalized absorption and emission spectra of the conjugated acid−base pairs are presented in Table 2. Information about the excited-state equilibrium constants can also be derived from fitting nonexponential fluorescence decays of a conjugated acid to the numerical solution of the Debye−Smoluchowski equation. This method, known as the spherically symmetric diffusion problem (SSDP) approach, was recently successfully applied to various photoacids.[59]

The fluorescence decay at the wavelength corresponding to the neutral emitter band typically displays a bimodal character. The short decay component corresponds to emission from the neutral emitter quenched by ESPT (with rate constant k_{PT}), whereas the long tail is attributed to the reversible geminate recombination process (k_r) (SI Figure S6). Such nonexponential decay is clearly visible in the emission from 4-**MeOxyLH** recorded at 450 nm (Figure 4a). The fitting procedure

Table 2. Spectroscopic Parameters and Equilibrium Constants for Firefly Oxyluciferin and Its Analogues in Aqueous Solutions

	λ_{abs}/nm			λ_{em}/nm		
compound	neutral	anion	pK_a	neutral	anion	pK_a*
4,6′-**DMeOxyL**	367	-	-	445	-	-
4-**MeOxyLH**	367	406	8.7	∼450	560	0.9 ± 0.3
6′-**MeOxyLH**	371	414	7.3	∼450	555	−0.3 ± 0.3
6′-**Me**-5,5-**Cpr-OxyL**	388	-	-	525	-	-
5,5-**Cpr-OxyLH**	388	482	7.8	n.d.[a]	637	−1.0 ± 0.5
OxyLH$_2$	371	414[b]	7.1[e]	∼450	539[c]	−0.9 ± 0.5[g]
					555[b]	−0.5 ± 0.3[e]
		425[c]	9.0[f]			1.2 ± 0.3[h]
					634[d]	7.5 ± 0.3[f]

[a]n.d. = not detectable. [b]Phenol-enolate-**OxyLH**$^-$. [c]**OxyL**$^{2-}$. [d]Phenolate-keto-**OxyLH**$^-$. [e]Phenol-enol/phenol-enolate. [f]Phenol-enolate/phenolate-enolate. [g]Phenol-keto/phenolate-keto. [h]Phenol-enol/phenolate-enol.

employed by using the SSDP software of Krissnel and Agmon[59] provided the rate constants of the proton transfer, $k_{PT} = 4.1 \times 10^9$ s^{-1}, and geminate recombination in the excited state, $k_r = 17 \times 10^9$ Å s^{-1}. The ratio k_{PT}/k_r[57] gives pK_a* = 2.0, in reasonable agreement with the value obtained by Förster cycle analysis. Unfortunately, the emission decays of the non-dissociated forms of the other compounds are nearly as short as our instrumental response (∼50 ps), and the SSDP approach could not be applied.

In contrast to the reversible recombination, the irreversible process takes the molecule to the ground state with rate constant k_q (SI Figure S6). This process is characterized by the presence of a short component in the fluorescence decay of anionic species in acidic conditions. This component is absent in basic solutions because the molecule is deprotonated before excitation (Figure 4b, Table 1). Interestingly, the relative contribution of this short component throughout the decay depends on the functional group of the photoacid. 4-**MeOxyLH** exhibits a time constant ∼1.5 ns with relative amplitude of 11%, whereas 6′-**MeOxyLH** has a component of 0.17 ns with an amplitude of 42%. This result indicates that the irreversible geminate proton quenching is significantly more effective for the enol group. **OxyLH$_2$** has the highest contribution from the short decay component (52%) because the quenching takes place at both deprotonation sites.

5. CONCLUSIONS

A combination of model compounds with thorough study of the pH-dependent steady-state and time-resolved fluorescence spectra revealed, for the first time, the emission spectra and luminescence lifetimes for all tautomeric forms and protonation states of firefly oxyluciferin in TRIS-buffered aqueous solutions. Using the Förster cycle approach, the excited-state equilibrium constants were also calculated. The most important conclusions from this study are as follows:

(1) Unlike some previous observations[42] with blue emission from the neutral phenol-keto isomer in nonaqueous solutions, we found a keto-oxyluciferin analogue (a cyclopropyl derivative) which is a green emitter (525 nm) in aqueous solution.

dx.doi.org/10.1021/jp508905m | J. Phys. Chem. B 2015, 119, 2638−2649

Scheme 2. Photoluminescence Pathways of Oxyluciferin in Aqueous Solution

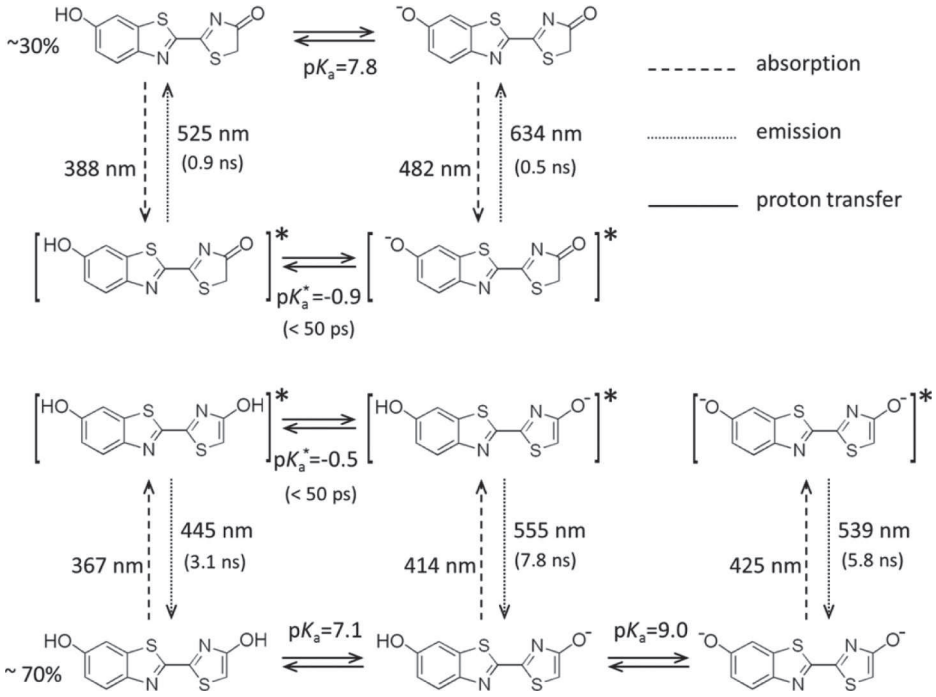

(2) We confirmed earlier conclusions[47] that ESPT from the enol group of the phenol-enol form is more favorable in the excited state than ESPT from the phenol group.
(3) The phenol-keto form is the strongest photoacid among the isomers.
(4) The phenolate-keto ion has the lowest emission energy (634 nm).
(5) The order of emission energies of the chemical forms of oxyluciferin and global analysis of the fluorescence decay indicates that some processes in the first excited state are not likely to take place in strongly polar environment with strong hydrogen bonding potential, such as water. In particular, a second deprotonation at the phenol group after the enol deprotonation (i.e., deprotonation of the phenol-enolate) is not likely to occur in the excited state. Moreover, the keto-enol tautomerism reaction, observed previously in toluene in the presence of a strong base,[47] is not favorable in water.

Finally by combining these data with our previous results as well as with the equilibrium constants determined in this work, we can propose Scheme 2 for the complete photoluminescence cycle of **$OxyLH_2$** in a wide pH range in buffered aqueous solution. These results could be useful to gain better insight into the firefly bioluminescence. Indeed although these results do not directly apply to the luciferase where the active site is considered to be of low polarity, they provide support to the hypothesis that the excited-state potential energy surface and the related dynamics are affected by the environment of the active site.

■ ASSOCIATED CONTENT

Supporting Information

Stability, absorption, emission and time-resolved fluorescence decays data for oxyluciferin and its analogues. This material is available free of charge via the Internet at http://pubs.acs.org.

■ AUTHOR INFORMATION

Corresponding Authors

*E-mail: pascal.didier@unistra.fr (P.D.).
*E-mail: michel.sliwa@univ-lille1.fr (M.S.).
*E-mail: pance.naumov@nyu.edu (P.N.).

Author Contributions

#These authors contributed equally to this study. The manuscript was written through contributions of all authors. All authors have given approval to the final version of the manuscript.

Notes

The authors declare no competing financial interest.

■ ACKNOWLEDGMENTS

This work was financially supported by the Human Frontier Science Program (project RGY0081/2011, "Excited-State Structure of the Emitter and Color-Tuning Mechanism of the Firefly Bioluminescence"). We also acknowledge financial support from the PICS CNRS-FWO Fund and New York University Abu Dhabi. Authors are thankful to Gilles Ulrich UMR 7515-ECPM-CNRS for providing facilities to measure absolute quantum yield of reference derivatives.

■ REFERENCES

(1) Shimomura, O. *Bioluminescence: Chemical Principles and Methods*; World Scientific: Singapore, 2012.
(2) McCapra, F. Chemical mechanisms in bioluminescence. *Acc. Chem. Res.* **1976**, *9*, 201−208.
(3) Branchini, B. R.; Southworth, T. L.; Murtiashaw, M. H.; Magyar, R. A.; Gonzalez, S. A.; Ruggiero, M. C.; Stroh, J. G. An Alternative Mechanism of Bioluminescence Color Determination in Firefly Luciferase. *Biochemistry* **2004**, *43*, 7255−7262.
(4) Suzuki, N.; Goto, T. Studies on Firefly Bioluminescence. III. Synthesis of 4-Thiazolone Derivatives Related to Firefly Oxyluciferin. *Agric. Biol. Chem.* **1972**, *36*, 2213−2221.
(5) White, E. H.; Rapaport, E.; Seliger, H. H.; Hopkins, T. A. The chemi- and bioluminescence of firefly luciferin: An efficient chemical

production of electronically excited states. *Bioorg. Chem.* **1971**, *1*, 92−122.
(6) Ando, Y.; Niwa, K.; Yamada, N.; Enomot, T.; Irie, T.; Kubota, H.; Ohmiya, Y.; Akiyama, H. Firefly bioluminescence quantum yield and colour change by pH-sensitive green emission. *Nat. Photonics* **2008**, *2*, 44−47.
(7) Greer, L. F.; Szalay, A. A. Imaging of light emission from the expression of luciferases in living cells and organisms: A review. *Luminescence* **2002**, *17*, 43−74.
(8) Griffiths, M. W. The role of ATP bioluminescence in the food industry. *Food Technol.* **1996**, *50*, 62−73.
(9) Kricka, L. J. Application of bioluminescence and chemiluminescence in biomedical sciences. *Methods Enzymol.* **2000**, *305*, 333−345.
(10) Ohkuma, H.; Abe, K.; Kosaka, Y.; Maeda, M. Detection of luciferase having two kinds of luminescent colour based on optical filter procedure: Application to an enzyme immunoassay. *Luminescence* **2000**, *15*, 21−27.
(11) Shinde, R.; Perkins, J.; Contag, C. H. Luciferin derivatives for enhanced in vitro and in vivo bioluminescence assays. *Biochemistry* **2006**, *45*, 11103−11112.
(12) Sun, Y.-Q.; Liu, J.; Wang, P.; Zhang, J.; Guo, W. D-Luciferin Analogues: A Multicolor Toolbox for Bioluminescence Imaging. *Angew. Chem., Int. Ed.* **2012**, *51*, 8428−8430.
(13) Ugarova, N. N. Interaction of firefly luciferase with substrates and their analogs: A study using fluorescence spectroscopy methods. *Photochem. Photobiol. Sci.* **2008**, *7*, 218−227.
(14) Ugarova, N. N.; Brovko, L. Y. Protein structure and bioluminescent spectra for firefly bioluminescence. *Luminescence* **2002**, *17*, 321−330.
(15) Hosseinkhani, S. Molecular enigma of multicolor bioluminescence of firefly luciferase. *Cell. Mol. Life Sci.* **2011**, *68*, 1167−1182.
(16) Wang, Y.; Hayamizu, Y.; Akiyama, H. Spectroscopic Study of Firefly Oxyluciferin in an Enzymatic Environment on the Basis of Stability Monitoring. *J. Phys. Chem. B* **2014**, *118*, 2070−2076.
(17) Branchini, B. R.; Murtiashaw, M. H.; Magyar, R. A.; Portier, N. C.; Ruggiero, M. C.; Stroh, J. G. Yellow-Green and Red Firefly Bioluminescence from 5,5-Dimethyloxyluciferin. *J. Am. Chem. Soc.* **2002**, *124*, 2112−2113.
(18) Branchini, B. R.; Rosenberg, J. C.; Ablamsky, D. M.; Taylor, K. P.; Southworth, T. L.; Linder, S. J. Sequential bioluminescence resonance energy transfer−fluorescence resonance energy transfer-based ratiometric protease assays with fusion proteins of firefly luciferase and red fluorescent protein. *Anal. Biochem.* **2011**, *414*, 239−245.
(19) Gandelman, O. A.; Brovko, L. Y.; Chikishev, A. Y.; Shkurinov, A. P.; Ugarova, N. N. Investigation of the interaction between firefly luciferase and oxyluciferin or its analogues by steady state and subnanosecond time-resolved fluorescence. *J. Photochem. Photobiol., B* **1994**, *22*, 203−209.
(20) Gandelman, O. A.; Brovko, L. Y.; Ugarova, N. N.; Shchegolev, A. A. The Bioluminescent System of Fireflies - Investigation of the Interaction of the Reaction-Product, Oxyluciferin, and its Analogs with Luciferase by Methods of Fluorescence Spectroscopy. *Biochemistry (Moscow)* **1990**, *55*, 785−789.
(21) Min, K.-L.; Steghens, J.-P. The Emitting Species Dissociated from the Enzyme Can Emit the Light in *Photinus pyralis* Luciferase System. *Biochem. Biophys. Res. Commun.* **1999**, *265*, 273−278.
(22) Nakatsu, T.; Ichiyama, S.; Hiratake, J.; Saldanha, A.; Kobashi, N.; Sakata, K.; Kato, H. Structural basis for the spectral difference in luciferase bioluminescence. *Nature* **2006**, *440*, 372−376.
(23) Niwa, K.; Ichino, Y.; Kumata, S.; Nakajima, Y.; Hiraishi, Y.; Kato, D.-i.; Viviani, V. R.; Ohmiya, Y. Quantum Yields and Kinetics of the Firefly Bioluminescence Reaction of Beetle Luciferases. *Photochem. Photobiol.* **2010**, *86*, 1046−1049.
(24) Ugarova, N. N.; Maloshenok, L. G.; Uporov, I. V.; Koksharov, M. I. Bioluminescence Spectra of Native and Mutant Firefly Luciferases as a Function of pH. *Biochemistry (Moscow)* **2005**, *70*, 1262−1267.
(25) Viviani, V. R.; Arnoldi, F. G. C.; Neto, A. J. S.; Oehlmeyer, T. L.; Bechara, E. J. H.; Ohmiya, Y. The structural origin and biological function of pH-sensitivity in firefly luciferases. *Photochem. Photobiol. Sci.* **2008**, *7*, 159−169.
(26) Wang, Y.; Akiyama, H.; Terakado, K.; Nakatsu, T. Impact of Site-Directed Mutant Luciferase on Quantitative Green and Orange/Red Emission Intensities in Firefly Bioluminescence. *Sci. Rep.* **2013**, *3*, 2490.
(27) Yanagisawa, Y.; Kageyama, T.; Wada, N.; Tanaka, M.; Ohno, S.-y. Time Courses and Time-Resolved Spectra of Firefly Bioluminescence Initiated by Two Methods of ATP Injection and Photolysis of Caged ATP. *Photochem. Photobiol.* **2013**, *89*, 1490−1496.
(28) Anselmi, M.; Marocchi, S.; Aschi, M.; Amadei, A. Theoretical modeling of the spectroscopic absorption properties of luciferin and oxyluciferin: A critical comparison with recent experimental studies. *Chem. Phys.* **2012**, *392*, 205−214.
(29) Chen, S.-F.; Liu, Y.-J.; Navizet, I.; Ferré, N.; Fang, W.-H.; Lindh, R. Systematic Theoretical Investigation on the Light Emitter of Firefly. *J. Chem. Theory Comput.* **2011**, *7*, 798−803.
(30) Pinto da Silva, L.; Esteves da Silva, J. C. G. Computational Studies of the Luciferase Light-Emitting Product: Oxyluciferin. *J. Chem. Theory Comput.* **2011**, *7*, 809−817.
(31) Hiyama, M.; Akiyama, H.; Wang, Y.; Koga, N. Theoretical study for absorption spectra of oxyluciferin in aqueous solutions. *Chem. Phys. Lett.* **2013**, *577*, 121−126.
(32) Kim, H. W.; Rhee, Y. M. On the pH Dependent Behavior of the Firefly Bioluminescence: Protein Dynamics and Water Content in the Active Pocket. *J. Phys. Chem. B* **2013**, *117*, 7260−7269.
(33) Li, Z.-w.; Ren, A.-m.; Guo, J.-f.; Yang, T.; Goddard, J. D.; Feng, J.-k. Color-Tuning Mechanism in Firefly Luminescence: Theoretical Studies on Fluorescence of Oxyluciferin in Aqueous Solution Using Time Dependent Density Functional Theory. *J. Phys. Chem. A* **2008**, *112*, 9796−9800.
(34) Nakatani, N.; Hasegawa, J.-Y.; Nakatsuji, H. Red Light in Chemiluminescence and Yellow-Green Light in Bioluminescence: Color-Tuning Mechanism of Firefly, *Photinus pyralis*, Studied by the Symmetry-Adapted Cluster−Configuration Interaction Method. *J. Am. Chem. Soc.* **2007**, *129*, 8756−8765.
(35) Navizet, I.; Liu, Y.-J.; Ferré, N.; Xiao, H.-Y.; Fang, W.-H.; Lindh, R. Color-Tuning Mechanism of Firefly Investigated by Multi-Configurational Perturbation Method. *J. Am. Chem. Soc.* **2010**, *132*, 706−712.
(36) Navizet, I.; Roca-Sanjuán, D.; Yue, L.; Liu, Y.-J.; Ferré, N.; Lindh, R. Are the Bio- and Chemiluminescence States of the Firefly Oxyluciferin the Same as the Fluorescence State? *Photochem. Photobiol.* **2013**, *89*, 319−325.
(37) Orlova, G.; Goddard, J. D.; Brovko, L. Y. Theoretical Study of the Amazing Firefly Bioluminescence: The Formation and Structures of the Light Emitters. *J. Am. Chem. Soc.* **2003**, *125*, 6962−6971.
(38) Pinto da Silva, L.; Esteves da Silva, J. C. G. Computational Investigation of the Effect of pH on the Color of Firefly Bioluminescence by DFT. *ChemPhysChem* **2011**, *12*, 951−960.
(39) Ren, A.-M.; Guo, J.-F.; Feng, J.-K.; Zou, L.-Y.; Li, Z.-W.; Goddard, J. D. TDDFT Study of the Electronic Structure, Absorption and Emission Spectra of the Light Emitters of the Amazing Firefly Bioluminescence and Solvation Effects on the Spectra. *Chin. J. Chem.* **2008**, *26*, 55−64.
(40) Song, C.-I.; Rhee, Y. M. Dynamics on the Electronically Excited State Surface of the Bioluminescent Firefly Luciferase−Oxyluciferin System. *J. Am. Chem. Soc.* **2011**, *133*, 12040−12049.
(41) Naumov, P.; Kochunnoonny, M. Spectral−Structural Effects of the Keto−Enol−Enolate and Phenol−Phenolate Equilibria of Oxyluciferin. *J. Am. Chem. Soc.* **2010**, *132*, 11566−11579.
(42) Naumov, P.; Ozawa, Y.; Ohkubo, K.; Fukuzumi, S. Structure and Spectroscopy of Oxyluciferin, the Light Emitter of the Firefly Bioluminescence. *J. Am. Chem. Soc.* **2009**, *131*, 11590−11605.

(43) Rebarz, M.; Kukovec, B. M.; Maltsev, O. V.; Ruckebusch, C.; Hintermann, L.; Naumov, P.; Sliwa, M. Deciphering the protonation and tautomeric equilibria of firefly oxyluciferin by molecular engineering and multivariate curve resolution. *Chem. Sci.* **2013**, *4*, 3803−3809.
(44) Maltsev, O. V.; Nath, N. K.; Naumov, P.; Hintermann, L. Why is firefly oxyluciferin a notoriously labile substance? *Angew. Chem., Int. Ed.* **2014**, *53*, 847−850.
(45) Hirano, T.; Hasumi, Y.; Ohtsuka, K.; Maki, S.; Niwa, H.; Yamaji, M.; Hashizume, D. Spectroscopic Studies of the Light-Color Modulation Mechanism of Firefly (Beetle) Bioluminescence. *J. Am. Chem. Soc.* **2009**, *131*, 2385−2396.
(46) Wang, Y.; Kubota, H.; Yamada, N.; Irie, T.; Akiyama, H. Quantum Yields and Quantitative Spectra of Firefly Bioluminescence with Various Bivalent Metal Ions. *Photochem. Photobiol.* **2011**, *87*, 846−852.
(47) Solntsev, K. M.; Laptenok, S. P.; Naumov, P. Photoinduced Dynamics of Oxyluciferin Analogues: Unusual Enol "Super"photoacidity and Evidence for Keto−Enol Isomerization. *J. Am. Chem. Soc.* **2012**, *134*, 16452−16455.
(48) Sundlov, J. A.; Fontaine, D. M.; Southworth, T. L.; Branchini, B. R.; Gulick, A. M. Crystal Structure of Firefly Luciferase in a Second Catalytic Conformation Supports a Domain Alternation Mechanism. *Biochemistry* **2012**, *51*, 6493−6495.
(49) Erez, Y.; Presiado, I.; Gepshtein, R.; Pinto da Silva, L.; Esteves da Silva, J. C. G.; Huppert, D. Comparative Study of the Photoprotolytic Reactions of d-Luciferin and Oxyluciferin. *J. Phys. Chem. A* **2012**, *116*, 7452−7461.
(50) Ando, Y.; Akiyama, H. pH-Dependent Fluorescence Spectra, Lifetimes, and Quantum Yields of Firefly-Luciferin Aqueous Solutions Studied by Selective-Excitation Fluorescence Spectroscopy. *Jpn. J. Appl. Phys.* **2010**, *49*.
(51) Hiyama, M.; Akiyama, H.; Mochizuki, T.; Yamada, K.; Koga, N. Analysis of Photoexcitation Energy Dependence in the Photoluminescence of Firefly Luciferin. *Photochem. Photobiol.* **2014**, *90*, 820−828.
(52) Throughout this work, unprimed locants refer to the thiazole/thiazolone part, and primed locants refer to the benzothiazole part of oxyluciferin and its analogs.
(53) Lakowicz, J. R. *Principles of Fluorescence Spectroscopy*; Springer: New York, 2006.
(54) White, E. H.; Roswell, D. F. Analogs and Derivatives of Firefly Oxyluciferin, the Light Emitter in Firefly Bioluminescence. *Photochem. Photobiol.* **1991**, *53*, 131−136.
(55) Leonteva, O. V.; Vlasova, T. N.; Ugarova, N. N. Dimethyl- and monomethyloxyluciferins as analogs of the product of the bioluminescence reaction catalyzed by firefly luciferase. *Biochemistry (Moscow)* **2006**, *71*, 51−55.
(56) Calculation was performed using the formula $pK^* = pK + (E_{HA} - E_A)/2.3RT$, where pK is the value for the ground state, T is absolute temperature, R is the gas constant and E_{HA} and E_A are the energies of the protonated and dissociated form estimated from absorption maxima.
(57) Solntsev, K. M.; Huppert, D.; Agmon, N. Photochemistry of "Super"-Photoacids. Solvent Effects. *J. Phys. Chem. A* **1999**, *103*, 6984−6997.
(58) Gandelman, O. A.; Brovko, L. Y.; Ugarova, N. N.; Chikishev, A. Y.; Shkurimov, A. P. Oxyluciferin fluorescence is a model of native bioluminescence in the firefly luciferin—luciferase system. *J. Photochem. Photobiol., B* **1993**, *19*, 187−191.
(59) Krissinel, E. B.; Agmon, N. Spherical symmetric diffusion problem. *J. Comput. Chem.* **1996**, *17*, 1085−1098.

Supporting Information

Emission Properties of Oxyluciferin and its Derivatives in Water: Revealing the Nature of the Emissive Species in Firefly Bioluminescence

Avisek Ghose[†,¶], Mateusz Rebarz[‡,¶], Oleg V. Maltsev[§], Lukas Hintermann[§], Cyril Ruckebusch[‡], Eduard Fron[∥], Johan Hofkens[∥], Yves Mély[†], Pance Naumov[#], Michel Sliwa*[‡], Pascal Didier*[†]*

Contents:

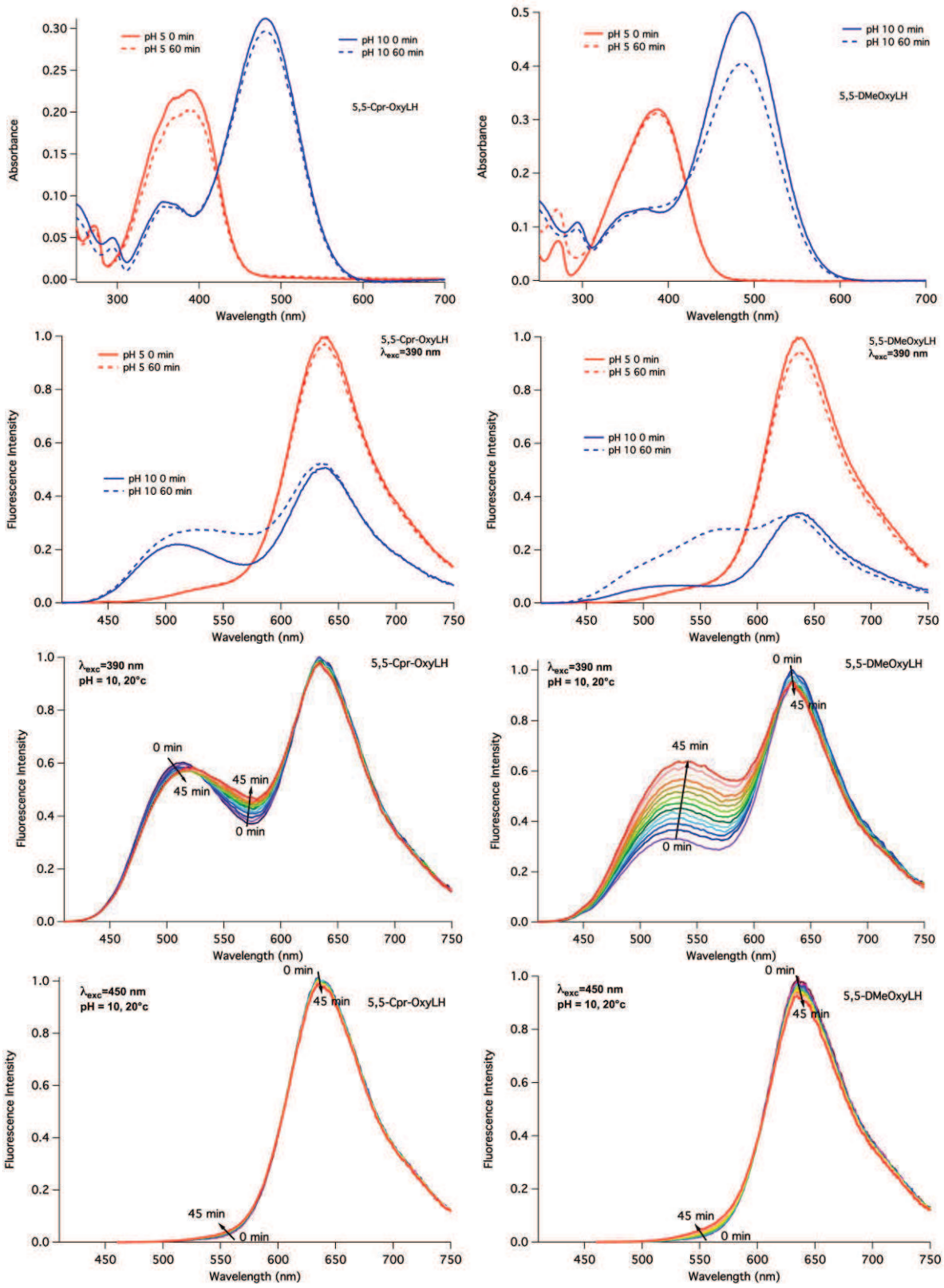

Figure S1. Relative stability and photo-stability of 5,5-**Cpr-OxyLH** and 5,5-**DMeOxyLH**. Row 1 and 2: Absorption and emission changes measured at t=0 min and t=60 min at pH 5 and 10 (irradiation was stopped between the two measured spectra). Row 3 and 4: time dependent emission under continuous illumination at 390 and 450 nm measured at pH 10. All experiments were performed at T=20°C.

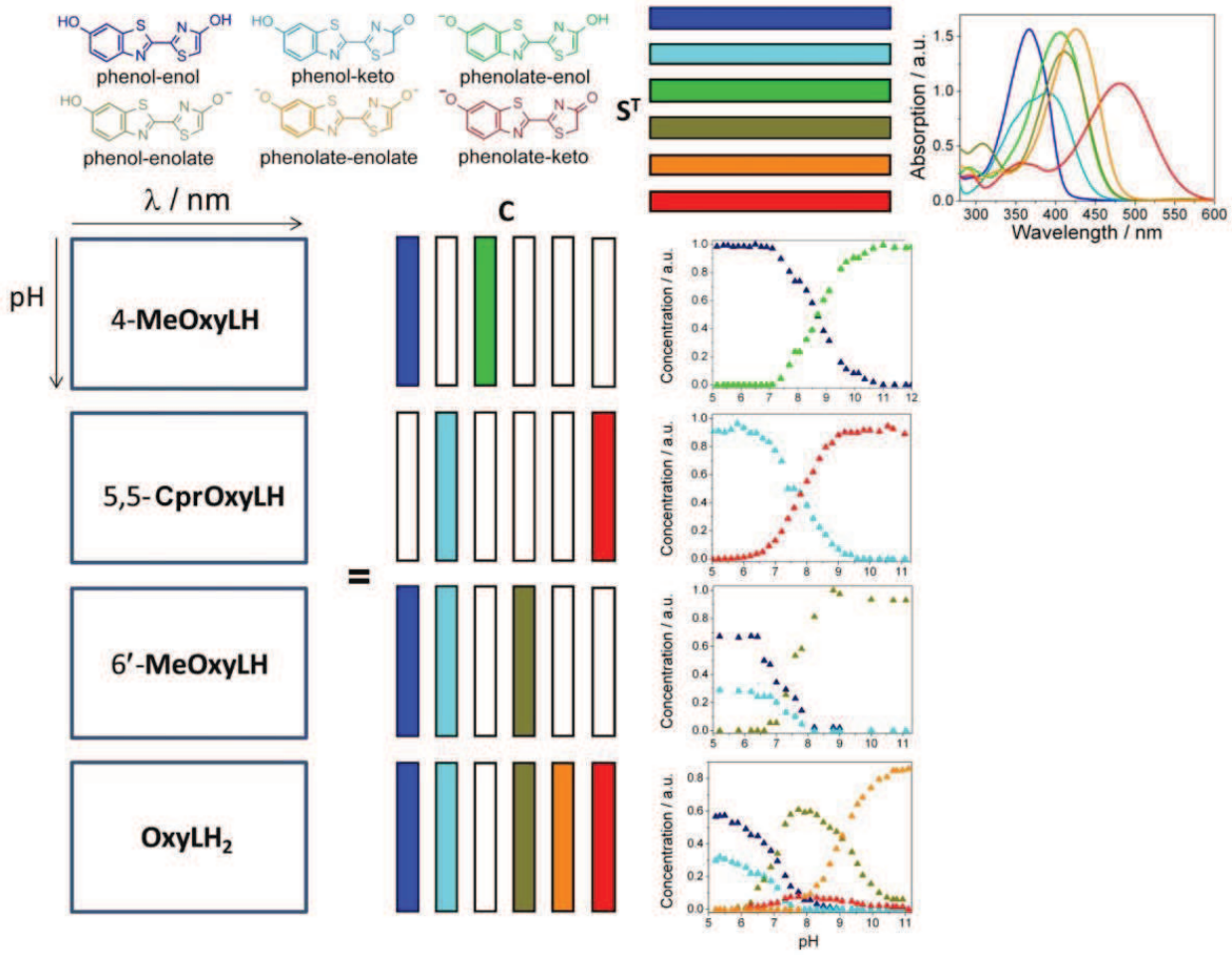

Figure S2. Absorption spectra and corresponding concentration profiles for **$OxyLH_2$** and three model compounds (4-**MeOxyLH**, 5,5-**Cpr-OxyLH** and 6′-**MeOxyLH**) obtained by multi-set MCR-ALS analysis.

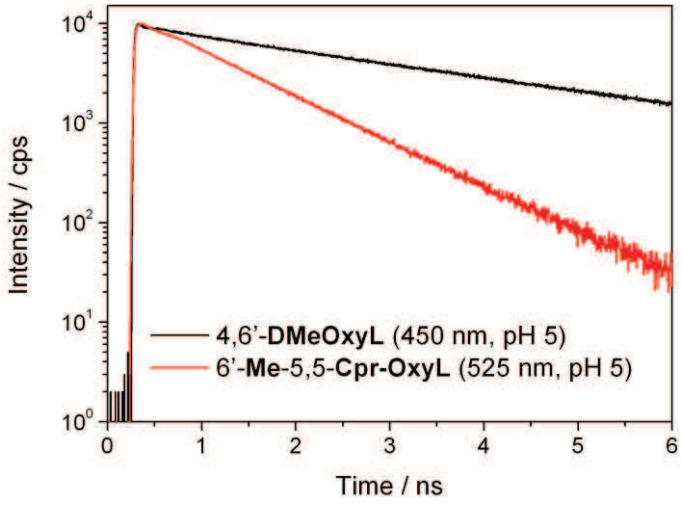

Figure S3. Fluorescence decays of two model compounds (4,6′-**DMeOxyL** and 6′-**Me** 5,5-**Cpr-OxyL**) recorded in aqueous solutions.

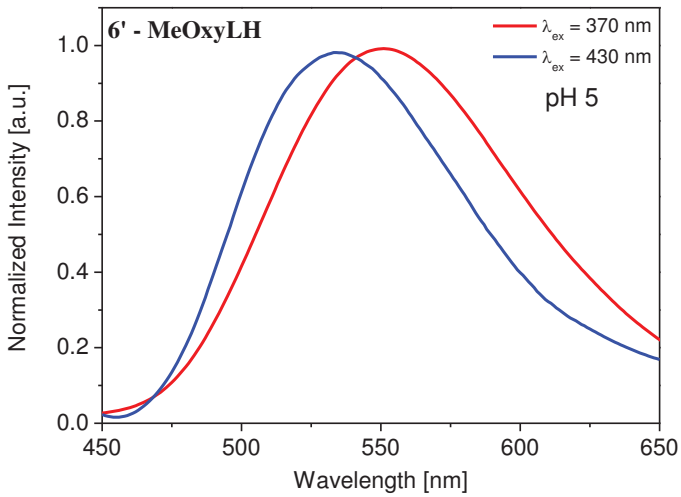

Figure S4. Emission spectra of 6′-**MeOxyLH** recorded in aqueous solutions at pH 5 and excitation at 370 nm (red line) and 430 nm (blue line).

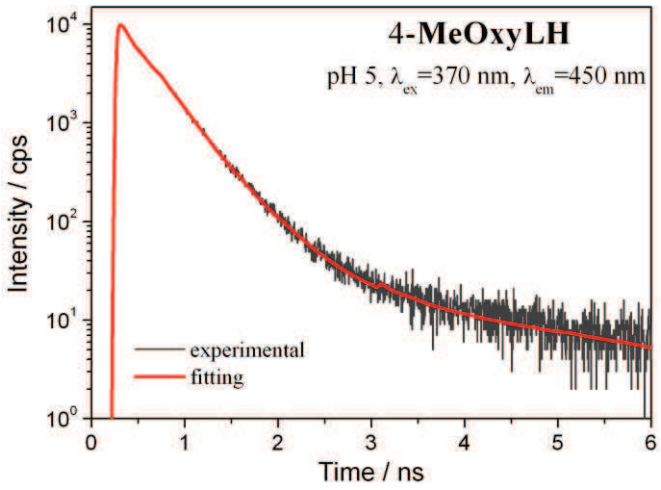

Figure S5. Fluorescence decay of neutral form of 4-**MeOxyLH** recorded in aqueous solutions at pH 5 and excitation at 370 nm (black line) with fitting by SSDP model (red line).

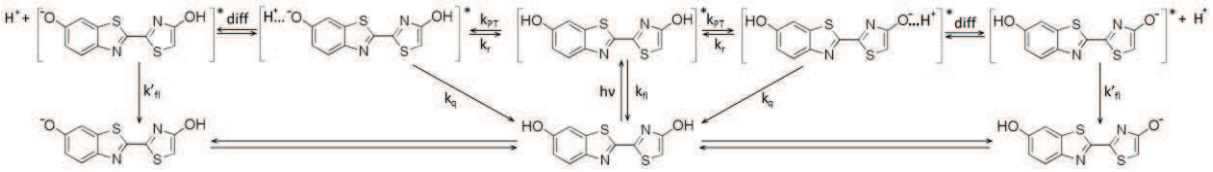

Figure S6. Mechanism of ESPT for enol tautomer of oxyluciferin.

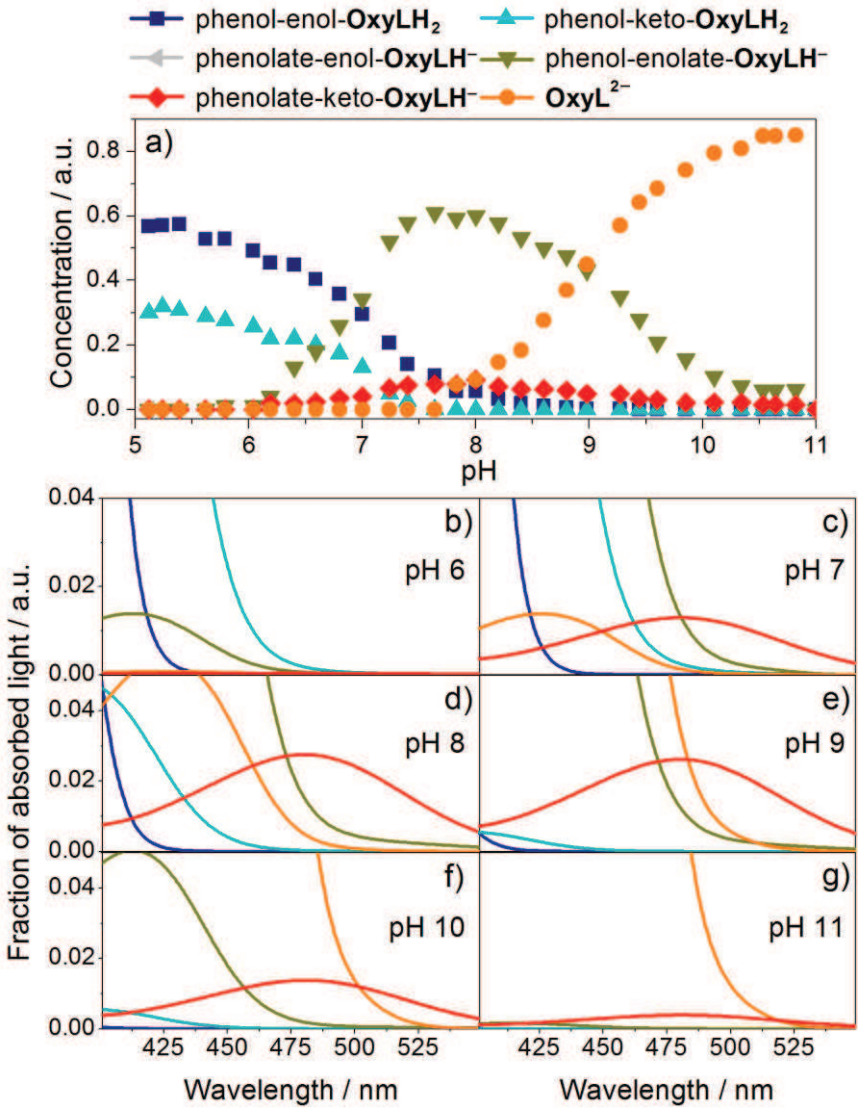

Figure S7. Absorption spectra and pH-concentration profiles of five forms of firefly oxyluciferin obtained by MCR-ALS analysis. The concentration of the phenolate-enol-**OxyLH**$^-$ form under these conditions is negligible.

Chapter 04

Results & Discussions

Oxyluciferin and Luciferase luminescence mechanism

Luciferase and Oxyluciferin Luminescence Mechanism

We have so far discussed about photophysical properties of the firefly Oxyluciferin in aqueous buffer and identified its different chemical forms responsible for its luminescence color tuning mechanism. In addition, we have discussed about the role of different chemical forms of Oxyluciferin on the de-excitation or emission mechanism, ESPT involved in the process, excited state lifetime and most importantly the role of solvent pH in the emission mechanism. All these experiments were performed in the absence of the enzyme. However, Oxyluciferin is formed as a product of the chemical reaction between Luciferin and Luciferase in presence of ATP. The photo product is formed within the pocket of the enzyme. The local properties of the microenvironment of the enzyme pocket (hydrophobicity, polarity etc.), the bond strength between the emitter and the surrounding amino acids affect the emission mechanism of Oxyluciferin. Indeed, as already described in the previous chapter, variations in the microenvironment (solvent pH, solvent composition etc.) of the dye has a strong impact on the emission properties of Oxyluciferin. To understand the photodynamics of the bioluminescence process in a more real context, it is necessary to decipher the optical properties of the Oxyluciferin-Luciferase complex in physiological conditions. By mimicking the exact physiological condition, we were able to draw the exact color tuning mechanism of the firefly bioluminescence. In this chapter, we will discuss about the structure of Japanese firefly *Luciola cruciata* Luciferase followed by a discussion about the photophysical properties of selective chemical forms the Oxyluciferin-Luciferase complex in aqueous buffer. Results presented in this chapter will be communicated soon for publication in a peer reviewed journal.

4.1 pH dependent bioluminescence spectra of Luciferase/d-Luciferin/ATP complex

Prior to observe pH dependent emission properties of firefly Oxyluciferin in complex with Luciferase, it was necessary to characterize the firefly bioluminescence in its natural environment. With this aim, we mimic the exact physiological condition where, bioluminescence from the natural photo-emitter, d-Luciferin/Luciferase/ATP at different pH has been observed as a function of time and solvent pH. Also their emission spectra have been recorded when a steady luminescence could be observed from the system (after ~25 minute).

Commercially available partially premix of d-Luciferin, Luciferase and ATP were purchased from Sigma Aldrich (Ref: FL-AA) and prepared according to the provided protocol. The assay was performed in aqueous buffers at pH ranging from 5 to 11 at 20°C. Composition of buffers has been described in chapter 2. The bioluminescence spectra were recorded on spectrofluorometer by manually blocking the excitation light (as described in the following section 4.3 and figure 4.5. In addition, the corresponding emission spectra were recorded by exciting at 360 nm after ~25 min of the beginning of the reaction.

The results are completely in line with the data obtained by Ando et al. as explained earlier[5]. In basic solutions (pH > 7.0) the spectral maxima has been observed at 557 nm from the enol form. The spectral maxima gradually red-shifts to 612 nm in acidic solutions (pH < 7.0) confirming formation of the keto form. We have observed the similar spectral behavior as reported earlier[5].

Spectra depicted in figure 4.1a represent bioluminescence of firefly Luciferase and d-Luciferin/ATP in aqueous buffer at different pH arises due to *chemi-excitation* of different chemical forms of Oxyluciferin. Due to chemi-excitation, emission from different chemical forms (enol and/or keto) of Oxyluciferin with different emission maxima could be observed. While, the fluorescence emission due to *photo-excitation* (at 360 nm) of only the enol-Oxyluciferin(-luciferase complex) in aqueous buffer at different pH has been measured in the figure 4.1c. The emission spectra recorded upon photo-excitation of this system is in complete agreement with the emission spectra of **$OxyLH_2$** reported in the previous chapter, figure 3.8f.

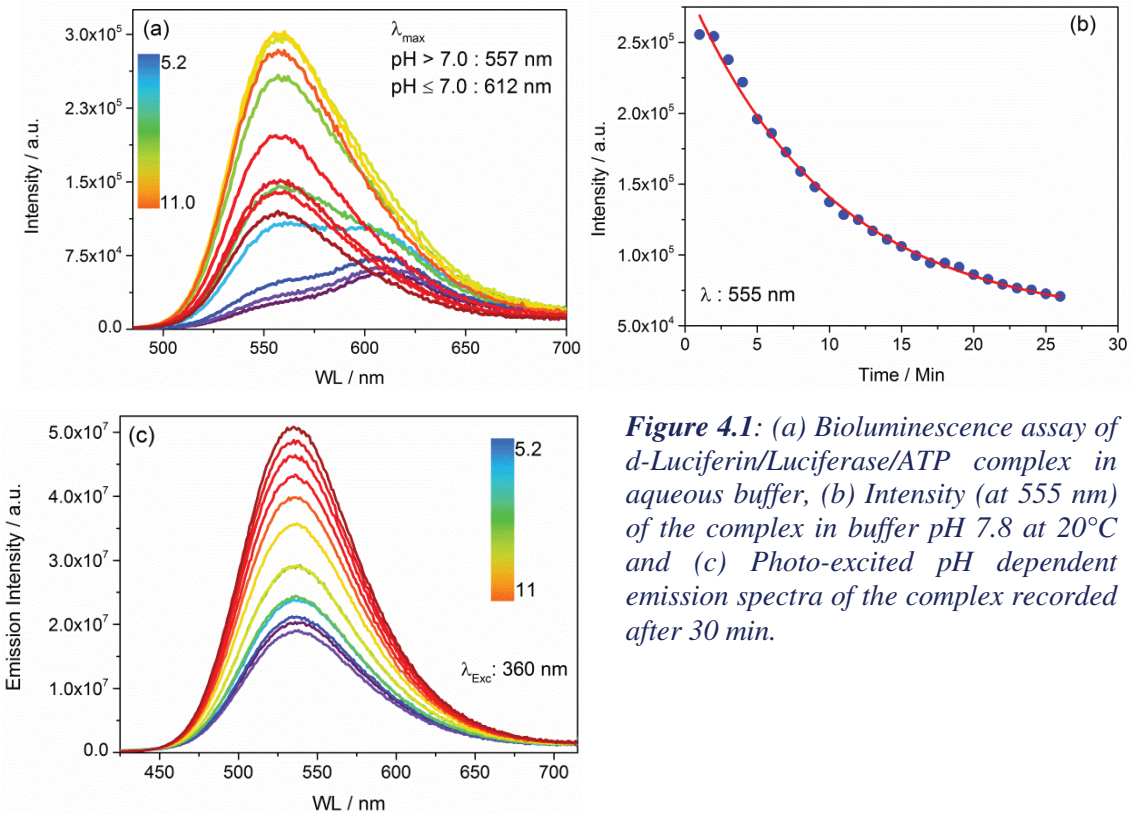

***Figure 4.1**: (a) Bioluminescence assay of d-Luciferin/Luciferase/ATP complex in aqueous buffer, (b) Intensity (at 555 nm) of the complex in buffer pH 7.8 at 20°C and (c) Photo-excited pH dependent emission spectra of the complex recorded after 30 min.*

4.2 Structure of *Luciola cruciata* Luciferase

All known Luciferase (obtained from 17 insects) consists of one common polypeptide chain (with 542-552 amino acid residues) without any co-factor and display identical amino acid alignments. More than half of the amino acids are non-polar while number of charged amino acids is identical in all Luciferase. The main difference lies in the number of Cysteine and Tryptophan residues[52].

Firefly Luciferase is a member of giant superfamily of adenylating enzymes known as ANL superfamily. (ANL refers to the group of subfamilies **a**cyl-CoA synthetase, the adenylation domains of the modular **n**on-ribosomal peptide synthetase and **l**uciferase). ANL plays a very important role in both primary and secondary metabolism. These three subfamilies catalyze the chemi-luminescence reaction sharing an initial adenylating step to produce Luciferyl-AMP intermediate. CoA ligase links –COOH of Adenylate to the phosphoryl moiety of AMP in the following steps[7,56]. Adenylate is further being used by the acyl-CoA synthatase and non ribosomal peptide synthatase adenylation domain, for thioester forming reaction. ANL enzymes contain 400-500 amino acid residues as a N terminal domain and a comparatively smaller C-terminal domain consisting 110-130 amino acids. The enzyme active site is located at the interface of these two domains. There are ten conserved regions termed as A1-A10 motifs which play critical role in either or both partial reactions[7,53,56]. Domain alteration catalytic strategy has been adapted by ANL enzyme where after formation of adenylate and release of pyrophosphate, a rotation (about 140°) of C terminal domain allows the enzyme to adopt a further conformation that can be used for second partial reaction[7,53]. For firefly Luciferase, two Lysine (Lys) residues on each face of the C-terminal domain are required for each partial reaction which suggests that a similar domain rotation is required for the catalysis of the full reaction. The two targeted residues are 37Å apart in *Luciola cruciata* Luciferase and can be susceptible to cross-linking while the enzyme adopts the second conformation. Indeed, this trapped enzyme was competent for catalysis of the oxidative reaction when in complex with the Luciferyl-AMP intermediate, and the activity is dependent on the side chain of the A8 motif residue, Lys443[53]. The primary sequence of firefly Luciferase shares extensive sequence similarity with acyl-CoA ligases[7,56].

The firefly Luciferase folds into two distinct domains: the major portion of the structure, containing amino acid residues 4–436, consist in a compact domain with a distorted anti-parallel β-barrel and two β-sheets, which are in sequence on both side of α-helices. The C terminus of the protein (440–544) separately forms a small α+β domain[56]. The crystal structure of *Luciola cruciata* has been explained by Nakatsu et al. (Nature Letter, 440; 2006)[7] in a very well fashioned manner. They resolved crystal structure of wild type *Luciola cruciata* (LcrLucWT) in complex with Luciferyl-AMP. The structure has been determined with 1.3Å resolution by the molecular replacement method and compared with the same of Luciferase form American firefly (*Photinus pyralis*). In their study, Luciferyl-AMP has been replaced by an intermediate analogue 5'-O-{N-(dehydroluciferyl)-sulfamoy}adenosine (**DLSA**). According to Nakatsu et al., LcrLuc(WT) in complex with DLSA consists of a large amino-terminal domain and a small carboxy terminal domain connected by a flexible linker loop (amino acid residues 438–442). This spatial arrangement of both domains in the LcrLuc(WT)+DLSA complex is different from that in the *Photinus pyralis* structure, but similar to those in non ribosomal peptide synthetases structures[7].

The dehydroluciferin moiety in the active site of LcrLuc(WT)+DLSA complex adopts a *trans* conformation with a rotational angle of ~7° with respect to the C2–C2'

bond, and is bound in a hydrophobic pocket consisting of α8 (amino acid residues 248–260), β12 (286–289), β13 (313–316), β14 (339–342), β15 (351–353) and a loop (343–350), while the entrance of the pocket is blocked by the adenosine moiety. The benzothiazole ring of DLSA is in Van-der Waals contact with the side chains of Phe249, Thr253, Ile288 and Ala350, and with the main chains of the β13 and β14 strands. A water molecule, Wat1, is hydrogen-bonded to N3' of Luciferyl-AMP (2.83Å) and Ser349Oγ (2.70Å)[7]. Figure 4.2 and 4.3 show structure of *Luciola cruciata* bound with DLSA; its ribbon structure and DLSA binding site.

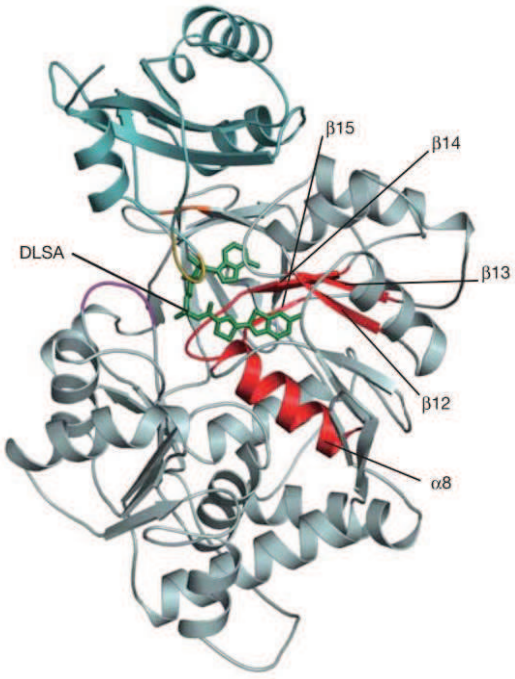

***Figure 4.2**: Ribbon diagram of LcrLuc(WT)+DLSA, large N terminal (grey) and small C terminal (blue) accompanied by the active site loop (yellow) are shown here (Nakatsu et al. Reprinted with corresponding author's acknowledgement)*[7]

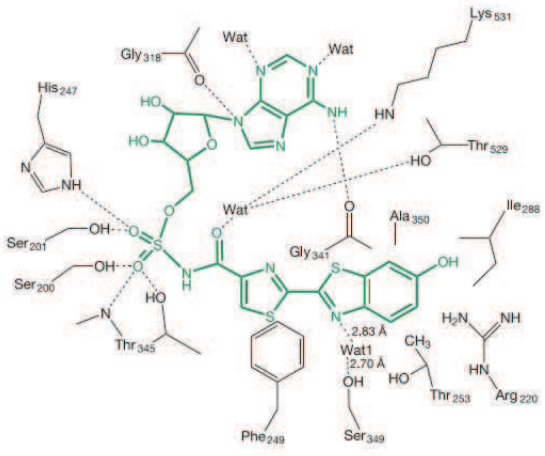

***Figure 4.3**: A schematic drawing of DLSA (green) binding site (Nakatsu et al. Reprinted with corresponding author's acknowledgement)*[7]

Nakatsu et al. also studied structure of LcrLucWT in complex with Mg-ATP (reactant) and with AMP-Oxyluciferin (product) at 2.3Å and 1.6Å resolutions, respectively and compared them with LcrLuc(WT)+DLSA complex. These structures shown in figure 4.4 (in complex with Mg-ATP and AMP-Oxyluciferin) are found to be identical but they observed significant structural difference with DLSA complex. The β12

strand in DLSA complex is much closer to the luciferin binding site than in the other structure. Particularly, Cα of Ile288 is 1.5Å closer in the DLSA complex while also side chain of Ile288 is closer to the complex and rotated by 131°. Nakatsu et al. considered this structural movement to be linked to the switching of a hydrogen bonding network involving Ser286 side chain which is hydrogen-bonded to Glu313 in LcrLucWT in complex with AMP-Oxyluciferin, but is no longer hydrogen-bonded to Glu313 in the structure of the DLSA complex. Instead, Ser286 in the DLSA complex forms new hydrogen bonds with Tyr257 and Asn231 via a water molecule Wat2. This conformational change is also accompanied by 68° rotation of the side chain of Phe249 towards DLSA. As a consequence of these movements all together a « closed form » of the active site is formed, creating a structure in which the benzothiazole ring of DLSA is tightly sandwiched inside a hydrophobic pocket, with the side chains of Ile288 and Phe249 on one side and the side chain of Ala350 and the main chain of Gly341 on the other side. Therefore, the LcrLucWT changes its conformation during catalysis process to make an extremely hydrophobic microenvironment by transient movement of the side chains of Ile288[7].

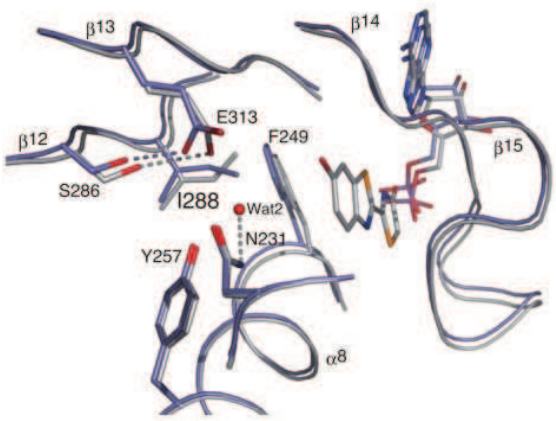

***Figure 4.4**: Superposition of the structures of LcrLuc(WT)+MgATP (light blue) and LcrLucWT+ AMP-Oxyluciferin (white) complex (Nakatsu et al. Reprinted with corresponding author's acknowledgement)*[7]

4.2.1 Amino acid sequence of *Luciola cruciata* (Japanese Firefly Luciferase, used in this study)

Sequence chain: Length: 548 AA, Mol. Weight: 60017 Da (Checksum: 2052D6189E79109F) PDB Reference: P13129- LUCI_LUCCR

MENMENDENI VVGPKPFYPI EEGSAGTQLR KYMERYAKLG AIAFTNAVTG	50
VDYSYAEYLE KSCCLGKALQ NYGLVVDGRI ALCSENCEEF FIPVIAGLFI	100
GVGVAPTNEI YTLRELVHSL GISKPTIVFS SKKGLDKVIT VQKTVTTIKT	150
IVILDSKVDY RGYQCLDTFI KRNTPPGFQA SSFKTVEVDR KEQVALIMNS	200
SGSTGLPKGV QLTHENTVTR FSHARDPIYG NQVSPGTAVL TVVPFHHGFG	250
MFTTLGYLIC GFRVVVMLTKF DEETFLKTLQ DYKCTSVILV PTLFAILNKS	300
ELLNKYDLSN LVEIASGGAP LSKEVGEAVA RRFNLPGVRQ GYGLTETTSA	350
IIITPEGDDK PGASGKVVPL FKAKVIDLDT KKSLGPNRRG EVCVKGPMLM	400
KGYVNNPEAT KELIDEEGWL HTGDIGYYDE EKHFFIVDRL KSLIKYKGYQ	450
VPPAELESVL LQHPSIFDAG VAGVPDPVAG ELPGAVVVLE SGKNMTEKEV	500
MDYVASQVSN AKRLRGGVRF VDEVPKGLTG KIDGRAIREI LKKPVAKM	548

4.3 Activity test of Luciferase

The enzyme, Luciferase has been expresses and purified as described in the section « Materials and Methods » and its biological activity was verified by monitoring its bioluminescence, by addition of d-Luciferin (CAS No. 2591-17-5) in presence of ATP in Tris/NaCl buffer containing Mg^{2+}at pH 8.0 at 20°C. The reaction mixture was kept in complete darkness from the beginning. The bioluminescence from the mixture was measured by classical steady state fluorescence method using Fluorolog (Jobin Yvon) spectrofluorometer where incoming excitation light was manually blocked but the emission slit and the PMT were active to detect the emitted photons (see figure 4.5). Due to the manual blockage in the path, no excitation light could reach to the sample and the emission spectra recorded was due to *chemi-excitation* only. The bioluminescence emission from the reaction mixture were measured with the PMT every minute during ~30 min. Bioluminescence emission centered at ~560 nm has been observed and displayed an intensity decreases with time (see figure 4.6 and 4.7) due to the decomposition of Luciferin. As a negative control, the same experiment was repeated without ATP. In this case, no emission was observed (only Instrument's response characteristics could be recorded). Therefore it can be postulated that the spectra recorded was a result of pure bioluminescence of Luciferin and Luciferase reaction and the protein expressed by us is chemically active.

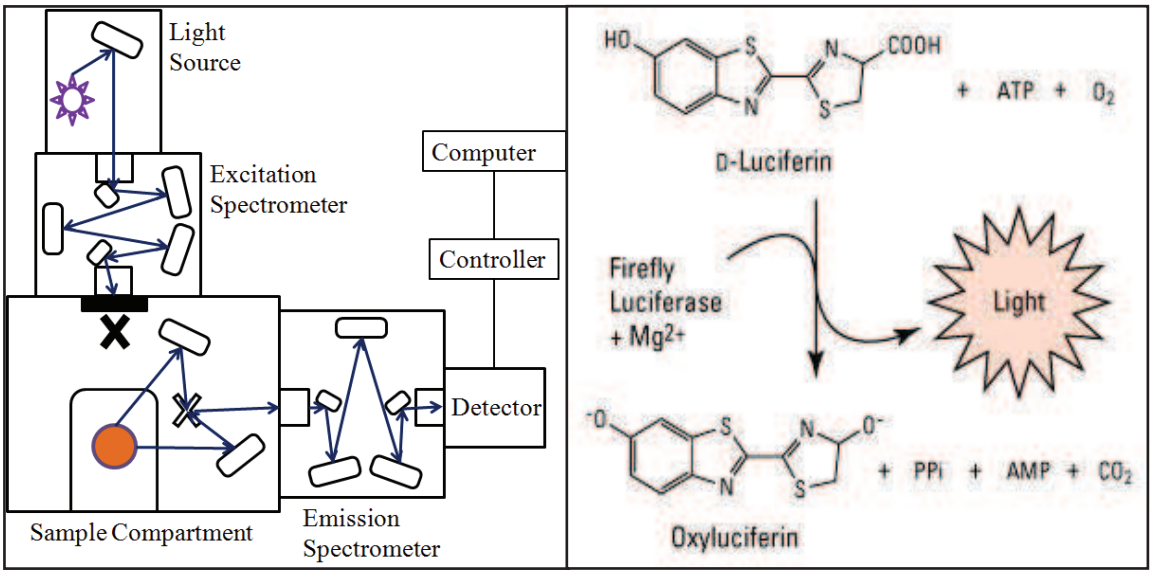

***Figure 4.5**: Manual blocking (marked as* X*) of the incoming excitation light of the spetrofluorometer (left) and bioluminescence reaction of Luciferin and Luciferase (right, ©Thermo Scientific, Adapted Form).*

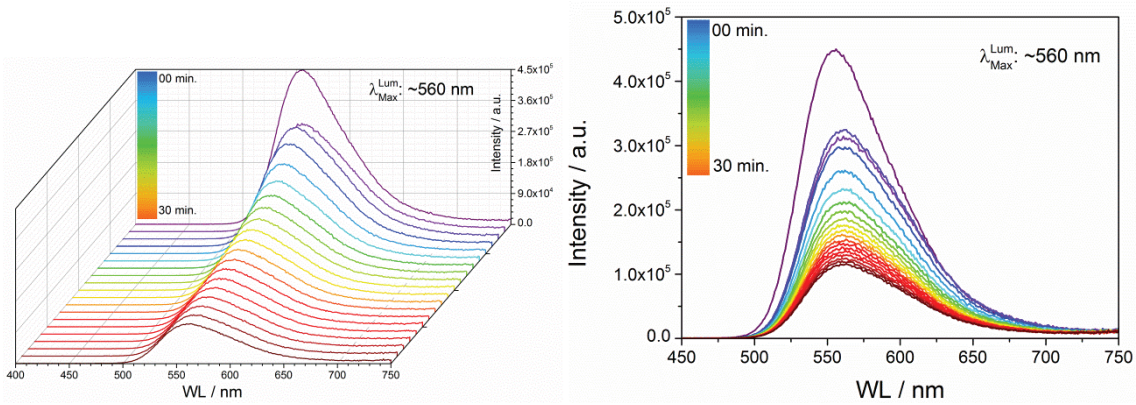

***Figure 4.6**: Bioluminescence spectra of Luciferase-Luciferin in presence ATP in buffer pH 8.0 at 20°C*

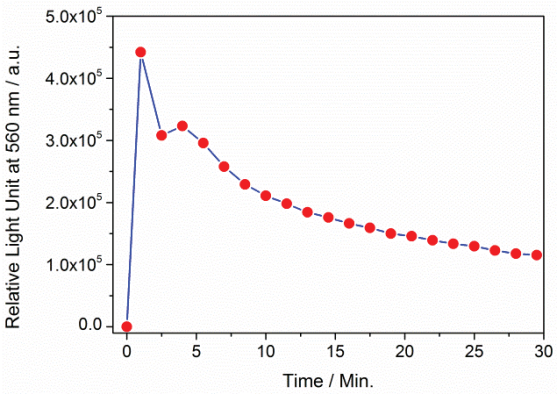

***Figure 4.7**: Relative luminescence intensity of **Luciola cruciata** (expressed by us) with d-Luciferin and ATP at 560 nm in buffer pH 8.0 has an identical profile as reported in review by Marques et al.*[66]

4.4 Oxyluciferin-Luciferase assay protocol

To understand the photophysical properties of Oxyluciferin inside the active pocket of Luciferase, we performed several steady state and time resolved fluorescence spectroscopic studies with different analogues of Oxyluciferin bound with Luciferase in the presence of Adenosin monophosphate (AMP) in aqueous buffer at three different pH; 5.0, 7.4 and 10.0 at room temperature (20°C). Such experimental conditions were used to mimic the exact physiological conditions required to observe bioluminescence. Based on the results presented in the previous chapter, steady state and time resolved fluorescence emission were recorded by using selective excitation, allowing us to specifically visualize the contribution from the different chemical forms of Oxyluciferin.

We have mainly studied Oxyluciferin (**$OxyLH_2$**) and three model compounds **4-MeOxyLH**, **4,6'-DMeOxyL** and **5,5-Cpr-OxyLH** (see chart 4.1) in complex with Luciferase in presence of AMP. The reaction mixture has been prepared in aqueous buffer at desired pH consist of ~1.0 µM Luciferase, ~0.1 µM Oxyluciferin and 320 µM AMP. To be sure that all Oxyluciferin molecules were inside the active pocket of Luciferase, a ten-fold higher concentration of protein was used. Doing so, there was a high probability that no free Oxyluciferin was available in the solution. From the initial steady state anisotropy experiments, explained in the following section (see figure 4.8),

we have determined that the appropriate concentration ratio can be 1:10. For pH 5.0 and 10.0 same buffer as for our previous experiments have been used and for pH 7.4, commercially available Phosphate Buffered Saline (PBS 1x) has been used.

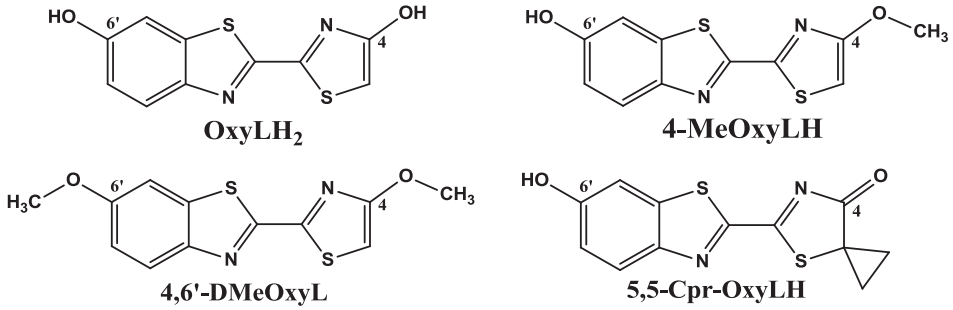

***Chart 4.1**: Oxyluciferin and its derivatives used in this study*

4.5 Steady state anisotropy titration of $OxyLH_2$ and 4-MeOxyLH with Luciferase

Fluorescent anisotropy measurement of Oxyluciferin-Luciferase complex can be a powerful tool to determine the binding affinity of the fluorophore to the protein. When exposed to the polarized light, the Oxyluciferin molecules in perfectly homogeneous solvent, which are having absorption transition moment aligned with the electric vector of the incident light, are preferentially excited. Hence the excited state population is partially oriented[135]. Therefore, fluorescence anisotropy measurement was found to be the most suitable technique to characterize the complex formation and to measure the binding affinity between Luciferase and Oxyluciferin. Indeed the measured anisotropy will be strongly modified when the fluorophore is bound to the protein. It can be assumed that the molecular weight of the complex (fluorophore bound to the protein) must be much higher than the free fluorophore. When the molecule is free, it has less anisotropy value as compared to the bound one. Thus, gradual change in the anisotropy with increasing concentration of Luciferase, gives a confirmation that the molecule is properly bound with Luciferase.

To determine the binding affinity of Oxyluciferin to Luciferase, we have performed anisotropy titration experiments with of **$OxyLH_2$** and **4-MeOxyLH** with increasing concentration of Luciferase in PBS (at physiological pH). The titrations were performed with 0.2 µM **$OxyLH_2$** or **4-MeOxyLH** in PBS with increasing concentration of Luciferase from 0 to ~3.0 µM with an increment of 100 nM. Fluorescence anisotropy at each concentration has been calculated from the polarized emission (See « Materials and Methods » for more detail) collected through long pass filters to eliminate scattered light from the excitation. The anisotropy curves were plotted in figure 4.8. By analyzing the increase of anisotropy of both compounds with a Scatchard model[157] the dissociation constant (K_D) could be calculated (see Appendix-B.1 for a brief discussion about Scatchard function). Almost identical dissociation constants (K_D) have been observed for both compounds (0.29 µM). From the anisotropy plateau we determined that a 1:7.5 concentration ratio between the fluorophore and the protein is sufficient to neglect the

contribution from the free fluorophore. So, we decided to use 1:10 for Oxyluciferin:Luciferase concentration for our further experiments. Despite the change in lifetime of the compounds in the presence of Luciferase (see table 4.2a), we decided to work with this ratio because of the limited amount of Luciferase.

Because of limited amount of produced protein, we avoid this titration experiment with the neutral compound **4,6'-DMeOxyL**. In addition, dissociation constant for **5,5-Cpr-OxyLH** could not be calculated even in complex with > 3 µM of protein due to the absence of a plateau. Indeed, in the case of **5,5-Cpr-OxyLH**, the quantum yield of the compound was modified by the binding process avoiding accurate determination of the anisotropy value.

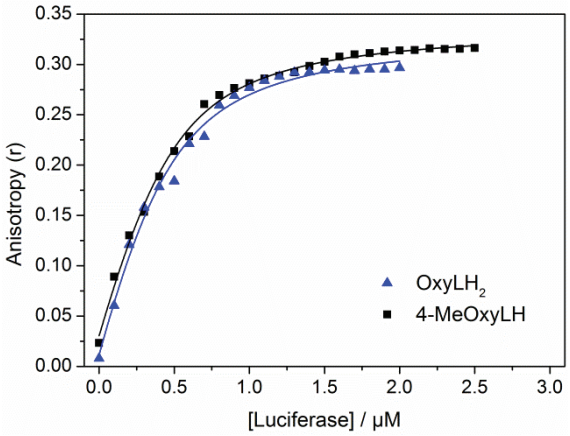

***Figure 4.8**: Anisotropy titration of **OxyLH$_2$** (K_D 0.29 µM) and 4-**MeOxyLH** (K_D 0.28 µM) with Luciferase in PBS. (Dissociation constant, K_D calculated by using Scatchard model)*

4.6 pH dependent emission mechanism of Oxyluciferin in complex with Luciferase

Emission spectra of all model compounds and Oxyluciferin were measured in aqueous buffers at three different pH, considering that at lowest pH 5.0, compounds are in their neutral form and at pH 10, compounds are already at their deprotonated form in the ground state. To mimic the exact physiological condition, we also characterized their photophysical properties in PBS (pH 7.4). Emission spectra of Oxyluciferin (**OxyLH$_2$**) and model compounds (**4-MeOxyLH**, **4,6'-DMeOxyL** and **5,5-Cpr-OxyLH**) were recorded by exciting at 395 nm, 385 nm, 370 nm and 425 nm respectively. **4-MeOxyLH** and **5,5-Cpr-OxyLH** were excited at their isosbestic point while **4,6'-DMeOxyL** was excited at its absorption maxima. **OxyLH$_2$** was excited at 395 nm (see figure 3.2). In addition, to observe emission particularly from **phenol-keto-OxyLH$_2$** and **phenol-enolate-OxyLH$^-$**, spectra of the neutral-keto Oxyluciferin (**6'-Me-5,5-Cpr-OxyL)** and **6'-MeOxyLH** in complex with Luciferase were also recorded respectively. Emission spectra of free Oxyluciferin and in complex with a 10 fold molar excess of Luciferase have been recorded and represented in figure 4.9. Their anisotropy values (free and bound) have been presented in the table 4.1. In most of the conditions (except boldface fonts in table 4.1) blue shift in the emission maxima was observed when Oxyluciferin is bound with Luciferase. In addition, a significant increase in their anisotropy was also observed. All these measured parameters are presented in table 4.1.

***Table 4.1**: Photophysical parameters of the complex in different buffers*

Compound	λ_{Exc}	pH	Oxyluciferin (Free)		Oxyluciferin+Luciferase			
	(nm)		Anisotropy, r	Em. Max./nm	Anisotropy, r	Em. Max./nm	Δ-Anisotropy	Blue Shift/nm
4-MeOxyLH	385	5.0	0.02528	558	0.2465	537	0.22122	21
		7.4	0.0271	558	0.3233	528	0.2962	30
		10.0	0.01099	558	0.2146	521	0.20361	37
4,6'-DMeOxyL	370	5.0	0.01469	444	0.1624	437	0.14771	7
		7.4	0.01465	444	0.3226	437	0.30795	7
		10.0	0.01544	444	0.1916	437	0.17616	7
$OxyLH_2$	395	5.0	0.02116	552	0.2873	515	0.26614	37
		7.4	0.007624	548	0.3019	509	0.294276	39
		10.0	0.0108	536	0.01754	536	**0.00674**	**0**
5,5-Cpr-OxyLH	425	5.0	0.08384	637	0.1145	626	**0.03066**	11
		7.4	0.07125	637	0.2754	612	0.20415	25
		10.0	0.06124	637	0.0712	637	**0.00996**	**0**

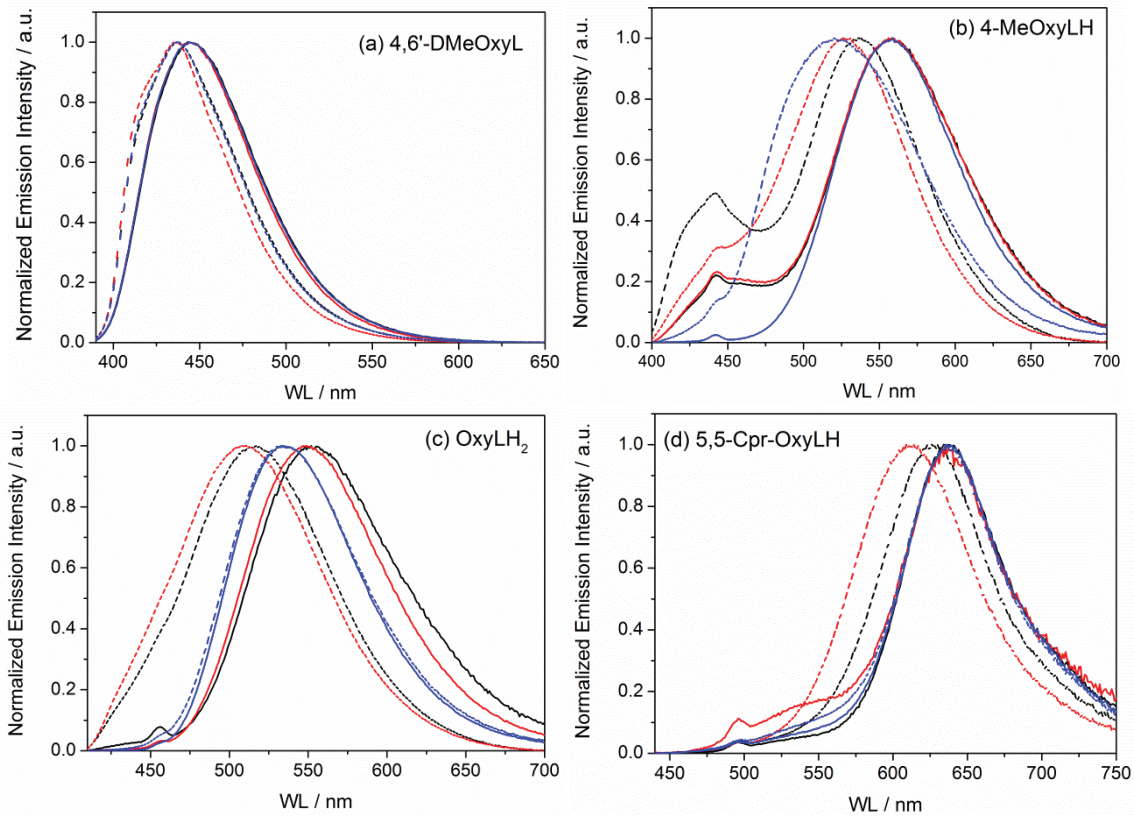

***Figure 4.9**: Emission spectra of different Oxyluciferin-Luciferase complexes at different pH. Spectra represents emission of different compounds in buffer pH 5.0 (Black), 7.4 (Red) and 10.0 (Blue) without (solid line) and with 10x Luciferase (dashed line). Their excitation wavelength, emission maxima and anisotropy values at different conditions are mentioned in the table 4.1. (due to weak emission intensity, contribution from the Raman scattering could not be avoided and are visible in the spectra as a very small peak)*

From the analysis of the results discussed in the previous chapter, we can identify the exact contribution that corresponds to a particular chemical form of Oxyluciferin « see figure 3.2 ». In addition, for specific pH and excitation energy, our model compound can have an emission that can unambiguously be associated with a particular chemical form of Oxyluciferin. With the help of those results, we were able to selectively excite our model compounds and **$OxyLH_2$** to observe an emission dominated by single specie.

We have observed that fluorescence emission of Oxyluciferin in aqueous buffer is red shifted with respect to the spectra obtained in any apolar solvent e.g. DMSO, although their absorption spectra were quite similar (see previous chapter section 3.2). Because of the change in the dipole moment of the molecule in the excited state, the molecule always has a higher dipole moment than that in the ground state, when in complex with Luciferase. Also the ionic strength of the solvent is to be considered. In the excited state, Oxyluciferin is caged inside the protein pocket, which likely induces electrostatic interaction of dipole with its microenvironment. Electrostatic interaction depends inversely on the dielectric constant of the solvent. So, in a polar environment Coulombic contribution will decrease with respect to a less polar environment. This interpretation can be used to explain the blue shift in emission spectra of Oxyluciferin when bound with Luciferase. In addition, the amplitude of the blue shift differs with the solvent pH and structure of Oxyluciferin analogue. For instance, if Oxyluciferin is bound on the surface of the protein, it is exposed to the solvent, and fluorescence emission will be identical to the emission spectra of the free Oxyluciferin[12,43,48,100]. In a hydrophobic cavity, where non-polar side chain of amino acid residue is predominant, blue shift in emission spectra can be observed. For a higher hydrophobicity, a larger blue shift can be observed. Not only the environment can have an effect, but also the rigidity of the complex affects the emission spectra. This can be studied by comparing anisotropy of the complex with free Oxyluciferin in buffers at different pH. To understand this mechanism in a much better way time resolved anisotropy experiments can be employed which can have a major impact in this concern.

While observing excitation spectra (recorded at emission maxima, data not shown) for all free and Luciferase bounded compounds, no spectral shift has been observed from which we can conclude that the excited specie is the one associated with the ground state of the dye.

*4.6.1 Fluorescence emission of nonionizable model compound **4,6'-DMeOxyL** in complex with Luciferase*

We have already observed that because of the absence of acidic group (where deprotonation is inhibited), the position and shape of the emission spectra as well as the fluorescence lifetime do not evolve with buffer pH (see table 3.1)[48]. **4,6'-DMeOxyL** exhibits a single emission band from neutral **phenol-enol-$OxyLH_2$** centered at 444 nm. Also the time resolved fluorescence emission decays monoexponentially with a lifetime of 3.1 ns for the studied buffer pH (5-7.4-10). **4,6'-DMeOxyL** presents, when in complex

with Luciferase in presence of AMP, a 7 nm blue shift in the emission maxima together with a 1.25 fold increase in the fluorescence intensity for the entire pH range without modification of its spectral shape. Fluorescence emission decays monoexponentially with a lifetime of 3.7 ns (see figure 4.10 and table 4.2a). On the basis of the results obtained in the previous chapter, we can attribute this emission to the neutral **phenol-enol-OxyLH$_2$**. A fluorescence anisotropy close to zero (of about 0.015) was recorded for free **4,6'-DMeOxyL** for all pH while exciting with a polarized light at 370 nm. By adding Luciferase and AMP, a increase in the fluorescence anisotropy was observed. These data confirms probability of formation of a pH independent complex of **4,6'-DMeOxyL** with Luciferase and AMP.

In addition, to observe emission from **phenol-keto-OxyLH$_2$**, emission spectra of **6'-Me-5,5-Cpr-OxyL** in complex with Luciferase has been recorded in buffer pH 10 with an excitation at its absorption maxima i.e. 390 nm. Like **4,6'-MeOxyL**, this neutral-keto form can have a pH independent emission spectra and as expected emission centered at 523 nm with a negligible blue shift (2 nm) has been observed for the complex. This can be postulated that the fluorophore was not properly bounded with the protein. This observation has to be confirmed further by measuring anisotropy of the complex.

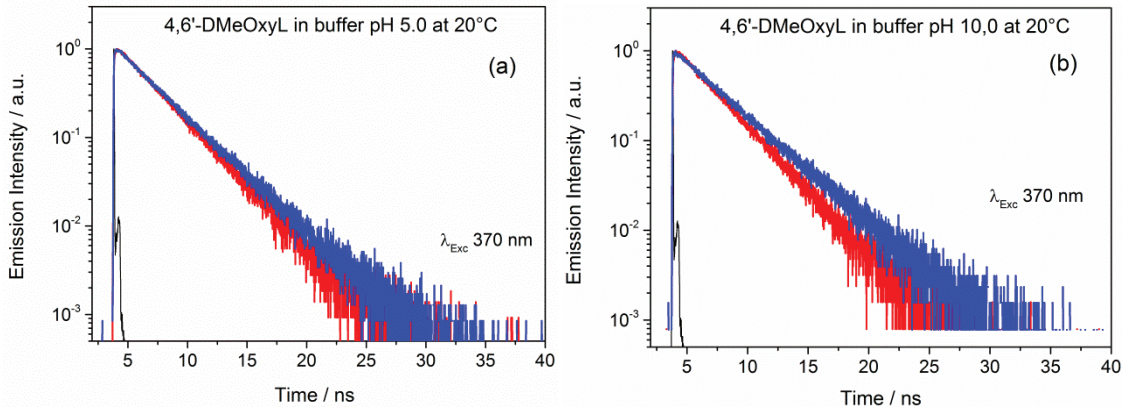

***Figure 4.10**: Time resolved fluorescence emission of **4,6'-DMeOxyL** (λ_{Em} 440 nm) bound to Luciferase in aqueous buffer. Red line represents emission decay of free compound while blue line represents fluorescence decay of the complex (instrument's response function has been represented by black line). Time resolved data reported in table 4.2a.*

*4.6.2 Fluorescence emission of ionizable model compounds **4-MeOxyLH** and **5,5-Cpr-OxyLH** in complex with Luciferase*

Fluorescence spectra of **4-MeOxyLH** was recorded in aqueous buffer at different pH at an excitation wavelength that corresponds to its isosbestic point of 383 nm (see figure 3.2)[48]. The spectra of **4-MeOxyLH** in pH 5 and 7.4 are characterized by two emission bands; a strong band centered at 560 nm from the anion is accompanied by a weaker band centered at 445 nm associated the neutral form, both decay with different fluorescence lifetime values as mentioned in the table 4.2a. At higher pH (10.0), where deprotonation occurs already in the ground state, the emission from the neutral form (λ_{max}: 445 nm) is quenched and disappears. The generation of both emission bands of **4-MeOxyLH** has

already been described before. While compared with **4-MeOxyLH**-Luciferase complex, blue shift in emission maxima has been observed which linearly increases with solution pH.

The emission of **4-MeOxyLH**-Luciferase at pH 5.0 centered at 440 nm is attributed to its neutral form. Excitation of this neutral form (Abs/Em: 370/440 nm) lead to a fluorescence decay characterized by a short component of 380 ps together with a biexponential decay with lifetimes of 1.7 and 3.96 ns, similar to the **phenol-enol-OxyLH$_2$** (see figure 4.11a). At pH 7.4, because of solvent deprotonation, a small increase of these parameters was observed. In all three pH, anionic form of this compound decays monoexponentially with a lifetime of ~5.5 ns which is attributed from the **phenolate-enol-OxyLH$^-$** form (see figure 4.11b). A strong blue shift of 37 nm and a 20 fold increased in the fluorescence anisotropy have been observed for buffer at pH 10.0 (see table 4.2a) which is likely associated with the presence of a more hydrophobic environment in this conditions.

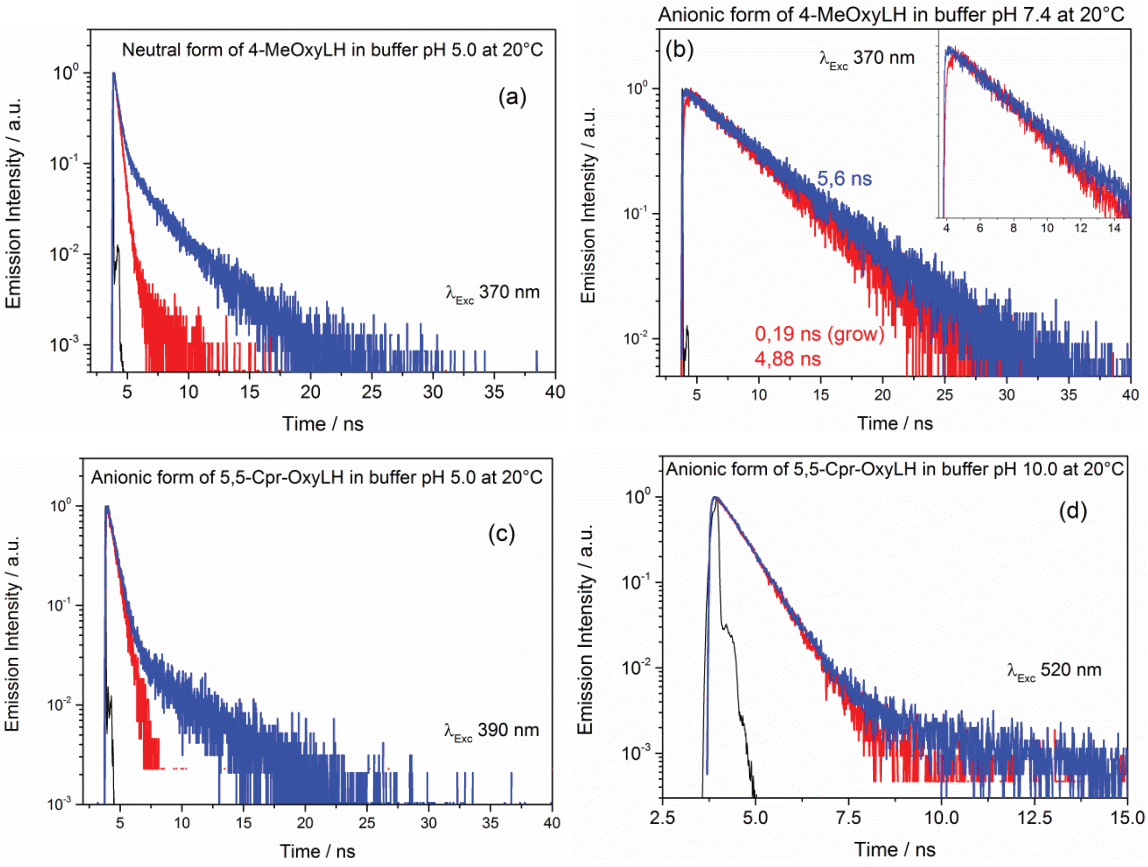

***Figure 4.11**: Time resolved fluorescence emission of **4-MeOxyLH** (a & b) and **5,5-Cpr-OxyLH** (c & d) in complex with Luciferase in aqueous buffer. Red line represents emission decay of free compound while blue line represents fluorescence decay of the complex (instrument's response function has been represented by black line)*

Fluorescence decay of the other ionizable model compound **5,5-Cpr-OxyLH** (see figure 4.11c & 4.11d) recorded at 520 nm (the neutral form) corresponds to the **phenol-keto-OxyLH$_2$**. Because of much higher photoacidity and very efficient ESPT, the neutral form of this compound (Abs/Em: 390/520 nm) is rapidly quenched with a lifetime shorter

than the instrumental response function (IRF) of the set up (<0.05 ns). Indeed, the decay measured at 630 nm characterized by an additional component of 5.5 ns, apart from other component similar to its unbound form. At pH 10.0, no spectral shift and no change in anisotropy could be observed likely meaning that for this condition, the derivative is not bound to luciferase. This hypothesis is supported by the monoexponential fluorescence decay observed at 640 nm with a lifetime of 600 ps (similar to the value of free Oxyluciferin). In addition, to observe emission from the **phenol-enolate-OxyLH$^-$** the emission spectra of **6'-MeOxyLH** in complex with Luciferase in buffer pH 10.0 has been recorded with an excitation at 430 nm, where negligible blue shift of 3 nm could be observed.

***Table 4.2a**: Time-resolved fluorescence parameters of non-ionizable and ionizable model compounds in aqueous buffers.*

Compound		Neutral Emission				Anionic Emission			
		pH	λ_{Ex}/nm	λ_{Em}/nm	τ/ns (%)	pH	λ_{Ex}/nm	λ_{Em}/nm	τ/ns (%)
4,6'-DMeOxyL	w/Luc	5-11	370	450	3.1				
	+Luc			440	3.7				
4-MeOxyLH	w/Luc	5	370	450	0.24[a]	5	370	560	0.21[b] 1.47 (11) 4.86 (89)
	+Luc			440	0.38 (86.7) 1.7 (8.6) 3.96 (4.7)			540	5.50
	w/Luc	7.4	370	450	0.41[a]	7.4	370	560	0.19[b] 4.88
	+Luc			430	0.405 (95.8) 2.18 (4.8) 6.17 (3.3)			525	5.6
	w/Luc					10	430	560	4.88
	+Luc							520	5.20
5,5-Cpr-OxyLH	w/Luc	5	390	525	<0.05[a]	5	390	640	0.16 (25) 0.61 (75)
	+Luc			520	<0.05[a]			630	0.65 (97) 5.53 (3)
	w/Luc					7.4	390	640	<0.06[a] 0.64
	+Luc							615	0.73 (62.5) 5.5 (37.5)
	w/Luc					10	520	640	0.63
	+Luc							640	0.60

w/Luc: Without Luciferase/Free compound, +Luc: Bound with Luciferase, a: Short component for nonexponential decay, b: Time constant for the growing part

*4.6.3 Fluorescence emission of **OxyLH$_2$** in complex with Luciferase*

A mixture of all chemical forms could be visible in the emission of the real emitter **OxyLH$_2$**. Thus accurate spectral characterization of **OxyLH$_2$** bound to Luciferase was a complex task. Depending upon the excitation wavelength and solution pH, emission from different chemical forms could be observed. To decipher emission from different chemical forms, time resolved fluorescence decay of **OxyLH$_2$** in complex with

Luciferase has been recorded with excitation at UV (370 nm) as well as at visible light (430, 510 nm). The results have been compared with the same for unbound **OxyLH$_2$**.

Excitation at 370 nm

In acidic condition (pH 5), emission decay from unbound **phenol-enol-OxyLH$_2$** recorded at 450 nm indicates that the neutral form is strongly quenched with time < 50 ps. On the contrary when in complex with Luciferase neutral **phenol-enol-OxyLH$_2$** decays biexponentially (see figure 4.12a) with lifetime of 2 ns and 9.5 ns as mentioned in the table 4.2b. Compared to our previous experiments with unbound **OxyLH$_2$**, fluorescence emission measured for bound **phenol-enolate-OxyLH$^-$** (Em. max. 515 nm) as well as for bound **phenolate-keto-OxyLH$^-$** (Em. max. 630 nm), decay multiexponentially (see figure 4.12b and 4.12c). In addition to the contribution of the geminate recombination (~0.18 ns), the bound **phenolate-keto-OxyLH$^-$** decays with a lifetime of ~10 ns, much higher to the same measured for unbound **OxyLH$_2$.** Bound **phenol-enolate-OxyLH$^-$** decays with a lifetime of 11.3 ns that is higher too as compared to the unbound one. With little increase in pH emission from both **phenol-enolate-OxyLH$^-$** and **phenolate-enolate-OxyL^{2-}** can be expected.

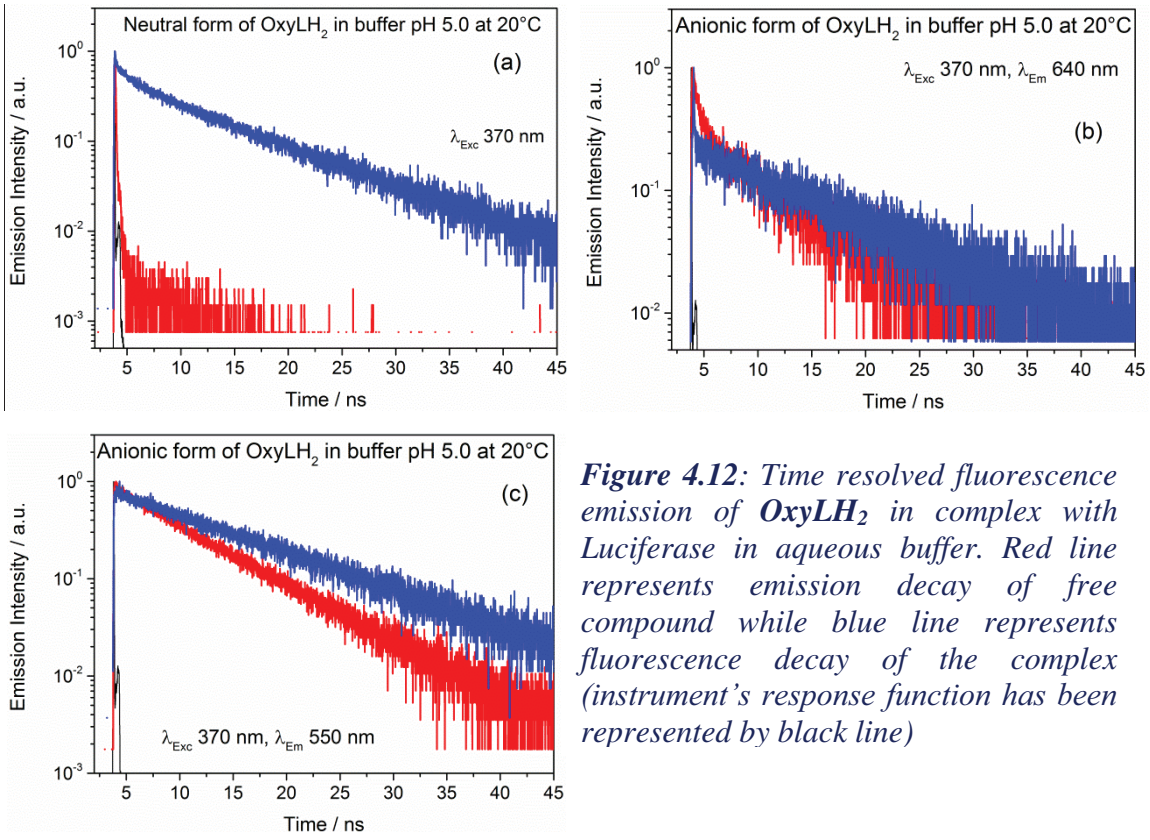

***Figure 4.12**: Time resolved fluorescence emission of **OxyLH$_2$** in complex with Luciferase in aqueous buffer. Red line represents emission decay of free compound while blue line represents fluorescence decay of the complex (instrument's response function has been represented by black line)*

Excitation with visible light (430 and 510 nm)

A different photoluminescence pathway has been observed for unbound **OxyLH$_2$**. At pH 7.4 with an excitation at 510 nm, emission occurs from **phenolate-keto-OxyLH$^-$** (Em. max. 634 nm). This emission decays monoexponentially with a lifetime of 0.4 ns. **OxyLH$_2$** when in complex with Luciferase has an identical lifetime measured at 630 nm

for this condition (see figure 4.13a). The **phenolate-keto-OxyLH$^-$** emission was further characterized with its emission spectra in buffer pH 7.4 with an excitation at 510 nm (see figure 4.13a) and compared with figure 3.11. **OxyLH$_2$** in buffer pH 7.4 when in complex with Luciferase readily undergo tautomerization and presence of both forms was visible in the emission spectra. Emission of unbound Oxyluciferin has a single band emission centered about 625 nm while the bound form has a dual emission from both enol and keto form. A decrease in emission energy could also be observed. This observation is likely showing that the emission property of **phenolate-keto-OxyLH$^-$** is affected by the protein environment but not the lifetime. At pH 7.4, with an excitation at 430 nm, mixture of **phenolate-keto-OxyLH$^-$**, **phenolate-enolate-OxyL^{2-}** and **phenol-enolate-OxyLH$^-$** have been observed for unbound **OxyLH$_2$**. However, when bound to Luciferase, we observed redistribution in the amplitude of the different contributions. When bound with Luciferase, **OxyLH$_2$** decays multiexponentially (see figure 4.13b) with lifetime of 0.13 ns, 2.2 ns and 9.7 ns.

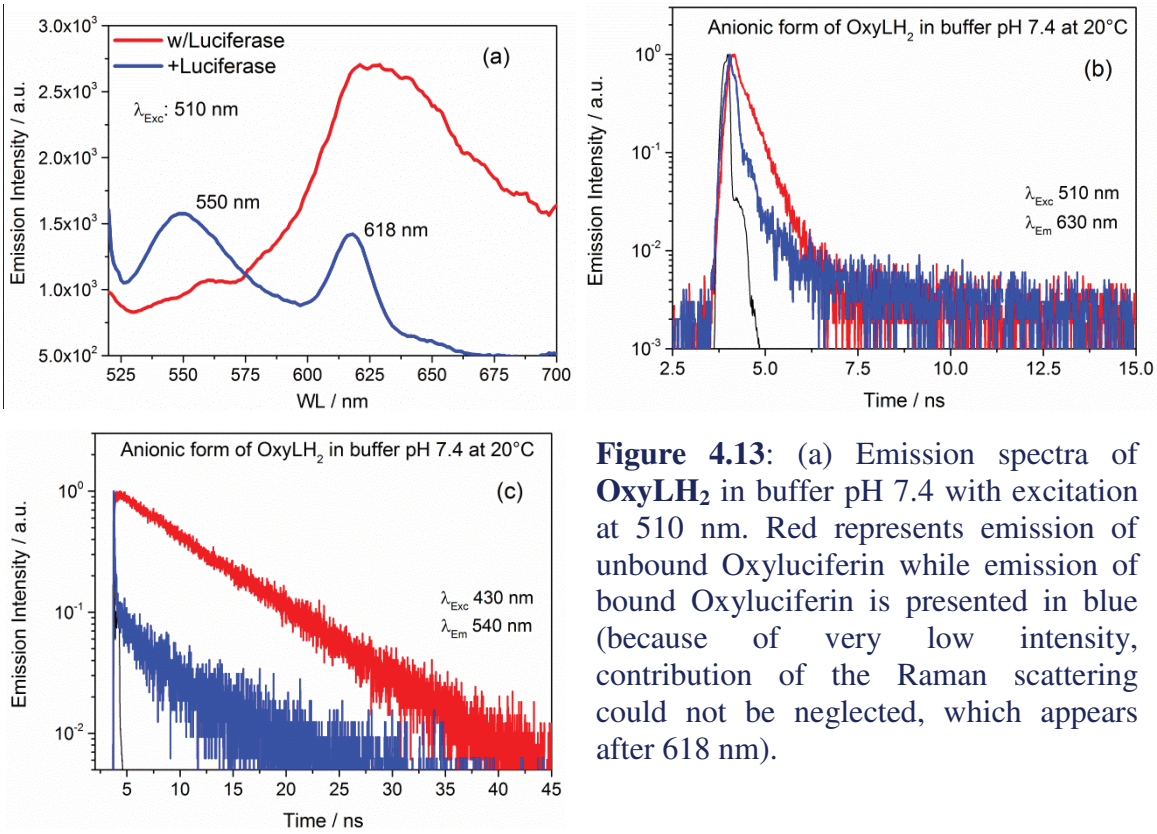

Figure 4.13: (a) Emission spectra of **OxyLH$_2$** in buffer pH 7.4 with excitation at 510 nm. Red represents emission of unbound Oxyluciferin while emission of bound Oxyluciferin is presented in blue (because of very low intensity, contribution of the Raman scattering could not be neglected, which appears after 618 nm).

Figure 4.13 b-c: *Time resolved fluorescence emission of **OxyLH$_2$** complex with Luciferase in aqueous buffer; Red line represents emission decay of free compound while blue line represents fluorescence decay of the complex (instrument's response function has been represented by black line)*

***Table 4.2b**: Time-resolved fluorescence parameters of **$OxyLH_2$**-Luciferase complexes in aqueous buffers.*

Compound		Neutral Emission				Anionic Emission			
		pH	λ_{Ex}/nm	λ_{Em}/nm	τ/ns (%)	pH	λ_{Ex}/nm	λ_{Em}/nm	τ/ns (%)
$OxyLH_2$	w/Luc	5	370	450	<0.05[a]	5	370	550	0.16 (52) 1.04 (8) 7.63 (40)
	+Luc			445	2.04 (39) 9.5 (61)			515	11.28
	w/Luc						370	640	0.16 (12) 0.56 (80) 7.28 (8)
	+Luc							630	0.18 (62.8) 9.8 (27.5) 20.5 (9.7)
	w/Luc					7.4	430	550	0.17 (32) 0.53 (19) 3.95 (6) 7.68 (43)
	+Luc							540	0.13 (71.8) 2.2 (16.7) 9.66 (11.4)
	w/Luc						510	640	0.41
	+Luc							630	0.41
	w/Luc					10	430	540	5.91
	+Luc							535	6.11

w/Luc: Without Luciferase/Free compound, +Luc: Bounded with Luciferase, a: Short component for nonexponential decay

4.7 Conclusion

In the previous chapter, we have already discussed about the proposed model of the photoluminescence pathway of different chemical forms of Oxyluciferin in aqueous buffer. We have compared those results with the ones obtained in the presence of Luciferase. By using selective photo-excitation of particular chemical form of Oxyluciferin in complex with Luciferase in aqueous buffer and with the help of these preliminary results, we could decipher the photophysical properties of those chemical forms inside the Luciferase pocket. From the analysis of the fluorescence anisotropy and blue shift in the emission maxima, we could interpret the effect of the microenvironment (that is induced by the binding to the protein) on the optical properties of the dye. In addition we could re-draw and propose the photoluminescence pathway of the emitter in aqueous buffer (scheme 4.1) when in complex with the enzyme i.e. the photoluminescence pathway in the exact natural condition. We have observed that the ground state properties (absorption) are not modified by the binding process of Oxyluciferin (or its analogues). Based on this observation, the emission mechanism of the Oxyluciferin-Luciferase complex can be interpreted in these terms:

i. increase in emission intensity has been observed for the spectra when it is in complex with Luciferase. Rigidity of the microenvironment is responsible for the increase in the emission intensity. In a rigid microenvironment blue shift

in the emission maxima can be expected. In a rigid structure, Oxyluciferin can be tightly linked with Luciferase active site (inside the pocket) via hydrogen bonds. The rigidity of the active site pocket restricts any structural adjustment which can result into insufficient time delay for structural relaxation of Oxyluciferin before de-excitation (emission) starts. Therefore average fluorescence intensity increases and along with blue shift in the spectra. Although spectral shape remains identical. Binding site polarity/hydrophobicity and rigidity are to be considered for this argument.

ii. as proposed in earlier studies[12,43,48,100] and as discussed in the above section, the increase in the emission blue shift and the anisotropy can be associated with the change in the local environment of the dye. More the hydrophobicity, larger the blue shift is. In addition, the amplitude of the blue shift is also related to the accessibility of the solvent to water inside the protein. Small blue shift is associated with a fluorophore close to the surface of the protein (e.g. **phenol-enol-OxyLH$_2$**) because of an increase in the water accessibility. A high blue shift in the emission refers to the deeper access of the fluorophore inside the active site pocket of the protein (e.g. **phenolate-enol-OxyLH$^-$**). Fluorescence anisotropy is directly correlated with the strength of the encapsulation of the fluorophore inside the pocket. Also, it is noteworthy to mention that when bound to the protein molecular weight of the fluorophore (complex) increases. Therefore its anisotropy increases.

iii. this parameter of the protein-fluorophore complex can be studied further by time resolved fluorescence anisotropy. We have observed increase in excited state lifetime parameters of Oxyluciferin due to binding to protein. Depending on the rigidity and packing inside the active pocket, the fluorophore may rotate faster and shows short rotational correlation time components. But when the fluorophore is properly encapsulated inside the pocket, because of higher molecular weight of the complex and less water accessibility, longer rotational correlation time can be expected[120,158].

iv. The strongest modification in the optical properties has been observed for the **phenolate-enol-OxyLH$^-$**. We can conclude that, in this condition, the complex experience the highest hydrophobic environment. **Phenolate-enol-OxyLH$^-$** when free of Luciferase has negligible contribution in the absorption spectra (see figure 3.6) but when bounded to Luciferase it can have a large blue shift with a monoexponential fluorescence decay of ~5.5 ns.

v. except in physiological pH, keto-Oxyluciferin (**5,5-Cpr-OxyLH**) could not bind to the protein properly. Changes in the fluorescent anisotropy values are negligible in these conditions. Similarly, at pH 10 (**phenolate-enolate-OxyL^{2-}**), **OxyLH$_2$** was also unable to bind with the protein. Indeed, neither any blue shift in the emission maxima nor any changes in the fluorescence anisotropy were observed except for **5,5-Cpr-OxyLH** in pH 5 where a blue shift of 11 nm was recorded. This blue shift can likely be associated with the change in its litetime values (see figure 4.11c). For rest of the conditions, negligible changes in the lifetime values could be observed.

These conditions are not in the favor of the complex formation (see boldface fonts in table 4.1).

vi. the order of emission energies is almost identical to the same reported by us in the previous chapter, except the shift of phenolate-enol OxyLH$^-$ form. The emission energies of the complex is: *phenol-enol-OxyLH$_2$ (437 nm) > phenolate-enol-OxyLH$^-$ (521 nm) > phenol-keto-OxyLH$_2$ (523 nm) > phenolate-enolate-OxyL^{2-} (536 nm) > phenol-enolate-OxyLH$^-$ (552 nm) > phenolate-keto-OxyLH$^-$ (637 nm).*

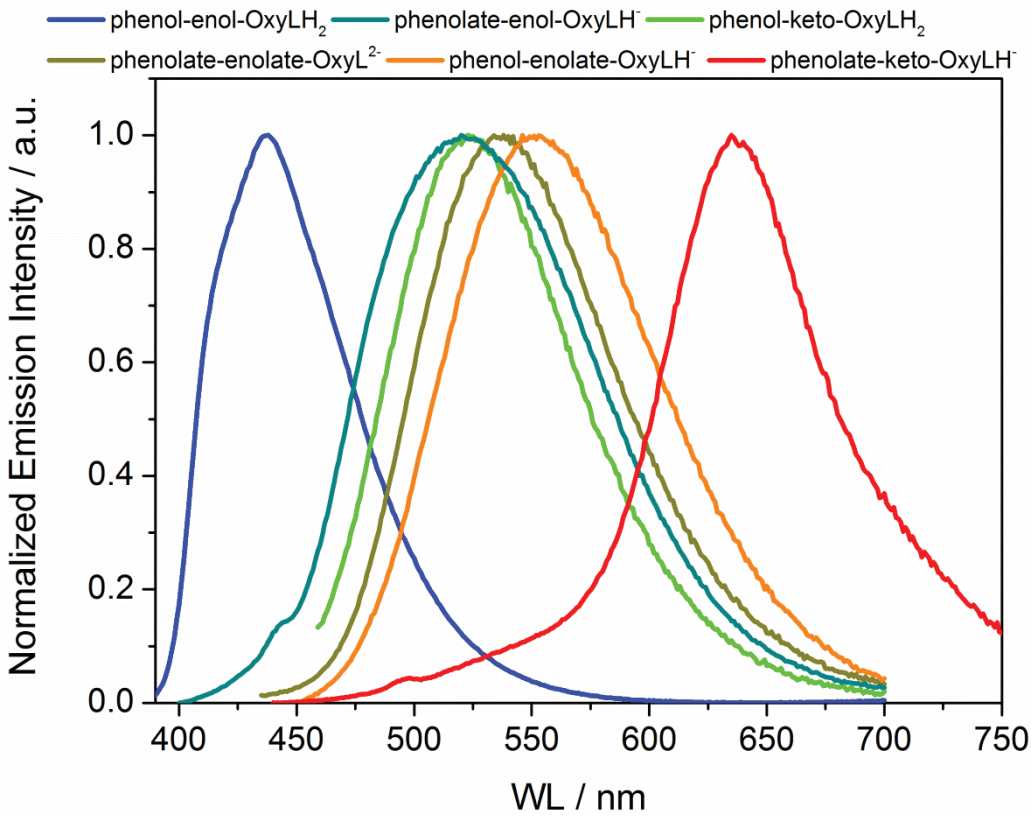

***Figure 4.14**: Emission spectra of different chemical forms of Oxyluciferin-Luciferase complexes in aqueous buffer.*

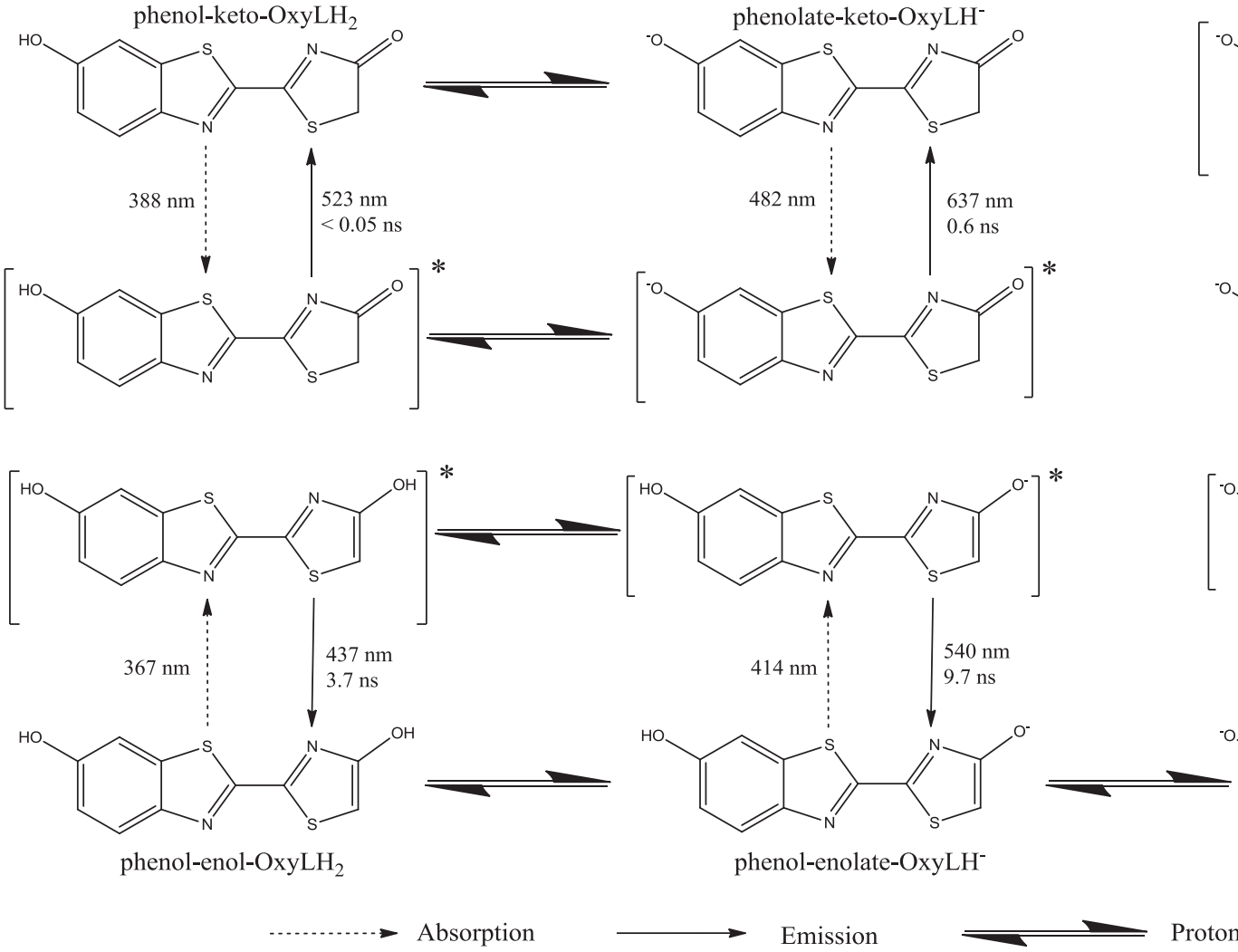

***Scheme 4.1**: Proposed Photoluminescence pathway of Oxyluciferin-Luciferase complex in*

Appendix-B

B.1 Scatchard Function[157]

Scatchard model function is a method of linearisation of data from a saturation binding experiment in order to determine binding constants (k). The model can be expressed as *r/c = (nka-rka)*, where *r* is the ratio of the concentration of bounded ligand to total available binding sites, *c* is the concentration of free ligand, and *n* is the number of binding sites per protein molecule. The plot yields a linear function with a slope corresponding to the binding affinity. Dissociation constant K_D is equal to inverse of ka.

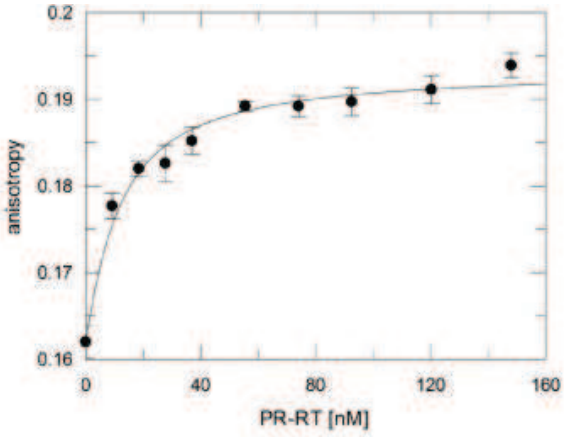

***Figure B.1**: Determination of k_D value from fluorescence anisotropy of labeled DNA by using Scatchard function (Leo B. et al. Adapted Form)*[8]

For calculating dissociation constant (K_D) of the binding of the protein (P) with the ligand (L), modified Scatchard function was used. Modified Scatchard function can be represented as:

P+L → PL $\qquad r_T = (1-f_L)r_L + f_L r_L \qquad f_L = \dfrac{[P_T][L_T] + K_D - \sqrt{\Delta}}{2[P_T]}$

$$\Delta = ([P_T] + [P_T] + K_D)^2 - 4[P_T][L_T]$$

Where,

$[P_T]$	:	Concentration of protein
$[L_T]$	:	Concentration of ligand
r_L	:	Anisotropy of the ligand free of protein (unbound ligand)
r_T	:	Anisotropy of the protein-ligand complex

B.2 Fluorescence time resolved parameters of other Oxyluciferin-Luciferase complexes

The following figure represents remaining (other than reported in figure 4.10-4.13) fluorescence time resolved decay (also compared with free Oxyluciferin) of studied Oxyluciferin-Luciferase complexes in aqueous buffer at different experimental conditions.

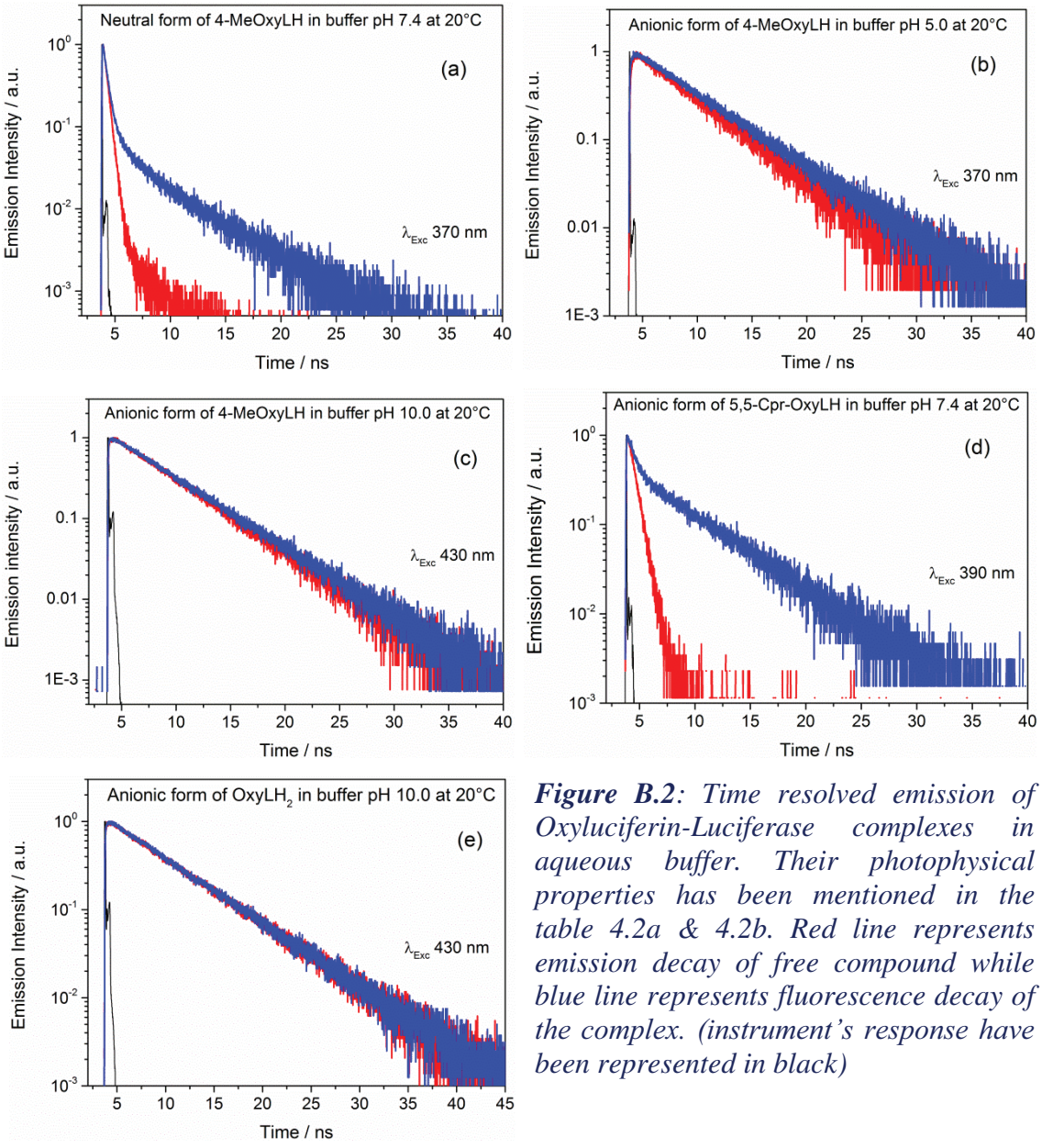

***Figure B.2**: Time resolved emission of Oxyluciferin-Luciferase complexes in aqueous buffer. Their photophysical properties has been mentioned in the table 4.2a & 4.2b. Red line represents emission decay of free compound while blue line represents fluorescence decay of the complex. (instrument's response have been represented in black)*

Chapter 05

Results & Discussions

Application of Oxyluciferin as a bio-analytical probe

Application of Oxyluciferin as a Bio-Analytical Probe

Fluorescence based techniques have become an invaluable tool for investigating biomolecular interactions[105]. For potential biological applications of fluorescence emission from firefly Oxyluciferin, a better knowledge of photophysical properties of this natural fluorophore in biological context is essential. Triple acid/base and keto/enol equilibrium (pKa, pKa*)[48] of natural and five closely related analogues of Oxyluciferin have been elucidated by analyzing their steady state and time resolved characteristics in aqueous buffers at physiologically relevant pH range[24 9,42,97].

Firefly Luciferin and Oxyluciferin are highly specific to the substrate. Methylation at 6'C-benzothiazole and/or 4C-thiazole inhibit the interaction between Oxyluciferin and its microenvironment[48]. Because of its better ability to convert chemical energy into light and exceptionally high signal-to-noise ratio, (therefore, very high fluorescence quantum yield),[5,48] Oxyluciferin can be used for sensitive bio-imaging applications[32] overcoming the major limitation of chemi-luminescence reaction which has much lower fluorescence quantum yield.

From the steady state and time resolved data interpretations[48], it has been understood that Oxyluciferin and its prime analogues can be good candidates to be employed for studying *in-vivo* or *in-vitro* biomolecular interactions. In particular, the environment sensitive properties of Oxyluciferin can be used to evidence biomolecular interaction. Fluorescence lifetime imaging and fluorescence quenching mechanism have been the key parameters to promote Oxyluciferin as a bio-analytical tool.

Herein, we will present the results obtained by using Oxyluciferin and its classic polarity dependent fluorescence mechanism as a tool to monitor biomolecular interactions. Oxyluciferin (**$OxyLH_2$**) and its two prime analogues **4-MeOxyLH** and **4,6'-DMeOxyL** have been coupled to proteins of Human Immunodeficiency Virus type-1 (HIV-1) and their photophysical properties have been studied *in-cellulo* and in complex with different oligonucleotide sequences. By monitoring distinct fluorescence emission properties of these derivatives, for the first time, we were able to study *in-vitro* biomolecular interactions using Oxyluciferin as a sensor. Also, it could be possible to use high affinity to thiol reactive group of keto-Oxyluciferin as a site specific fluorescent label for human protein Alpha-1 Antitrypsin (α1-AT). Results presented in this chapter will be communicated soon for publication in a peer reviewed journal.

5.1 *In-cellulo* Fluorescence Lifetime Imaging Microscopy with Oxyluciferin

It has been observed that **$OxyLH_2$** has different excited state lifetime within the physiological pH region. Its excited state lifetime decay is prominently sensitive to the change in environmental pH. Significant variation at different pH ranging 5-11 has been observed from its time resolved spectroscopic parameters (see table 3.1). In particular, **$OxyLH_2$** can be used to map the intracellular pH profile. To this aim, we used the very

specialized cell penetrating characteristics of HIV-1 Tat peptide labeled with **$OxyLH_2$**, and its neutral analogue **4,6'-DMeOxyL.** Next, Fluorescence Lifetime Imaging Microscopy (FLIM) allowed us to observe distribution pattern of excited state lifetime within the cytoplasm. Structurally modified **$OxyLH_2$** and **4,6'-DMeOxyL** have been attached to the N terminal of Tat(44-61) peptide acting as a cargo protein and cellular internalization imaging experiments were performed. The neutral Oxyluciferin analogue, **4,6'-DMeOxyL**, is not responsive to ESPT mechanism and has only one excited state lifetime invariable throughout the entire pH range (5-11)[48]. This neutral analogue of Oxyluciferin served as a negative control where changes in fluorophore lifetime correlated with pH variation cannot be expected.

Human Immunodeficiency Virus type-1 (HIV-1), the causative agent of AIDS (Acquired immunodeficiency syndrome), has two essential core proteins that can bind RNA sites and contain basic domains i.e. trans activator (Tat) protein and nucleocapsid protein (NCp7)[112,114]. Tat is a very crucial protein involved in HIV-1 life-cycle during viral transcription. Importantly, this protein is the most ideal target for drugs intervening with lentiviral growth[159]. Tat is a very small protein with 86-101 amino acids constituted with a highly cationic cluster which includes six Arginine and two Lysine residue in the middle of the peptide sequence along with an α-helical structure at the N terminal[132,160]. A number of studies showed that this unique structure has a very strong cell translocation property[160,161] where covalent conjugate bond between the cell penetrating peptide (CPP) and various types of cargo molecule allows easy intracellular cytoplasmic cargo delivery[161]. This N terminal part of Tat is used to introduce foreign molecules inside the cell[161]. The α-helical conformation and cationic cluster is also ready to adopt the extended structure[132,160] i.e. CPP-cargo molecule conjugate. Due to its highly cationic nature, several anionic cellular entrants can be accessible to control the cell penetration mechanism of this peptide. It has already been shown that delivery of protein and other biomolecules into cells is possible by cationic peptides like Tat[160] which can facilitate cytoplasmic delivery of its cargo. The most remarkable fact about this CPP is its ability to carry diverse range of cargo as a vector system. Very small molecules (~100 Da) to massive biomolecule with a diameter of ~200 nm can be transduced inside the cell using this CPP[132,160]. Several articles reported already that this ATP and temperature independent cellular uptake technique allows safe delivery of wide range of cargo molecules including low molecular weight drugs, small oligonucleotide, peptides, full length proteins etc. with expected functional activity *in-vivo* or *in-vitro*[160].

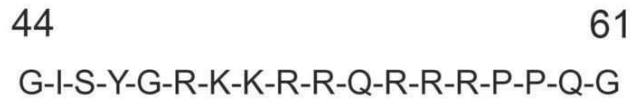

***Figure 5.1**: Amino acid sequence of HIV-1 Tat(44-61) used in this study[112]*

5.1.1 Two-Photon Excitation microscopy of $OxyLH_2$ labeled HeLa cells

Cellular internalization, uptake and cytoplasmic distribution of **$OxyLH_2$** were the main concerns before monitoring *in-cellulo* fluorescence lifetime distribution pattern of the fluorophore. Indeed, two significant properties have to be satisfied i. cellular internalization and distribution of Tat peptide labeled with Oxyluciferin has to be like the staining of non-labeled Tat and ii. possibility of using 2-photon excitation with Oxyluciferin. Prior to proceed for FLIM experiments, HeLa cells were incubated with 0.3-0.7 µg/ml $OxyLH_2$ labeled Tat(44-61) peptide for 30-45 min. Then cytoplasmic distribution of labeled peptide was visualized with two-photon excitation at 780 nm. In the figure 5.2, HeLa cells incubated with **$OxyLH_2$** can be observed with two-photon excitation. As depicted in figure 5.2, Tat peptide labeled with Oxyluciferin can be efficiently internalized within the living cell. In addition, the observed fluorescence staining of the cells are in line with the usual localization of free Tat peptide reported earlier with the help of other fluorophores[162-164] and most importantly, the fluorophore can easily be excited by two-photon excitation.

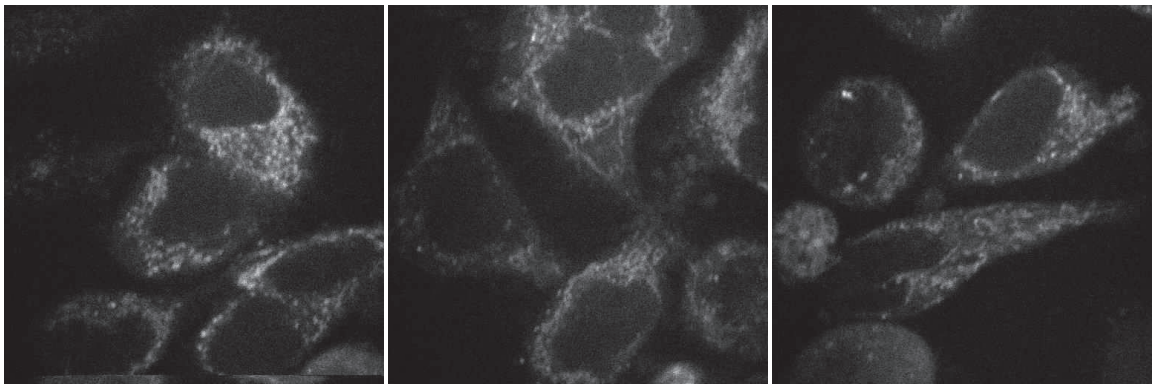

***Figure 5.2**: Two photon excitation microscopy of HeLa cells incubated with Tat peptide labeled with **$OxyLH_2$** (λ_{Exc} 780 nm, avg. laser power < 0.5 mW, 50x50 µm)*

5.1.2 Fluorescence Lifetime Imaging Microscopy (FLIM)

HeLa cells were incubated with Tat peptide whose N terminal has been coupled to either Oxyluciferin (**$OxyLH_2$**) or to its neutral analogue **4,6'-DMeOxyL**. Their excited state lifetime distribution pattern within the cytoplasm has been observed with fluorescence lifetime imaging microscopy with pulsed two-photon excitation at 780 nm with an average laser power lower than 0.5 mW in the sample plane. The labeled peptide concentration was 0.3-0.7 µg/ml and the incubation time was set to 30-45 min, next cells were washed with the media as described in « Materials and Methods » and further incubated with same media. To monitor the distribution pattern of excited state lifetime generally a single cell or two fused cells have been observed and fluorescence decays were recorded for 120-180 seconds.

As presented in the third chapter, **$OxyLH_2$** displays optical properties that are very sensitive to pH. In particular, the excited state lifetime of **$OxyLH_2$** varies significantly within a pH range that is perfectly comparable to the cytosolic pH of HeLa

cells. Intracellular pH can vary from as low as 4.5 (Lysosomal pH) to as high as 8.0 (Mitochondrial pH)[165]. Hence different excited state lifetime values of **$OxyLH_2$** can be expected when it is scattered within the heterogeneous pH environment of the cytoplasm. The fluorophore lifetime is completely dependent on the microenvironment surrounding the molecule. On the other hand, doubly methylated analogue (**4,6'-DMeOxyL**) is neutral in nature and does not respond to pH modifications in the microenvironment. Its absorption, emission and excited state lifetime values cannot be modified through pH changes as both –OH group positions (6'C-benzothiazole and 4C-thiazole) are methylated to prevent this molecule to undergo any protonation or deprotonation reaction. **4,6'-DMeOxyL** is not responsive to ESPT mechanism and has only one excited state lifetime value throughout the entire physiological pH region (5-11)[48]. Therefore, this analogue has been preferred as a negative control to the FLIM experiment of HeLa cells stained with Tat(44-61) labeled with **$OxyLH_2$. $OxyLH_2$** and **4,6'-DMeOxyL** have absorption spectra which are ideal for the excitation at 390 nm. Absorption maxima for **4,6'-DMeOxyL** is 367 nm and isosbestic point for **$OxyLH_2$** is 385 nm in aqueous buffer[48] (see figure 3.2).

To monitor the photodynamic response of **$OxyLH_2$** within the cytoplasm, another control mechanism has been used. Influence of Monensin Sodium Salt (CAS No. 22373-78-0) on living cells ought to be a good means to further prove that the distribution of fluorophore lifetime within living cells[166-168] can be associated with spatial pH changes. Monensin is an ionophore capable of breaking down Na^+ and H^+ gradients within the living cell[168]. Monensin, with an affinity to form a complex with monovalent cations, has an ability to diffuse through the cellular and sub-cellular lipid membranes by ion exchange method. It can block intracellular protein transport and other biological activities by causing lysosomal acidification that results in an increased H^+ concentration inside cells and homogenize cytosolic pH[168,169]. The effect of Monensin could be followed by monitoring Oxyluciferin fluorescence lifetime distribution pattern further evidencing the ability to use Oxyluciferin as a bio-analytical fluorophore.

Due to the acidification of the cytoplasm, nearly homogeneous cytoplasmic pH can be expected. So, different lifetime distribution pattern can be expected for **$OxyLH_2$** as at certain pH it must have a particular excited state lifetime value. The presence of Monensin should not alter the excited state fluorescence lifetime for **4,6'-DMeOxyL** because the photophysical properties of this derivative is not pH dependent. HeLa cells were incubated with 0.3-0.7 µg/ml Tat(44-61) peptide labeled with either **$OxyLH_2$** or **4,6'-DMeOxyL**. Their lifetime distribution within the cell has been recorded. Further the cells were treated with Monensin salt and again their lifetime distribution was recorded. The lifetime distributions for both derivatives at two different conditions (normal/heterogeneous pH and Monensin treated/homogeneous pH) are represented in figure 5.3.

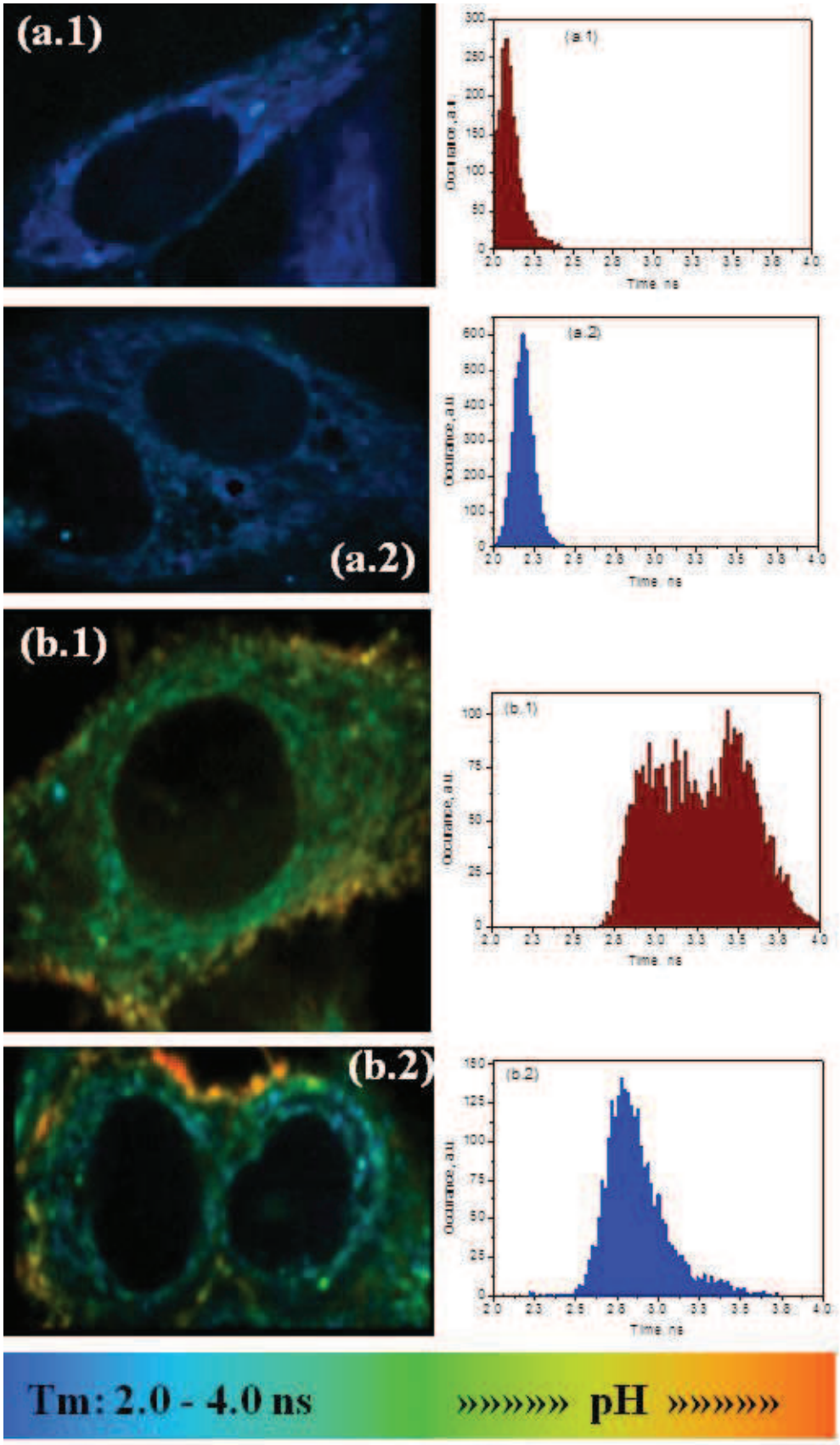

***Figure 5.3**: FLIM images (left panel) and lifetime distribution (right panel) of HeLa cell incubated with Tat labeled with different Oxyluciferin; (a) **4,6'-DMeOxyL**, (b) **OxyLH$_2$**; with (row 2 & 4) and without (row 1 & 3) Monensin salt (λ_{Exc} 780 nm, avg. laser power < 0.5 mW)*

In figure 5.3, left panel displays the lifetime distribution images obtained within living cells with: (a) **4,6'-DMeOxyL**, (b) **$OxyLH_2$** in normal condition (row 1 & 3) and with Monensin treated conditions (row 2 & 4). Their corresponding lifetime distribution histograms are reported in right panel respectively. Cells incubated with Tat(44-61) labeled with **4,6'-DMeOxyL** shows a very narrow lifetime distribution (centered around 2.1 ns) which is not significantly affected when the cells are further treated with 20 µg/ml Monensin salt and are having a homogeneous cytosolic pH. For both conditions (homogeneous and heterogeneous cytosolic pH) the lifetime distribution pattern is identical (see figure 5.3a) and centered at 2.1 ns. Such observation is in full line with the results presented in chapter 3.

Significant changes in the lifetime distribution were observed with cells incubated with Tat(44-61) labeled with **$OxyLH_2$**. Cells incubated with **$OxyLH_2$** at normal condition shows a broad distribution of lifetime (see figure 5.3b1) ranging between 2.75-4.0 ns. Such observation can be associated with the heterogeneous pH pattern within the cell, which is possible because the excited state lifetime of **$OxyLH_2$** is pH dependent. While incubated with 20µg/ml Monensin salt (at homogeneous cytosolic pH) a significant change in lifetime distribution could be noticed (see figure 5.3b2). In a homogenous pH environment, the lifetime distribution remains very narrow and centered about 2.80 ns. Due to the Lysosomal acidification, cytosolic pH become homogeneous and at a certain pH and thus a specific excited state lifetime is expected from **$OxyLH_2$**. The presence of orange particles in figure 5.3b2 can correspond to the undamaged endosomes. Lowering in the lifetime value are perfectly in accordance with its steady state data. In aqueous solutions at lower pH, **$OxyLH_2$** has low excited state lifetime value which increases with pH due to change in proton transfer mechanism. It is also noteworthy to mention that no damages were observed on cells during data acquisition. Although, cells treated with Monensin lost their morphology within 30-45 min after Monensin injection.

From the in-vitro analysis, existence of multi component in the excited state lifetime of **$OxyLH_2$** was observed[48]. Due to the higher signal to noise ratio in measurements performed in living cells, the FLIM images were re-analyzed by using a two population model with an iterative deconvolution algorithm. Apart from the mean lifetime distribution, contributions of individual components have been analyzed and the amplitudes (α) distributions have been plotted (see figure 5.4). A significant change in the distribution (represented in figure 5.4) is observed with cells displaying homogeneous and heterogeneous cytosolic pH. This multi-component analysis further strengthens the possible use of **$OxyLH_2$** as pH sensitive probe that can be useful for *in-cellulo* pH monitoring.

The results presented above demonstrate that Oxyluciferin can be used to probe pH within living cells. We were indeed able to sense the *in-cellulo* pH and shown that the fluorophore was not toxic for the cells. In addition, the staining procedure was quite simple. To determine intracellular pH in an absolute manner, further experiments have to be performed to correlate the fluorescence lifetime of the dye with a specific pH value. To this aim, calibration FLIM measurements will be done with prepared solution displaying a certain pH.

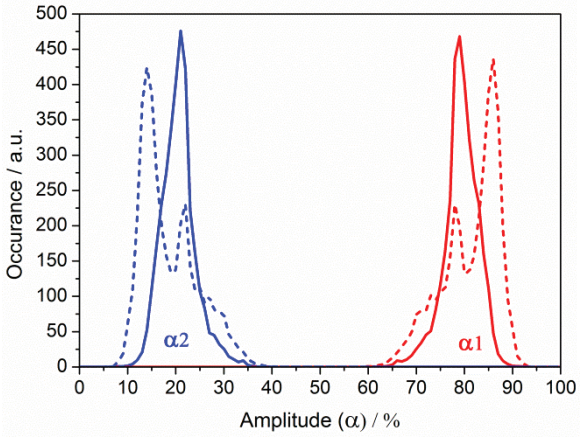

Figure 5.4: *Contribution of individual lifetime components of Tat peptide labeled with* ***OxyLH$_2$*** *inside HeLa cells. (Solid line represents normal condition while dotted line represents distributions within Monensin treated cells. Blue lines represent occurance of first component while red lines represent occurance of the second component).*

5.1.3 Most of the commercially available fluorophores are insensitive to in-cellulo pH

The most common commercial fluorophores (applicable for biological event monitoring) which are sensitive to pH are Cy-5, Cy-7, Texas Red, Dylight-649, TMR-Dextran, Alexa-647 Alexa-750, Atto-647, Carboxyfluoresceine based fluorophores, Napthofluoresceine, FITC-Dextran etc.[165] Although, the pH range, within which their photophysical profile varies, differs broadly. For example, Alexa-647 and Alexa-750 shows ~18% fluorescence quenching at pH 3-4 while Atto-647 shows increased emission at pH < 4.0 and so on. It has been established that the intracellular pH varies from 4.5 to 8.0. So, it can be argued that to monitor intracellular pH, the fluorophore must be sensitive in terms of its photophysical properties within this range. Most of the commercially available fluorophores, except Carboxyfluoresceine based fluorophores and FITC-Dextran, are insensitive in this physiological pH range (4.5-8.0). In additions, these fluorophores are excitable either in the green or NIR region and their Stokes Shift is also very less (most of the cases < 30 nm). On the contrary, Oxyluciferin is excitable at UV region and has much larger Stokes Shift.

Analysis of FLIM results obtained with **OxyLH$_2$** can be compared with commercially available lysosome tracking fluorophores. These commercially available fluorophores exhibit pH dependent increase in fluorescence intensity upon acidification. Their photophysical properties change according to the solvent pH. Lysosome tracking probes are used to investigate acidification of lysosomes and alterations of its function or other intracellular activities that can be associated, e.g. lysosomes in some tumor cells have a lower pH than usual while other tumor cells can have higher pH. In addition, cystic fibrosis and other diseases result in decrease in intracellular pH of some intracellular organelles and the lysosome tracking fluorophores are useful to study these aberrations[170-172]. OxyLH$_2$ also exhibits exactly similar photophysical properties and possibility of its application for the above said methodology cannot be neglected.

5.2 Monitoring interactions between HIV-1 NCp7 and oligonucleotides

Another protein, HIV-1 NCp7 plays essential multiple roles in viral replication. Antiviral drugs can target various steps during this virus replication[115]. Although, several attempts failed because of emergence of resistant strain in the target part of HIV-1 and needs a wider exploration of these molecular targets to resolve this disappointment[115]. One of these possible targets is the HIV-1 nucleocapsid-7 protein (NCp7), a 72 amino acids long basic protein with two highly conserved zinc-finger (ZF) motifs[115,173] which binds to the viral genomic RNA[173]. A highly basic linker sequence "RAPRKKG" connects these two ZFs[111]. NC can bind specifically or non-specifically, to any oligonucleotide (NT) sequence such as stem-loop structured cTAR (complementary Transactivation Response Region) or single-stranded sequences with a binding affinity in micro/nanomolar range. This binding affinity strongly depends on several parameters including amino acid sequence of the peptide, concentration, nature and folding of the NT sequence etc. Ionic strength plays an vital role for the affinity of binding[105,111,114,115,133,174,175]. NCp7 shows strong salt dependent affinity to bind any small NT sequence (5-8 in length) mostly unspecifically through electrostatic interactions, as well as it shows specific binding to some long single-stranded and stem-loop sequences. This specific binding is strongly promoted by the hydrophobic platform formed on the top of ZFs by several amino acid residues e.g. Val13, Thr24, Trp37, Met46 etc. which allows a non-electrostatic interaction between the oligonucleotide and NCp7[111].

Several previous studies[105,111,114,115,133,173,175] show, how NCp7 can bind with different stem-loop and single-stranded oligonucleotide sequences. Solvatochromic fluorophores are ideal to understand molecular interaction between NCp7 and different NT sequences. Short peptides labeled with these fluorophores have been used for studying protein-protein interactions and/or protein-NT interactions. These interactions are commonly studied by monitoring change in polarity of the microenvironment at the active site, readily detected from the change in fluorescence emission[105]. However studying interaction of labeled peptide and NT becomes more challenging as oligonucleotide environment is relatively polar and may not be dramatically affected by the polarity change. Polarity sensitive fluorophore like Oxyluciferin[48] can be very much useful in this concern. At pH 7.4 (physiologically relevant pH) Oxyluciferin analogue **4-MeOxyLH** has dual emission band; one centered at ~450 nm and other centered around 560 nm. Change in intensity at these two emission energies can be very useful for monitoring environmental modifications induced by the interaction between NCp7 and NT.

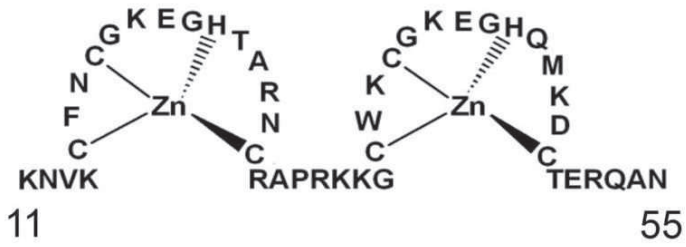

***Figure 5.5**: Amino acid sequence of HIV-1 NCp7(11-55) used in this study*[112]

5.2.1 Site-specific interaction between NCp7 and oligonucleotides (NT) sequences

NCp7 can non-specifically bind small NT sequence or specifically bind to some long single-stranded and stem-loop sequences such as TAR sequence with a binding affinity in nanomolar to a few micromolar range. The binding affinity strongly depends on the ionic strength of the system, structure of the protein, concentration, nature and folding of the NT sequence etc.[105,111,114,115,133,174,175] The site specific binding of NCp7 and stem-loop oligonucleotide is strongly promoted by the hydrophobic platform formed on the top of ZFs. Amino acid residues which are actively involved in the non-electrostatic interaction between NCp7 and NT are Val13, Phe16, Asn17, Thr24, Arg32, Ala35, Trp37, Gln45 and Met46[111,113]. The hydrophobic platform created by Val13, Phe16, Thr24, Trp37 and Gln45 specifically supports interaction of GGAG or GGCG sequence. The stabilization of the complex is provided by the Trp37 residue through its stacking with the central G residue[111]. For very short specific NT sequences (5 or 6 nucleotides) specific binding is possible with an affinity of 330-400 nM. Trp37 can bind to C and/or G residue present in the middle of the sequence[105,111].

Interaction of NCp7 with stem-loop structures is more site specific[111]. NMR study by Bourbigot et al. confirmed how NCp7 can bind and destabilize (-)Primary Binding Site (-PBS) sequences during reverse transcription phase[116]. The adjacent figure[116] represents nucleotide sequence of ΔP(-)PBS. Two independent binding sites, one with a high affinity of protein (80nM) and other with ~10 times lower affinity (910 µM), have been identified by NMR studies. Study of Bourbigot et al. on (-)PBS and ΔP(-)PBS interaction with different mutant of NCp7, confirmed site specific binding of NCp7 with this NT sequence. Almost two NCp7 per ΔP(-) PBS is required for the binding. An insertion of Trp37 and Phe16 in between T6 and G7 in the loop is reported by the NMR studies[116,176]. The first residues of the loop T6 and G7 force NCp7 to interact with C5 which is in paired with G11 on the stem. Identified binding sites of NCp7 for ΔP(-)PBS are 5-CTG-7 (higher affinity) and 10-CGG-12 (lower affinity).

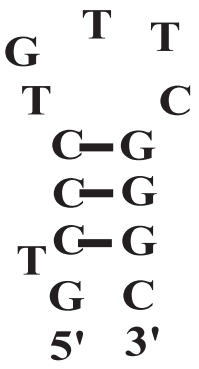

Role of fluorescence quenching of solvatochromic fluorophore in monitoring interaction between NCp7 and NT has been explained nicely by Godet et al.[120], Shvadchak et al.[105] and Beltz et al.[133]. They have monitored NCp7 induced structural and

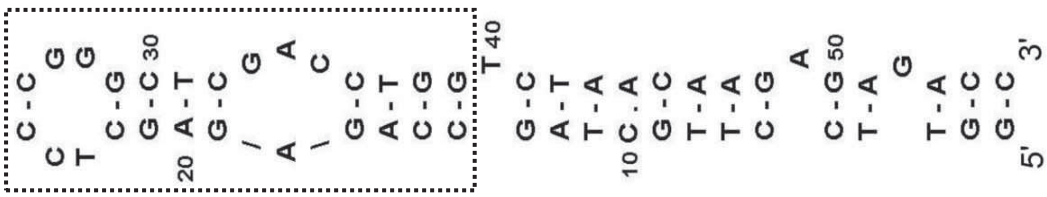

dynamical perturbations in the cTAR structure. The adjacent figure represent nucleotide sequence of cTAR[120] and sequence outlined by dotted box represent mini-cTAR[119]. cTAR is highly dynamic in nature specially at the lower stem. Its terminal loop is found to be highly flexible while its internal loop is highly constrained. At a ratio of 1:1

NCp7/cTAR, the peptide shows a preferential binding to cTAR. The major NCp7 induced structural conformation can be observed at the lower stem (notably at the position 9/10 and 49/50) where direct interaction of Trp37 with G residue has been identified,[120] resulting to destabilization of cTAR stem. This NC induced restriction on the flexibility of cTAR prevents very fast transition of the complex (generally in picoseconds timescale) and form a locally destabilized domain with longer lifetime. Moreover they suggested that cTAR destabilization is result of progressive coating of cTAR by NCp7. The preferential binding of NCp7 at G9 or G50 residues confirms that NCp7 can specifically discriminate these two positions and can bind preferentially. Mini-cTAR shares same DNA-nucleotide sequence with cTAR. Upper hairpin part of cTAR (C14 to G26) has been proposed to be named as mini-cTAR.[119] NCp7 binding site for mini-cTAR have been identified at its lower stem 24-TGG-26 with an dissociation constant of 1.6 µM[118,119]. Identification of binding site of mini-cTAR proposes the other binding site for cTAR. Dissociation constants reported for different NT sequences at different experimental conditions are briefly summarized in the following table:

Sequence	K_D/µM	Buffer Sol^n/pH	[NaCl] /mM	NCp7	Method	Reference
DNA-5nt	0.33	Hepes/6.5	----	12-53	TFQ	Morellet et al.[113]
DNA-6nt	0.41	Tris/7.5	30	11-55	TMR/2f-FCS	Didier et al.[28]
DNA-12nt	0.71	Hepes/7.5	100	1-55	2ApF	Avilov et al.[177]
SL-20nt	1.0	Hepes/7.5	100	12-53	TFQ	Vuilleumier et al.[178]
cTAR	0.06	Tris/7.5	30	11-55	TFQ	Beltz et al.[133]
mini-cTAR	1.6	Tris/7.5	30	11-55	ITC	Bazi et al.[119]
ΔP(-) PBS	0.5	Tris/7.5	30	12-55	TFQ	Bourbigot et al.[116]

TFQ: Tryptophan Fluorescence Quenching, 2ApF: 2-Aminopurine Fluorescence, 2f-FCS: 2-focus FCS, ITC: Isothermal Calorimetry

*5.2.2 Labeling of NCp7(11-55) with **4-MeOxyLH** and selection of NT sequences*

In a next step, **4-MeOxyLH** was used to monitor the interaction of the NCp7 protein from HIV-1 with oligonucleotides. As reported in chapter 3, this Oxyluciferin derivative displays optical properties that can be explained by the coexistence of two spectral forms: the neutral (N*) and anionic (A*) forms. The ratio between these two forms (N*/A*) is strongly dependent on the local environment. In particular, both polarity and pH can tune the ratio. It has an isosbestic point at 383 nm with pKa of 8.7. At pH 7.4 (Abs Max 367 nm) with excitation at 385 nm, a dual emission band can be observed (see figure 5.6). A strong emission band centered at ~560 nm is the contribution from anionic Oxyluciferin which is accompanied by a weaker band centered at ~450 nm originating from neutral form of Oxyluciferin (see figure 5.6a). At pH 5.0 time resolved fluorescence decay of the neutral form (~450 nm) is strongly quenched and decays non-exponentially with a very short component of ~0.24 ns and the fluorescence emission at ~560 nm rises with an average time constant (~0.21 ns) that corresponds to the proton transfer rate and disappears biexponentially with ~l.5 and ~4.9 ns[48] time constants. Figure

5.6b shows time resolved fluorescence decay of NCp7(11-55) labeled with **4-MeOxyLH** recorded at both emission energies in buffer pH 7.4.

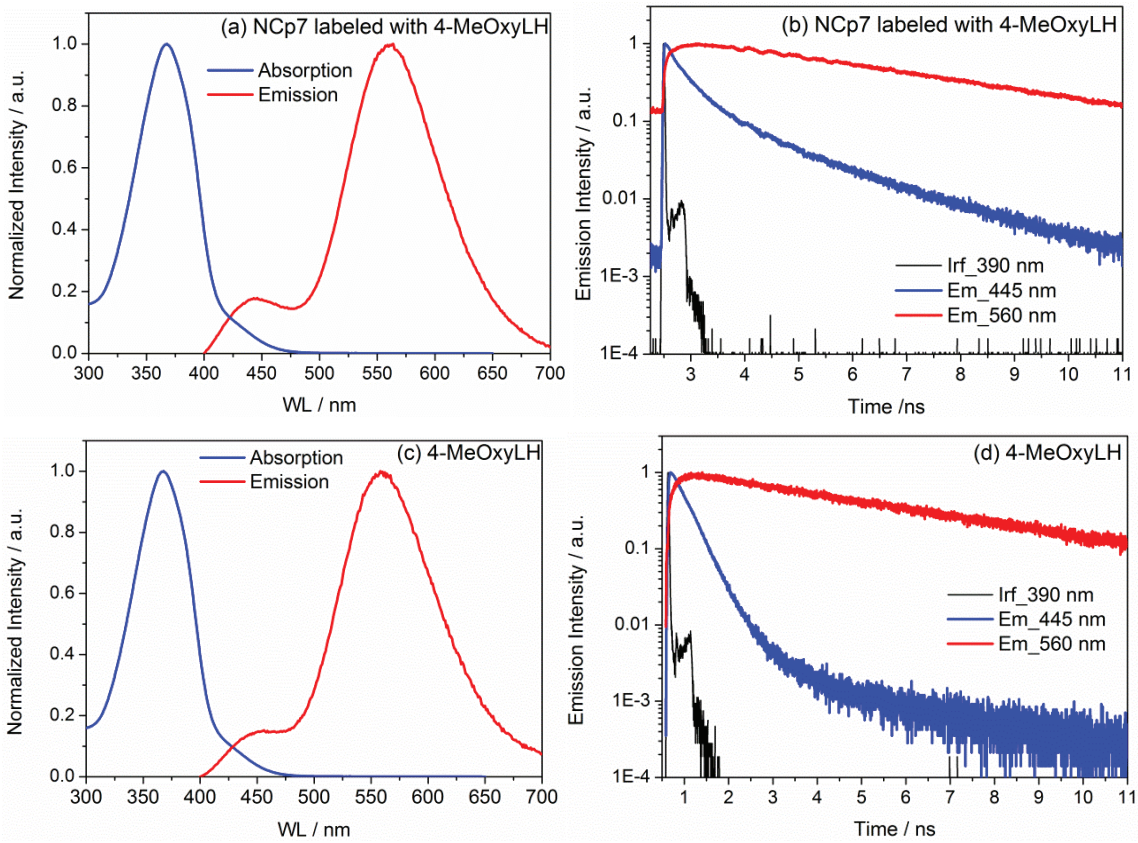

***Figure 5.6**: Photophysical properties of **4-MeOxyLH** coupled to NCp7(11-55) in buffer pH 7.4 at 20°C; (a) absorption and emission spectra, (b) time resolved fluorescence decay.*
*(c) absorption and emission spectra and (d) time resolved fluorescence decay **4-MeOxyLH** in buffer pH 7.3 at 20°C.*

Absorption, emission and time resolved data obtained for **4-MeOxyLH** coupled to NCp7 in aqueous buffer pH 7.4 are similar to that of free **4-MeOxyLH**[48]**.** Time resolved fluorescence decay of the neutral form (~450 nm) is quenched with a very short component of ~0.3 ns and decays biexponentially with time constants of ~0.7 and 2.6 ns. While the fluorescence emission at ~560 nm rises with an average time constant (~0.5 ns) that corresponds to the proton transfer rate and disappears with ~5.5 ns time constants. Figure 5.6b shows time resolved fluorescence decay of **4-MeOxyLH** coupled to NCp7(11-55) recorded at both emission energies in buffer pH 7.4. Thus, coupling of NCp7 with the fluorophore does not affect the photophysical properties of the dye.

When NCp7 is in complex with some other biomolecules (e.g. DNA/RNA) the emission properties of the dye can be affected. The conformational changes in the complex endorse fluorescence quenching on the either way. Fluorescence emission properties of **4-MeOxyLH**, when coupled to NCp7, can be affected when the protein is in complex with other biomolecules (see figure 5.8). The interaction affects the ratio between two emission energies. Ratio of these two emission intensities can then be used

to monitor the interaction between NCp7(11-55) and different oligonucleotide sequences. It has already been discussed that NCp7 can bind, specifically and non-specifically, to oligonucleotide sequences of different length and structure. To monitor this binding mechanism by using **4-MeOxyLH** as a reporter fluorophore, an experimental model has been developed where interaction between different single strand and stem-loop NT sequences has been observed through fluorescence quenching of **4-MeOxyLH** coupled to NCp7(11-55) with increasing NT concentration. Steady state fluorescence anisotropy and time resolved fluorescence decays were also used in the experiments. C and/or G rich different NT sequences ranging from small single-stranded (ss) to stem-loop (sl) structures used in this study were selected from the bibliographic studies and presented in the next table. The boldface underlined nucleotides correspond to the identified binding sites with maximum affinity for NCp7.

Name	Nucleotide sequences	No. of binding sites
Single-strand sequence (5'-3')		
DNA-5nt[113]	A**CG** CC	1
DNA-6nt[28,111]	AA**T G**CC	1
DNA-12nt[111,177]	TGA CC**G TG**A CCG	2
Stem-loop sequence (5'-3')		
SL-20nt[111,178]	GGA CTA GC**G GAG** GCT AGT CC	1
cTAR[120,133]	GGT TCC TT**G** CTA GCC AGA GAG CTC CCG GGC TCG ACC **TGG** TCT AAC AAG A**G**A GAC C	8
mini-cTAR[119]	CCA GAG AGC TCC CGG GCT CGA CC**T GG**	2
ΔP(-) PBS[116]	GTC C**CT G**TT **CGG** GC	2

These particular NT sequences have been obtained from earlier studies where NCp7 labeled with other fluorophores have been employed to monitor the interaction by means of fluorescence quenching mechanism. To decipher the exact structural conformation where NCp7 can bind to the NT sequence we include mini-cTAR and ΔP(-) PBS in our study (e.g. NCp7(11-55) can bind to the TGG sequence in the lower stem of mini-cTAR[119].

With the aim to monitor binding mechanism of NCp7 and DNA by using **4-MeOxyLH** as an indicator, N terminal of NCp7(11-55) has been coupled with **4-MeOxyLH** by solid phase synthesis method « see Materials & Methods ».

5.3 Activity test of NCp7(11-55) labeled with 4-MeOxyLH

In order to verify that NCp7(11-55) labeled with **4-MeOxyLH** is still biologically active, we used the classical cTAR destabilization experiment[179], where NC is known to promote changes in the fluorescence emission during unwinding of doubly-labeled cTAR[133]. Emission of cTAR labeled with TMR (Rh6-G) at 5' end and Dabcyl at 3' end has been recorded by exciting Rh6-G at 520 nm with and without NCp7 labeled with **4-**

MeOxyLH. In presence of NCp7, it is expected that the stem-loop of cTAR will unwind which can be determined by increased fluorescence emission of the donor (Rh6-G)[179]. In principle, the emission of Rh6-G is quenched by its structurally close neighbor Dabcyl. In presence of NCp7, bond between base pairs break and the stem starts to destabilize or unwind itself. The quenching efficiency of Dabcyl decreases as the distance between both fluorophores increases. A 4-fold increase in the intensity of Rh6-G emission (centered at 558 nm) has been observed due to unwinding of cTAR (see figure 5.7) in presence of 10x concentration of NCp7. Wild type NCp7 was used as a positive control and the obtained results were very similar. This test hence proved that the labeled peptide is biologically active.

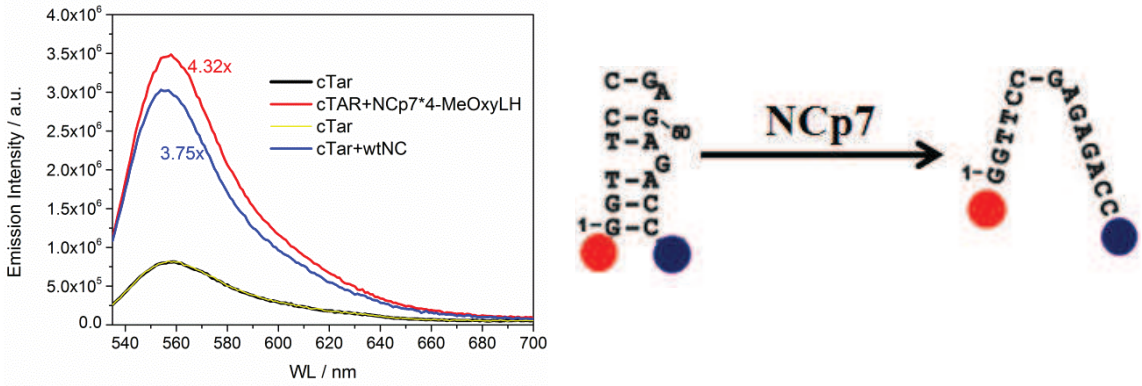

Figure 5.7: *In left, activity test of NCp7(11-55) labeled with* ***4-MeOxyLH****: Emission spectra of Rh6-G, attached to cTAR, in absence and presence of NCp7 labeled with* ***4-MeOxyLH*** *(Exc. WL 520 nm) and its comparison with wild type/non-labeled NCp(11-55). In right, schematic representation of dynamics of lower stem of labeled cTAR in presence of NCp7 (red circle represents Rh6-G and blue circle represents Dabcyl).*

5.4 Fluorescence quenching of NCp7(11-55) labeled with 4-MeOxyLH in complex with oligonucleotide

Fluorescence quenching of NCp7(11-55) labeled with **4-MeOxyLH** (NC) was monitored by increasing the concentration of different DNA (NT) in 25mM Tris/30 mM NaCl/0.2 mM $MgCl_2$ aqueous buffer at pH 7.4 (at 20°C). Their emission spectra have been recorded by exciting at 383 nm. In order to present results that are not dependent on the dye concentration, intensities of both emission bands were plotted in the form of a ratio (N*/A*) as a function of NT concentration. In parallel, fluorescence anisotropy of 0.25-0.5 µM NCp7(11-55) labeled with **4-MeOxyLH** has also been recorded with increasing concentration of NT (0 to > 3 µM). Fluorescence quenching of labeled NC has been observed when in complex with seven selective[111] NT sequences. By analyzing fluorescence anisotropy and N*/A* separately, using Scatchard function[157] (see Appendix-B.1), dissociation constants (k_D) for all DNA-NCp7 complexes could be calculated (see table 5.1).

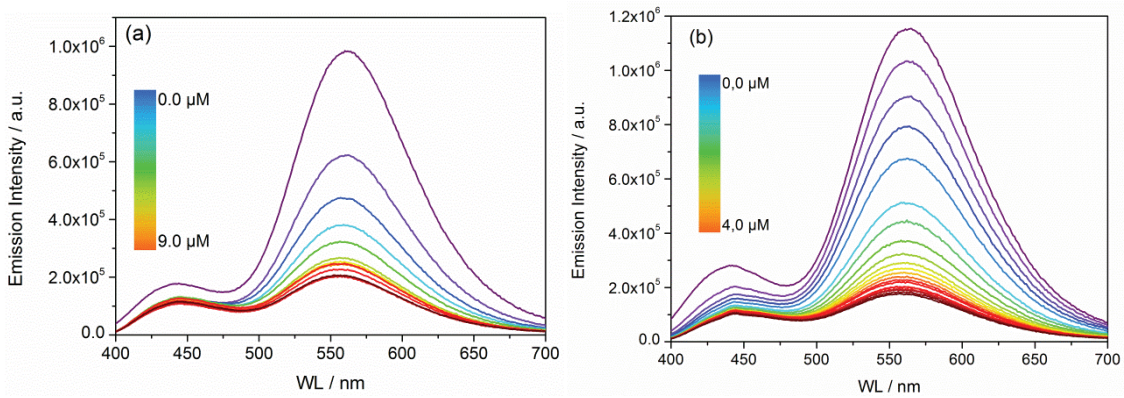

***Figure 5.8**: Fluorescence quenching of NCp7(11-55) labeled with **4-MeOxyLH** with increasing concentration of (a) DNA-12nt and (b) mini-cTAR.*

With the increase of the NT concentration, the NC starts to form a complex leading to an increase in the anisotropy. In parallel, the local electrostatic properties of the dye are modified by the binding event leading also to an increase of the N*/A* ratio. As reported in table 5.1, the changes in anisotropy and N*/A* ratio strongly depends on the NT sequence used.

Next, the interaction was monitored by measuring time resolved fluorescence decays. Both emission bands of **4-MeOxyLH** coupled to NCp7have their distinct excited state lifetime parameters. Emission at 445 nm is strongly quenched and decays multiexponentially while band at 560 nm grows with an average time constant corresponding to rate of proton transfer and disappear biexponentially.

Excited state lifetimes of NCp7(11-55) labeled with **4-MeOxyLH** have been recorded without and saturated concentration of NT. Change in the rate of ESPT could be observed when NC is in complex with a saturated (> 3 µM) NT concentration in the solution. As reported in table 5.1, additional components were observed both at 445 and 560 nm. In particular, a significant increase in lifetime can be observed (boldface fonts, table 5.1) which is likely due to a less efficient proton transfer associated with a change in the local environment of the dye. (although for very small ssDNA sequence of 5nt and 6nt change in lifetime could not be observed due to their unspecific binding with NC).

NC can bind specifically or non-specifically to NT. However the binding constant is strongly dependent on the nature and folding mechanism of the interacting NT sequence. Different NT sequences and their active binding sites that are interacting with the NC affect the strong variation in the binding constants. The NC-NT binding is strongly dependent on the ionic strength of the complex. In addition, buffer composition, pH and amino acid sequence of NC plays vital role for determination of the binding constant. NC can bind non-specifically to 5-8 NT sequences through low affinity electrostatic mode. NC shows sequence specific binding properties to selective single strand and stem-loop structures. In the NC-NT complex condensing and chaperon activity of NC sequences is dependent on the degree of sequence occupancy by NC. Different factors that are associated with the NC-NT complex formation, depends on this degree of occupancy that varies from low (1 NC per 100 NT) to high (1 NC per 2-5 NT) values. At very low degree of occupancy (1:100) NC binds with specific NT with a very high

affinity (e.g. cTAR in our case) without promoting any aggregation or chaperone activity. NC can bind to stem-loop NT structure with nanomolar affinity. But at very high degree of occupancy (1:10), NC-NT interaction can lead to aggregation with macromolecular crowding effect which in turn constrains remodeling of interacting molecules. At a very high degree of occupancy, NC can cover NT extensively.

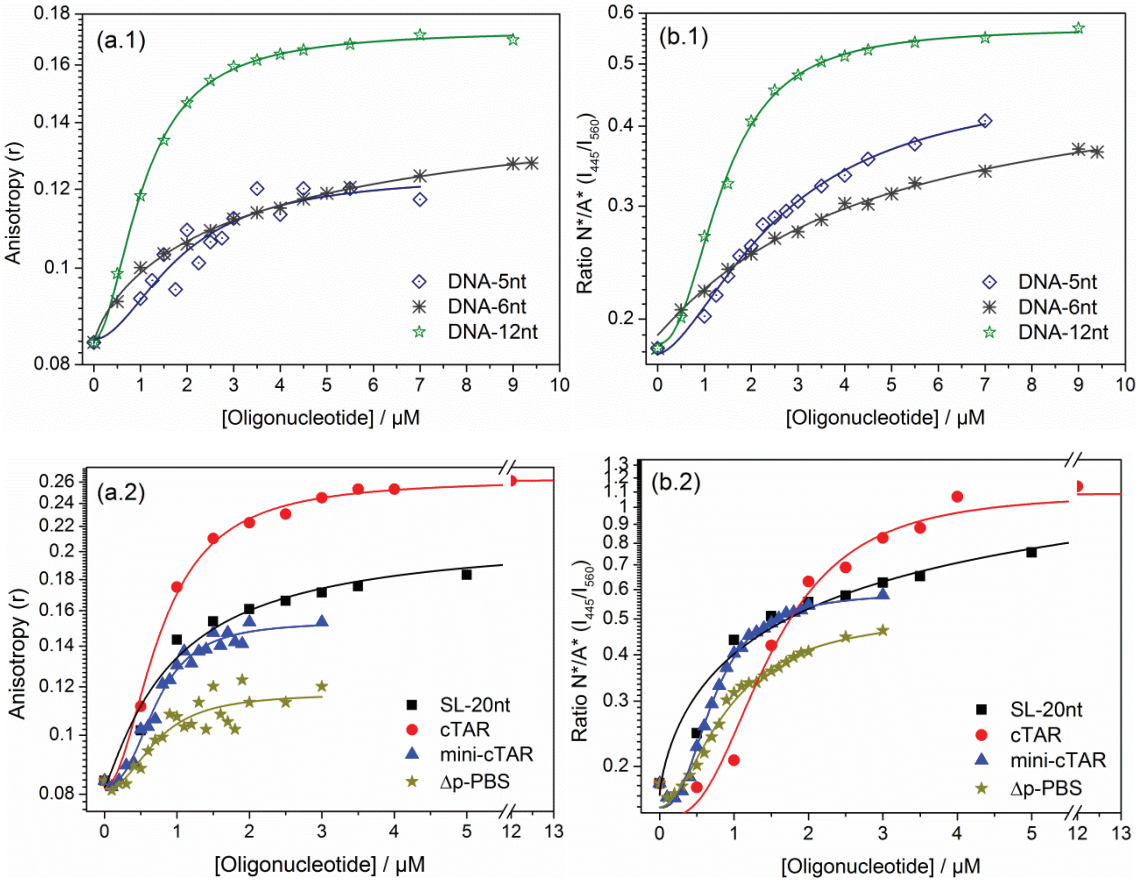

***Figure 5.9**: (a) Fluorescence anisotropy (b) N*/A* ratio (I_{445}/I_{560}) of NCp7(11-55) labeled with **4-MeOxyLH** in complex with different oligonucleotide sequences as mentioned in the above table.*

From the steady state and time resolved data of NCp7 labeled with **4-MeOxyLH**, different binding affinity could be observed which is comparable with earlier theoretical and experimental values. Ratiomatric analysis (N*/A*) of the complex recorded as a function of NT concentration is in very good agreement with corresponding anisotropy data. When NCp7 is in complex with NT, for small NT sequences (DNA-5nt and DNA-6nt), no change could be observed in the time resolve parameters of the anionic emission. However, significant changes, as expected, could be observed in the time resolved parameters of the NCp7 complexes with stem-loop and long DNA structures (see table 5.1). From this point of view it can be postulated that **4-MeOxyLH** with its dual emission can be used as a tool to monitor interaction between DNA and peptide. Distinct variations in ratiometric and excited state parameters are capable to find out conformational changes into peptide-DNA complex at different conditions. The analogue can thus be used as a ratiometric fluorescence probe to monitor such kind of biomolecular interactions.

***Table 5.1**: Dissociation constant (K_D) and time resolved parameters of NCp7 and DNA complexes.*

		Labeled NCp7		**Labeled NCp7+Oligonucleotide**	
NCp7+DNA complex	K_D, µMol	Tau, ns (%)			
		λ_{Em} 445 nm	λ_{Em} 560 nm	λ_{Em} 445 nm	λ_{Em} 560 nm
NCp7+ DNA-5nt	1.09	0.3 (68) 0.7 (25) 2.6 (7)	0.5[a] 5.5	0.3 (65) **1.5 (25)** **3.3 (10)**	0.8[a] 5.5
NCp7+ DNA-6nt	0.60			0.3 (62) **1.4 (30)** **3.4 (8)**	0.5[a] 5.7
NCp7+ DNA-12nt	2.75			0.3 (61) **1.4 (31)** **4.0 (8)**	**2.4**[a] 5.1
NCp7+ SL-20nt	1.26			0.3 (53) **1.2 (37)** **4.3 (10)**	**3.0**[a] 5.1
NCp7+ cTAR	0.04			0.3 (52) **1.6 (37)** **3.0 (11)**	**3.0**[a] 5.4
NCp7+ mini-cTAR	3.14			0.3 (59) **1.4 (29)** **3.5 (12)**	**2.7**[a] 5.3
NCp7+ ΔP (-)PBS	3.04			0.25 (64) **1.6 (27)** **4.0 (9)**	**2.3**[a] 5.1

a : growing time for decay

5.5 Fluorescence labeling of protein by 5,5-Cpr-OxyLH

Environment-sensitive (or solvatochromic) fluorescent dyes are efficient to monitor biomolecular interactions by sensing the changes in their microenvironment at the labeled site[105]. Different phenomenon associated with the biomolecular complex, can be monitored by observing the changes in the photophysical properties of a solvatochromic fluorophores attached to the structure of interest. To study protein-protein interaction or protein-foreign vector interactions, fluorescence is found to be one of the best techniques that can be applied to understand the complex formation mechanisms, conformational/structural changes in the complex, environmental effect on the complex etc. The proteins or peptides labeled by solvatochromic fluorophores, such as Prodan derivatives[180,181], dimethylaminophtalimide[182], dimethylaminonaphtamides[183-185] have been centre of interest so far. Biomolecular interactions commonly decrease the polarity at the labeled site by the binding of the protein partner. This variation in the polarity can be readily detected by solvatochromic fluorophores either through their spectral shift or by their fluorescence quenching[105]. An example of application of fluorescence quenching to monitor peptide-oligonucleotide interaction have been presented in the previous section.

Most of the protein or large biomolecules have at least one Cysteine residue. Keeping this in mind we proposed a model mechanism of protein labeling where a solvent accessible Cysteine residue is available for site-specific labeling with keto

analogue of Oxyluciferin (**5,5-Cpr-OxyLH**). In this way the protein could be labeled by Oxyluciferin analogue. The labeling efficiency can be monitored by using the emission properties of the dye.

*5.5.1 Spectral behavior of **5,5-Cpr-OxyLH** in aqueous buffer in presence of Cysteine*

The **5,5-Cpr-OxyLH** was initially designed to mimic the keto form of Oxyluciferin. In addition, this compound is able to specifically react with Cysteine residues through the ring opening on the spiro moiety of the compound. This reaction occurs only in basic conditions (pH > 9) and can be monitored both with absorption and emission spectra. In figure 5.10, we have reported the time dependent absorption and emission properties in the presence of Cysteine. The absorption spectrum of **5,5-Cpr-OxyLH** shows a significant spectral change in the presence of 1000x Cysteine with time, as reported in the figure 5.10a. **5,5-Cpr-OxyLH** has an absorption maximum of the phenolate-keto form centered at 482 nm in buffer at pH 9.5. By adding Cysteine, the absorption maxima blue shifted to 432 nm. In a similar way, the fluorescence emission of the dye is strongly modified by the presence of Cysteine. As reported in figure 5.10b, in presence of 1000 fold excess Cysteine in solution, a growing emission band centered about 567 nm was observed. The emission intensity at 567 starts increasing as the reaction proceeds (figure 5.10c). In absence of Cysteine in the solution, this spectral blue shift has not been observed. This emission (λmax 567 nm) can be attributed to its enol tautomer.

In **5,5-Cpr-OxyLH** thiazole subunit is restricted to keto tautomeric form of Oxyluciferin via 5,5 distribution pattern (see chart 5.1). At the ground state its phenol group is already deprotonated in basic media where absorption of phenolate ion of the keto form can be observed with a maxima at 482 nm. This mimics **phenolate-keto-OxyLH$^-$** form. This absorption is due to л-л* transition from the keto group and to n-л* transition from the 6'C hydroxyl group[9]. Emission spectrum of **5,5-Cpr-OxyLH** has only one band maximum at 637 nm that does not evolve with pH. Much higher photoacidity and very efficient ESPT could be observed for this molecule at this deprotonated form while exciting at its isosbestic point (423 nm). Although a weak contribution in emission at this basic condition, appears as a tail, which likely corresponds to photo-degradation of neutral keto-OxyLH_2 emission (530 nm) can be observed. ESPT from the phenol group is much faster (< 50 ps) than the responding time of the instrument and thus emission from deprotonated form (maxima at 637 nm) could only be observed with classical steady state spectroscopy[48].

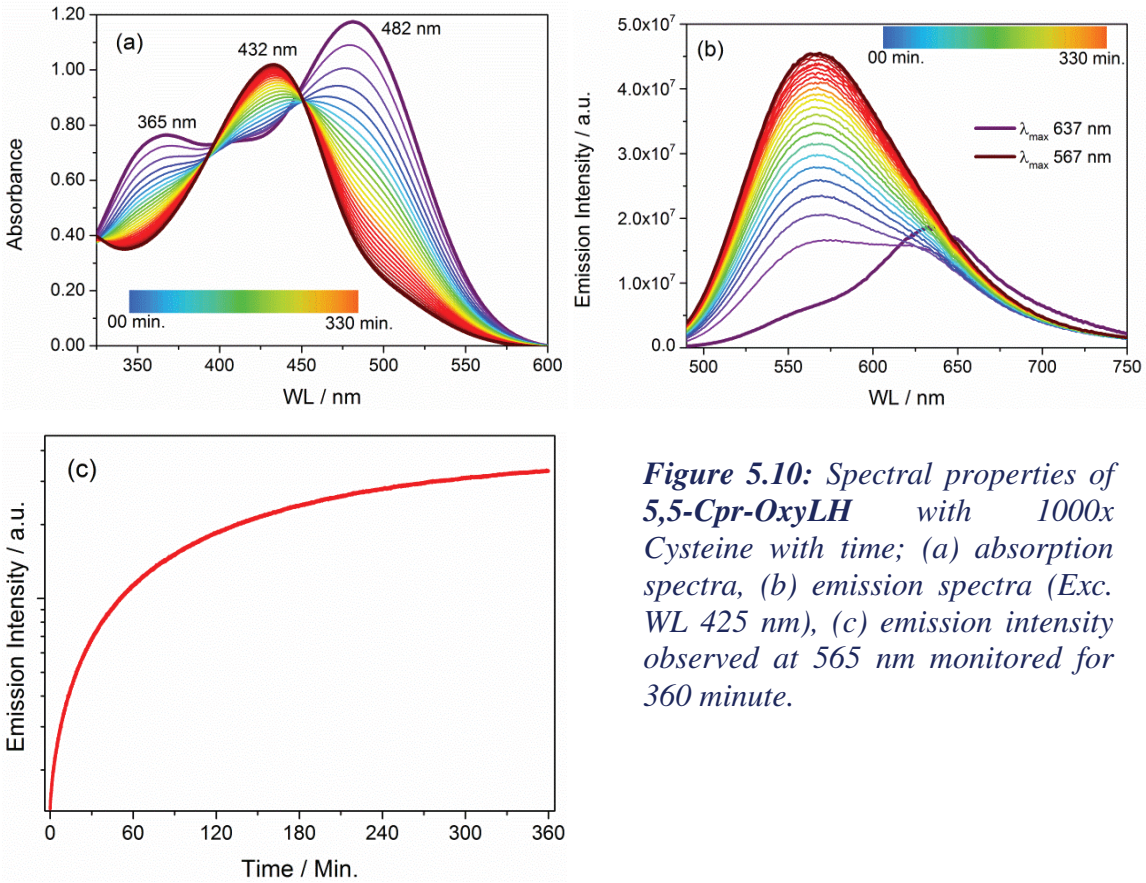

Figure 5.10: *Spectral properties of* ***5,5-Cpr-OxyLH*** *with 1000x Cysteine with time; (a) absorption spectra, (b) emission spectra (Exc. WL 425 nm), (c) emission intensity observed at 565 nm monitored for 360 minute.*

The formation of sulfhydryl group is very crucial phenomenon as the hydrogen can be easily replaced by some other radicals or groups and can form a covalent bond with other molecules (such as Cystine formation). The disulfide bridge formed may be a weaker bond than a peptide bond and can be split easily but is quite stronger than other interactions like salt bridge or hydrogen bonding. The formation of this covalent bond is strongly dependent on the pH of the solution and redox potential of the micro-environment. Under basic conditions, –SH tends to be more oxidized and replaced by –SR (R ≠ Hydrogen)[186].

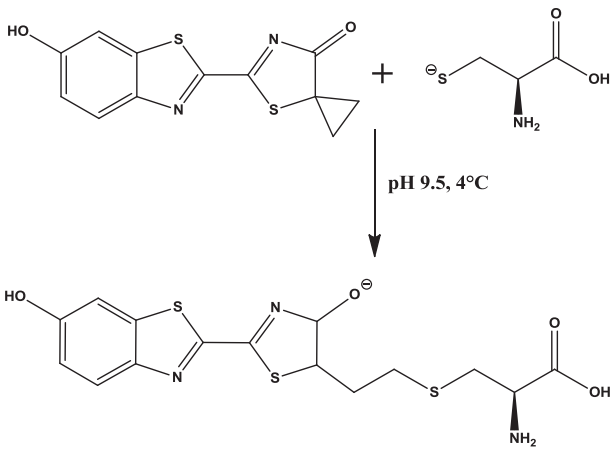

Chart 5.1*: Concept of cysteine (thiol) labeling of keto-Oxyluciferin*

When a covalent disulfide bridge has been established in between Oxyluciferin and Cystine, significant blue shift in both absorption (~48 nm) and emission spectra (~71

nm) could be observed. Absorption maxima shifts to 432 nm which can be due to n-л* transition of phenol-phenolate species. Whereas emission maxima shifts to 567 nm confirming keto-enol tautomerization of **phenolate-keto-OxyLH**$^{-}$ to **phenolate-enol OxyLH**$^{-}$[48]. This spectral blue shift of **5,5-Cpr-OxyLH** emission can be used to follow the specific binding of the dye Cysteine residue in basic conditions and therefore protein containing Cysteine residue.

5.5.2 Human Alpha1-Antytrypsin (α1-AT) and its Cysteine residue

Human Alpha1-Antytrypsin (α1-AT), a single chain glycoprotein, commonly found among several eukaryotic organisms and plants as well as in viruses, is a protease inhibitor, which belongs to "serpin" (Serine Proteinase Inhibitors) family. This ~46 kDa/412 amino acid (Ref: UniprotKB code Q00896) protease inhibitor shares a very high structural homology consisting eight α-helices and three β-sheets. A multi step reaction mechanism is involved in irreversible binding of α1-AT to its associated enzyme[117,187]. The enzyme recognition site of α1-AT is composed of eight amino acids (P5-P'3) within its reactive centre loop (RCL); an exposed and flexible sequence of ~17 amino acids[117]. A unique free Cysteine residue, sufficiently exposed to the solvent, at position 232 of the C terminus end of β-strand 1B in α1-AT can easily be labeled by –SH reactive fluorescent probes[117]. This specific part of α1-AT (Cysteine-232) has no direct involvement in the enzyme interaction within RCL or the β-sheet A or in the proteinase translocation mechanism[117]. To investigate potential rearrangement of α1-AT in presence of enzyme, Cysteine-232 was labeled with solvent polarity sensitive fluorescent probe like **5,5-Cpr-OxyLH**. The advantage of presence of only one Cysteine residue is to avail an opportunity to easily perform a site specific fluorescence labeling of this protein.

Cysteine (abbreviated as Cys or C) is an α-amino acid, which can be synthesized biologically in human. This sulfur group biogenic amino acid is one of the 20 biologically essential amino acids required for cell-metabolism. This can be genetically encoded by two mRNA codons UGU and UGC. Cysteine or α-Amino-β-mercapto-propanoic acid ($C_3H_7NO_2S$, Mol. Wt. 121.15 gm/mol) structurally belongs to sulfur amino acid groups with a sulfur atom appears on its side chain (see chart 5.2)[186].

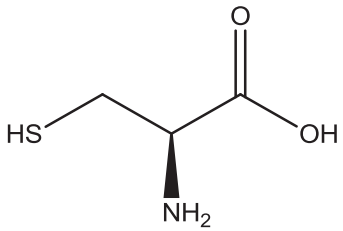

***Chart 5.2**: Chemical structure of Cysteine (CAS No. 52-90-4)*

The sulfur on its side chain creates a highly reactive sulfydryl group that make this amino acid less hydrophobic and more reactive than its methyl counterpart Metheonine (Met). Cysteine can easily be oxidized and form a dimer (or known as *Cystine*) with a covalent disulfide bridge between two Cysteine molecules. This dimer or

Cystine is very crucial for analysing the structure and dynamics of the protein at different stages. Sulfhydral bond formed in Cystine is considered to be very strong reducing factor that can control various activities of several proteins[188-190].

Cysteine can be found (at least one) in 88% of proteins and peptides (according to Swiss-Port database). To investigate structure and dynamics of biomolecules by using fluorescence methods, Cysteine is the most popular target especially because of its unique nature which helps to study protein folding mechanism[188-190].

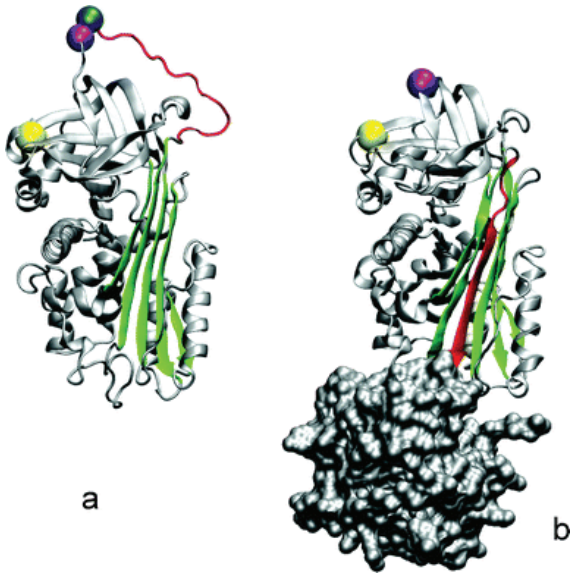

***Figure 5.11**: 3-D model representation of human α1-AT in its (a) free state and (b) in complex with Procine Pancreatic Elastase (PPE) (grey surface). The C-terminus side (in red) of the RCL becomes part of β-sheet A (in green) in the complexed state of the protein. Yellow sphere represents the unique Cys-232 residue. The P1 and P'1 residues of RCL are represented by blue and purple spheres, respectively. The figures were prepared with the pdb files 1hp7 and 2d26 (Boudier et al. Reprinted with permission)[117].*

*5.5.3 Fluorescence labeling of Alpha1-Antytrypsin (α1-AT) by **5,5-Cpr-OxyLH** and its purification*

To further evidence the ability to use Oxyluciferin derivatives to probe biomolecular interactions, in the next step, we labeled α1-AT by **5,5-Cpr-OxyLH**. To label α1-AT at Cystein-232 position by **5,5-Cpr-OxyLH**, α1-AT was dissolved in 25mM Tris/75 mM NaCl/0.2mM $MgCl_2$ buffer at pH 9.5 at 20°C. In order to work with an excess of dye to ensure an efficient labeling of α1-AT, five-fold more concentrated **5,5-Cpr-OxyLH** was added to the solution and kept at +4°C for 24 hours in dark. Concentrations of α1-AT (ε_{280} 19060 $M^{-1}.cm^{-1}$)[117] and **5,5-Cpr-OxyLH** (ε_{375} 62700 $M^{-1}.cm^{-1}$) were calculated from their absorption spectra. In parallel, spectral signature of **5,5-Cpr-OxyLH** without α1-AT in the same solution has been observed continuously as a negative control.

At the end of the labeling procedure, emission spectra of the solution were recorded. Emission from both, keto (637 nm) and enol (562 nm) Oxyluciferin could be

observed when excited at 423 nm (see figure 5.12-red). The band centered at 562 nm arises due to emission from the enol form which is already bound to Cysteine-232 residue of α1-AT while the emission centered at 631 nm is due unbound/free **5,5-Cpr-OxyLH** (excess Oxyluciferin molecule available in the solution). Then entire solution was passed through PD-10 desalting column, purchased from GE healthcare UK, equilibrated with same buffer, and only labeled protein was collected as filtrate. High molecular weight labeled proteins can be separated by the gravitational force from the mixture of both labeled protein and free Oxyluciferin.

Emission spectra of filtrate has been recorded again by exciting at 423 nm and as depicted in the figure 5.12 only emission from enol Oxyluciferin bound to Cysteine was observed. This confirms complete removal of free **5,5-Cpr-OxyLH** from the mixture. The filtrate was lyophilized under vacuum and re-dissolved in PBS at pH 7.4 at 20°C. Concentration was calculated from absorption at 280 nm; ε_{280} 19060 $M^{-1}.cm^{-1}$.

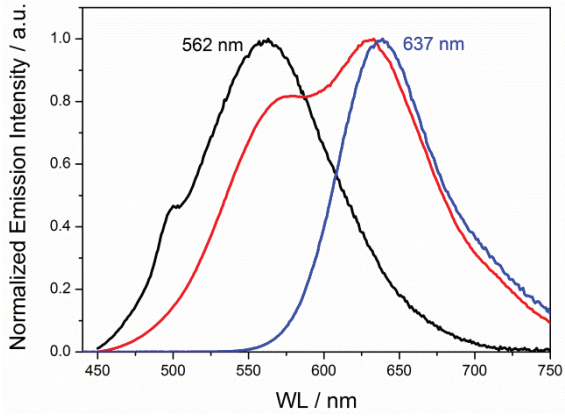

***Figure 5.12**: Normalized emission spectra (Exc. WL 425 nm) of **5,5-Cpr-OxyLH** during labeling process. (Blue: at beginning; Red: before filtration; Black: after filtration)*

5.5.4 Activity test of Alpha1-Antytrypsin (α1-AT) labeled with 5,5-Cpr-OxyLH

To verify the activity of the labeled protein and to monitor the interaction between labeled α1-AT and another biomolecule, we adopted the similar model as proposed by Boudier et al.[191] RCL of α1-AT can easily inhibit Porcine Pancreatic Elastase (PPE), a member of subfamily of Serine, by catalyzing hydrolysis of ester substrate of certain peptide bonds of α1-AT[191]. The interaction between PPE and labeled α1-AT can be studied through the fluorescence quenching of Oxyluciferin derivative that is associated with conformational changes resulting from reaction between α1-AT and PPE. Boudier et al. shows how fluorescence quenching of labeled α1-AT in presence of PPE can be monitored by studying steady state (time dependent) fluorescence emission[117]. The reaction of PPE with oxyluciferin labeled α1-AT has been studied in similar way. In ~700 nM solution of labeled α1-AT, PPE was added with increasing concentration up to 1µM (Δ100 nM). Fluorescence spectra were recorded at each concentration by exciting at 425 nm. Significant fluorescence quenching has been observed between 0 and 1µM of PPE confirming the structural changes of the labeled α1-AT in complex with PPE (see figure 5.13). Boudier et al. has reported the similar fluorescence quenching properties of labeled α1-AT with increasing PPE concentration in their work[117].

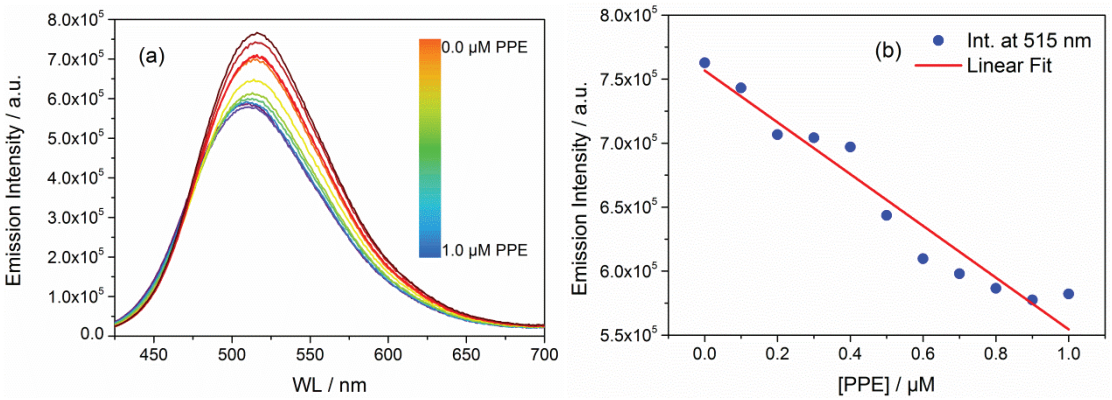

***Figure 5.13**: Fluorescence quenching of α1-AT labeled with **5,5-Cpr-OxyLH** (a) with increasing conc. of PPE,(b) Emission int. at 515 nm with increasing conc. of PPE*

5.6 Conclusion

Fluorescence emission properties of oxyluciferin and its structural analogues can be used to monitor different biological processes. Upon two-photon excitation, *in-cellulo* local/cyosolic pH can be visualized and the change in cytosolic pH can be monitored. Moreover oxyluciferin appeared to be a non toxic solvatochromic fluorophore. Next we demonstrated that peptide-DNA interactions can be monitored by observing dual emission spectrum of **4-MeOxyLH** labeled peptide. **4-MeOxyLH** can thus be a good candidate to study structural dynamics of protein-DNA complexes involved in viral life cycle of HIV-1. Labeling of Cysteine-232 of α1-AT by **5,5-Cpr-OxyLH** is a classic example of application of keto-enol tautomerization of oxyluciferin as a site specific fluorescent labeling probe for studying structural dynamics and protein folding mechanism.

Appendix-C

C.1 Schematic of Oxyluciferin analogues used for peptide conjugation

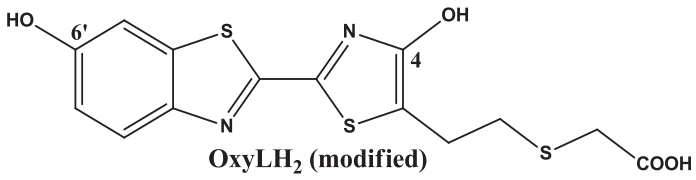

$OxyLH_2$ (modified)

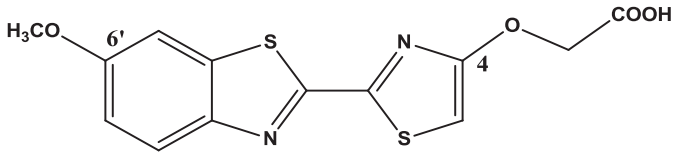

4,6'DMeOxyL (modified)

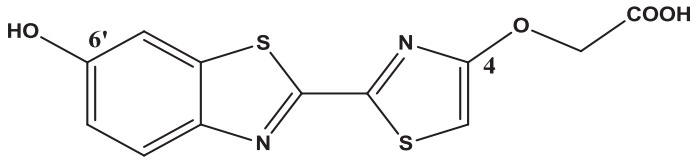

4-MeOxyLH (modified)

Compound	Mol. Wt. (g/mol)
$OxyLH_2$	368.45
4,6'-DMeOxyL	322.36
4-MeOxyLH	308.33

C.2 Amino Acid sequence of Alpha-1-antitrypsin, used in this study (PDB Q00896- A1AT3_MOUSE)

Sequence chain: Length: 412 AA, Mol. Weight: 45823 Da (Checksum: FFA3BF10ABC1B8AE)

MTPSISWGLL LLAGLCCLVP SFLAEDVQET DTSQKDQSPA SHEIATNLGD	50
FAISLYRELV HQSNTSNIFF SPVSIATAFA MLSLGSKGDT HTQILEGLQF	100
NLTQTSEADI HKSFQHLLQT LNRPDSELQL STGNGLFVNN DLKLVEKFLE	150
EAKNHYQAEV FSVNFAESEE AKKVINDFVE KGTQGKIVEA VKKLDQDTVF	200
ALANYILFKG KWKKPFDPEN TEEAEFHVDE STTVKVPMMT LSGMLDVHHC	250
STLSSWVLLM DYAGNATAVF LLPDDGKMQH LEQTLSKELI SKFLLNRRRR	300
LAQIHFPRLS ISGEYNLKTL MSPLGITRIF NNGADLSGIT EENAPLKLSQ	350
AVHKAVLTID ETGTEAAAVT VLLAVPYSMP PILRFDHPFL FIIFEEHTQS	400
PLFVGKVVDP TH	412

C.3 Molar Extinction coefficient of Oxyluciferin and its analogues

To calculate the molar extinction coefficient (Ɛ) of oxyluciferin and its few analogues, Fluorescence Correlation Spectroscopy (FCS) has been used. Diffusion of Oxyluciferin derivatives (diluted in PBS) within an open volume created by a focused laser beam were monitored with FCS[123]. Absolute local concentration of oxyluciferin within this open volume can be calculated from a reference volume (V = 0.45 fl) and number of flurophore (N) observed in this volume, by using the equation N/(V*Va),

where Va is Avogadro No. 6.022 x10^{23}[123]. Number of fluorophore inside the volume was calculated by Igor pro (from WaveMetrices) run under MATLAB (MathWorks) platform. 50nM of Tetramethylrhodamine (TMR) solution in water was used as reference. From this calculated concentration (C), taking into consideration of dilution factor (~1/50x), and measured absorbance (A) at 375 nm, Ɛ values for each compound were calculated by applying simplified Beer-Lamberts equation C = A/(Ɛ*l).

The calculated Ɛ of these compounds have been mentioned in the following table:

Compound	Molar Extinction coefficient (Ɛ) at 375 nm ($M^{-1}.cm^{-1}$)
6'-MeOxyLH	1,30 x 10^4
4-MeOxyLH	6,31 x 10^4
4,6'-DMeOxyL	4,82 x 10^4
$OxyLH_2$	2,23 x 10^4
5,5-Cpr-OxyLH	6,27 x 10^4

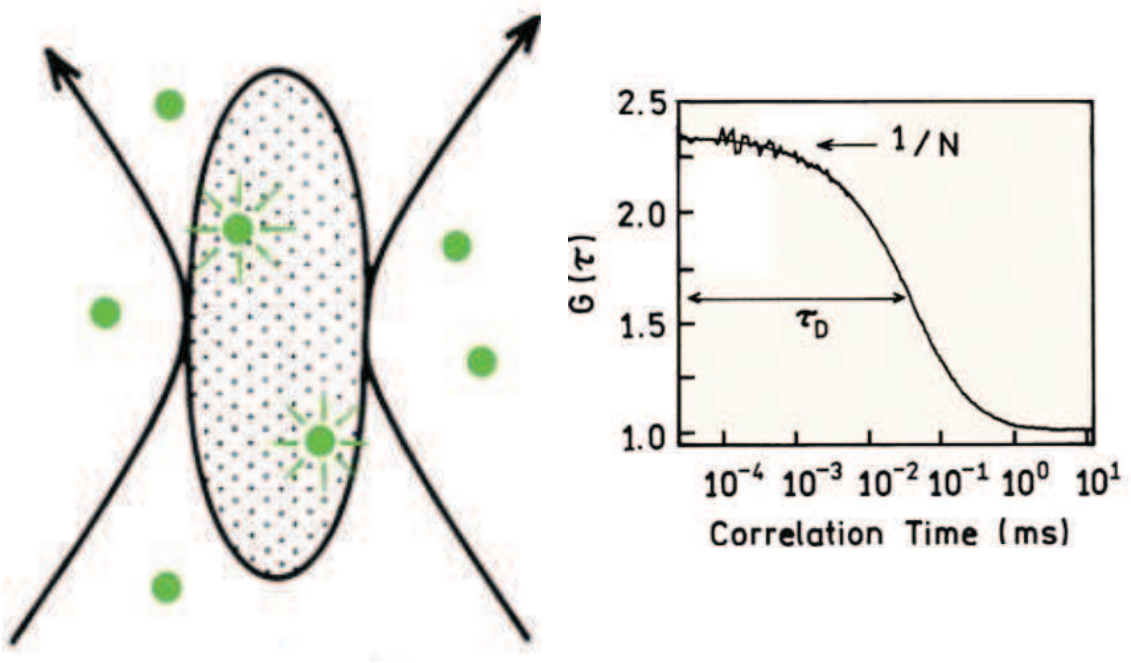

Figure C.2: *Schematic representation of a fluorophore inside the focal volume illuminated by FCS (left) and calculation of correlation time from the observed decay (Princ. of Flr. Spetr; J. Lakowich, Adapted Form)*[135]

C.4 Molecular brightness of Oxyluciferin analogue 4-MeOxyLH

Another interesting feature of **4-MeOxyLH** is its high molecular brightness. About 47% of relative fluorescence quantum yield could be observed in pH 10.0[48]. Molecular brightness of **4-MeOxyLH** was found to be 1500 photon/sec per fluorophore.

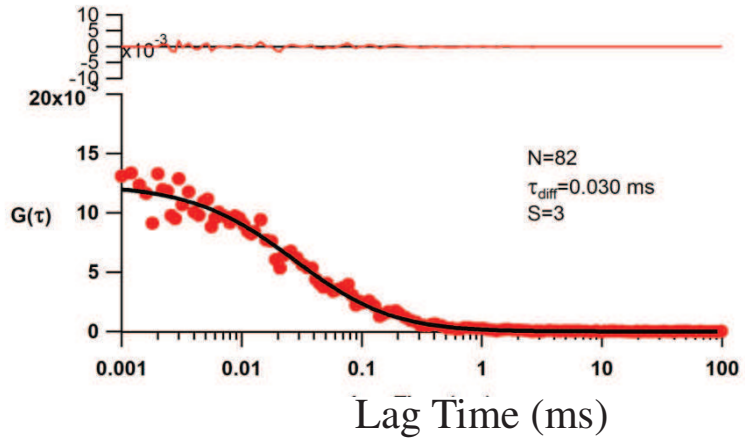

***Figure C.3**: The molecular brightness of **4-MeOxyLH** in buffer pH 10 is 1500 ph.s-1 per fluorophore (P=15 mW).*

Conclusion & Prospective

General Conclusions and Prospective

General conclusion of the work

To obtain a better insight of firefly bioluminescence color tuning mechanism and the phenomenon governing the excited state photodynamics of this natural fluorophore, the absorption, emission and fluorescence lifetime of structural analogues of Oxyluciferin have been studied in aqueous buffer. Photodynamic study of different chemical forms of Oxyluciferin reveals that the emission mechanism is strongly dependent on the solvent pH. With the help of different chemometric approaches it was possible to decipher the exact chemical form that is responsible for a particular color of the emission. In addition, it was possible to establish a pH dependent photophysical profile of the firefly Oxyluciferin. Also, we were able to provide a strong evidence of ESPT mechanism involved in the de-excitation process as well as we provided a photoluminescence pathway of different chemical forms of the emitter along with their ground and excited state equilibrium constants.

By mimicking the exact physiological conditions of the natural bioluminescence system, we identified the photophysical properties of the emitter inside the pocket of the enzyme, firefly Luciferase at a preliminary stage. The emission mechanism of Oxyluciferin inside the pocket of Japanese firefly *Luciola cruciata* in the presence of AMP have been studied. The binding affinity of the fluorophore to the protein was calculated. The effect of microenviroenment of the protein on the emission mechanism of the fluorophore have been studied and with these preliminary results an enhanced photophysical profile has been established by combining results obtained from the analysis of free Oxyluciferin.

In addition, keeping in mind the extraordinary photophysical mechanism of the fluorophore, its application as a bio-analytical tool to monitor different biological events have been proposed in this study. Proven models have been presented in this study where this environment sensitive fluorophores have been applied for *in-cellulo* pH monitoring and to monitor interaction between HIV-1 NCp7 & different oligonucleotide sequences. A classical example has been presented where the very strong thiol affinity of the fluorophore have been applied for fluorescence labeling of another human protein Alpha-1 Antitrypsin.

All together,

i. we deciphered different chemical forms of Oxyluciferin (individually and when in complex with Luciferase) involved in color tuning mechanism of firefly bioluminescence by studying its different structural analogues in aqueous buffer.
ii. we established the photoluminescence pathway of the Oxyluciferin and Oxyluciferin-Luciferase complex in aqueous buffer.
iii. we did an interpretation the exact excited state structure of the photo emitter in natural conditions and in complex with the enzyme Luciferase and also interpret ESPT mechanism involved in color tuning mechanism of firefly bioluminescence.

iv. we could propose Oxyluciferin as a promising bio-analytical tool specially to monitor different biomolecular interactions *in-vivo* or *in-vitro*.
v. the results we obtained have a potential contribution to put light on the study of bioluminescence mechanism of firefly Luciferin-Luciferase.

Prospective of the work

Combing these results, advancement of the study of Oxyluciferin as a bio-analytical probe may be opted. Although a detail photophysical profile of the color tuning mechanism for the firefly bioluminescence has been proposed, further analysis of this phenomenon is required,, especially when the photo-emitter is bound with the enzyme. To understand the structure, fluorescence time-resolved anisotropy parameters of the protein-fluorophore complex at different experimental conditions need to be studied. For better understanding of the excited state structure of the protein-fluorophore complex, it will be excellent to combine their crystallographic structural analysis with these photophysical parameters. The result can further be validated by applying different theoretical model functions for constructing a more reliable excited-state structure of the photo-emitter and its color-tuning mechanism in the natural context. Also the effect of buffer composition (ionic strength etc.) should be studied theoretically as well as experimentally. Effect of ionic strength on pka has briefly been discussed in the chapter 3 but not when bound to Luciferase. To draw a more realistic excited-state structure of the photo-emitter, contribution of different buffers compounds and effect of different salts and their concentrations on the emission spectra of the protein-fluorophore complex must be considered. In particular, the chemometric approach can be used to characterize these properties.

From the application point of view of the dye, further more detailed *in-cellulo* and/or *in-vivo* investigations are required for better understanding about cellular pH monitoring. Time dependent cellular imaging, effect of other extracellular factors etc. needs to be included in the study. Also it would be a good idea to quantify the exact *in-cellulo* pH dependent excited state lifetime profile of the fluorophore, so that the exact pH variation for specific cellular organelle/location can be monitored. The fluorophore can be opted as an alternative for lysosome tracking mechanism. Experimental data of this approach can be excellently supported by the theoretical model. To elucidate other possibilities of protein labeling, different additional proteins can be studied, e.g full length NCp7 or any other protein can be labeled with the fluorophore and its interaction with oligonucleotides at different conditions may be studied. Ionic strength, buffer composition, pH of the solution affects binding of the fluorophore to the protein. These parameters can also be studied to tune the photophysical parameters required for monitoring biomolecular interactions. Time resolved fluorescence anisotropy and crystallographic structural measurements of labeled protein must be included in the analysis to have a better knowledge about the complex formation, which can be further validated with their theoretical models. In addition, application of ultrafast time resolved fluorescence techniques to understand the photodynamics of the dye free as well as in complex with the protein will be having an added value to the analysis.

Résumé en Français

Résumé en Français

Au cours de la dernière décennie, la compréhension du processus de bioluminescence a connu un intérêt croissant en raison du très grand nombre d'applications en particulier dans le domaine de l'analyse biologique (*in vivo*/*in vitro*, imagerie, caractérisation des interactions biomoléculaires etc.). Malgré de vastes connaissances expérimentales et théoriques de cette réaction chimique complexe, la photophysique de l'**$OxyLH_2$** reste encore mal comprise. En fonction des conditions expérimentales, la partie optiquement active peut exister sous la forme de six espèces chimiques différentes en raison de l'ionisation des groupements hydroxyle et de l'équilibre céto-énolique de la sous-unité thiazole. Cet équilibre chimique complexe en solution aqueuse est fortement influencé par la nature du solvant, le pH et les interactions spécifiques avec des bases. En outre, lorsque l'**$OxyLH_2$** forme un complexe avec l'enzyme luciférase, les propriétés spectrales de chaque forme chimique peuvent être affectées par la nature du site actif, tel que la polarité, la présence d'ions supplémentaires et l'empilage de type л-л. Les études récentes ont montrés que non seulement les espèces phénolate-céto générées à l'état excité, mais aussi le tautomère de la forme énol sont des formes contribuant à l'émission de fluorescence. Ce mécanisme implique un transfert de protons à l'état excité (ESPT excited state proton transfer) à partir de l'un ou l'autre des groupes hydroxyles. En outre, des études antérieures menées sur la luciférine provenant de la luciole (le précurseur de réaction) ont montré que le mécanisme de photoluminescence dépend fortement de diverses conditions, y compris le pH de la solution et la longueur d'onde d'excitation.

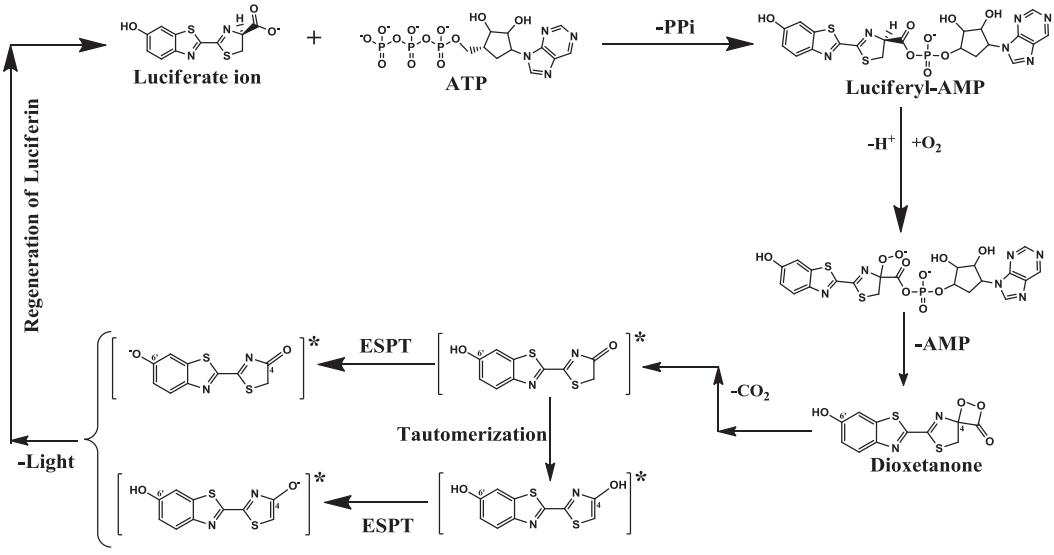

Mécanisme réactionnel de la bioluminescence de la luciole

Ce travail de thèse fait parti d'un projet intitulé « *Excited-State Structure of the Emitter and Color-Tuning Mechanism of the Firefly Bioluminescence* » (RGY-0081/2011) soutenu financièrement par l'Human Frontier Science Program (HFSP). Quatre collaborateurs sont impliqués dans ce projet: i) Prof. Lukas HINTERMANN, Département de chimie, Université de Munich, Allemagne; ii) Dr Pance NAUMOV, Université de New York, Abu Dhabi; iii) le Dr Pascal DIDIER, Université de Strasbourg, FRANCE et iv) le Dr Michel SLIWA, Université de Lille, FRANCE. Les différents

analogues structuraux de l'oxyluciférine ont été synthétisés par le groupe du Prof. HINTERMANN et leurs études structurales cristallographiques ont été effectuées par l'équipe du Dr NAUMOV. L'étude des propriétés photophysiques ainsi que les possibles applications biologiques ont été réalisées au Laboratoire de Biophotonique et de Pharmacologie sous la supervision du Dr DIDIER. A Lille, le Dr SLIWA et son équipe ont étudié les propriétés optiques dans le domaine infra-rouge de ces dérivés.

Le premier objectif de la thèse était d'identifier les différentes formes de l'**$OxyLH_2$** responsables de l'accordabilité de l'émission de fluorescence (445-637 nm) en solution aqueuse. Aussi, il était important de comprendre le mécanisme ESPT impliqué dans ce processus et de fournir un modèle permettant d'expliquer les processus de de-excitation de l'**$OxyLH_2$** en solution aqueuse.

Pour comprendre le mécanisme d'émission de l'**$OxyLH_2$**, l'équipe du Prof. Lukas HINTERMANN a synthétisé chimiquement différents analogues de **$OxyLH_2$** pour lesquels, les groupements -OH sont remplacés par un groupe -OCH_3, de manière à bloquer la déprotonation de la molécule en en solution aqueuse (voir le tableau ci-dessous). Différentes procédures expérimentales impliquant des techniques de spectroscopie de fluorescence à l'état stationnaire et résolues en temps ont été utilisées pour étudier les propriétés optiques de ces dérivés structurellement modifiés. Les spectres d'absorption, d'émission et les durées de vie de fluorescence des différents analogues de **$OxyLH_2$** ont été mesurés en solution aqueuse à différent pH.

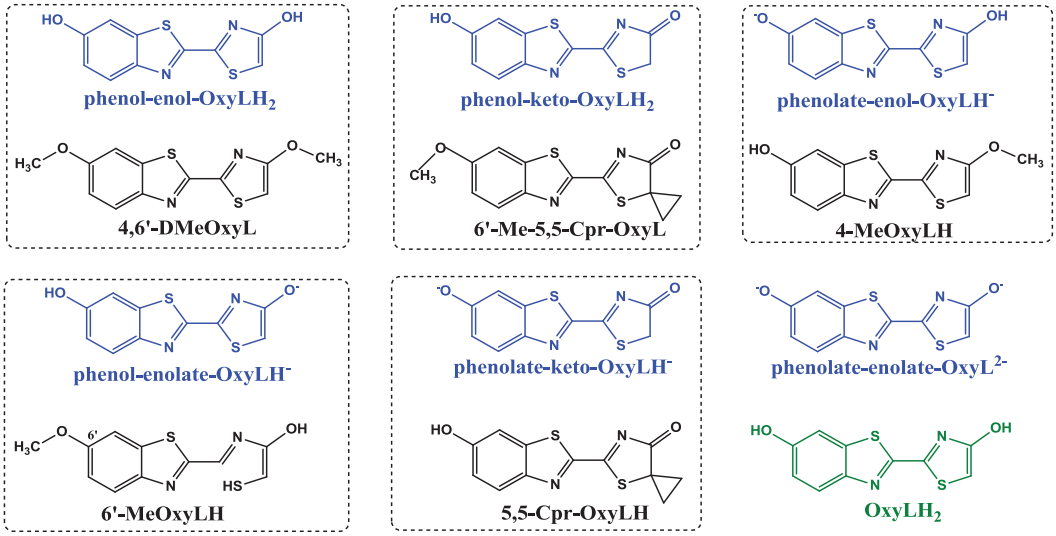

*Structures chimiques de l'**$OxyLH_2$** et de ses dérivés, utilisés dans cette étude comme analogues des différentes formes de l'oxyluciférine*

La thèse est divisée en cinq chapitres. Le premier chapitre traite de l'introduction générale du système suivi par la description des différentes techniques qui ont été utilisées pour étudier le système. Les résultats qui ont été obtenus pour comprendre le mécanisme de bioluminescence ainsi que les différentes applications sont présentés dans les trois chapitres suivants puis le manuscrit se termine par une conclusion générale et une présentation succincte des perspectives envisageables dans le domaine.

Le **chapitre 1** fait le point sur les travaux existants qui ont été menés sur la bioluminescence de la luciole. Ce chapitre comprend une description détaillée du mécanisme de réaction, du rôle de l'enzyme de la luciole etc. Dans le **chapitre 2**, une description détaillée des différentes techniques employées au cours de l'étude est présentée : mesures à l'état stationnaire, spectroscopie résolue en temps (nanoseconde), microscopie à deux photons, anisotropie de fluorescence, préparation des différents échantillons (émetteur de lumière et les échantillons biologiques), expression et la purification de l'enzyme luciférase, synthèse et étiquetage des peptides du VIH-1.

Les résultats présentés dans le **chapitre 3** ont été valorisés à travers un article paru dans J. Phys. Chem. B "Emission properties of oxyluciferin and its derivatives in water: revealing the nature of the emissive species in firefly bioluminescence". Les mesures à l'état stationnaire et résolues en temps, effectuées dans des solutions aqueuses tamponnées dans une gamme de pH physiologiquement pertinent, ont permis pour la première fois d'obtenir les spectres d'absorption et d'émission associés à chacune des formes (six) de l'**$OxyLH_2$** impliquées dans le mécanismes d'émission. En outre, nous avons mesuré les constantes cinétiques à l'état excité et proposer un schéma réactionnel de la photoluminescence de l'**$OxyLH_2$** en solution aqueuse.

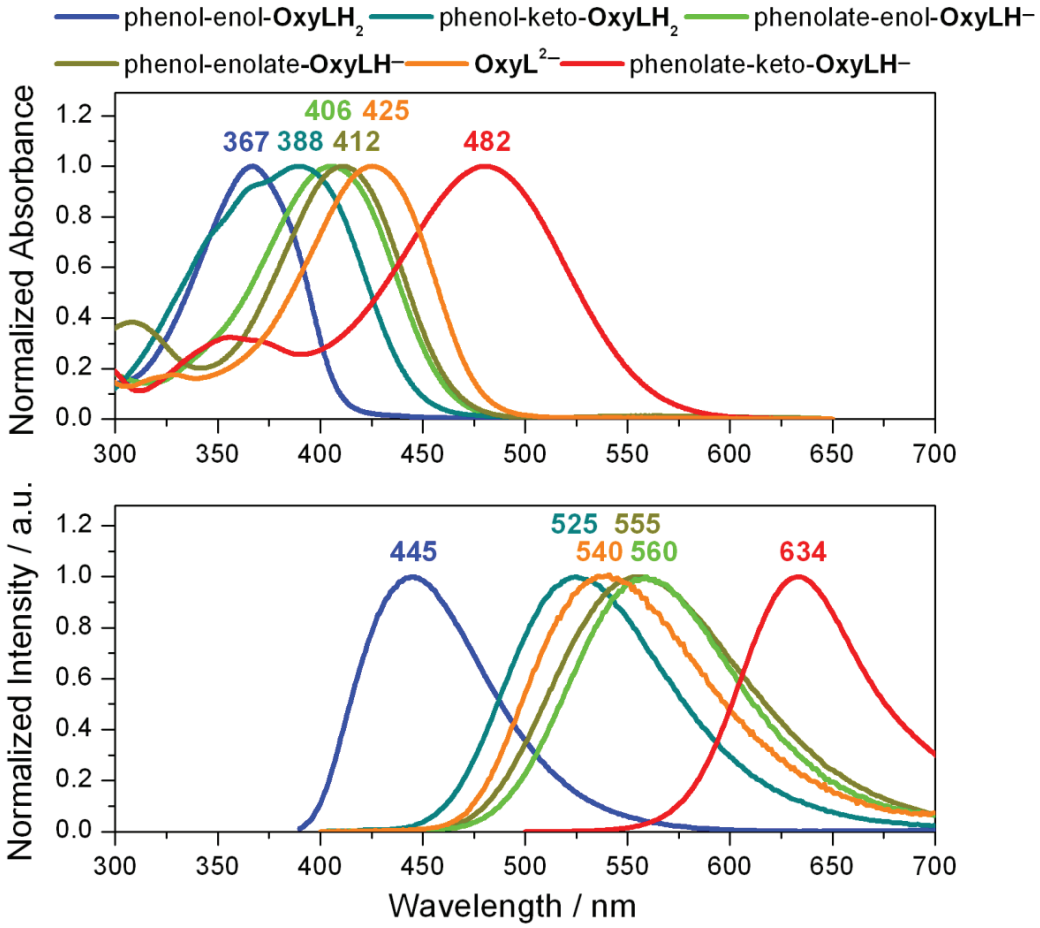

Spectres d'absorption (en haut) et d'émission (en bas) des espèces chimiques individuelles de l'oxyluciférine obtenus par une approche analytique basée sur une méthode d'analyse multidimensionnelle.

Dans le **chapitre 4**, nous avons produit et purifié l'enzyme luciférase (exprimée en bactéries E. coli et purifiée par la technique FPLC) afin d'étudier les propriétés photophysiques de complexes **$OxyLH_2$**-luciférase en tampon aqueux à différent pH. Les analogues de l'oxyluciférine en complexe avec la luciférase ont été étudiés (de manière à mimer le complexe oxyluciférine-luciférase) pour obtenir des informations sur la photophysique du complexe naturel. Nous avons d'abord déterminé le meilleur ratio protéine/oxyluciférine en utilisant l'anisotropie de fluorescence de manière à n'avoir que des molécules liées en solution. Ensuite, nous avons utilisé la spectroscopie de fluorescence à l'état stationnaire et résolue en temps en excitant de manière sélective chacune des formes chimiques de oxyluciférine pour étudier les différents paramètres du complexe oxyluciférine-luciférase. Les résultats préliminaires obtenus nous ont permis de mettre en évidence le rôle clé joué par l'environnement protéique sur les propriétés optiques de l'oxyluciférine à l'intérieur de la poche protéique.

En comparant les résultats obtenus avec ceux présentés dans le **chapitre 3**, nous avons pu mettre en évidence les modifications dues à l'environnement protéique. De plus ces résultats nous ont permis de proposer un modèle pour décrire l'équilibre chimique entre les différentes espèces.

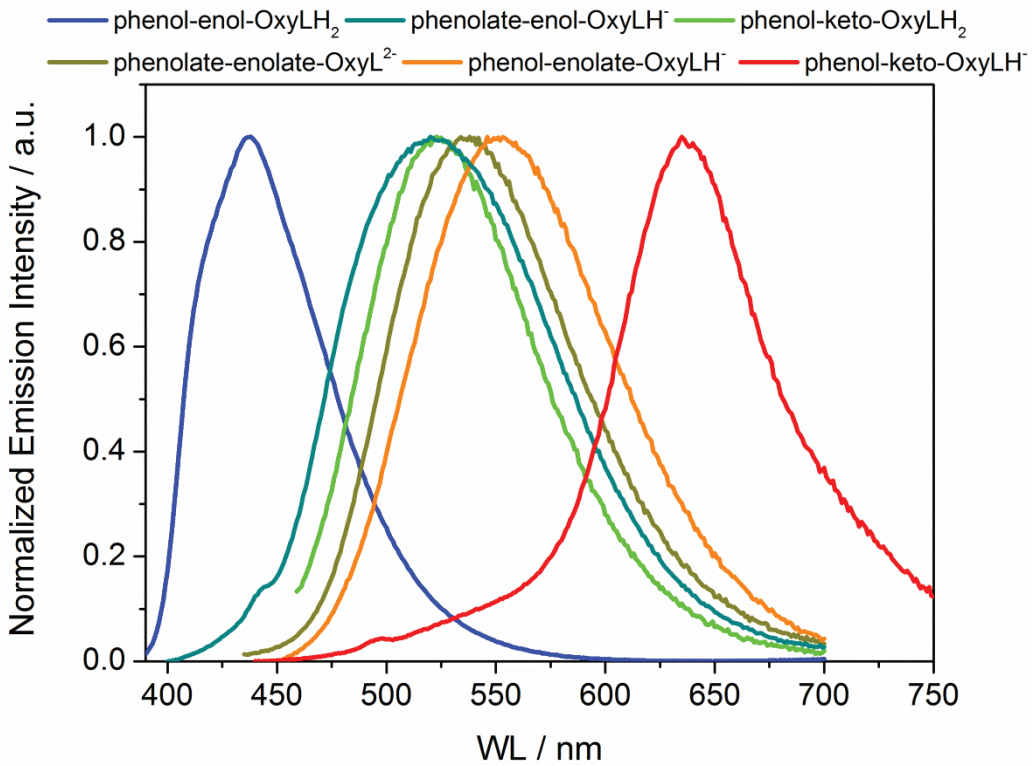

Les spectres d'émission de différentes formes chimiques des complexes oxyluciférine-luciférase dans un tampon aqueux.

Dans la dernière partie de notre travail, l'**$OxyLH_2$** et ses deux analogues structuraux; **4-MeOxyLH** et **4,6'-DMeOxyL** (voir graphique ci-dessus) ont été choisis pour démontrer la capacité potentielle d'utilisation de dérivés de l'oxyluciférine pour des applications biologiques. En particulier, ces dérivés ont été modifiés chimiquement et couplés à des peptides du VIH-1[Tat (44-61) et/ou NCp7(11-55)] par synthèse peptidique en phase solide. Différentes approches analytiques ont été employées pour utiliser les

propriétés optiques des dérivés de l'**$OxyLH_2$** pour suivre l'interaction biomoléculaire en milieu cellulaire ou in vitro. Ces approches expérimentales implique l'imagerie par durée de vie de fluorescence (Fluorescence Lifetime Imaging Microscopy FLIM) avec des cellules HeLa incubées avec le peptide Tat du VIH-1 marqué avec l'oxyluciférine, ainsi que des mesures à l'état stationnaire et résolues en temps pour suivre l'interaction de la NCp7 marqué avec par le **4-MeOxyLH** avec des séquences oligonucléotidiques.

Le FLIM est une technique d'imagerie, dans laquelle le contraste en chaque pixel est donné par la durée de vie de fluorescence du fluorophore. Ces expériences nous ont permis de montrer que l'oxyluciférine pouvait être utilisée comme sonde de pH en milieu cellulaire. En effet, comme nous l'avons décrit dans le **chapitre 3**, l'**$OxyLH_2$** présente des propriétés d'émission qui dépendent du pH. En milieu cellulaire, nous obtenons une distribution des durées de vie fluorescence qui dépend de la localisation cellulaire du pixel considéré. Ces observations ont été confirmées par l'utilisation d'un dérivé qui ne présente pas de dépendance par rapport au pH (Tat marqué avec **4,6'-DMeOxyL**). Les résultats obtenus dans ces expériences ont démontré que l'oxyluciférine peut être utilisé avec le FLIM comme outil d'analyse pour cartographier les variations de pH intracellulaire.

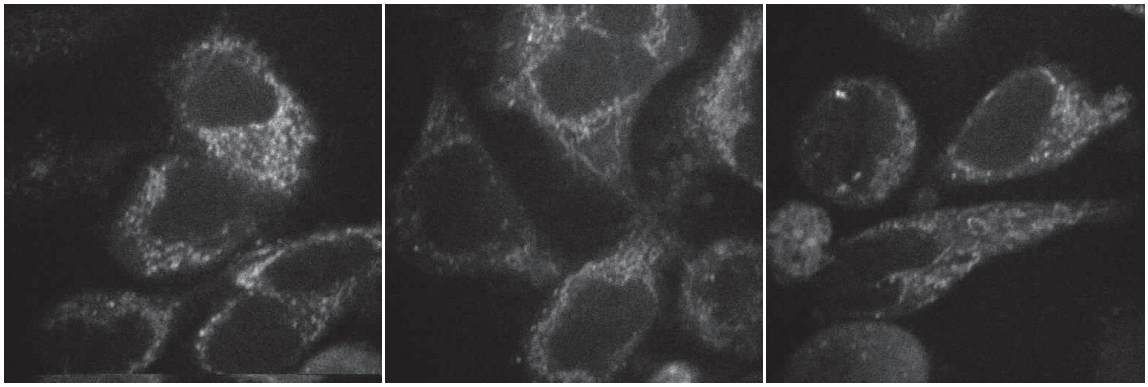

*Images obtenues par excitation à deux photons de cellules HeLa incubées avec le peptide Tat marqué avec l'**$OxyLH_2$** (exc 780 nm, puissance du laser <0,5 mW, 50x50 µm)*

En parallèle, nous avons marqué la protéine de la nucléocapside avec le dérivé **4-MeOxyLH** et observé, à travers son extinction de fluorescence, l'interaction de la protéine avec des séquences d'oligonucléotides. Ce dérivé de l'oxyluciférine présente un spectre d'émission double associé à deux états de protonation du fluorophore. Le rapport d'intensité entre ces deux bandes d'émission peut alors être utilisé pour suivre les modifications de l'environnement proche du marqueur. Nous avons titré en ajoutant une concentration croissante d'oligonucléotide, de manière à suivre l'interaction simultanèment par anisotropie de fluorescence et par mesure ratiométrique. Les résultats obtenus à partir de ces expériences montre que le rapport d'émission entre les deux formes du fluorophores permet de suivre l'interaction entre la protéine et l'oligonucléotide avec une dynamique plus importante que celle obtenue avec l'anisotropie de fluorescence.

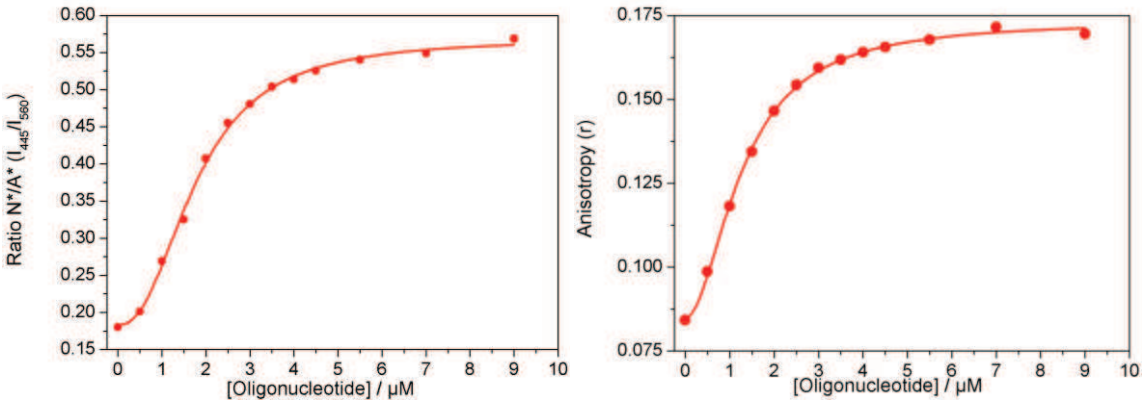

Suivi de l'interaction entre la NCp7 et l'oligonucléotide

Dans le but de stabiliser la forme cétone de l'**OxyLH$_2$**, le dérivé **5,5-Cpr-OxyLH** (voir figure ci-dessus) a été synthétisé par nos collègues allemands. Ce composé offre également la possibilité de marquer sélectivement les résidus cystéine permettant ainsi d'étiqueter des protéines qui présentent une cystéine exposée au solvant. De plus lors de la liaison à la cystéine, le dérivé **5,5-Cpr-OxyLH** voit ses propriétés optiques changer. En absence de cystéine, le composé a un spectre d'émission centrée à 637 nm alors que lié à la cystéine, le maximum d'émission est fortement décalé vers le bleu (environ 70 nm). L'hypothèse est que, en présence du thiol de la cystéine, le cycle spiro du thiazole en position 5 s'ouvre et réagit avec le groupe thiol de la cystéine conduisant à la formation de la forme énol de l'oxyluciférine. Environ 88% de toutes les protéines présentent au moins un résidu cystéine. Cette approche offre donc la possibilité de marquer sélectivement les résidus cystéine. De plus, lors de la liaison le spectre d'émission change et permet de purifier facilement l'excès de sondes libres.

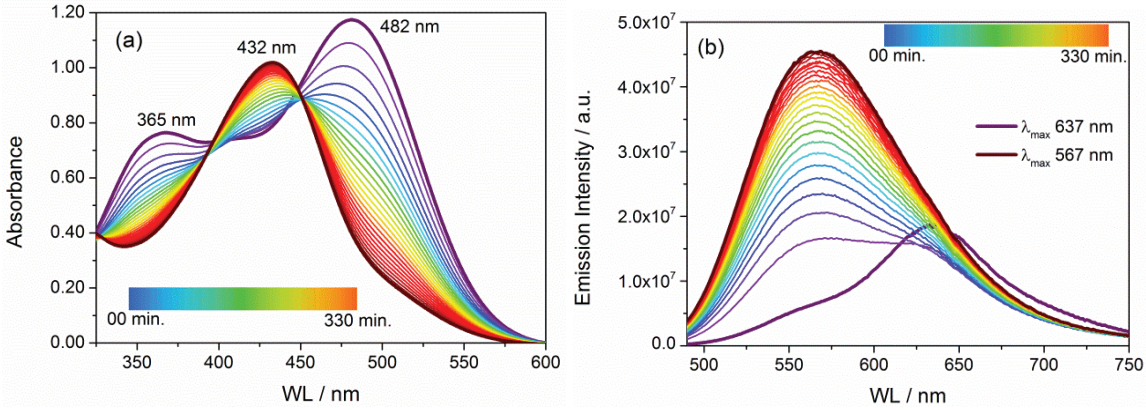

*Propriétés spectrales de **5,5-Cpr-OxyLH** avec un excès de cystéine (1000x) en fonction du temps; (a) spectres d'absorption, (b) spectres d'émission (Exc. WL 425 nm)*

Ce dérivé **5,5-Cpr-OxyLH** a été utilisé pour marquer la protéine humaine alpha-1 antitrypsine (α1-AT) qui est un inhibiteur de protéase (protéine longue de 412 acides aminés) et qui possède un résidu Cys232 accessible. Un changement significatif a été enregistré dans les spectres d'émission (~ 75 nm) avant et après étiquetage. Après l'achèvement de la procédure de marquage et de purification, l'extinction de fluorescence de l'α1-AT marquée avec une concentration croissante d'élastase pancréatique (PPE) a

été étudiée. En présence de PPE l'extinction de la fluorescence a été observée confirmant l'intégrité biologique de la protéine dans un tampon physiologique.

Les résultats présentés dans les **chapitre 4** et **chapitre 5** vont faire l'objet de publications dans des journaux à comite de lecture.

Dans le but obtenir une meilleure description du mécanisme de bioluminescence de la luciole et de la dynamique à l'état excité, nous avons étudié les propriétés optiques d'analogues structuraux de l'oxyluciférine dans un tampon aqueux. En particulier, nous avons pu montrer que le mécanisme d'émission est fortement dépendant du pH. A l'aide de différentes méthodes chimiométriques il a été possible de déterminer les formes spectrales associées à chacune des espèces chimiques de l'oxyluciférine. De plus, nous avons mesurés les constantes cinétiques qui régissent l'équilibre entre ces différentes espèces à l'état fondamental et à l'état excités.

En mimant les conditions physiologiques requises par la bioluminescence naturelle, nous avons caractérisé les propriétés photophysiques de l'émetteur à l'intérieur de la poche de l'enzyme : la luciférase. Dans un premier temps, nous avons déterminé les paramètres de la liaison du fluorophore à la protéine. L'effet du microenvironnement à l'intérieur de la protéine sur le mécanisme d'émission du fluorophore a été étudié et comparé aux propriétés photophysiques mesurées en solution avec de l'oxyluciférine libre.

Finalement dans une dernière série d'expériences, nous avons pu montrer que cette famille de fluorophore pouvait être utilisée pour caractériser des interaction entre biomolécules. En effet, les propriétés optiques de ces marqueurs sont très sensibles aux modifications de l'environnement proche du fluorophore, ce qui permet de les utiliser comme sondes. En particulier, nos expériences ont mis en évidence que l'oxyluciférine pouvait être utiliser pour suivre les variations de pH intracellulaires ; le dérivé **4-MeOxyLH** a quant à lui été utilisé pour suivre l'interaction d'une protéine du VIH-1 avec des oligonucléotides. Finalement, nous avons également montré que le dérivé **5,5-Cpr-OxyLH** pouvait marquer de manière spécifiques les résidus cystéine et que la liaison peut être suivie à travers les modifications des propriétes spectrales du fluorophore.

En résumé,

i. nous avons identifié les différentes formes chimiques de l'oxyluciférine (individuellement et lorsque dans un complexe avec la luciférase) impliqués dans le mécanisme de la bioluminescence de la luciole par l'étude de ses analogues structuraux en solution aqueuse.

ii. nous avons proposé un mécanisme permettant de décrire la photoluminescence de l'oxyluciférine.

iii. nous avons obtenu des résultats préliminaires sur le mécanisme d'émission du complexe dans des conditions naturelles.

iv. nous avons montré que l'oxyluciférine et ses dérivés peuvent être utilisés comme outils permettant de caractériser des interactions biomoléculaires in vivo ou in vitro.

v. les résultats que nous avons obtenus contribuent de manière forte à l'avancement de la compréhension de la photophysique de la bioluminescence.

Bien que les études en solutions aqueuses nous aient permis de proposer un schéma réactionnel du mécanisme de bioluminescence, il reste nécessaire d'élucider précisément le mécanisme d'émission au sein de la protéine. Pour obtenir des informations sur la structure, des expériences d'anisotropie résolues en temps seront menées avec le complexe protéine-fluorophore. En outre, afin d'obtenir une meilleure compréhension de la structure du complexe protéine-fluorophore à l'état excité, il sera utile de combiner nos résultats avec ceux obtenus par analyse cristallographique. Ces résultats pourront être interprétés par des modèles théoriques reposant sur des méthodes de chimie quantique. En outre l'effet de la composition du tampon (force ionique etc.) doit être étudié théoriquement et expérimentalement. L'effet de la force ionique sur le pka a brièvement été discuté dans le **chapitre 3**, mais pas lorsqu'il est lié à la luciférase. Pour obtenir une structure du photoémetteur à l'état excité plus réaliste, la contribution de différents composés du tampon ainsi que l'effet de différents sels et leurs concentrations sur les spectres d'émission du complexe protéine-fluorophore doivent être considérés. En particulier, l'approche chimiométrique pourra être utilisée pour caractériser ces propriétés.

De manière à accroitre le champ des applications de ces dérivées, il est également nécessaire d'approfondir les études au niveau cellulaire. En particulier, l'effet du temps ainsi que celui des facteurs extracellulaires et d'autres paramètres doivent être étudiés. En ce qui concerne les expériences de mesure de pH intracellulaire, des expériences de calibration doivent être réalisées de manière à pouvoir déterminer de manière absolue le pH à partir de la durée de vie. Pour cela, nous prévoyons d'utiliser des solutions de référence (pH connu) avec lesquelles nous calibrerons la méthode. L'oxyluciférine pourra alors être par exemple utilisée pour suivre spécifiquement certain compartiment cellulaire (lysosome). Pour démontrer d'autres possibilités d'étiquetage de protéines, nous marquerons d'autres protéines connues pour interagir avec des oligonucléotides (transcriptase inverse du VIH-1). En particulier, l'effet de paramètres physico-chimiques (force ionique, la composition du tampon, pH) seront caractériser à partir des modifications des propriétés spectrales du fluorophore. Ces études permettront également de mettre en évidence les paramètres capables de modifier la photophysique de la sonde. Dans le cas du complexe oxyluciférine-luciférase, des mesures d'anisotropie résolue en temps ainsi que des mesures cristallographiques de la protéine marquée devront être incluses dans l'analyse pour avoir une meilleure connaissance de la formation du complexe. Finalement, l'utilisation de techniques de fluorescence résolues en temps ultrarapides (femtoseconde) permettra de d'étudier finement la dynamique du système à l'état excité du colorant libre ainsi que dans un complexe avec la protéine.

Bibliography

References

Due to some unavoidable technical difficulties, reappearance of few references could not be avoided. Their detail is as follows:

	Reference No.	Reappeared as	Reference detail
1	3	83	Branchini et al. 2004, Biochem. 43(23): 7255-7262
2	4	42	Naumov et al. 2009, JACS 131(32): 11590-11605
3	5	43	Ando et al. 2008, Nature Photonics 2(1): 44-47
4	8	136	Rebarz et al. 2013, Chem. Sc. 4(10): 3803-3809
5	10	101	White et al. 1971, Bioorg. Chem. 1(1-2) : 92-122
6	20	141	White et al. 1991, Photochem. and Photobiol. 53(1): 7
7	29	72	Erez et al. 2012, J. of Phy. Chem. A 116(28): 7452-7461
8	31	77	Sun et al. 2012, Angewandte Chemie Int. Ed., Wiley 51: 8428-8430
9	40	46	Nakatani et al. 2007, JACS 129(28): 8756-8765
10	51	53	Ugarova et al. 2002, Luminescence 17(5): 321-330
11	64	109	Razgulin et al. 2011, Chem Sc. Rev 40 : 4186-4216
12	69	138	Naumov et al. 2010, JACS 132: 11566-11579
13	122	134	Principles of Fluorescence Spectroscopy, J. R. Lakowicz
14	135	166	Greiner et al. 2011, Biochim. 93(10): 1647–1658
15	150	156	Leontieva et al. 2006, Biochem.-Moscow 71(1): 51-55
16	153	154	Krissinel et al. 1996, J. Comp. Chem 17(9) : 1085-1098
17	172	173	Vercruyesse et al. 2012, Retrovirology 9(95)

1 Shimomura, O. *Bioluminescence: Chemical Principles and Methods*. (World Scientific, 2012).

2 McCapra, F. Chemical mechanisms in bioluminescence. *Accounts of Chemical Research* **9**, 201-208, doi:10.1021/ar50102a001 (1976).

3 Branchini, B. R. *et al.* An Alternative Mechanism of Bioluminescence Color Determination in Firefly Luciferase. *Biochemistry* **43**, 7255-7262, doi:10.1021/bi036175d (2004).

4 Naumov, P., Ozawa, Y., Ohkubo, K. & Fukuzumi, S. Structure and Spectroscopy of Oxyluciferin, the Light Emitter of the Firefly Bioluminescence. *Journal of the American Chemical Society* **131**, 11590-11605, doi:10.1021/ja904309q (2009).

5 Ando, Y. *et al.* Firefly bioluminescence quantum yield and colour change by pH-sensitive green emission. *Nature Photonics* **2**, 44-47, doi:10.1038/nphoton.2007.251 (2008).

6 Yuval Erez, I. P., Rinat Gepshtein, Dan Huppert. Excited state Intermolecular Proton Transfer of firefly Luciferin IV.Temperature and pH Dependence. *Journal of American Chemical Society* **115**, 1617-1626, doi:10.1021/jp110889v (2011).

7 Toru Nakatsu, S. I., Jun Hiratake, Adrian Saldanha, Nobuyuki Kobashi, Kanzo Sakata, Hiroaki Kato. Structural basis for the spectral difference in luciferase bioluminescence. *Nature Letter* **440**, 372-376, doi:10.1038/nature04542 (2006).

8 Berit Leo, M. J. H., Kristian Schweimer, Florian Mayr, Birgitta M Wöhrl. Insights into the structure and activity of prototype foamy virus RNase H. *Retrovirology* **9**, doi:10.1186/1742-4690-9-14 (2012).

9 Mateusz Rebarz, B.-M. K., Oleg V. Maltsev, Cyril Ruckebusch, Lukas Hintermann, Pance Naumov, Michel Silwa. Deciphering the Protonation and Tautomeric Equilibria of Firefly Oxyluciferin by Molecular Engineering and Multivariate Curve Resolution. *Chemical Science* **4**, 3803-3809, doi:10.1039/c3sc50715g (2013).

10 Suzuki, N., Goto, T. Studies on Firefly Bioluminescence .3. Synthesis of 4-Thiazolone Derivatives Related to Firefly Oxyluciferin. *Agricultural and Biological Chemistry* **36**, 2213-2221 (1972).

11 White, E. H., Rapaport, E., Seliger, H. H. & Hopkins, T. A. The chemi- and bioluminescence of firefly luciferin: An efficient chemical production of electronically excited states. *Bioorganic Chemistry* **1**, 92-122 (1971).

12 Hirano, T., Hasumi, Yosuke, Ohtsuka, Kazuhiro, Maki, Shojiro, Niwa, Haruki, Yamaji, Minoru, Hashizume, Daisuke. Spectroscopic Studies of the Light-Color Modulation Mechanism of Firefly (Beetle) Bioluminescence. *Journal of the American Chemical Society* **131**, 2385-2396, doi:10.1021/ja808836b (2009).

13 Fraga, H. Firefly luminescence: A historical perpective and recent developments. *Photochemical & Photobiological Science* **7**, 146-158, doi:10.1039/b719181b (2008).

14 Chase, A. M. The Absorption Spectrum of luciferin and oxydized Luciferin. *Journal of Biological Chemistry* **150**, 433-445 (1943).

15 McElroy WD, S. B. Factors influencing the response of the bioluminescent reaction to adenosine triphosphate. *Arch. Biochem.* **22**, 420-433 (1949).

16 Hastings JW, M. W., Coulombre J. The effect of oxygen upon the immobilization reaction in firefly luminescence. *J Cell Physiol.* **42**, 137-150 (1953).

17 JW., H. Firefly flashes and royal flushes: life in a full house. *J Biolumin Chemilumin.* **4**, 29-30 (1989).

18 Bowie, L. J. Synthesis of firefly luciferin and structural analogs. *Methods in Enzymology* **57**, 15-28, doi:10.1016/0076-6879(78)57004-3 (1978).

19 Rajesh Shinde, J. P., Christopher H. Contag. Luciferin Derivatives for Enhanced in Vitro and in Vivo Bioluminescence Assays. *Biochemistry* **45**, 11103-11112, doi:10.1021/bi060475o (2006).

20 Emil H. White, H. W., Howard H. Seliger, William D. McElroy. Amino Analogs of Firefly Luciferin and Biological Activity There of. *Journal of American Chemical Society* **88**, 2015-2019, doi:10.1021/ja00961a030.

21 Emil H. White, D. F. R. Analogs and Derivatives of Firefly Oxyluciferin, the Light Emitter in Firefly Bioluminescence. *Photochemistry and Photobiology* **53**, 7 (1991).

22 Emil Henry White , E. R., Thomas A. Hopkins , Howard H. Seliger. Chemi- and Bioluminescence of Firefly Luciferin. *Journal of American Chemical Society* **91**, 2178-2180, doi:10.1021/ja01036a093 (1969).

23 Gadarla Randheer Reddy , W. C. T., Stephen C. Miller Robust Light Emission from Cyclic Alkylaminoluciferin Substrates for Firefly Luciferase. *Journal of American Chemical Society* **132**, 13586-13587, doi:10.1021/ja104525m (2010).
24 Nicholas R. Conley, A. D.-A., Jianghong Rao, W. E. Moerne. A Selenium Analogue of Firefly d-Luciferin with Red-Shifted Bioluminescence Emission. *Bioluminescence* **124**, 3406–3409, doi:10.1002/ange.201105653 (2012).
25 Li, Z.-w., Ren, Ai-min, Guo, Jing-fu, Yang, Tianxiao, Goddard, John D., Feng, Ji-kang. Color-Tuning Mechanism in Firefly Luminescence: Theoretical Studies on Fluorescence of Oxyluciferin in Aqueous Solution Using Time Dependent Density Functional Theory. *The Journal of Physical Chemistry A* **112**, 9796-9800, doi:10.1021/jp8014047 (2008).
26 Ugarova, N. N. Interaction of firefly luciferase with substrate and their analogs: a study using fluorescence spectroscopy methods *Photochemical & Photobiological Science* **7**, 218-227, doi:10.1039/b712895a (2008).
27 Ren, A.-M., Guo, Jing-Fu, Feng, Ji-Kang, Zou, Lu-Yi, Li, Zhong-Wei, Goddard, John David. TDDFT Study of the Electronic Structure, Absorption and Emission Spectra of the Light Emitters of the Amazing Firefly Bioluminescence and Solvation Effects on the Spectra. *Chinese Journal of Chemistry* **26**, 55-64, doi:10.1002/cjoc.200890038 (2008).
28 Pascal Didier, J. G., Yves Mély. Two-Photon Two-Focus Fluorescence Correlation Spectroscopy with a Tunable Distance Between the Excitation Volumes. *Journal of Fluorescence* **19**, 561-565, doi:10.1007/s10895-008-0424-0 (2009).
29 Galina Orlova , J. D. G., and Lioubov Yu. Brovko. Theoretical Study of the Amazing Firefly Bioluminescence: The Formation and Structures of the Light Emitters. *Jaournal of American chemical Society* **125**, 6962–6971, doi:10.1021/ja021255a (2003).
30 Yuval Erez, I. P., Rinat Gepshtein, Luís Pinto da Silva, Joaquim C. G. Esteves da Silva, Dan Huppert. Comparative Study of the Photoprotolytic Reactions of d-Luciferin and Oxyluciferin. *Journal of Physical Chemistry A* **116**, 7452–7461, doi:10.1021/jp301910p (2012).
31 Itay Presiado, Y. E., Ron Simkovitch, Shay Shomer, Rinat Gepshtein, Luís Pinto da Silva, Joaquim C.G. Esteves da Silva, Dan Huppert. Excited-State Proton Transfer of Firefly Dehydroluciferin. *J. Physical Chemistry A* **116**, 10770-10779, doi:10.1021/jp308818r (2012).
32 Yuan-Qiang Sun, J. L., Pi Wang, Jingyu Zhang, Wei Guo. D-Luciferin Analogues: a Multicolor Toolbox for Bioluminescence Imaging. *Angewandte Chemie International Edition, Wiley* **51**, 8428-8430, doi:10.1002/anie.201203565 (2012).
33 Chang-ik song, Y. M. R. Dynamics on the Electronically Excited State Surface of the Bioluminescent Firefly Luciferase-Oxyluciferin System *Journal of American Chemical Society* **133**, 10, doi:10.1021/ja201752p (2011).
34 Pinto da Silva, L., Esteves da Silva, Joaquim C. G. . Computational Investigation of the Effect of pH on the Color of Firefly Bioluminescence by DFT. *ChemPhysChem* **12**, 951-960, doi:10.1002/cphc.201000980 (2011).
35 Luís Pinto Da Silva, J. C. G. E. D. S. Theoretical modulation of the color of light emitted by firefly oxyluciferin. *Journal of Computational Chemistry* **32**, 2654–2663, doi:10.1002/jcc.21845 (2011).

36 Pinto da Silva, L., Esteves da Silva, Joaquim C. G. Computational Studies of the Luciferase Light-Emitting Product: Oxyluciferin. *Journal of Chemical Theory and Computation* **7**, 809-817, doi:10.1021/ct200003u (2011).

37 V.R. Viviani, F. G. C. A., A.J.S. Neto, T.L. Oehlmeyer, E.J.H. Bechara, Y. Ohmiya. The structural origin and biological function of pH sensitivity in firefly luceferase. *Photochemical & Photobiolgical Science* **7**, 159-169, doi:10.1039/b714392c (2008).

38 Luís Pinto da Silva, J. C. G. E. d. S. Firefly luciferin as a multifunctional chemiluminescence molecule. *Photochem. Photobiol. Sci* **12**, 1615-1621, doi:10.1039/C3PP50086A (2013).

39 Ju Mei, J. T., Jian Wang, Anjun Qin, Jing Zhi Sun, Ben Zhong Tang. Discriminative fluorescence detection of cysteine, homocysteine and glutathione via reaction-dependent aggregation of fluorophore-analyte adducts. *Journal of Materials Chemistry* **22**, 17063-17070, doi:10.1039/C2JM32892E (2012).

40 Ai-Min Ren, J. D. G. Predictions of the electronic absorption and emission spectra of luciferin and oxyluciferins including solvation effects. *Journal of Photochemistry and Photobiology B: Biology* **81**, 163-170, doi:10.1016/j.jphotobiol.2005.07.007 (2005).

41 Nakatani, N., Hasegawa, J.-Y. & Nakatsuji, H. Red Light in Chemiluminescence and Yellow-Green Light in Bioluminescence: Color-Tuning Mechanism of Firefly, Photinus pyralis, Studied by the Symmetry-Adapted Cluster−Configuration Interaction Method. *Journal of the American Chemical Society* **129**, 8756-8765, doi:10.1021/ja0611691 (2007).

42 Kristian Støchkel, C. N. H., Jørgen Houmøller, Lisbeth Munksgaard Nielsen, Kelvin Anggara, Mathieu Linares, Patrick Norman, Fernando Nogueira, Oleg V. Maltsev, Lukas Hintermann, Steen Brøndsted Nielsen, Panče Naumov, Bruce F. Milne. On the Influence of Water on the Electronic Structure of Firefly Oxyluciferin Anions from Absorption Spectroscopy of Bare and Monohydrated Ions in Vacuo. *J. Am. Chem. Soc.* **135**, 6485–6493, doi:10.1021/ja311400t (2013).

43 Pance Naumov, Y. o., Kei Ohkubo, Shunichi Fukuzumi. Structure and Spectroscopy of Oxyluciferin, the Light Emitter of the Firefly Bioluminescence. *Journal of American Chemical Society* **131**, 11590-11605, doi:10.1021/ja904309q (2009).

44 Yoriko Ando, K. N., Nobuyuki Yamada, Toshiteru Enomoto, Tstutomu Irie, Hidehiro Kubota, Yoshihiro Ohmiya, Hidefumi Akiyama. Firefly bioluminescence quantum yield and colour change by pH-sensitive green emission. *Nature Photonics* **2**, 44-47, doi:10.1038/nphoton.2007.251 (2008).

45 Takashi Hirano, H. N., Takuto Matsuhashi, Yosuke Hasumi, Satoshi Iwano, Kazuto Ito, Shojiro Maki, Haruki Niwaa, Vadim R. Vivianib Spectroscopic studies of the color modulation mechanism of firefly (beetle) bioluminescence with amino-analogs of luciferin and oxyluciferin. *Photochem. Photobiol. Sci.* **11**, 1281-1284, doi:10.1039/C2PP25106J (2012).

46 Bruce R. Branchini, M. H. M., Rachelle A. Magyar, Nathan C. Portier, Maria C. Ruggiero, Justin G. Stroh. yellow-Green and Red Firefly Bioluminescence from 5,5-Dimethyloxyluciferin. *Journal of American Chemical Society* **124**, 2112-2113, doi:10.1021/ja017400m (2002).

47 Naoki Nakatani , J.-y. H., and Hiroshi Nakatsuji. Red Light in Chemiluminescence and Yellow-Green Light in Bioluminescence: Color-Tuning Mechanism of Firefly, Photinus pyralis, Studied by the Symmetry-Adapted

Cluster−Configuration Interaction Method. *Journal of American Chemical Society* **129**, 8756–8765, doi:10.1021/ja0611691 (2007).

48 Avisek Ghose, M. R., Oleg V. Maltsev, Lukas Hintermann, Cyril Ruckebusch, Eduard Fron, Johan Hofkens, Yves Mély, Panče Naumov, Michel Sliwa, Pascal Didier. Emission Properties of Oxyluciferin and its Derivatives in Water: Revealing the Nature of the Emissive Species in Firefly Bioluminescence *Journal of Phy. Chem. B* **119**, 2638-2649, doi:10.1021/jp508905m (2015).

49 Itay Presiado, Y. E., Dan Huppert. Excited State Intermolecular Proton Transfer of Firefly Luciferin III. Proton Transfer to a Mild Base. *J. Physical Chemistry A* **114**, 13337-13346, doi:10.1021/jp107360d (2010).

50 Yuval Erez, D. H. Excited State Intermolecular Proton Transfer of the Firefly's Chromophore D-Luciferin. *J. Physical Chemistry A* **114**, 8075-8082, doi:10.1021/jp103264y (2010).

51 Jianzhang Zhao, S. J., Yinghui Chen, Huimin Guo, Pei Yanga Excited state intramolecular proton transfer (ESIPT): from principal photophysics to the development of new chromophores and applications in fluorescent molecular probes and luminescent materials. *Phys. Chem. Chem. Phys.* **14**, 8803-8817, doi:10.1039/C2CP23144A (2012).

52 Ugarova NN, B. L. Protein structure and bioluminescent spectra for firefly bioluminescence. *Luminescence* **17**, 321-330, doi:10.1002/bio.688 (2002).

53 Jesse A. Sundlov, D. M. F., Tara L. Southworth, Bruce R. Branchini, Andrew M. Gulick. Crystal Structure of Firefly Luciferase in a Second Catalytic Conformation Supports a Domain Alternation Mechanism. *Biochemistry, Am. Chem. Sc.* **51**, 6493–6495, doi:10.1021/bi300934s (2012).

54 Ugarova, N. N. B., L. Yu. Protein structure and bioluminescent spectra for firefly bioluminescence. *Luminescence* **17**, 321-330, doi:10.1002/bio.688 (2002).

55 Baldwin, T. O. Firefly luciferase: the structure is known, but the mystery remains. *Structure, Current Biology*, 223-228 (1996).

56 Elena Conti, N. P. F., Peter Brick. Crystal structure of firefly luciferase throws light on a superfamily of adenylate-forming enzymes. *Structure, Current Biology*, 287–298 (1996).

57 Bruce R. Branchini, J. C. R., Danielle M. Fontaine, Tara L. Southworth, Curran E. Behney, Lerna Uzasci. Bioluminescence Is Produced from a Trapped Firefly Luciferase Conformation Predicted by the Domain Alternation Mechanism. *Journal of American Chemical Society* **133**, 11088–11091, doi:10.1021/ja2041496 (2011).

58 Wang, Y. A., Hidefumi Terakado, Kanako Nakatsu, Toru. Impact of Site-Directed Mutant Luciferase on Quantitative Green and Orange/Red Emission Intensities in Firefly Bioluminescence. *Sci. Rep.* **3**, doi:10.1038/srep02490 (2013).

59 Mikhail I. Koksharova, N. N. U. Approaches To Engineer Stability Of Beetle Luciferases. *Computational and Structural Biotechnology Journal* **2**, 1-7, doi:10.5936/csbj.201209004 (2012).

60 Yuichi Oba, N. M., Mayumi Yoshida, Satoshi Inouye. Identification and Characterization of a Luciferase Isotype in the Japanese Firefly, Luciola cruciata, Involving in the Dim Glow of Firefly Eggs. *ACS Biochemistry* **49**, 10788–10795, doi:10.1021/bi1016342 (2010).

61 Ali Moradi, S. H., Hossein Naderi-Manesh, Majid Sadeghizadeh, Bagher Said Alipour. Effect of Charge Distribution in a Flexible Loop on the Bioluminescence Color of Firefly Luciferases. *ACS Biochemistry* **48**, 575–582, doi:10.1021/bi802057w (2009).

62 Bruce R. Branchini, R. A. M., Martha H. Murtiashaw, Shannon M. Anderson, Lisa C. Helgerson, arc Zimmer. Site-Directed Mutagenesis of Firefly Luciferase Active Site Amino Acids: A Proposed Model for Bioluminescence Color. *ACS Biochemistry* **38**, 13223–13230, doi:10.1021/bi991181o (1999).

63 J P Steghens, K. L. M., J C Bernengo. Firefly luciferase has two nucleotide binding sites: effect of nucleoside monophosphate and CoA on the light-emission spectra. *Biochem Journal* **336**, 109-113 (1998).

64 Greer, L. F., Szalay, Aladar A. Imaging of light emission from the expression of luciferases in living cells and organisms: a review. *Luminescence* **17**, 43-74, doi:10.1002/bio.676 (2002).

65 Andrew razgulin, N. M., Jianghong rao. Strategis for in vivo imaging of enzyme activity: an overview and recent advances. *RSC* **40**, 31, doi:10.1039/c1cs15035a (2011).

66 Simone M. Marques, J. C. G. E. d. S. Firefly bioluminescence: A mechanistic approach of luciferase catalyzed reactions. *IUBMB Life* **61**, 6-17, doi:10.1002/iub.134 (2009).

67 Ryosuke Kojima, D. H. T., Prof. Takeaki Ozawa, Yukio Tada, Prof. Tetsuo Nagano, Prof. Yasuteru Urano. Rational Design and Development of Near-Infrared-Emitting Firefly Luciferins Available In Vivo. *Angewandte Chemie International Edition* **52**, 1175-1179, doi:10.1002/anie.201205151 (2013).

68 Genevieve C. Van de Bittner, C. R. B., Christopher J. Chang. Strategy for Dual-Analyte Luciferin Imaging: In Vivo Bioluminescence Detection of Hydrogen Peroxide and Caspase Activity in a Murine Model of Acute Inflammation. *Journal of American Chemical Society* **135**, 1783-1795, doi:10.1021/ja309078t (2013).

69 Jing Li, L. C., Lupei Dua, Minyong Li. Cage the firefly luciferin! – a strategy for developing bioluminescent probes. *Chemical Society Reviews* **42**, 662-676, doi:10.1039/C2CS35249D (2013).

70 pance Naumov, M. K. Spectral-Structural Effects of the Keto-Enol-Enolate and Phenol-Phenolate Equilibira of Oxylucifering. *Journal of American Chemical Society* **132**, 11566-11579, doi:10.1021/ja102885g (2010).

71 Kyril M. Solntsev, S. P. L., Panče Naumov. Photoinduced Dynamics of Oxyluciferin Analogues: Unusual Enol “Super”photoacidity and Evidence for Keto–Enol Isomerization. *Journal of American Chemical Society* **134**, 16452-16455, doi:10.1021/ja3045212 (2012).

72 Luís Pinto da Silva, J. C. G. E. d. S. Chemiexcitation Induced Proton Transfer: Enolate Oxyluciferin as the Firefly Bioluminophore. *Journal of Physical Chemistry B*, doi:10.1021/jp5036458 (2014).

73 Erez, Y. *et al.* Comparative Study of the Photoprotolytic Reactions of d-Luciferin and Oxyluciferin. *The Journal of Physical Chemistry A* **116**, 7452-7461, doi:10.1021/jp301910p (2012).

74 Ekaterina I. Dementieva, E. A. F., Lubov Yu. Brovko, Alexander P. Savitskii, Natalya N. Ugarova. Fluorescent properties of firefly luciferases and their complexes with luciferin. *Bioscience Reports* **20** (2000).

75 Griffiths, M. W. The role of ATP bioluminescence in the food industry. *Food Technology* **50**, 62-73 (1996).

76 Kricka, L. J. Application of bioluminescence and chemiluminescence in biomedical sciences. *Methods in Enzymology* **305**, 333-345, doi:10.1016/S0076-6879(00)05498-7 (2000).

77 Ohkuma, H., Abe, K., Kosaka, Y., Maeda, M. Detection of luciferase having two kinds of luminescent colour based on optical filter procedure: application to an enzyme immunoassay. *Luminescence* **15**, 21-27 (2000).
78 Sun, Y.-Q., Liu, Jing, Wang, Pi, Zhang, Jingyu, Guo, Wei. D-Luciferin Analogues: a Multicolor Toolbox for Bioluminescence Imaging. *Angewandte Chemie International Edition* **51**, 8428-8430, doi:10.1002/anie.201203565 (2012).
79 Kajiyama, K. G. a. N. Oxyluciferin, a Luminescence Product of Firefly Luciferase, Is Enzymatically Regenerated into Luciferin. *J. Biol Chem* **276**, 36508-36513, doi:10.1074/jbc.M105528200 (2001).
80 Kunisuke Okada, H. I., Ichiro Kubota, Toshio Goto. Firefly Bioluminescence III. Conversion of Oxyluciferin to Luciferin in Firefly. *Tetrahedron letteres* **32**, 2771-2774 (1974).
81 Hosseinkhani, S. Molecular enigma of multicolor bioluminescence of firefly luciferase. *Cell. Mol. Life Sci.* **68**, 1167-1182, doi:10.1007/s00018-010-0607-0 (2011).
82 Wang, Y., Hayamizu, Yuhei, Akiyama, Hidefumi. Spectroscopic Study of Firefly Oxyluciferin in an Enzymatic Environment on the Basis of Stability Monitoring. *The Journal of Physical Chemistry B* **118**, 2070-2076, doi:10.1021/jp411476p (2014).
83 Bruce R. Branchini, T. L. S., Martha H. Murtiashaw, Rachelle A. Magyar, Susan A. Gonzalez, Maria C. Ruggiero, Justin G. Stroh. An Alternative Mechanism of Bioluminescence Color Determination in Firefly Luciferase. *Biochemistry* **43**, 7255-7262, doi:10.1021/bi036175d (2004).
84 Branchini, B. R., Rosenberg, Justin C., Ablamsky, Danielle M., Taylor, Kelsey P., Southworth, Tara L., Linder, Samantha J. Sequential bioluminescence resonance energy transfer–fluorescence resonance energy transfer-based ratiometric protease assays with fusion proteins of firefly luciferase and red fluorescent protein. *Analytical Biochemistry* **414**, 239-245, doi:10.1016/j.ab.2011.03.031 (2011).
85 Gandelman, O. A., Brovko, L. Yu, Chikishev, A. Yu, Shkurinov, A. P.,Ugarova, N. N. Investigation of the interaction between firefly luciferase and oxyluciferin or its analogues by steady state and subnanosecond time-resolved fluorescence. *Journal of Photochemistry and Photobiology B: Biology* **22**, 203-209, doi:10.1016/1011-1344(93)06970-E (1994).
86 Gandelman, O. A., Brovko, L. Y., Ugarova, N. N., Shchegolev, A. A. The Bioluminescent System of Fireflies - Investigation of the Interaction of the Reaction-Product, Oxyluciferin, and its Analogs with Luciferase by Methods of Fluorescence Spectroscopy. *Biochemistry-Moscow* **55**, 785-789 (1990).
87 Min, K.-L., Steghens, Jean-Paul, . The Emitting Species Dissociated from the Enzyme Can Emit the Light in Photinus pyralis Luciferase System. *Biochemical and Biophysical Research Communications* **265**, 273-278 (1999).
88 Niwa, K., Ichino, Yoshiro, Kumata, Shiho, Nakajima, Yoshihiro, Hiraishi, Yoshihiro, Kato, Dai-ichiro, Viviani, Vadim R., Ohmiya, Yoshihiro. Quantum Yields and Kinetics of the Firefly Bioluminescence Reaction of Beetle Luciferases. *Photochemistry and Photobiology* **86**, 1046-1049, doi:10.1111/j.1751-1097.2010.00777.x (2010).
89 Ugarova, N. N., Maloshenok, L. G., Uporov, I. V., Koksharov, M. I. Bioluminescence Spectra of Native and Mutant Firefly Luciferases as a Function of pH. *Biochemistry-Moscow* **70**, 1262-1267, doi:10.1007/s10541-005-0257-2 (2005).

90 Hiyama, M., Akiyama, Hidefumi, Wang, Yu, Koga, Nobuaki. Theoretical study for absorption spectra of oxyluciferin in aqueous solutions. *Chemical Physics Letters* **577**, 121-126, doi:10.1016/j.cplett.2013.05.053 (2013).

91 Yanagisawa, Y., Kageyama, Takeshi, Wada, Naohisa, Tanaka, Masatoshi, Ohno, Shin-ya. Time Courses and Time-Resolved Spectra of Firefly Bioluminescence Initiated by Two Methods of ATP Injection and Photolysis of Caged ATP. *Photochemistry and Photobiology* **89**, 1490-1496, doi:10.1111/php.12146 (2013).

92 Anselmi, M., Marocchi, Simone, Aschi, Massimiliano, Amadei, Andrea. Theoretical modeling of the spectroscopic absorption properties of luciferin and oxyluciferin: A critical comparison with recent experimental studies. *Chemical Physics* **392**, 205-214, doi:10.1016/j.chemphys.2011.11.021 (2012).

93 Chen, S.-F. *et al.* Systematic Theoretical Investigation on the Light Emitter of Firefly. *Journal of Chemical Theory and Computation* **7**, 798-803, doi:10.1021/ct200045q (2011).

94 Kim, H. W., Rhee, Young Min. On the pH Dependent Behavior of the Firefly Bioluminescence: Protein Dynamics and Water Content in the Active Pocket. *The Journal of Physical Chemistry B* **117**, 7260-7269, doi:10.1021/jp4024553 (2013).

95 Navizet, I., Liu, Ya-Jun, Ferré, Nicolas, Xiao, Hong-Yan, Fang, Wei-Hai, Lindh, Roland. Color-Tuning Mechanism of Firefly Investigated by Multi-Configurational Perturbation Method. *Journal of the American Chemical Society* **132**, 706-712, doi:10.1021/ja908051h (2010).

96 Navizet Isabelle, R.-S., Daniel Yue, Ling Liu, Ya-Jun Ferré, Nicolas Lindh, Roland. Are the Bio- and Chemiluminescence States of the Firefly Oxyluciferin the Same as the Fluorescence State? *Photochemistry and Photobiology* **89**, 319-325, doi:10.1111/php.12007 (2013).

97 Oleg V. Maltsev, N. K. N., Panče Naumov, Lukas Hintermann. Why is Firefly Oxyluciferin a Notoriously Labile Substance. *Angewandte Chemie International Edition, Wiley* **53**, 847-850, doi:10.1002/anie.201307972 (2013).

98 Ando, Y., Akiyama, H. pH-Dependent Fluorescence Spectra, Lifetimes, and Quantum Yields of Firefly-Luciferin Aqueous Solutions Studied by Selective-Excitation Fluorescence Spectroscopy. *Japanese Journal of Applied Physics* **49**, doi:10.1143/jjap.49.117002 (2010).

99 Hiyama, M. A., Hidefumi, Mochizuki, Toshimitsu, Yamada, Kenta Koga, Nobuaki. Analysis of Photoexcitation Energy Dependence in the Photoluminescence of Firefly Luciferin. *Photochemistry and Photobiology* **90**, 820-828, doi:10.1111/php.12243 (2014).

100 Wang, Y., Kubota, Hidehiro, Yamada, Nobuyuki, Irie, Tsutomu, Akiyama, Hidefumi. Quantum Yields and Quantitative Spectra of Firefly Bioluminescence with Various Bivalent Metal Ions. *Photochemistry and Photobiology* **87**, 846-852, doi:10.1111/j.1751-1097.2011.00931.x (2011).

101 Bruce R. Branchini, M. H. M., Rachelle A. Magyar, Shannon M. Anderson. The role of lysine 529, a conserved residue of the acyl-adenylate-forming enzyme superfamily, in firefly luciferase. *Biochemistry* **39**, 5433–5440, doi:10.1021/bi9928804 (2000).

102 Emil H. White Eliezer Rapaport, H. H. S., Thomas A. Hopkins. The chemi- and bioluminescence of firefly luciferin: An efficient chemical production of electronically excited states. *Bioorganic Chemistry* **1**, 92-122, doi:10.1016/0045-2068(71)90009-5 (1971).

103 Yoshihiro Ohmiya, T. H., Mamoru Ohashi. The structural origin of the color differences in the bioluminescence of firefly luciferase. *FEBS letteres* **384**, 83-86, doi:10.1016/0014-5793(96)00288-8 (1996).
104 Vadim Viviani, A. U., N. Suenaga, M. Ryufuku, Y. Ohmiya. Thr226 is a key residue for bioluminescence spectra determination in beetle luciferases. *Biochemical and Biophysical Research Communications* **280**, 1286-1291, doi:10.1006/bbrc.2001.4254 (2001).
105 Volodymyr V. Shvadchak, A. S. K., Hugues de Rocquigny and Yves Mely. Sensing peptide–oligonucleotide interactions by a two-color fluorescence label: application to the HIV-1 nucleocapsid protein. *Nucleic Acids Research* **37**, 12, doi:10.1093/nar/gkn1083 (2009).
106 Azadeh Kheirolomoom, D. E. K., Shengping Qin, Katherine E. Watson, Chun-Yen Lai, Lawrence J.T. Young, Robert D. Cardiff, Katherine W. Ferrara. Enhanced in vivo bioluminescence imaging using liposomal luciferin delivery system. *Journal of Controlled Release* **141**, 128-136, doi:10.1016/j.jconrel.2009.08.029 (2010).
107 Emelía Eiríksdóttir, I. M., Taavi Lehto, Samir El Andaloussi, Ülo Langel. Cellular Internalization Kinetics of (Luciferin-)Cell-Penetrating Peptide Conjugates. *Bioconjugate Chemistry* **21**, 1662-1672, doi:10.1021/bc100174y (2010).
108 ee F. Greer III, A. A. S. Imaging of light emission from the expression of luciferases in living cells and organisms: a review. *Luminescence* **17**, 43-74, doi:10.1002/bio.676 (2002).
109 Amit P. Jathoul, H. G., James C. Anderson, Martin A. Pule. A Dual-Color Far-Red to Near-Infrared Firefly Luciferin Analogue Designed for Multiparametric Bioluminescence Imaging. *Angewandte Chemie International Edition* **53**, 13059-13063, doi:10.1002/anie.201405955 (2014).
110 Andrew Razgulin, N. M., Jianghong Rao. Strategies for in vivo imaging of enzyme activity: an overview and recent advances. *Chem. Soc. Rev* **40**, 4186-4216, doi:10.1039/C1CS15035A (2011).
111 Jean-Luc Darlix, J. G., Roland Ivanyi-Nagy, Philippe Fossé, Olivier Mauffret, Yves Mély. Flexible Nature and Specific Functions of the HIV-1 Nucleocapsid Protein. *Journal of Molecular Biology* **410**, 17, doi:10.1016/j.jmb.2011.03.037 (2011).
112 Christian Boudier, N. H., Françoise Chaminade, Yingying Chen, Hugues de Rocquigny, Julien Godet, Olivier Mauffret, Philippe Fossé, Yves Mély. Dynamic interactions of the HIV-1 Tat with nucleic acids are critical for Tat activity in reverse transcription. *Nucleic Acids Research* **42**, 14, doi:10.1093/nar/gkt934 (2014).
113 Nelly Morellet, H. D., Valérie Teilleux, Tam Huynh-Dinh, Hugues de Rocquigny, Marie-Claude Fournié-Zaluski. Structure of the complex between the HIV-1 nucleocapsid protein NCp7 and the single-stranded pentanucleotide d(ACGCC). *Journal of Molecular Biology* **283**, 419-434, doi:10.1006/jmbi.1998.2098 (1998).
114 Mattia Mori, A. N., Maria Chiara Dasso Lang, Nicolas Humbert, Christian Boudier, Francois Debaene, Sarah Sanglier-Cianferani, Marjorie Catala, Patricia Schult-Dietrich, Ursula Dietrich, Carine Tisné, Yves Mely, Maurizio Botta. Functional and Structural Characterization of 2-Amino-4-phenylthiazole Inhibitors of the HIV-1 Nucleocapsid Protein with Antiviral Activity. *ACS Chemical Biology*, doi:10.1021/cb500316h (2014).
115 Alice Sosic, F. F., Elisa Perissutti, Laura Sinigaglia, Vincenzo Santagada, Giuseppe Caliendo, Elisa Magli, Antonio Ciano, Giuseppe Zagotto, Cristina

Parolinc and Barbara Gatto. Design, synthesis and biological evaluation of TAR and cTAR binders as HIV-1 nucleocapsid inhibitors. *Med. Chem. Comm. RSCqs* **2013**, 06, doi:10.1039/c3md00212h (2013).

116 Sarah Bourbigot, N. R., Christian Boudier, Gilmar F.J. Salgado, Bernard P. Roques, Yves Mély, Serge Bouaziz, Nelly Morellet. How the HIV-1 Nucleocapsid Protein Binds and Destabilises the (−)Primer Binding Site During Reverse Transcription. *Journal of Molecular Biology* **383**, 1112-1128, doi:10.1016/j.jmb.2008.08.046 (2008).

117 Christian Boudier, A. S. K., Yves Mely, Anny Follenius-Wund. Local environment perturbations in alpha1-antitrypsin monitored by a ratiometric fluorescent label. *Photochemical and Photobiological Sciences* **8**, 8, doi:10.1039/b902309g (2009).

118 Loussiné Zargarian, I. K., Ali Bazzi, Jonathan Boynard, Françoise Chaminade, Philippe Fossé, Olivier Mauffret. Structural and dynamic characterization of the upper part of the HIV-1 cTAR DNA hairpin. *Nucleic Acids research* **37**, 4043-4054, doi:10.1093/nar/gkp297 (2009).

119 Ali Bazzi1, L. Z., Françoise Chaminade, Christian Boudier, Hughes De Rocquigny, Brigitte René, Yves Mély, Philippe Fossé, Olivier Mauffret. Structural insights into the cTAR DNA recognition by the HIV-1 nucleocapsid protein: role of sugar deoxyriboses in the binding polarity of NC. *Nucleic Acids Research* **39**, 3903-3916, doi:10.1093/nar/gkq1290 (2011).

120 Julien Godet, C. K., Frédéric Przybilla, Ludovic Richert, Guy Duportail, Yves Mély. Site-selective probing of cTAR destabilization highlights the necessary plasticity of the HIV-1 nucleocapsid protein to chaperone the first strand transfer. *Nucleic Acids Research* **41**, 5036-5048, doi:10.1093/nar/gkt164 (2013).

121 Kengo Suzuki, A. K., Shigeo Kaneko, Kazuyuki Takehira, Toshitada Yoshihara, Hitoshi Ishida, Yoshimi Shiina, Shigero Oishic, Seiji Tobita. Reevaluation of absolute luminescence quantum yields of standard solutions using a spectrometer with an integrating sphere and a back-thinned CCD detector. *Phys. Chem. Chem. Phys.* **11**, 9850-9860, doi:10.1039/B912178A (2009).

122 Adolfas K. Gaigalas, L. W. Measurement of the Fluorescence Quantum Yield using a spectrometer with an Integrating Sphere Detector. *journal of research of the National Institue of Standards and Technology* **113**, 17-28 (2008).

123 Lakowicz, J. R. *Principles of Fluorescence Spectroscopy*. 3rd edn, (Springer, 2006).

124 Becker, W. in *The bh TCSPC Handbook* (2012).

125 GmbH, B. H. (2013).

126 N. B. Sankaran, P. K. M., Bhaswati Bhattacharya, Anunay Samanta. Fluorescence response of mono- and tetraazacrown derivatives of 4-aminophthalimide with and without some transition and post transition metal ions. *J. Mater. Chem* **15**, 2854-2859, doi:10.1039/B417926A (2005).

127 Jeffrey R. De Wet, K. V. W., Donald R. Helinski, Marlene Deluca. Cloning of firefly luciferase cDNA and the expression of active luciferase in E.Coli. *Proc. Natl. Acad. Sci* **82**, 7870-7873 (1985).

128 de Wet JR, W. K., DeLuca M, Helinski DR, Subramani S. Firefly luciferase gene: structure and expression in mammalian cells. *Mol. Cell. Biol.* **7**, 725-737 (1987).

129 Merrifield, R. B. Sloid Phase Peptide Synthesis. I. The synthesis of a Tetrapeptide. (1963).

130 Hussein Ftouni, F. B., Hugues de Rocquigny, jean-François Nicoud. Functionalized two-photon absorbing diketopyrrolopyrrole-based fluorophores for

living cells fluorescent microscopy. *ACS Bioconjugate Chemistry*, 9, doi:10.1021/bc300623q (2013).

131 Oleksandr M. Zamotaiev, V. Y. P., Volodymyr V. Shvadchak, Vasyl G. Pivovarenko, Andrey S. Klymchenko, Yves Mély. Improved Hydration-Sensitive Dual-Fluorescence Labels For Monitoring Peptide−Nucleic Acid Interactions. *ACS Bioconjugate Chemistry* **22**, 8, doi:10.1021/bc100434d (2011).

132 Hilary Brooks, B. L., Eric Vivès. Tat peptide-mediated cellular delivery: back to basics. *Advanced Drug Delivery Reviews* **57**, 19, doi:10.1016/j.addr.2004.12.001 (2005).

133 Hervé Beltz, C. C., Etienne Piémont, Damien Ficheux, Robert J. Gorelick, Bernard Roques, Caroline Gabus, Jean-Luc Darlix, Hugues de Rocquigny, Yves Mély. Structural Determinants of HIV-1 Nucleocapsid Protein for cTAR DNA Binding and Destabilization, and Correlation with Inhibition of Self-primed DNA Synthesis. *Journal of Molecular Biology* **348**, 14, doi:10.1016/j.jmb.2005.02.042 (2005).

134 Joëlle V Fritz, P. D., Jean-Pierre Clamme, Emmanuel Schaub, Delphine Muriaux, Charlotte Cabanne, Nelly Morellet, Serge Bouaziz, Jean-Luc Darlix, Yves Mély, Hugues de Rocquigny. Direct Vpr-Vpr Interaction in Cells monitored by two Photon Fluorescence Correlation Spectroscopy and Fluorescence Lifetime Imaging. *Retrovirology* **5**, doi:10.1186/1742-4690-5-87 (2008).

135 Lakowicz, J. R. (ed Springer) (2006).

136 Vanille J. Greiner, V. S., Joëlle Fritz, Youri Arntz, Pascal Didier, Benoît Frisch, Christian Boudier, Yves Mély, Hugues de Rocquigny. Characterization of the mechanisms of HIV-1 Vpr(52–96) internalization in cells. *Biochimie* **93**, 1647–1658, doi:10.1016/j.biochi.2011.05.033 (2011).

137 Rebarz, M., Kukovec, B. M., Maltsev, O. V., Ruckebusch, C., Hintermann, L., Naumov, P., Sliwa, M. Deciphering the protonation and tautomeric equilibria of firefly oxyluciferin by molecular engineering and multivariate curve resolution. *Chemical Science* **4**, 3803-3809, doi:10.1039/c3sc50715g (2013).

138 Miyabi Hiyama, H. A., Yu Wang, Nobuaki Koga. Theoretical study for absorption spectra of oxyluciferin in aqueous solutions. *Chemical Physics Letters* **577**, 121-126, doi:10.1016/j.cplett.2013.05.053 (2013).

139 Naumov, P., Kochunnoonny, Manoj. Spectral−Structural Effects of the Keto−Enol−Enolate and Phenol−Phenolate Equilibria of Oxyluciferin. *Journal of the American Chemical Society* **132**, 11566-11579, doi:10.1021/ja102885g (2010).

140 Jagannath Kuchlyan, D. B., Arpita Roy, Niloy Kundu, Nilmoni Sarkar. Excited-State Proton Transfer Dynamics of Firefly's Chromophore D-Luciferin in DMSO–Water Binary Mixture. *J. Physical Chemistry B*, doi:10.1021/jp510389d (2014).

141 White, E. H. & Roswell, D. F. Analogs and Derivatives of Firefly Oxyluciferin, the Light Emitter in Firefly Bioluminescence. *Photochemistry and Photobiology* **53**, 131-136, doi:10.1111/j.1751-1097.1991.tb08478.x (1991).

142 Gandelman, O. A., Brovko, L. Yu, Ugarova, N. N., Chikishev, A. Yu, Shkurimov, A. P. Oxyluciferin fluorescence is a model of native bioluminescence in the firefly luciferin—luciferase system. *Journal of Photochemistry and Photobiology B: Biology* **19**, 187-191, doi:10.1016/1011-1344(93)87083-Y (1993).

143 S.Y. Goldberg, E. P., D. Huppert. Proton scavenging in photoacid geminate recombination processes *Chem. Phy. Letters* **192**, 77-81 (1992).

144 Benjamin J. Schwartz, J. C. K., Jin Z. Zhang, Charles B. Harris. Direct femtosecond measurements of single collision dominated geminate recombination times of small molecules in liquids. *Chemical Physics Letters* **203**, 203-508, doi:10.1016/0009-2614(93)85300-D.
145 Rackovsky, S. Theory of Geminate Recombination as a Molecular Process. *Physical Rev. Letter* **178**, 19-23 (1991).
146 Rackovsky, S. Molecular Theory of Geminate Recombination. V. Recombination of Polarons on the 2-D Square Lattice. *J. Phys. Chem. B* **104**, 3795-3803, doi:10.1021/jp993114 (2000).
147 L. Song, S. F. S., R. C. Dorfmanf, K. Weidemaier, M. D, Fayer. Photoinduced Electron Transfer and Geminate Recombination in Solution *J. Phys. Chem.* **97**, 1374-1382 (1993).
148 L.V. Lukin, B. S. Y. Two state electron model for geminate recombination of electron–ion pairs in liquid isooctane. *Chem. Physics* **382**, 58-67, doi:10.1016/j.chemphys.2011.02.011 (2011).
149 R. C. Dorfman, M. D. F. The influence of diffusion on photoinduced electron transfer and geminate recombination. *J. Chem. Phys.* **96**, 7410-7422 (1992).
150 Leonteva, O. V., Vlasova, T. N. & Ugarova, N. N. Dimethyl- and monomethyloxyluciferins as analogs of the product of the bioluminescence reaction catalyzed by firefly luciferase. *Biochemistry-Moscow* **71**, 51-55, doi:10.1134/s000629790601007x (2006).
151 Solntsev, K. M., Huppert, Dan,Agmon, Noam. Photochemistry of "Super"-Photoacids. Solvent Effects. *The Journal of Physical Chemistry A* **103**, 6984-6997, doi:10.1021/jp9902295 (1999).
152 Peter Clifford, N. J. B. G., Michael J. Pilling. Analysis of the Debye-Smoluchowski equation. Approximations for high-permittivity solvents. *J. Phys. Chem.* **88**, 4171-4176, doi:10.1021/j150662a064 (1984).
153 Krissinel, E. B. A., Noam. Spherical symmetric diffusion problem. *Journal of Computational Chemistry* **17**, 1085-1098 (1996).
154 Krissinel, E. B., Agmon, Noam. Spherical symmetric diffusion problem. *Journal of Computational Chemistry* **17**, 1085-1098 (1996).
155 Solntsev, K. M., Laptenok, S. P. & Naumov, P. Photoinduced Dynamics of Oxyluciferin Analogues: Unusual Enol "Super"photoacidity and Evidence for Keto–Enol Isomerization. *Journal of the American Chemical Society* **134**, 16452-16455, doi:10.1021/ja3045212 (2012).
156 Leontieva O. V, V. T. N., Ugarova N. N. Dimethyl and monomethyl oxyluciferins as analogs of the product of the bioluminescence reaction catalyzed by firefly luciferase. *Biohimiâ* **71**, 65-69 (2006).
157 *The Proteins*. 3 edn, Vol. I (Academic Press Inc. london, 1975).
158 Julien Godet, N. R., Kamal K. Sharma, Ludovic Richert, Hugues de Rocquigny, Jean-Luc Darlix, Guy Duportail, Yves Mély. Specific implications of the HIV-1 nucleocapsid zinc fingers in the annealing of the primer binding site complementary sequences during the obligatory plus strand transfer. *Nucleic Acids Research* **39**, 6633-6645, doi:10.1093/nar/gkr274 (2011).
159 P. Bayer, M. K., A. Ejchart, M. Westendorp, R. Frank, P. Rosch. Structural Studies of HIV-1 tat Protein. *Journal of Molecular Biology*, 529-535 (1995).
160 Jean Philippe Richard, K. M., Hilary Brooks, Paul Prevot, Bernard Lebleu, Leonid V. Chernomordik. Cellular Uptake of Unconjugated TAT Peptide Involves Clathrin-dependent Endocytosis and Heparan Sulfate Receptors. *The Journal of Biological Chemistry* **280**, 7, doi:10.1074/jbc.M401604200 (2005).

161 John J. Turner, G. D. I., Birgit Verbeure, Donna Williams, Andrey A. Arzumanov, Saïd Abes, Bernard Lebleu, Michael J. Gait. Cell-penetrating peptide conjugates of peptide nucleic acids (PNA) as inhibitors of HIV-1 Tat-dependent trans-activation in cells. *Nucleic Acids Research* **33**, 13, doi:10.1093/nar/gki991.

162 Terra B. Potocky, A. K. M., Samuel H. Gellman. Cytoplasmic and Nuclear Delivery of a TAT-derived Peptide and a β-Peptide after Endocytic Uptake into HeLa Cells. *J. Biol Chem* **278**, 50188-50194, doi:10.1074/jbc.M308719200 (2003).

163 Paul G. Coupland, S. J. B., Jonathan W. Aylott. Using fluorescent pH-sensitive nanosensors to report their intracellular location after Tat-mediated delivery. *RSC Integr. Biol.* **1**, 318-323, doi:10.1039/B822569A (2009).

164 Jean Philippe Richard, K. M., Eric Vives, Corinne Ramos, Birgit Verbeure, Mike J. Gait, Leonid V. Chernomordik, Bernard Lebleu. Cell-penetrating Peptides A Revolution of the Mechanism of Cellular Uptake. *J. Biol Chem* **278**, 585-590, doi:10.1074/jbc.M209548200 (2003).

165 Antony K. Chen, Z. C., Mark A. Behlke, Andrew Tsourkas. Assessing the Sensitivity of Commercially Available Fluorophores to the Intracellular Environment. *Anal. Chem* **80**, 7437–7444, doi:10.1021/ac8011347 (2008).

166 Franz Gabor, U. K., Michael Wirth. The Interaction between wheat germ agglutinin and other plant lectins with prostate cancer cells Du-145. *International Journal of Pharmaceutics* **221**, 13, doi:10.1016/S0378-5173(01)00650-0 (2001).

167 Vanille J. Greiner, V. S., Joëlle Fritz, Youri Arntz, Pascal Didier, Benoît Frisch, Christian Boudier, Yves Mély, Hugues de Rocquigny. Characterization of the mechanisms of HIV-1 Vpr(52–96) internalization in cells. *Biochimie* **93**, 12, doi:10.1016/j.biochi.2011.05.033 (2011).

168 Hilton H. Mollenhauer, D. J. M., Loyd D. Rowe. Alteration of intracellular traffic by monensin; mechanism, specificity and relationship to toxicity. *Biochimica et Biophysica Acta (BBA) - Reviews on Biomembranes* **1031**, 22, doi:10.1016/0304-4157(90)90008-Z (1990).

169 Benjamin E. Steinberg, K. K. H., Alexandre Brodovitch, Sabrina Jabs, Tobias Stauber, Thomas J. Jentsch, Sergio Grinstein. A cation counterflux supports lysosomal acidification. *Journal of Cell Biology* **189**, 16, doi:10.1083/jcb.200911083 (2010).

170 L W Jiang, V. M. M., J J McCormick, M Schindler. Alkalinization of the lysosomes is correlated with ras transformation of murine and human fibroblasts. *Journal of Biol. Chem.* **265**, 4775-4777 (1990).

171 S S Chauhan, X. J. L., A W Su, A Pai-Panandiker, D W Shen, J A Hanover, M M Gottesman. Reduced endocytosis and altered lysosome function in cisplatin-resistant cell lines. *British Journal of Cancer* **88**, 1327-1334, doi:10.1038/sj.bjc.6600861 (2003).

172 Sarah J. Swanson, P. C. B., Russell L. Jones. Barley Aleurone Cells Contain Two Types of Vacuoles: Characterization of Lytic Organelles by Use of Fluorescent Probes. *The Plant Cell* **10**, 685-698, doi:10.1105/tpc.10.5.685 (1998).

173 Thomas Vercruysse, B. B., Wim Dehaen, Nicolas Humbert, Jan Balzarini, François Debaene, Sarah Sanglier-Cianférani, Christophe Pannecouque, Yves Mély and Dirk Daelemans. A phenyl-thiadiazolylidene-amine derivative ejects zinc from retroviral nucleocapsid zinc fingers and inactivates HIV virions. *Retrovirology* **9**, 14, doi:10.1186/1742-4690-9-95 (2012).

174 Thomas Vercruysse, B. B., Wim Dehaen, Nicolas Humbert, Jan Balzarini, François Debaene, Sarah Sanglier-Cianférani, Christophe Pannecouque, Yves

Mély, Dirk Daelemans. A phenyl-thiadiazolylidene-amine derivative ejects zinc from retroviral nucleocapsid zinc fingers and inactivates HIV virions. *Retrovirology* **9**, 7, doi:10.1186/1742-4690-9-95 (2012).

175 Joel Azoulay, J.-P. C., Jean-Luc Darlix, Bernard P. Roques, Yves Mély. Destabilization of the HIV-1 Complementary Sequence of TAR by the Nucleocapsid Protein Through Activation of Conformational Fluctuations. *Journal of Molecular Biology* **326**, 10, doi:10.1016/S0022-2836(02)01430-4 (2003).

176 Nelly Morellet, N. J., Hugues De Rocquigny, Bernard Maigret, Jean-Luc Darlix, Bernard P.Roques. Determination of the structure of the nucleocapsid protein NCp7 from the human immunodeficiency virus type 1 by H NMR. *The EMBO* **11**, 3059-3065 (1992).

177 Sergiy V. Avilov, J. G., Etienne Piémont, Yves Mély. Site-Specific Characterization of HIV-1 Nucleocapsid Protein Binding to Oligonucleotides with Two Binding Sites. *Biochemistry* **48**, 2422-2430, doi:10.1021/bi8022366 (2009).

178 C. Vuilleumier, E. B., N. Morellet, D. Gérard, B. P. Roques,Y. Mély. Nucleic Acid Sequence Discrimination by the HIV-1 Nucleocapsid Protein NCp7: A Fluorescence Study. *Biochemistry* **38**, 16816-16825, doi:10.1021/bi991145p (1999).

179 Igor Kanevsky, F. C., Yingying Chen, Julien Godet, Brigitte René, Jean-Luc Darlix, Yves Mély, Olivier Mauffret, Philippe Fossé. Structural determinants of TAR RNA-DNA annealing in the absence and presence of HIV-1 nucleocapsid protein. *Nucleic Acids Research* **39**, 8148-8162, doi:10.1093/nar/gkr526 (2011).

180 Bruce E. Cohen1, T. B. M., Eun Sun Park, Yuh Nung Jan, Steven G. Boxer, Lily Yeh Jan. Probing Protein Electrostatics with a Synthetic Fluorescent Amino Acid. *Science* **296**, 1700-1703, doi:10.1126/science.1069346 (2002).

181 Vazquez, M., Nitz, M, Stehn, J, Yaffe MB, Imperiali B. Fluorescent caged phosphoserine peptides as probes to investigate phosphorylation-dependent protein associations. *J. Am. Chem. Soc.* **125**, 10150-10151, doi:10.1021/ja0351847 (2003).

182 Vazquez, M., Rothman DM, Imperiali B. A new environment-sensitive fluorescent amino acid for Fmoc-based solid phase peptide synthesis. *Org. & Biomol. Chem.* **2**, 1965-1966, doi:10.1039/b408001g (2004).

183 Bruce E. Cohen, A. P., XiaoJie Yao, Gayathri Swaminath, Chris S. Gandhi, Yuh Nung Jan, Brian K. Kobilka, Ehud Y. Isacoff, Lily Y. Jan. A fluorescent probe designed for studying protein conformational change. *PNAS* **102**, doi:10.1073/pnas.0409469102 (2005).

184 Vazquez ME, B. J., Imperiali B. Photophysics and biological applications of the environment-sensitive fluorophore 6-N,N-Dimethylamino-2,3-naphthalimide. *J. Am. Chem. Soc.* **127**, 1300-1306, doi:10.1021/ja0449168 (2005).

185 Loving G, I. B. A versatile amino acid analogue of the solvatochromic fluorophore 4-N,N-dimethylamino-1,8-naphthalimide: A powerful tool for the study of dynamic protein interactions. *J. Am. Chem. Soc.* **130**, 13630-13638, doi:10.1021/ja804754y (2008).

186 Stryer, L. *Biochemistry*. 2 edn, (W. H. Freeman and Company, 1981).

187 Eun Joo Seo, C. L., Myeong-Hee Yu. Concerted Regulation of Inhibitory Activity of α1-Antitrypsin by the Native Strain Distributed throughout the Molecule. *Journal of Biological Chemistry* **277**, 5, doi:10.1074/jbc.M110272200 (2002).

188 Raquel Requejo, T. R. H., Nikola J. Costa andMichael P. Murphy. Cysteine residues exposed on protein surfaces are the dominant intramitochondrial thiol

and may protect against oxidative damage. *The FEBS Journal* **277**, 1465-1480, doi:10.1111/j.1742-4658.2010.07576.x (2010).

189 Brosnan, J. T. B. a. M. E. The Sulfur-Containing Amino Acids: An Overview. *The Journal of Nutrition* **136**, 16365-16405 (2006).

190 Fahey RC, H. J., Windham GC. On the cysteine and cystine content of proteins. Differences between intracellular and extracellular proteins. *J. Mol. Evol.* **10**, 155-160 (1977).

191 Harold L. James, A. B. C. Mechanism of Inhibition of Porcine Elastase by Human Alpha-1-Antitrypsin. *Journal of Clinical Investigation* **62**, 10, doi:10.1172/JCI109255 (1978).

192 Yuste, R. Fluorescence Microscopy Today. *Nature Method* **2**, 3 (2005).

193 Bi-Chang Chen, W. R. L., Kai Wang, Lin Shao, Daniel E. Milkie, Michael W. Davidson, Chris Janetopoulos, Xufeng S. Wu, John A. Hammer III, Zhe Liu, Brian P. English, Yuko Mimori-Kiyosue, Daniel P. Romero, Alex T. Ritter, Jennifer Lippincott-Schwartz, Lillian Fritz-Laylin, R. Dyche Mullins, Diana M. Mitchell Joshua N. Bembenek, Anne-Cecile Reymann, Ralph Böhme, Stephan W. Grill, Jennifer T. Wang, Geraldine Seydoux, U. Serdar Tulu, Daniel P. Kiehart, Eric Betzig. Lattice light-sheet microscopy: Imaging molecules to embryos at high spatiotemporal resolution. *Science* **346**, 439-451, doi:10.1126/science.1257998 (2014).

Avisek GHOSE

Etude des propriétés photophysiques de dérivés de l'oxyluciférine et leurs applications à l'étude d'interactions entre biomolécules

Résumé: Dans ce travail, nous avons étudié le mécanisme d'émission de la partie optiquement active du complexe luciférine-luciférase. Ce système bioluminescent est largement utilisé dans un très grand nombre d'approches bioanalytiques. Ce phénomène naturel résulte en l'émission de lumière visible (vert-jaune-rouge) à partir du photoproduit : l'oxyluciférine. Une des hypothèses couramment admise pour expliquer le mécanisme d'émission de l'oxyluciféreine fait intervenir un équilibre complexe entre six espèces chimiques, mais le détail exact du mécanisme reste à élucider. Les principales conclusions présentées ici repose sur l'identification des six formes chimiques de l'oxyluciférine impliquées dans le mécanisme d'émission de fluorescence et la caractérisation d'un point de vu dynamique du transfert de proton à l'état excité. Ces résultats ont été obtenus par l'étude des propriétés optiques de différents analogues structuraux de l'oxyluciférine dans un tampon aqueux. Différent techniques de spectroscopie (état stable et résolue en temps) et des approches chimiométriques ont été appliquées pour étudier ce mécanisme d'émission. En outre, les propriétés photophysiques de l'oxyluciférine en complexe avec l'enzyme luciférase (*Luciola cruciata)* ont été étudiées également en milieu aqueux. En parallèle, les dérivés présentant des propriétés d'émission sensibles à l'environnement ont été utilisés pour visualiser l'interaction entre biomolécules. En particulier, nous avons démontré que l'oxyluciférine peut être utilisée pour cartographier le pH intracellulaire à l'aide de la microscopie de fluorescence dans des cellules vivantes. Avec l'aide d'un autre dérivé de l'oxyluciférine nous avons été en mesure de caractériser l'interaction entre une protéine du VIH-1 et des séquences d'oligonucléotide au moyen de mesures ratiométriques. Enfin, nous avons développé une approche basée sur le marquage de résidus cystéine pour suivre, *in vitro*, l'interaction protéine-protéine.

Mots clés : oxyluciférine, fluorescence résolue en temps, spectroscopie, ESPT, sonde sensible à l'environnement, technique bio-analytique

Abstract: In this work, we investigated the emission mechanism of the optically active part of the firefly luciferin-luciferase complex. This bioluminescent system is widely used in bioanalytical assay. This amazing natural phenomenon results in the emission of visible light (yellow-green-red) from the photoproduct *Oxyluciferin*. This color tuning mechanism involves six chemical species, but their active involvement in the excited state proton transfer (ESPT) mechanism was poorly understood so far. One of the main finding presented here relies on the identification of six chemical forms of Oxyluciferin involved in the color tuning fluorescence emission mechanism. This result was obtained by studying the optical properties of different structural analogues of firefly Oxyluciferin in aqueous buffer. Different spectroscopic (steady state and time-resolved) and chemometric approaches have been applied to reveal the emission mechanism. In addition, the photophysical properties of Oxyluciferin in complex with the Luciferase enzyme *Luciola cruciata* have been studied in aqueous buffer as well. In parallel, derivatives displaying environment sensitive emission were used to monitor biomolecular interactions. In particular, we demonstrated that Oxyluciferin can be employed to map intracellular pH by using fluorescence microscopy within living cells. With the help of another Oxyluciferin derivative we were able to monitor the interaction between a HIV-1 protein and different oligonucleotide sequences by means of ratiometric measurements. Finally we develop an approach based on cysteine labeling to monitor *in vitro* protein-protein interaction.

Keywords: Oxyluciferin, time resolved fluorescence, spectroscopy, ESPT, environment sensitive dye, bio-analytical assay